UNIVERSITY OF SOUTHAMPTON

FACULTY OF ENGINEERING, SCIENCE AND MATHEMATICS

School of Ocean and Earth Sciences

Iron inputs from sediments to the oceans

by

William Bela Homoky

Thesis for the degree of Doctor of Philosophy

December 2009

UNIVERSITY OF SOUTHAMPTON

ABSTRACT

FACULTY OF ENGINEERING, SCIENCE & MATHEMATICS
SCHOOL OF OCEAN & EARTH SCIENCES

Doctor of Philosophy

IRON INPUTS FROM SEDIMENTS TO THE OCEANS

by William Bela Homoky

This thesis explores the nature and ubiquity of iron (Fe) inputs from sediments to the oceans. In the last 10 years continental shelf sediments have become widely recognised as important vectors for dissolved Fe inputs to the oceans, where bacterial dissimilatory Fe-reduction (DIR) promotes the flux of Fe to the water column during the oxidation of sedimentary organic matter. Deep-sea and volcanogenic sediments however, are important reservoirs of Fe, which have not yet been investigated as sources of Fe to seawater. Furthermore knowledge of the nature of Fe phases involved in sediment, pore-fluid and seawater cycling is limited.

The nature of Fe cycling was investigated in deep-sea volcaniclastic surface-sediments (0-20 cmbsf). Pore-fluid and sediment samples were collected from tephra-rich sites near the active volcanic island of Montserrat, Caribbean Sea, and mixed biosiliceous sites around the dormant Crozet Island archipelago, Southern Ocean. Analyses reveal both regions maintain high pore-fluid Fe concentrations close to the sediment surface (up to 20 μM 0-5 cmbsf), despite relatively low organic carbon supply and contrasting oxygen utilization pathways. The oxidation of young tephra is thought to maintain the steep oxygen gradient measured in Montserrat sediments, and is considered to be an important component of Fe, and in particular manganese (Mn), cycling with local bottom water. Unlike Montserrat dissolved Fe and Mn in Crozet pore-fluids are dominated by colloidal phases (0.02-0.2 μm), and in both oxic and sub-oxic sediment layers. Thus mixed biosiliceous-volcaniclastic sediments are shown to host important colloidal-Fe generating reactions, which it is argued, promote the exchange of Fe with the overlying bottom waters. Re-cycling processes close to the seafloor are likely to determine the impact of this flux on seawater Fe budgets.

Low-cost ex-situ incubation experiments were used to measure a benthic Fe flux on sediments from the river-dominated Californian margin (6.3 ± 5.9 μmol Fe m^{-2} yr^{-1}) consistent with previous studies. Fe and Mn fluxes from Montserrat tephra deposits were also assessed; Differences in oxidation kinetics are shown to prevent the accumulation of Fe, yet permit the accumulation of Mn (~27 μmol m^{-2} yr^{-1}) in Montserrat bottom waters. Studies indicate temporospatial variations to bioirrigation and sediment re-suspension are important aspects of sedimentary Fe inputs that are poorly represented by conventional sampling methods.

In an effort to trace the biogeochemical processing of pore-fluid Fe in Crozet sediments, its isotopic composition was determined, representing the first measurements of their kind in deep-sea pore-fluids. Unique relative to previous studies of pore-fluid Fe isotopes, the near-crustal δ^{56}Fe compositions, demonstrate that DIR does not impart the same *light* Fe-isotopic signature that characterises previous sub-oxic pore-fluids. Comparison of reactive Fe contents between Crozet and pacific margin sediments indicates pore-fluid Fe isotopes reflect the extent to which Fe is recycled by redox processes. This discovery brings to light the potential for Fe isotopes to trace the input of Fe from shelf sediments, where redox re-cycling of Fe is extensive. The mean oceanic Fe isotope composition (δ^{56}Fe) is predicted to be -0.1 to -3.2‰ depending on the balance of uncertainty in input terms. The predicted surface water Fe isotope composition in the Crozet region (-2.0 to -2.2‰) is shown to reflect the *light* composition of shelf-derived Fe for a Fe inventory already constrained for this region.

TABLE OF CONTENTS

LIST OF FIGURES

LIST OF TABLES

DECLARATION OF AUTHORSHIP

I, William Bela Homoky, declare that the thesis entitled "Iron inputs from sediments to the oceans" and the work presented in the thesis are both my own, and have been generated by me as the result of my own original research. I confirm that:

- this work was done wholly or mainly while in candidature for a research degree at this University;
- where any part of this thesis has previously been submitted for a degree or any other qualification at this University or any other institution, this has been clearly stated;
- where I have consulted the published work of others, this is always clearly attributed;
- where I have quoted from the work of others, the source is always given. With the exception of such quotations, this thesis is entirely my own work;
- I have acknowledged all main sources of help;
- where the thesis is based on work done by myself jointly with others, I have made clear exactly what was done by others and what I have contributed myself;
- parts of this work have been published as:

Homoky, W.B., Severmann, S., Mills, R.A., Statham, P.J., and Fones, G.R., 2009, Pore-fluid Fe isotopes reflect the extent of benthic Fe redox recycling: Evidence from continental shelf and deep-sea sediments: Geology, v. 37, p. 751-754

Signed: ……

Date:……

ACKNOWLEGEMENTS

My greatest thanks are to my three supervisors Peter Statham, Rachel Mills and Gary Fones. Gary has played a vital role in supervising the generation and interpretation of data, and I'll very much miss the trips to Portsmouth, running the ICP and ducking out for a bacon sandwich on a construction site. I only hope I have also inherited some of Gary's meticulousness in trace metal analyses. Rachel is brimming with ideas and suggestions and has been a continuous source of motivation throughout this research. She has opened many doors during my training and provided great feedback. Despite encouragement from a former student (Silke), I never made her cry (though I think I came close with her first triathlon). Peter has been a great supervisor; his breadth of experience in ocean and earth science and trace metal analyses is reflected in the exchange of his ideas, as is his breadth of experience of riding bicycles. For sharing both of these I am truly grateful. I feel lucky to have had three supervisors of such complementary qualities - with so many points of view writing this thesis could have been a nightmare, but I am pleased to say you've all played together nicely! There's no doubt your combined support and tenacity has been crucial to the generation of this thesis and I am grateful, if not indebted to you all.

Upon arrival at the University of California (UC), Riverside, Silke Severmann offered support as friend, mentor, kayak instructor, margarita drinker, and geochemistry critique during my research visit. She shared many ideas and introduced me to many people in my field. I'm indebted to Silke for long nights in the lab, a bed on her living room floor, road-trips before dawn and cold Pacific swims, and for taking such an active role in my development as a researcher (for point of reference, this thesis contains just 2147 data points, meriting a nod of respect to her own doctoral research). My stay at UC Riverside was all the more fun and made a success thanks the welcome from Tim Lyons, his family and his research group. Particular thanks goes to Jeremy Owens for his assistance in the labs at UC Riverside. I would like to acknowledge James (Jim) McManus and family for welcoming me in their home while in the US. My time at Oregon State University was largely thanks to Jim's involvement, and experiments central to this thesis would not have been achieved without his support and stimulating discussion - what is more, for Jim to choose his own name as my nickname at sea, was a great honour and compliment. Further thanks are to Will Berelson, his research group at USC and in particular Tim Riedel, for their input to experiments conducted at Sea.

I've been lucky enough to benefit from four research-cruises, and each has been central to the work presented here. There are too many individuals to name here, but my sincere thanks goes to all the scientists and crews who worked together with me on RSS *Discovery*, RSS *James Cook*, and RV *Wecoma*. They have helped yield these results and made my experiences at sea so far life-long memories.

Back on home soil, I'd like to thank Martin Palmer for dropping in on discussion meetings with my supervisors, his insights have been welcomed and his support appreciated. There're a number of people at NOCS thanks to whom this work has been accomplished: Laura Hepburn's assistance with sediment digestion procedures was indispensable, as was input from Darryl Green and Belinda Alker; Doug Connelly was a great mentor on the graphite furnace and Paul Gooddy had a habit of finding just what I was missing in the lab; Eric Achterberg offered welcome criticism in panel meetings and Ray Collins and Ian Jenkinson provided

the care and craftsmanship for experimental apparatus developed in this thesis. For all their help and countless (Hélène Planquette, Paul Morris, Florence Nédélec, Sergio Balzano, Sarah Taylor, Sarah Bennett, Rich Marsh, Debbie Hembury, Morgan Jones...) other's input while I've been at Southampton, thank you.

Lastly, I'd like to acknowledge the friends and family who have supported me (often unknowingly) through difficult times: when things got tough, the surrogate job as bicycle mechanic at 'The Hub' gave me the perfect practical means to vent my frustrations; my family have provided a steady flow of encouragement, love and perception and my grandfather has seen me "go well" through it all on a good wooden chair. The production of this thesis (with the help of all mentioned above) has come to fruition thanks to Catherine, in part for editing my mistakes, but most of all thanks to her untold patience and belief.

LIST OF DEFINITIONS AND ABBREVIATIONS

ArO^+	Argide
BBL	Benthic boundary layer
C	Carbon
$CaCO_3$	Calcium carbonate
CASS-4	Nearshore seawater reference material for trace metals
Ce	Cerium
CFe	Colloidal iron
CHNS	Carbon Hydrogen Nitrogen Sulphur
CMn	Colloidal manganese
Cmbsf	Centimeters below seafloor
Co	Cobalt
CTD	Conductivity, temperature and density
DFe	Truly dissolved iron (<0.02μm)
DIR	Dissimilatory iron reduction
DIRB	Dissimilatory iron reducing bacteria
DMn	Truly dissolved manganese (<0.02μm)
DSi	Dissolved silicon
ERS	Eel River shelf
Fe	Iron
[Fe]	Concentration of iron
$Fe_{h\text{-}lab}$	Highly-labile iron
Fe_{ox1}	Easily reducible iron oxides
Fe_{ox2}	Reducible iron oxides
Fe_{reac}	Reactive iron
Fe_{tot}	Total iron
GFAAS	Graphite Furnace Atomic Absorption Spectroscopy
HCl	Hydrochloric acid
$HClO_4$	Perchloric acid
HF	Hydrofluoric acid
HNLC	High Nutrient – Low Chlorophyll
HNO_3	Nitric acid
ICP-AES	Inductively Coupled Plasma – Atomic Emission Spectroscopy
ICP-MS	Inductively Coupled Plasma – Mass Spectrometry
IRMM	Institute for Reference Materials and Measurements

LDPE	Low density polyethylene
Li	Lithium
MC-ICP-MS	Multiple collector - Inductively Coupled Plasma – Mass Spectrometry
Mn	Manganese
MORB	Mid-ocean ridge basalt
Milli-Q	Deionised water
NO_3^-	Nitrate
NOCS	National Oceanography Centre, Southampton
POM	Particulate organic matter
PVC	Polyvinyl chloride
Q-	Quartz distilled
RSD	Relative standard deviation
SBDW	Sub-boiled distilled water
SD	Standard deviation
Si	Silicon
SLRS-4	Certified river water reference material for trace metals
$T_{1/2}$	Half-life
TC	Total carbon
Tl	Thallium
TOC	Total organic carbon
Ti	Titanium
TIC	Total inorganic carbon
UC	University of California
USGS	United States Geological Survey
UV	Ultra-violet radiation
Y	Yttrium

Chapter 1 Introduction

Why is iron (Fe) important in the oceans? Why should we study sediments as a source of Fe to seawater? What does this thesis aim to do?

These are questions that this chapter aims to answer, and in doing so demonstrate the relevance of this study to Ocean and Earth Science. Firstly, an overview of the current state of knowledge concerning the importance of Fe, its distribution throughout the oceans, and mechanisms controlling the input, removal and stabilization of Fe in seawater will be presented. Secondly, the state of understanding of Fe in the benthic environment will be discussed, giving consideration to key aspects of benthic Fe cycling in need of further investigation. At the end of the chapter the project aims and objectives of this study will be outlined, along with an overview of the chapters that follow and address these goals.

1.1 THE IMPORTANCE OF Fe IN THE OCEANS

Dissolved iron is crucial for the metabolic functioning of many marine organisms. Intracellular respiration, photosynthesis, the utilization of nitrate and the production of chlorophyll cannot be achieved without Fe (Martin, 1990; Johnson et al., 1997; Ussher et al., 2004). Primary production in most oceanic regimes is limited by the abundance of light and macronutrients such as nitrate, phosphate and dissolved silicon. In approximately 40% of the world's oceans however, these major nutrients are in abundance relative to the primary production they sustain. These regions have been termed High Nutrient Low Chlorophyll (HNLC) regions, and most notably include the Southern Ocean, the Equatorial Pacific, and the Subarctic Pacific (Johnson et al., 1997; Moore et al., 2002). A number of field studies have demonstrated that the addition of Fe to HNLC waters stimulates phytoplankton growth (Martin et al., 1994; Coale et al., 1996; Coale et al., 1998; Bollens and Landry, 2000; Boyd et al., 2000; Coale et al., 2004), supporting the modern Fe hypothesis, which states that primary production in the ocean can be limited by low Fe concentrations (Martin, 1990; Watson, 2001). The impact of Fe

fertilization experiments has prompted debate concerning the impact of Fe availability on oceanic carbon sequestration by the biological carbon pump and sinking organic matter. The extent to which Fe fertilization of the oceans might enhance organic carbon export to the deep-sea (below 1000 m) is still in the early stages of quantification. The possible benefits of Fe addition to the oceans for offsetting anthropogenic carbon emissions may be outweighed by limited carbon sequestration and/or large-scale environmental impacts. Initial results however demonstrate Fe inputs to HNLC regions are of great significance to biogeochemical cycles and potentially impact the Earth's climate (Pollard, 2009). Thus studying the natural Fe cycling processes in the oceans is of great importance to Ocean and Earth Science.

1.2 DISTRIBUTION AND SPECIATION OF Fe

Fe is the fourth most abundant element on earth, and comprises approximately 5.6 wt% of the earth's crust. In Earth's surface conditions Fe occurs in two oxidation states, Fe^{2+} and Fe^{3+}, and its highly stable ^{56}Fe nucleus and associated isotopes form compounds accounting for a significant proportion of rocks and soils. These Fe compounds are present as oxides, carbonates and sulphides, for example haematite (Fe_20_3), magnetite (Fe_3O_4), limonite ($2Fe_2O_3.3H_2O$), siderite ($FeCO_3$), and pyrite (FeS_2). The stability of these Fe compounds however, explain in part, why despite being ubiquitous in the Earth's crust, dissolved iron occurs in very low concentrations in most of the oceans, typically of the order of 1 nmol L^{-1} or less (Johnson et al., 1997).

The presence of oxygen in aqueous systems is the single most important factor in determining the oxidation state and subsequent solubility of Fe in seawater (Johnson et al., 1997). The very low Fe concentrations found in seawater relative to the crustal abundance of Fe is therefore a symptom of the oxygenated modern ocean (Ussher et al., 2004). The oxidation of soluble Fe^{2+} is predominantly through the Harber-Weiss mechanism (Equation 1-1), where a single oxygen molecule may be involved in the initiation and propagation of Fe^{2+} oxidation by formation of hydrogen peroxide as well as oxygen and hydroxide radicals. The presence of oxygen therefore drives the equilibrium between Fe redox reactions strongly in favour of relatively insoluble Fe^{3+} formation.

$$Fe^{2+} + O_2 \rightarrow Fe^{3+} + O^{\bullet}_2^{-}$$
$$Fe^{2+} + O^{\bullet}_2^{-} + 2H^{+} \rightarrow Fe^{3+} + H_2O_2$$
$$Fe^{2+} + H_2O_2 \rightarrow Fe^{3+} + OH^{-} + HO^{\bullet}$$
$$Fe^{2+} + HO^{\bullet} \rightarrow Fe^{3+} + OH^{-} \quad (1\text{-}1)$$

This reaction serves to establish a heterogeneous equilibrium between Fe redox reactions, negating the effects of Fe^{2+} production processes such as UV photochemical reduction, and thus maintains low Fe concentrations in the ocean (De Baar and De Jong, 2001).

Typically Fe mimics a nutrient-like profile in the oceans, with low concentrations in the surface layer <0.2 nmol L^{-1}, increasing with depth to ~0.75 nmol L^{-1} in the deeper ocean, below 1000 m (Landing and Bruland, 1987; Johnson et al., 1997; Landing and Powell, 1999; Klunder et al., In Press). Gradients in dissolved Fe concentration have been reported along transects close to continental and island margins, in some cases up to >1000 km off-shore (Bucciarelli et al., 2001; Boye et al., 2003; Nishioka et al., 2007; Planquette et al., 2007), and these observations will be revisited in Section 1.3. The relatively constant Fe concentration of the deep ocean is unique for a nutrient like profile as it suggests little inter-ocean fractionation of Fe occurs. Kuma et al. (2003) have shown dissolved Fe(II) concentrations in intermediate waters are largely controlled by Fe(III)hydroxide solubility associated with sinking particulate organic matter (POM). However, if the oceanic concentration of dissolved Fe were controlled by solubility reactions alone, then the Fe concentration in the deep-sea would be much lower than is observed (Millero, 1998). The existence of organic complexes capable of stabilizing soluble Fe for sufficient periods to allow inter-ocean mixing to occur is believed to account for this phenomenon (Rue and Bruland, 1995; Wu and Luther III, 1995; Johnson et al., 1997), and is discussed in greater detail below.

1.3 ORGANIC Fe STABILISATION

The significance of the organic stabilisation of dissolved Fe has been discussed for more than 30 years since the work of Stumm and Morgan (1970) and Theis and Singer (1974). It is now understood that >99% of dissolved Fe measured in the oceans appears to be Fe(III) complexed by organic ligands (van den Berg, 1995; Wu and Luther III, 1995; Kuma et al., 1998; van den Berg, 2006). Fe-binding ligands have been observed between 0.6 and 0.75 nmol/L throughout sites in the Atlantic, Pacific and Southern Oceans (Rue and Bruland, 1995; Wu and Luther III, 1995; Johnson et al., 1997; Boye et al., 2001). They are often found to be at saturation by Fe(III), which has led to the suggestion that the concentration of organic ligands could be a limiting factor controlling the concentration of dissolved Fe in the oceans (Gledhill et al., 1998). In the Southern Ocean surface waters however, organic ligands are measured in excess of Fe concentrations by ~0.5 nmol/L (Boye et al., 2001). The exact origins of organic ligands found in seawater, remains unknown. Fe-binding ligands appear to be released by phytoplankton during Fe fertilised incubation experiments (Boye and van den Berg, 2000). The associative distribution of organic ligands with algal blooms, and the similarity of their conditional stability constants to siderophores and other organically synthesised chelators, suggest they originate from marine organisms (Gledhill et al., 1998; Barbeau et al., 2001). It has been suggested the release of organic ligands by micro-organisms might help buffer dissolved Fe concentrations during temporal fluctuations to Fe sources to the oceans and subsequently help to sustain growth (van den Berg, 1995).

1.4 ORIGINS OF Fe IN SEAWATER

An excellent review covering the sources and sinks of Fe in seawater can be found by De Baar and De Jong (2001; and references therein). There are 5 major pathways by which Fe is now known to enter the oceans:

1. River discharge and continental run-off
2. Atmospheric (dry/wet) deposition and dissolution
3. Iceberg rafted particulate Fe dissolution
4. Hydrothermal discharge

5. Diagenetic sedimentary flux

Fe inputs from river discharge have been estimated (Chester, 1990) and represent one of the largest fluxes of dissolved Fe to seawater (~29 $x10^9$ mol Fe yr^{-1}). However, seasonal, diurnal, and isolated peak-discharge events that typify many river systems may be poorly reflected by many discharge estimates, and the associated Fe concentration of river waters will also be subject to considerable temporal variability, that is not well documented. Therefore some significant uncertainty remains concerning the Fe input from rivers. River and seawater mixing in estuarine zones promotes the flocculation of dissolved material and intense particulate scavenging effectively traps ~90% of dissolved riverine Fe entering the oceans in coastal zone sediments, limiting the estimated global riverine input of dissolved Fe to the oceans to 1.5 $x10^9$ mol Fe yr^{-1}.

Atmospheric deposition of mineral dust is an important pathway by which Fe reaches ocean surface waters (Duce and Tindale, 1991). It is estimated that the input of dissolved Fe to seawater from dissolution of atmospheric dust is greater than the magnitude of the riverine flux, ~13 $x10^9$ mol Fe yr^{-1} (Jickells and Spokes, 2001) or 10-26 $x10^9$ mol Fe yr^{-1} (De Baar and De Jong, 2001) . Atmospheric transport is of particular importance for delivering Fe directly to the surface waters of open ocean regions where Fe is often most scarce, and as such may represent the primary source of Fe to some HNLC regions (Sarthou et al., 2003).

Rates of hydrothermal fluid discharge are very high, however steep oxygen, pH and temperature gradients account for extensive particulate Fe sulphide and oxyhydroxide precipitation (Feely et al., 1987). Thus it has been assumed that hydrothermal systems are a negligible source of dissolved Fe to seawater (German et al., 1991; De Baar and De Jong, 2001). A recent study however has shown the stabilization of dissolved Fe in a hydrothermal plume by organic ligands contributes a fraction (~4%) of hydrothermal Fe to seawater Fe, with an extrapolated global flux of ~0.3 $x10^9$ mol Fe yr^{-1} (Bennett et al., 2008).

Recent studies have shown that cryogenic inputs are important vectors for dissolved, colloidal and nano-particulate Fe oxides and sulphides to the oceans. A fraction of which are bio-available, and are inferred to represent an important

source of dissolved Fe to the Southern Ocean (Raiswell et al., 2008), and to coastal waters near the Greenland Ice sheet (Statham et al., 2008).

Amongst the least well-quantified Fe inputs is the input from sedimentary sources. In the review by De Baar and De Jong (2001), the authors speculate as to the existence of a diagentic sedimentary Fe flux large enough to balance the estimated inputs of River, Aerosol, and Hydrothermal Fe with the amount of Fe-induced export production in the global oceans (the output of Fe). The estimated magnitude of this benthic balancing term is ~33 $x10^9$ mol Fe yr^{-1}, and later publication of revised flux estimates have not diminished the significance of this missing source term for Fe, which until recently remained largely unstudied. The release of Fe from sediments has previously been identified in estuarine environments (Watson et al., 1993), and associations of Fe induced productivity with re-suspended particulate Fe on the California margin lead to the understanding that continental shelves may be dominated by a sedimentary source, rather than riverine source, of Fe (Johnson et al., 1999). Elrod et al. (2004) suggested sediments were "a missing source for [dissolved] seawater Fe budget" and estimated the global flux of dissolved Fe from continental shelf sediments to be 2.2 $x10^9$ mol yr^{-1}. A recent model estimate for the global flux of Fe from shelf sediments was a more substantial 16 $x10^9$ mol yr^{-1} (Moore and Braucher, 2008). The highest estimate for shelf sedimentary Fe inputs to the oceans is based on the amount of reactive Fe enrichment in sediments beneath euxinic (sulphate reducing) bottom waters, and predicts the global contribution of Fe from shelf sediments to be ~410 $x10^9$ mol yr^{-1} (Raiswell and Anderson, 2005). The uncertainty between global flux estimates therefore remains high, yet the consensus of opinion is sediments are a major contributor of dissolved Fe to the oceans, and flux derivations to date for sedimentary inputs do not account for the observed Fe export or reactive Fe enrichment in deep-basin sediments.

1.5 BENTHIC Fe CYCLING

Sedimentary Fe inputs to seawater form part of a benthic Fe cycle. Fe reaches marine sediments via accumulating pelagic and terrigenous sedimentation sinking through the water-column, and by lateral transport of sediments accumulating on the margins by turbidite flows. Sediment accumulation rates are

much higher on the continental margins (1-10 mm yr^{-1}) than the deep-ocean (1-10 mm kyr^{-1}). Terrigenous Fe inputs contain a mixture of reactive Fe oxide minerals, silicate Fe minerals and Fe sulphides. Pelagic sedimentation carries mostly Fe as oxy(hydr)oxide phases associated with sinking POM. Thus sediments are the ultimate sink for particulate Fe in the oceans, from continental weathering and biological sources. The subsequent cycling of Fe between sediments and the overlying water column is driven by early diagenetic reactions in surface sediments which generates dissolved Fe in the pore-fluids.

Organic carbon reaching the seafloor is subject to decomposition by respiring microorganisms, which oxidise organic matter for the derivation of energy. Oxidants available for respiration (O_2, NO_3^-, MnO_2, Fe_2O_3, SO_4^{2-}) are utilised by bacteria in order of the energy yield from each reaction (Froelich et al., 1979; Lovley and Phillips, 1986; Lovley, 1991; Canfield et al., 1993). The result of successive oxidant utilisation in surface sediments has been described as biogeochemical zonation of respiratory processes, and is illustrated in Figure 1-1.

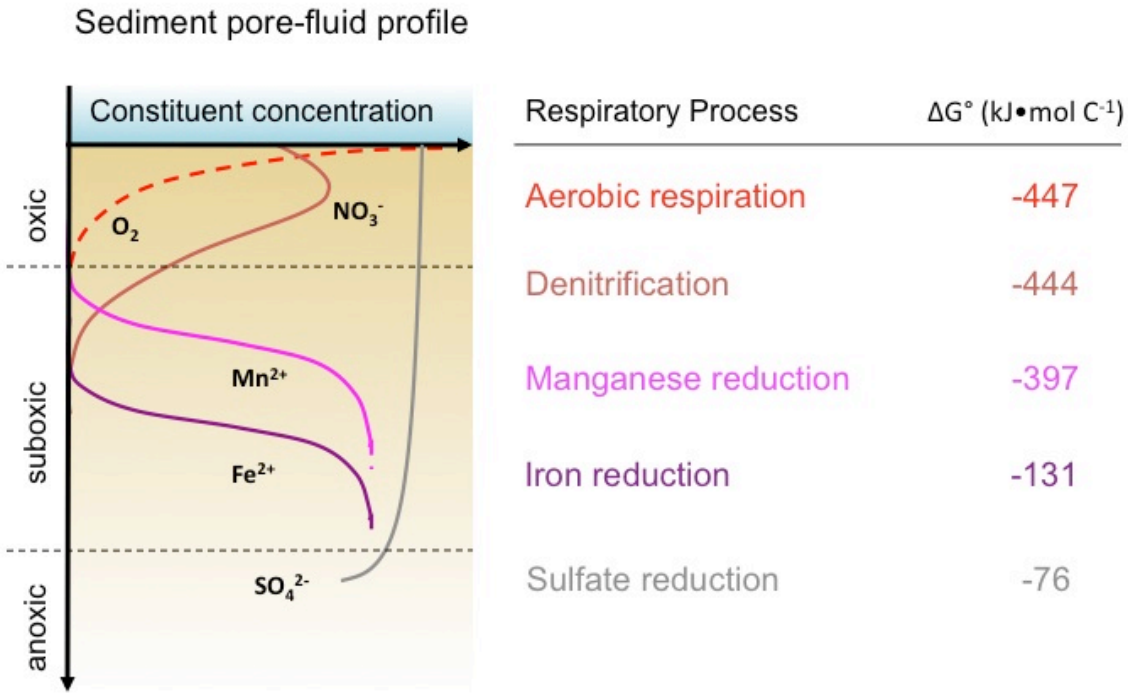

Figure 1-1. Biogeochemical zonation of respiratory processes in surface sediments, standard Gibbs free energy associations of each reaction, and the resulting distribution of depleted reactants and enriched products in the pore-fluids. Modified from Burdige, 2006.

Dissimilatory Fe reduction (DIR) in sub-oxic surface sediments by dissimilatory Fe reducing bacteria (DIRB) (Lovley and Phillips, 1986; Canfield, 1989; Lovley, 1991; Burdige, 1993; Thamdrup, 2000) is integral to early diagenetic reactions in sediments. Reduced Fe^{2+} liberated by DIRB accumulates in the pore-fluids in the absence of oxygen and diffuses towards regions of lower pore-fluid Fe concentration. Upward diffusing Fe^{2+} is balanced by the downward flux of oxygen at a redoxcline, where Fe re-precipitates as oxy(hydr)oxides in the sediment, and the upward transport of dissolved Fe is restricted. Downward diffusing Fe^{2+} meets free sulphide in the pore-fluids generated by bacterial sulphate reduction, and leads to the removal of Fe^{2+} from anoxic sediment pore-fluids by precipitation of Fe_2S or pyrite (Canfield et al., 1993). Dissolved Mn^{2+} behaves similarly to Fe^{2+}, diffusing upward to form MnO_x precipitates below the surface oxic layer, and diffusing downward to form carbonate precipitates, such as Rhodochrosite ($MnCO_3^2$).

A benthic flux of Fe requires the transport of a fraction of dissolved Fe in the pore-fluids to the overlying bottom water. The size of the benthic Fe flux is will be controlled by the thickness of the oxidizing sediment layer overlying sub-oxic zone and i.e. the concentration gradient of dissolved Fe (Berelson et al., 2008). The fate of Fe exiting the pore-fluids will strongly depend on the oxidation kinetics of Fe in the bottom water, the interactions of stabilizing organic complexes and particulate scavenging rates. Where oxygen concentrations are low, such as hypoxic bottom waters off the Oregon coastline, the concentration of Fe(II) has been shown to increase by two orders of magnitude in the waters overlying sediments suspected to generate an Fe(II) flux (Lohan and Bruland, 2008). In-situ lander deployments on the California coastline have also been used to measure the flux of Fe from sediments in low-oxygen bottom waters underlying regions of high surface water primary productivity (McManus et al., 1997; Berelson et al., 2003; Elrod et al., 2004; Severmann, 2008). Benthic Fe flux measurements however, have so far been restricted to continental shelf settings where organic-carbon accumulation (and DIR) rates are high.

Additional processes may contribute to the enhancement of Benthic Fe fluxes. Bioirrigation by megafauna promotes the injection of oxygenated bottom water into reducing zones in the sediment, and the ejection of reduced pore-fluids into the overlying bottom water (Aller, 1990; Polerecky et al., 2006). In effect this

process increases the surface area available to pore-fluid exchange by maintaining a 3-dimensional structure to the Fe redox front in surface sediments. It has been estimated that bioirrigation accounts for up to a 75% increase in the flux of Fe from continental margin sediments (Elrod et al., 2004) but the importance of this processes for generating benthic Fe flux is not well understood. It is possible that mediation of sediment diagenesis by macro-fauna might facilitate the flux of Fe, albeit smaller, from deeper ocean environments that remain to be investigated.

There is much uncertainty concerning the nature of Fe involved in its transfer from sediments to the water column. There is clearly evidence for the existence of a "dissolved" Fe flux (<0.45 μm) (McManus et al., 1997; Berelson et al., 2003; Elrod et al., 2004) from continental margin sediments to the overlying bottom waters, yet others highlight the significance of particulate Fe inputs to seawater from sediments in coastal and open ocean settings (Johnson et al., 1999; Lam et al., 2006; Nishioka et al., 2007). Improved understanding of Fe cycling between particulate and dissolved phases, in the sediments, pore-fluids and the water column is necessary to inform our understanding of the mechanisms of benthic Fe cycling (Figure 1-2).

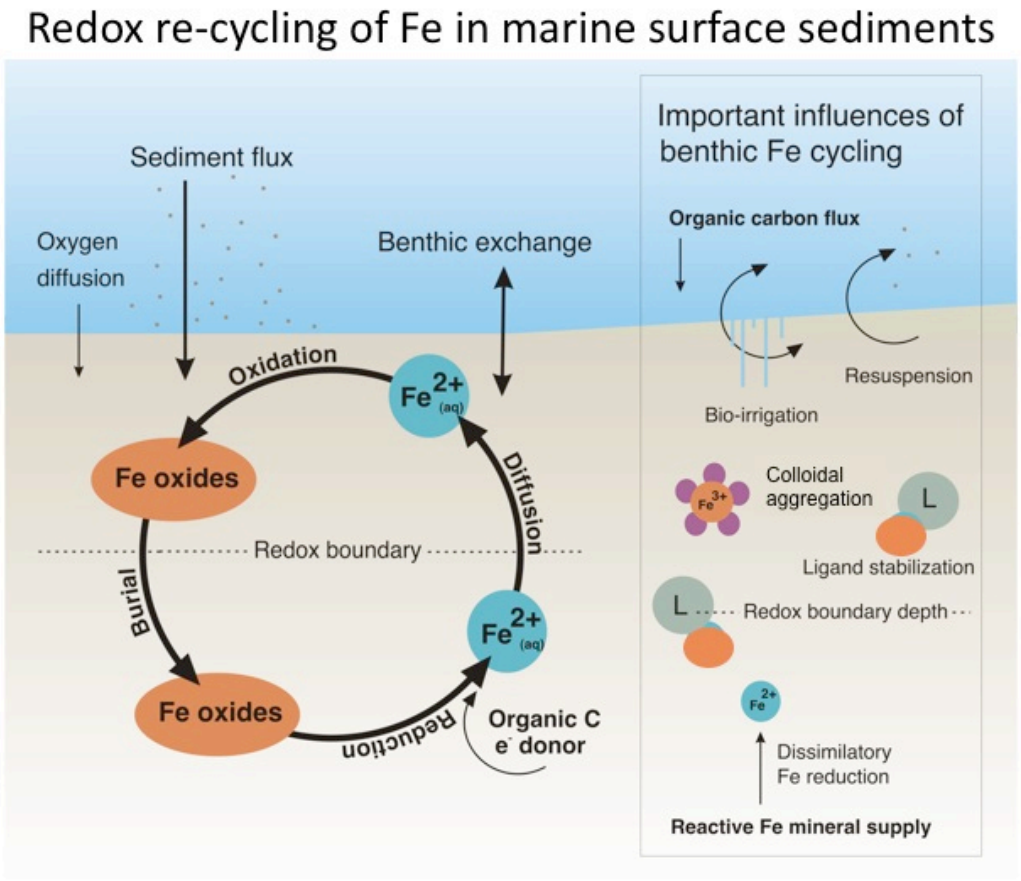

Figure 1-2. Redox re-cycling of Fe in marine surface sediments. Reactive Fe oxides are buried below a redoxcline where they become available to DIRB. Reduced Fe is enriched in the pore fluids and upward diffusion may lead to either the re-precipitation of Fe oxy(hydr)oxides (a return of Fe to the reactive sedimentary oxide pool) or diffusion into the overlying bottom waters. Downward diffusing Fe in the pore-fluids will be re-precipitated with free sulphide to form pyrite. Processes influencing the potential for, and magnitude of, a benthic Fe flux are summarised in the inset.

The geographical ubiquity or restriction of benthic Fe flux, and its impact on the open oceans is poorly constrained, and thus so too is the Fe inventory for the oceans. Knowledge of these processes will determine the impact of sedimentary Fe inputs on biogeochemical cycles.

1.6 Fe ISOTOPES IN PORE-FLUIDS - A SIGNATURE FOR BENTHIC Fe FLUX?

Iron isotopes have emerged as a new tool to evaluate iron cycling in aquatic environments, and may be a unique tracer of sediment respiration by dissimilatory Fe reducing bacteria (DIRB) (Anbar and Rouxel, 2007; Johnson et al., 2008). Due to the variations in atomic mass, many processes on earth may favour the fractionation of different isotopes, altering the relative abundance of each isotope in a given pool. The relative isotopic composition of Fe is described using the two most abundant Fe isotopes, ^{54}Fe and ^{56}Fe (Table 1-1), using the $\delta^{56}Fe$ standard notation described in Equation 1-2 and expressed in units per mil (‰).

$$\delta^{56}Fe = [(^{56}Fe/^{54}Fe_{sample})/(^{56}Fe/^{54}Fe_{standard})-1] \times 10^{3} \quad (1\text{-}2)$$

Table 1-1. Natural abundance of Fe isotopes in igneous rocks

Isotope	Abundance (%)
^{54}Fe	5.8
^{56}Fe	91.8
^{57}Fe	2.1
^{58}Fe	0.3

Incubation experiments have demonstrated that the reduction of Fe(III) in the presence of DIRB produces aqueous Fe^{2+} with $\delta^{56}Fe$ values that are 0.5–2‰ lower than the initial Fe(III) substrate (Beard et al., 1999; Icopini et al., 2004; Crosby et al., 2007). Pore-fluids from reducing shelf sediments, where organic matter oxidation proceeds through DIR, yield isotope compositions for dissolved Fe^{2+} that are ~1–3‰ lighter than average igneous rocks: the largest Fe isotope fractionation found in aqueous systems (Johnson et al., 2008). These observations suggest that benthic Fe inputs to seawater could potentially carry a unique DIR isotopic fingerprint (Severmann et al., 2006), and inform our understanding of sedimentary Fe inputs to seawater. Characterizing the Fe isotopic fingerprint of DIR in natural, aqueous systems is therefore important for developing the utility of Fe isotopes in biogeochemical cycles. Yet pore-fluid Fe isotope measurements have so far been restricted to the continental shelves where DIR is extensive (Bergquist and Boyle, 2006; Severmann et al., 2006), and no measurements have been made in low organic-carbon sediments or in deep-water settings where diagenetic rates are much slower than on the continental shelves.

1.7 AIMS AND OBJECTIVES

This thesis aims to:

1. Evaluate the processes a) involved in generating a benthic Fe flux and b) controlling the fate of Fe released from sediments to overlying waters;
2. Consider the geographical restriction or ubiquity of sedimentary Fe sources to the oceans and their significance for global seawater Fe budgets;
3. Identify important directions for future related research.

Specific objectives of this project are:

- To measure the concentration of Fe in sediment pore-fluids, from a range of diagenetic environments;
- To evaluate the partitioning of pore-fluid Fe between dissolved and colloidal size fractions
- To determine the abundance of Fe in different reactive solid-phases in sediments contemporaneous to pore-fluid Fe concentrations;
- To calculate the diffusive flux of Fe from pore-fluid concentration gradients;
- To design and build portable apparatus for the shipboard incubation of surface sediments and overlying bottom water;
- To measure concentration of Fe in overlying bottom water during shipboard sediment incubations, for comparison to diffusive flux calculations;
- To measure the composition of Fe isotopes in sediment pore-fluids from new and contrasting diagenetic environments

To meet these aims three marine sedimentary settings form the focus of this thesis: 1) Deep-sea sediments in the region of the Crozet Island archipelago in the Southern Ocean, 2) Deep-sea sediments close to the island of Montserrat in the Caribbean Sea, and 3) Continental shelf sediments from the Californian margin of the Northeast Pacific Ocean. The next chapter describes the methods of sampling and analysis used for all of the data presented in this thesis. This data is presented in Chapters 3-5, with the major conclusions presented in

Chapter 6. Chapter 3 presents pore-fluid Fe and Mn data from contrasting deep-water sedimentary regimes (Crozet and Montserrat), along with contemporaneous solid-phase distributions of Fe, to evaluate the controls on Fe and Mn in these regions. It also demonstrates the potential significance of deep-water and volcanogenic sediments for benthic Fe, and closely redox-coupled Mn, exchange with the overlying bottom waters, supporting previous observations of Fe release from intercalated volcaniclastics in the sedimentary record (Pirrie and Marshal, 1990; Bottrell and Morton, 1992; Pirrie et al., 1994). Chapter 4 introduces the apparatus designed and built for shipboard incubation of surface sediments and overlying bottom waters. The data presented compares the incubated Fe concentrations in bottom water overlying sediments from the Californian margin and Montserrat regions, which is used to evaluate the controls on benthic Fe flux process, the fate of Fe released from sediments, the validity of methods for Fe flux determinations, and to make recommendations for future Fe flux determination studies. Chapter 5 compares the pore-fluid Fe isotope composition of California margin sediments with deep-sea Crozet sediments, and uses ancillary solid-phase reactive Fe partitioning, to bring to light an improved understanding of Fe isotope processing in marine sediment pore-fluids, highlighting the potential for future studies to trace the benthic Fe fluxes from continental margins. Lastly Chapter 6 addresses the thesis' main objectives, drawing conclusions from the findings of individual chapters, and moves on to make recommendations for future research.

Chapter 2 Methods of sampling and analysis

2.1 INTRODUCTION

This chapter contains all methods used for the collection of pore-fluid and sediment samples, and describes how key parameters of these samples were analysed. Details of sampling locations and discussion of the data can be found in Chapters 3 to 6.

The pore-fluid sampling and sample processing described in this chapter required trace metal clean procedures. Unless otherwise stated, analyses were performed at the National Oceanography Centre, Southampton, and all sample and reagent containers were cleaned in a series of 50% HCl and 50% HNO_3 baths followed by thorough rinsing with Milli-Q. Volumetric transfer of solutions for volumes up to 50 ml used 20 μl to 10 ml gravimetrically calibrated Finnpipettes with 10% HCl cleaned and Milli-Q rinsed pipette tips. Immediately prior to use, each pipette tip was rinsed with a series of two tip rinses: firstly, in a 1-2% HCl Milli-Q solution and secondly, in a 0.1 % HCl Milli-Q solution. Where sufficient reagent/sample was available, the first aliquot of each pipette was passed to waste. Reagent volumes greater than 50 ml were gravimetrically determined, and reagent solutions were either analytical grade, or quartz distilled.

2.2 SEDIMENT CORING

Sediment samples were collected using a Bowers and Connelly Mega Corer and 10 cm diameter polycarbonate core tubes. Cores that were suspected of air leaking into the core tube during surface recovery, and thus either altering sediment redox conditions or physically disturbing the sediment–seawater interface, were not used in this study. Selected cores were removed from the Mega Corer and closed at each end by a neoprene bung, before being transferred to an upright core-rack to minimise disturbance during transportation to a

controlled temperature laboratory in preparation for pore-fluid and sediment sampling.

2.3 PORE-FLUID AND SEDIMENT SAMPLING

Three conventional methods were used for the collection of pore-fluids at sea: (1) centrifugation followed by filtration, (2) Diffusive Equilibrium in Thin-films (DET) gel probes, and (3) Pore-fluid extraction by Rhizon samplers. The anoxic filtration of centrifuged sediment was used as the primary method for the collection of pore-fluids and contemporaneous sediments. In some cores DET gel probes were used as an additional method to provide a validation of the filtration technique and a high-resolution sampling method for trace metals. Additionally Rhizon samplers were used in contemporaneous cores for comparison of methods, and are cited in Chapter 5 where nutrients collected by centrifugation were contaminated.

2.3.1 Pore-fluid sampling by centrifugation and filtration

Pore-fluids were sampled under nitrogen in a glove bag by conventional sectioning, centrifugation and filtration of the sediment recovered by Mega Core (Section 2.2). Firstly, the lower bung was removed and the core tube was transferred to an upright floor-mounted sediment extruder. Once in place, the upper bung was removed and excess overlying core water was carefully siphoned to waste using a Tygon tube, ensuring minimum disturbance to the sediment surface (Figure 2-1). The core was then pushed through the base of a glove bag containing all sediment sampling apparatus. The PVC flexible glove bag was filled with analytical grade nitrogen gas that had passed through a 0.45 μm glass fibre filter membrane, the gas was purged and this process was repeated 3 times to ensure effective removal of oxygen. An oxygen sensor was used to monitor the integrity of the anoxic environment in the glove bag. Any remaining excess overlying core water was removed using a Teflon tube and 20 ml syringe.

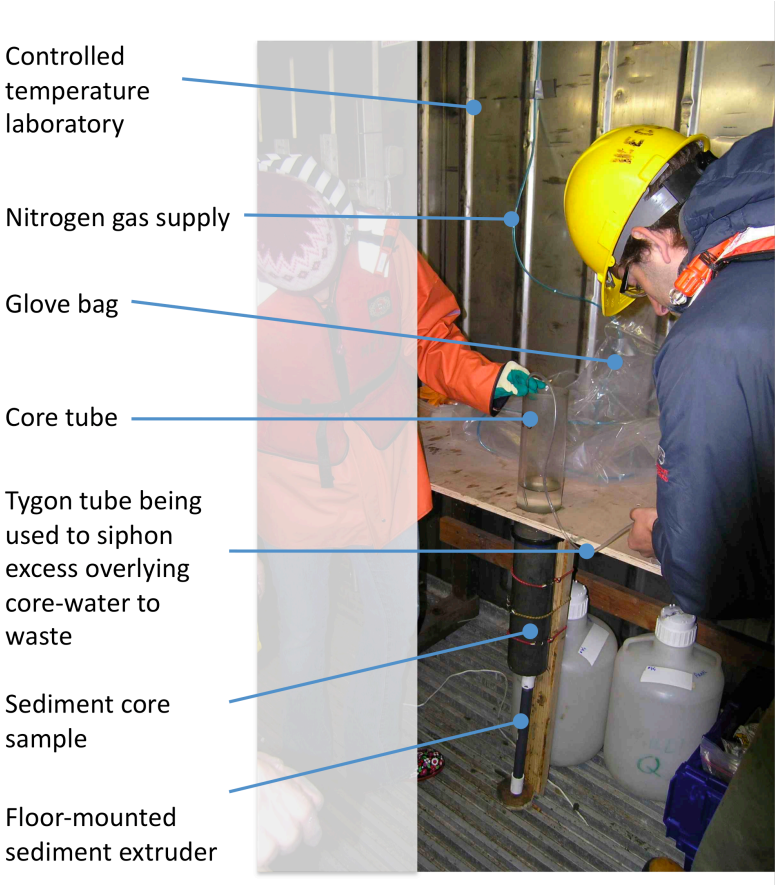

Figure 2-1. Sediment core sample mounted on extruder, while excess overlying cover-water is siphoned to waste. The core will then be sealed in a nitrogen-flushed glove bag ready for sediment sectioning.

The sediment core was then partially extruded and a sub-sample sectioned from the core tube at 1 or 2 cm depth intervals using a polycarbonate measuring ring and Teflon sectioning plate. A Teflon spatula was used to transfer the sediment sample from the sectioning plate to an 85 ml polycarbonate centrifuge bottle. The screw threads of the bottles were wiped clean using Kim Wipe to ensure an airtight seal of the lids. The extrusion and sectioning processes were repeated for each additional sample required. The deepest sediment sample was >5 cm from the base of the core and extrusion plunger. In some instances, centrifuge bottles were filled to the neck (85 ml) to ensure balancing in the centrifuge head and to maximise the volume of pore-fluid sampled. In this case, the mean depth of the sediment sample was back calculated from the sediment volume of each section. This means that every 85 ml of sediment transferred to a centrifuge tube from a 10 cm diameter core tube is equivalent to a sediment depth of 1.18 cm. Secure fitting of the centrifuge bottle lids was checked prior to removal from the glove bag to ensure there was no oxygen contamination. Samples were transferred to a

controlled temperature centrifuge, which was set to the same temperature as the as the bottom waters overlying the sampling site (between 4 and 8 ºC) and spun at 6000 rpm for 6 minutes, or 3000 rpm for 30 minutes.

Bottles were re-opened in a new glove bag under a new nitrogen atmosphere. Supernatant pore-fluids were separated from the sediment precipitate using a Teflon tube attached to a 20 ml nitrile-free syringe - any syringe used that might come into contact with the pore-fluid sample was trace-metal clean. The tube was removed and the sample divided for nutrient and trace metal analysis between two 15 ml low-density Polyethylene (LDPE) sample pots through a nitrogen flushed Whatman cellulose acetate 0.2 μm syringe filter. For some trace metal samples an aliquot was sequentially filtered through an additional 0.02 μm Whatman Anotop aluminium oxide filter. Trace metal pore-fluid samples were acidified to pH 1.7 using quartz distilled $HN0_3$ (Q-HNO_3) and refrigerated along with the sediment residues from centrifugation until later analysis.

2.3.2 Pore-fluid sampling by DET gel probes

Diffusive Equilibrium in Thin-film (DET) gel probes have been demonstrated to provide a robust alternative method for high resolution sampling of pore-fluid Fe and Mn in surface sediments (Fones et al., 2001; Morford et al., 2003). DET Gel probes were deployed in sediment cores collected from the same Mega-core deployment as used for pore-fluid sampling by filtration. Gel probes were allowed to equilibrate with the sediment pore-fluid for 24 hours at 4 ˚C. Gels were later sectioned at 2 mm depth resolution and eluted in 1M Q-HNO_3 for 36 hours at room temperature (20-22 ˚C) prior to dilution and analysis by Graphite Furnace Atomic Absorption Spectroscopy (GFAAS) (Section 2.4).

2.3.3 Pore-fluid extraction by Rhizon samplers

Rhizons have been demonstrated to be a robust method for the sampling of pore-fluid constituents across the sediment-seawater interface (Seeberg-Elverfeldt et al., 2005; Homoky et al., 2009). Eel River shelf nutrient data (Chapter 5) was derived by Rhizon sampling of sediment cores, where nitrate data from samples collected by centrifugation showed unreasonably high nitrate concentrations below the surface oxic zone. These samples were considered compromised with

respect to nutrient abundance, possibly due to cell lysis during centrifugation at speeds >10,000 rpm, and so comparison of pore-fluid constituent data with nutrient data from Rhizon sampling was considered reasonable. Pore-fluids were collected by 0.2 μm Rhizon samplers from cores at the same site as used for other pore-fluid constituent analysis and were analysed by Silke Severmann at the University of California, Riverside. The procedure followed is described by Seeberg-Elverfeldt, et al. (2005)

2.4 PORE-FLUID Fe AND Mn DETERMINATIONS BY GFAAS

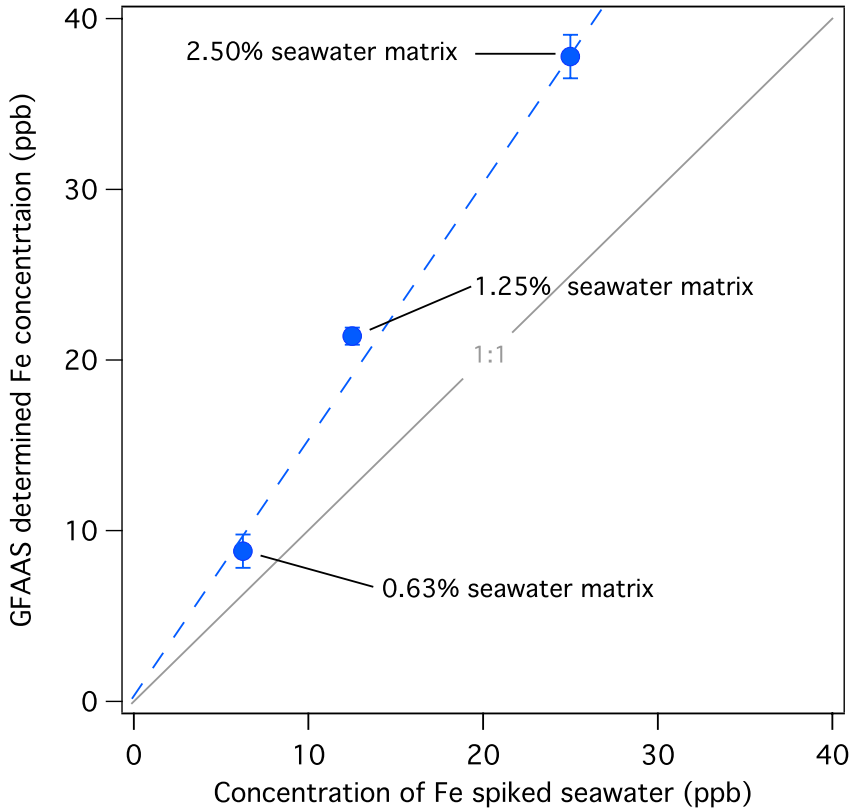

Figure 2-2. Concentration of Fe determined by Perkin Elmer AA800 GFAAS in a spiked Southern Ocean seawater sample following dilution between 40 and 160 fold with Milli-Q. The seawater sample was acidified to pH 1.7 using Q-HNO_3, and the initial Fe concentration was known to be <0.2 nmol/L or <0.0011 ppb (Planquette et al., 2007). The results show that saline interferences, thought to be caused by atomization of salt crystals accumulating in the sample tube during the drying step, produced artificially elevated absorption data for Fe, resulting in an apparent ~30% increase in the Fe concentration determined.

A Perkin Elmer AA800 atomic absorption spectrometer was initially used for the determination of Fe and Mn in DET gel probes and centrifuged pore-fluid samples. The interference of the pore-fluid matrix however could not be fully resolved (Figure 2-2) and the ICP-MS was used instead for analyses of pore-fluids and sediment extractions/digests thereafter (Section 2.5). DET gel probe data were unaffected by any matrix interference due to sufficient dilution during the sample elution and dilution process (<0.05% v/v seawater salts). The method described here is therefore used for the determination of Fe in DET gel probe data alone.

The GFAAS was equipped with background compensation with inverse longitudinal Zeeman-effect and transversely heated graphite atomiser (THGA). Pyrolytically coated graphite tubes and pyrolytic graphite platform were used. The instrument furnace programme used for the analysis of Fe is described in Table 2-1. Samples and standards were introduced to the furnace in 20 μl aliquots using an AS-800 auto-sampler. A single element hollow cathode Lumina lamp was used as the light source, and the manufacturer recommendations for operating parameters were followed (current: 25 mA; wavelength: 248.3 nm). Argon was employed in the graphite furnace as external and internal gas, and the flow of the internal gas was interrupted during atomization. Calibration ranges were between 12.5 and 50 μg/L, and an optimum linear absorbance range was achieved with a peak area of up to 0.33. Relative standard deviation (RSD) of analyses were <5% and calibration correlation coefficients were typically 0.998.

Table 2-1. GFAAS temperature programme.

Step	Temp/ ramp time (ºC/s)	Hold time (s)	Gas flow rate (ml/min)
1. Dry	110/10	30	250
2. Ash	1400/10	20	250
3. Atomise	2100/0	3	0 (read abs)
4. Cleaning	2450/1	3	250
5. Purge gas between samples			

2.5 PORE-FLUID Fe AND Mn DETERMINATION BY ICP-MS

Pore-fluid analyses were performed on an Agilent 7500cx series Inductively Coupled Plasma Mass Spectrometer (ICP-MS) with an Aligent Integrated Auto-sampler and an octopole reaction cell at the Universities of Portsmouth and California, Riverside. A 10 μg/L solution of Li, Y, Ce, Tl and Co in 2% HNO_3 was used for instrument tuning, and 2% Q-HNO_3 / 0.5% Q-HCl solution was used as a rinse. Argon was used as the carrier gas and was set to flow at 0.95 L min^{-1}. An internal standard was necessary to correct for any drift of signal intensity over time, and was performed automatically by the software. The standard must consist of one or more elements that are known to be either absent or present at negligible concentrations in the sample. All data presented here have been corrected using a 50 μg/L Indium and Rhenium internal standard solution prepared in 2% Q-HNO_3 and 0.5% Q-HCl.

A potential interference for the analysis of Fe is ArO^+, which shares the same mass as the major Fe isotope ^{56}Fe. The Octopole collision cell suppressed argide interferences and improved detection limits of the 7500cx Agilent compared with traditional ICP-MS techniques, despite the injection of sample solutions containing complex matrices such as dilute pore-fluids. Additionally, Fe was measured with Helium gas in the collision cell, which further eliminated potential polyatomic interferences that could have compromised the accuracy and consistency of analyses.

The mass spectrometer was calibrated using a series of external standards solutions prepared from 1 g/L analytical grade stock solutions by dilution with 2% Q-HNO_3 and 0.5% Q-HCl. Calibration ranges were linear between 0.1 μg/L and 500 μg/L. Detection limits were determined as 3-SD of the blank analyses, and typically 62 nmol/L for Fe and 0.45 nmol/L for Mn, with R-values between 0.998 and 1.000. Samples were diluted between 40 and 160 fold with the same 2% HNO_3/0.5% HCl solution used for preparation of calibration standard, internal standard, tuning, and rinse solutions. All samples were procedurally blank corrected, and blanks and standards were repeated after every 5 samples to monitor data quality. The precision of analyses was ± 10 nmol/L for Fe and ± 0.3 nmol/L for Mn (2-SD). The certified river water standard SLRS-4 was measured in

triplicate during each run on the ICP-MS and Fe and Mn concentrations were consistently within the accepted range of certified values (Table 2-2).

Table 2-2. Fe and Mn concentrations determined by ICP-MS in the certified river water standard SLRS-4

Certified standard	Fe (ppb)	Mn (ppb)
Consensus concentration		
SLRS-4	103 ± 5	3.37 ± 1.18
*Mean measured concentration (n=21)**		
SLRS-4	101 ± 3	3.68 ± 0.39

* Analytical uncertainty is expressed as 2-SD

2.5.1 Determination of Fe and Mn in 10% seawater matrices

The analysis of over-lying core-water from sediment core incubation experiments (Chapter 4) required the determination of Fe and Mn at nano molar concentrations (~0.1 ppb). The Octopole reaction cell works very effectively at reducing isobaric interferences, however, detection limits are greatly improved by 100-fold or greater dilutions of seawater or pore-fluid matrices. No studies appear to have measured Fe and Mn concentrations in samples containing 10% seawater matrix (~0.35 wt% matrix salts). In order to preserve the concentration of Fe and Mn in the core-water samples a valid method for determining Fe and Mn concentrations using a maximum 10-fold dilution was required.

To evaluate the validity of the method describe in Section 2.5, certified reference seawater (CASS-4), river water (SLRS-4) and a matrix matched standard solution (0.1ppb Fe and Mn spiked into a 10% CASS-4 solution) were analysed. Instrument set-up followed the previous description (Section 2.5), except clean cones were fitted to the plasma, all tuning and internal standards were newly prepared using fresh Q-distilled acids, and sample tubes were rinsed 3 times in the tuning solution (0.5% HCl / 2% HNO_3) prior to loading samples. The concentrations of Fe and Mn determined are plotted against the concentration predicted for each standard in Figure 2-3.

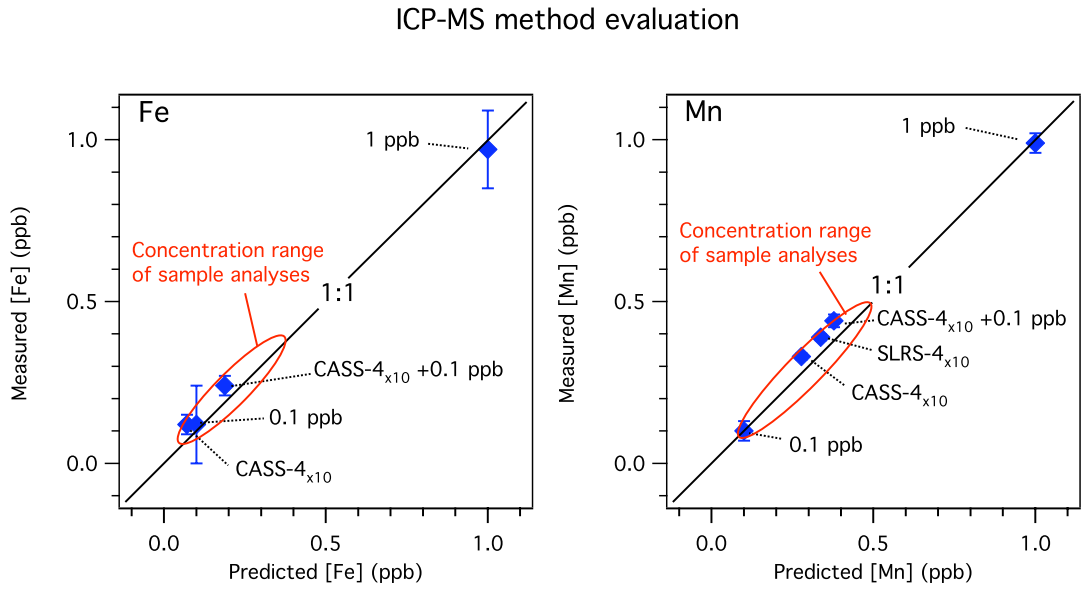

Figure 2-3. Evaluation of method used to determine Fe and Mn concentration in 10% seawater matrix. Measured versus predicted values of Fe and Mn in certified reference seawater (CASS-4), river water (SLRS-4) and a matrix matched standard solution (0.1 ppb Fe and Mn spiked into a 10% CASS-4 solution) as determined by direct injection to Agilent Octopole 7500cx ICP-MS with collision cell. Error bars are ±1 SD.

The concentration of Fe and Mn determined is largely within error of the predicted values, and the range of concentrations determined reflects the range of concentrations measured in the overlying core-samples. This approach is therefore considered sufficient for the determination of Fe and Mn in 10% v/v seawater solutions. The calibrated instrument detection limit was marginally improved for Fe (0.9 μg/L), while the precision of Fe determinations in 10% seawater samples was reduced (± 0.11 μg/L [2-SD]) compared with the method described in Section 2.5. The detection limit for Mn was largely unchanged (0.002 μg/L), as was the precision of Mn determinations in 10% seawater (± 0.013 μg/L [2-SD]).

2.5.2 Determination of Fe concentration using relative Fe isotope abundance

In order to determine the concentration of Fe in incubated overlying core-water samples from the Eel River shelf (Chapter 4), the abundance of ^{56}Fe normalised to

the abundance of quantitatively spiked ^{57}Fe was measured by ICP-MS following Section 2.5. This approach allowed for the determination of low (nano molar) Fe concentrations in samples with a high seawater salt matrix, by separating Fe from the sample matrix using anion exchange chromatography prior to analysis by ICP-MS. The anion exchange method is described in Section 2.7.1, with exceptions to this procedure outlined here.

Prior to sample loading on the exchange resin a ^{57}Fe isotopic standard was quantitatively added (~60 μg Fe) to each gravimetrically determined sample (~2 ml) and standard solutions between 10 and 500 nM. After elution from the exchange resin in 0.5 M HCl, samples were pre-concentrated by heating to dryness for ~6 hours at 110-160 ºC on a Teflon hotplate, then quantitatively re-dissolved in 20% Q-HNO_3 and further diluted by Mill-Q to produce a 2% HNO_3 sample solution in preparation for analysis by ICP-MS. Duplicate procedural determinations were performed on 9 samples and the accuracy of analyses was assessed, with a mean uncertainty of ± 4.2% or ± 1.6 nM Fe (2-SD).

2.6 Fe(II) and Fe(III) DETERMINATION BY SPECTROPHOTOMETRY

Anion exchange column calibrations (Section 2.7.1) and incubation experiments (Chapter 4) required a quick and transportable technique for the determination of Fe and/or Fe speciation in aqueous solutions. The disodium salt of 3-(2-pyridyl)-5,6-bis(4-phenylsulfonic acid)-1,2,4-triazine, hereafter referred to as Ferrozine, has been used extensively for the colorimetric determination of Fe(II) in aqueous solutions for more than 30 years (Stookey, 1970; Viollier et al., 2000). Sulphonate groups of the Ferrozine ligand maintain its solubility in water while coordinated nitrogen atoms allow for relatively stable complexation with Fe^{2+} (Figure 2-4).

Due to the specificity of the Ferrozine-Fe complex to iron in its lower oxidation state it is possible to determine the concentration of aqueous Fe present as either Fe (II) or Fe (III), by the colorimetric determination of Fe prior to, and after, the addition of a reducing agent and buffering of the final solution to between pH 5 and 8. This provides the concentration of Fe(II) and total Fe, allowing for Fe(III) determination by subtraction of the Fe(II) concentration from the total Fe concentration. Viollier et al. (2000) described this method for the sequential

determination of Fe(II) and Fe(III), which has been modified to accommodate a 40 mm path-length cell, to improve the detection limit of Fe.

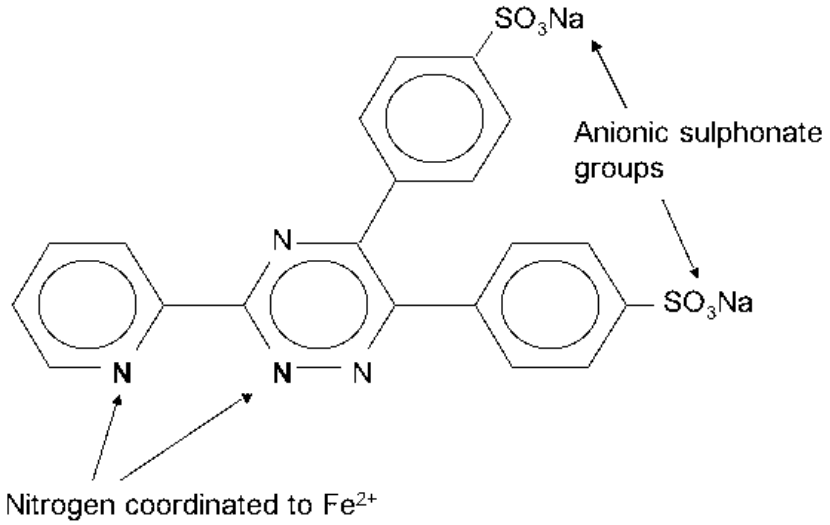

$$3Ferrozine^{2-} + Fe(H_2O)_6^{2+} \rightarrow Fe(Ferrozine)_3^{4-} + 6H_2O$$

Figure 2-4. The Ferrozine Fe(II) complex. Coordinated nitrogen atoms of three Ferrozine ligands complex an Fe^{2+} cation. The complex is strongly magenta in color and has an optimum light absorbance at a wavelength of 562nm.

The Ferrozine reagent was prepared by dissolution of the salt in an ammonium acetate solution made from sub-boiled distilled water and ammonium acetate crystals, which were produced from gaseous saturation of ammonium gas in Q-acetic acid. Hydroxylamine-HCl was prepared by the dissolution of analytical grade hydroxylamine-HCl in Q-HCl, and was used as the reducing agent for converting Fe (III) to Fe (II). The Ferrozine complex was buffered using ammonium acetate/ammonium hydroxide solution at a pH of 5.5 to give the optimum conditions for Ferrozine complexation, as described by Stookey (1970). Batches of reagents and Fe standards were refrigerated and stored in the dark between uses for a maximum period of one month prior to replacement. The analysis procedure was as follows, after Viollier et al. (2000):

(1) The buffered Ferrozine reagent was added to the sample.
(2) The absorbance of the sample-Ferrozine complex was determined by a spectrophotometer at a wavelength of 562 nm (Fe(II)).
(3) The reducing agent was added to the remaining sample-Ferrozine complex and left for 2 hours at room temperature.

(4) The reduced sample-reagent complex was re-buffered to pH 5.5.
(5) The absorbance of the sample-reagent complex was then re-analysed as in step (2) (total Fe).
(6) Fe(III) was determined by subtraction of Fe(II) from total Fe.

Linear calibrations were made by analysis of diluted Fe(II) and Fe(III) standard solutions. For anion exchange column calibrations (Section 2.7.1) a calibration range of 50 to 2000 μg/L Fe corresponded to a range of absorbance units from 0.007 to 0.123 respectively (R^2 = 0.9999), and a detection limit of 1.0 μmol L^{-1} Fe, using a 10 mm path-length cell. In order to measure Fe concentrations in incubation experiments (Chapter 4, Section 4.2.1), a calibration range of 5 to 1000 μg/L Fe was employed and corresponded to a range in absorbance units from 0.02 to 1.48 respectively (R^2 = 0.998), and a detection limit of 0.15 μmol L^{-1} Fe, using a 40 mm path-length cell. The mean relative standard deviation of triplicate analyses was ± 3.9%, and the overall analytical precision of the method was ± 0.018 μM Fe (2-SD).

2.7 PORE-FLUID Fe ISOTOPE MEASUREMENTS

Prior to Fe isotope analysis of pore-fluids it is necessary to separate Fe from the pore-fluid matrix and to pre-concentrate samples to near equal concentration to ensure accurate detection of all Fe isotopes, and to minimise mass bias effects during analysis. Fe samples were purified by standard anion exchange chromatography, where an anion exchange resin is used to separate pore-fluid Fe from the seawater matrix and allows for the individual pre-concentration of Fe to ~1000 μg/L for each sample. This procedure is based on Severmann et al. (2006) and is described below.

2.7.1 Anion exchange chromatography

All anion exchange chromatography was carried out under a class 100 laminar flow hoods, at the University of California, Riverside. Teflon columns were pre-cleaned in a 10% HCl bath for 48 hours and rinsed 3 times with Milli-Q water. Savllex Teflon sample bombs (15 ml) were cleaned sequentially in 10% Decon (24 hrs, 25 ºC), 50% HCl (24 hrs, 60 ºC), and 50% HNO_3 (24 hrs, 60 ºC) respectively,

and rinsed with, Milli-Q following each cleaning step.

Teflon columns (5 ml) were racked in a purpose built PVC stand for sample processing in batches of 10. A 750 μl aliquot of 200-400 mesh Bio-Rad AG-1x4 anion exchange resin was added to each column, and rinsed with 10 ml of 0.5 M Q-HCl, which was later transferred to waste. In order to optimise the pH in preparation for binding Fe^{2+}, columns were pre-treated using 2 ml of 7 M Q-HCl, which was passed to waste. Sample concentrations were determined by Ferrozine spectrophotometry (Section 2.6) and then adjusted to 7 M HCl prior to sample loading. A known aliquot of Fe was added to each pre-treated column. The pore-fluid sample matrix was passed through the column and transferred to waste while Fe^{2+} was bound to the exchange resin. A 10ml rinse of 7 M Q-HCl was applied to each column to ensure sufficient separation of the Fe in the sample from the sample matrix. A 15 ml Savillex Teflon pot was then used to collect the sample, which was eluted from the exchange resin by 7 ml of 0.5M Q-HCl. A 200 μl aliquot of the eluent was used to determine the fraction of Fe recovered from the anion exchange resin. Samples were then pre-concentrated by heating to dryness for ~6 hours at 110-160 ºC on a Teflon hotplate, and quantifiably re-dissolved in 20% Q-HNO_3 and further diluted by Mill-Q to produce ~1000 μg/L Fe in 2% HNO_3 in preparation for analysis.

Column calibrations were performed on a suite of Fe standards to determine the optimum reagent volumes and to ensure maximum Fe recovery and minimal unnecessary dilution during resin elution. Pore-fluid samples contained 1-4 μg Fe. This method enabled complete recovery of up to at least 5 μg of Fe, and the analysis of Fe isotope standards demonstrates that the column chemistry procedure imparted no significant isotopic fractionation on samples with 80-100% recovered Fe. A 50 μg Fe standard saturated the 750 μl anion exchange resin in each column. A serial elution determined the volume required for complete sample elution (Figure 2-5). Complete sample elution was achieved using 3 ml of eluent, thus the 7 ml used in this protocol is in excess of the required volume to ensure Fe recovery.

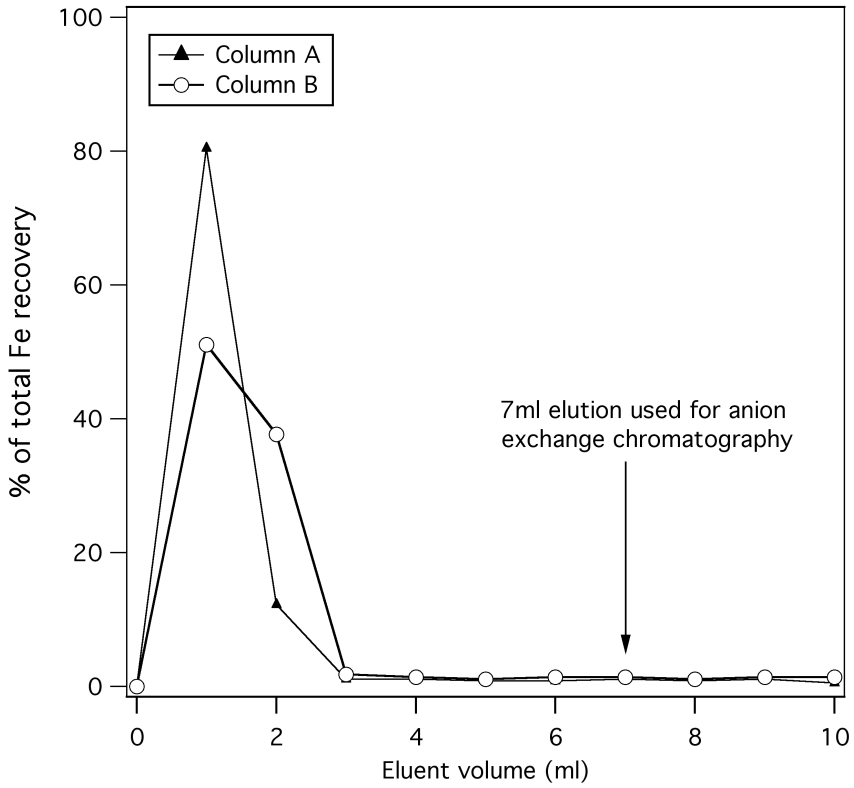

Figure 2-5. Percentage of total Fe recovered from anion exchange chromatography by 0.5 M Q-HCl, as a function of eluent volume. More than 99% of Fe loaded on the columns was recovered using 3 ml of eluent during replicate column calibrations.

2.7.2 Pore fluid Fe isotope analysis by Multi-Collector ICP-MS.

Iron isotope ratios were measured on a Thermo Finnigan High Resolution Multi-Collector ICP-MS (Neptune) at the University of California, Santa Cruz, following the procedure described in Arnold et al. (2004). Purified samples were introduced into the mass spectrometer as 1-2 ppm Fe solutions, mixed with equal amounts of Cu standard of known isotope composition, which was measured simultaneously for mass bias correction. In addition, samples were normalised to the average of two bracketing standards. Isotope ratios of $^{56}Fe/^{54}Fe$ and $^{57}Fe/^{54}Fe$ are reported using standard delta notation. Measured ratios are normalised relative to the average of igneous rocks, which have an isotope composition of $\delta^{56}Fe = 0 \pm 0.05‰$ (Beard et al., 2003). On this scale the isotope composition of the international Fe isotope reference material IRMM-014 is -0.08‰ for $\delta^{56}Fe$ (Table 2-3).

Table 2-3. Summary of δ^{56}Fe and δ^{57}Fe determinations and the standard deviations of repeat analyses for a range of Fe isotope standards. All certified reference materials are reported within error of their respective consensus values.

Standard	*n*	*Mean values relative to igneous rocks*			
		$\delta^{56/54}$Fe	2-SD	$\delta^{57/54}$Fe	2-SD
Itchen River water*	1	-2.44	0.07[†]	-3.62	0.11[†]
IRMM-14 spiked TMS-SW[§]	2	-0.07	0.12	-0.13	0.05
IRMM Col Chem[#]	2	-0.06	0.03	-0.12	0.15
IRMM-14	6	-0.08	0.06	-0.17	0.09
TAG	3	-1.01	0.10	-1.54	0.12
BCR2	3	-0.18	0.05	-0.29	0.14

*Southampton Estuary water (not certified standard)

[†]No replicates made. 2-SD estimated from mean of all standard measurements

[§]Trace-metal stripped seawater spiked with 2 mg to 5 mg of IRMM-14.

[#]IRMM-14 processed through replicate anion exchange columns.

The average analytical precision and the external precision for δ^{56}Fe (2-SD) are very similar at 0.13‰ and 0.06‰, respectively. Analysis of pore-fluid samples was limited to a maximum of two repeats, due to sample size. The calculation of meaningful standard error (St Err) was therefore not possible, and data uncertainty is expressed as 2-SD. Where the repeat of an individual sample was not made, the mean 2-SD of all replicate sample analyses (± 0.02‰) has been used. The mass dependence of Fe isotope fractionation was assessed (Figure 2-6) and as expected, all measurements fall within error of the δ^{56}Fe verses δ^{57}Fe linear regression, which provides a qualitative check against potential isotope-specific contamination of the samples. Several standard reference materials of known isotope composition, including IRMM-014, BCR-2 (a basalt standard reference material) and TAG (an in-house standard), were measured routinely for each sample batch and are summarised Table 2-3. TAG is a hydrothermal metalliferous sediment with an average isotope composition of -0.98 ± 0.10‰ (2-SD, n=28).

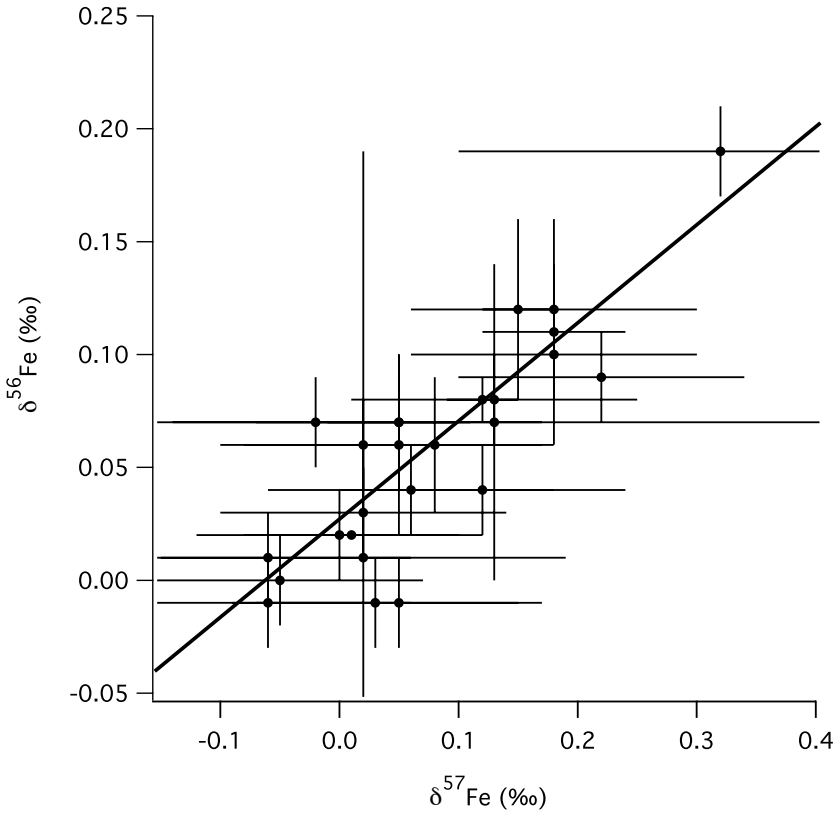

Figure 2-6. Measured δ^{56}Fe verses δ^{57}Fe in Crozet pore-fluids. Sample analyses lie within error (Error = ± 1-SD) of the mass dependant isotope fractionation line. Demonstrating there has been no significant isotopic contamination of the samples.

2.8 SEQUENTIAL Fe EXTRACTIONS FROM SEDIMENTS

A series of sediment leaches were used to assess the partitioning of Fe between different reactive mineral phases. Three extractions were used based on the method described by Poulton and Canfield (2005). Each step involves the reaction of dry pulverised sediment with a reducing agent under oxic conditions, and after the centrifugation and separation of the resultant supernatant the quantification of Fe liberated by each reduction step was achieved by ICP-MS (Section 2.5).

2.8.1 Preparation of leaching reagents

The composition of leaching reagents follows Poulton and Canfield (2005), and is summarised in Table 2-4. LDPE sample and reagent bottles were pre-cleaned in a 10% HCl bath for 24 hours, Milli-Q rinsed and dried under a class 100 laminar flow hood. Reagents were prepared by gravimetric determination to within

0.0001 g and further dilution was done volumetrically. The pH was measured using a digital pH meter that was calibrated by a certified buffer solution.

2.8.2 Sediment leaching protocol

Prior to the addition of reagents, sediments needed to be dried and homogenised. Sediments were prepared by desiccation in a warm oven (60-75 ˚C) in the presence of silica gel for 24 hours. Dry sediments were then ground by hand using an agate mill, and coarse sediments and rock samples were ground in a tungsten carbide milling machine. Ground samples were transferred to 30 ml LDPE sample pots. Prior to grinding each sample, agate and tungsten carbide mills were rinsed with Milli-Q, and wiped dry using acetone soaked Kim wipes to prevent cross contamination between samples. An aliquot (~250 mg) of each sample was quantitatively transferred to a 125 ml LDPE centrifuge bottle. Reagent (25 ml) was then added to the sediment sub sample.

Table 2-4 summarises the sequence of reagent additions and reaction conditions. Sediment-reagent mixtures were placed on a shaker table, secured, and left at room temperature (20-22 ˚C) for the duration of the reaction. After reaction, sediment-reagent mixtures were centrifuged at 6000 rpm for 6 minutes. Supernatant leachates were separated from sediment residue by carefully decanting into a 30 ml LDPE bottle. Leachates were then refrigerated for a maximum of 3 months prior to analysis by ICP-MS (Section 2.8.3). The sediment residue was immediately rinsed with 25 ml Milli-Q water and shaken by hand for 30 seconds. The sediment–Milli-Q mixture then under went a repeat centrifuge step and the supernatant rinse was discarded. The remaining sediment residue was then used for the next leaching step in the reagent sequence.

Poulton and Canfield (2005) demonstrate that these reagent sequences and reaction conditions allow for *optimum* recovery of the target Fe phases outlined in Table 2-4. However, the true mineralogy of Fe extracted in each leach cannot be determined by this method. Furthermore, a portion of one target Fe phase may be liberated by more than one leaching step. For example, the Na acetate leach has been shown to liberate approximately 2% of ferrihydrite from a mixed sediment standard prior to the Hydroxylamine-HCl leach where the remaining 98% of ferrihydrite was liberated (Poulton and Canfield, 2005). Consequently, this

method is used to describe the relative abundances of sedimentary Fe phases, as defined by their reactivity towards the leaching reagents described here.

Table 2-4. Summary of sequential leach reagents, reaction times, target Fe phases, and extractable mineralogy (Poulton and Canfield, 2005).

Reagent sequence and composition	Reaction time	Target Fe phases	Extractable mineralogy
1st - Na acetate: 1M Na acetate buffered to pH 4.5 with acetic acid	24 hrs	Highly-labile adsorped and carbonate associated ($Fe_{h\text{-}lab}$)	Fe^{2+}, Fe^{3+}, siderite: $FeCO_3$, ankerite; $Ca(Fe)(CO_3)_2$
2nd - Hydroxylamine-HCL: 1M Hydroxylamine HCL/25% v/v acetic acid	48 hrs	Easily reducible hydrous oxides (Fe_{ox1})	Ferrihydrite: $FeOOH \cdot 0.4H_2O$, lepidocrosite: γ-FeO(OH)
3rd - Na dithionite: 50 g/L Na dithionite buffered to pH 4.8 with 0.35M acetic acid/0.2M Na citrate solution	2 hrs	Reducible oxides (Fe_{ox2})	Goethite: FeO(OH), hematite: Fe_2O_3

2.8.3 ICP-MS determination of Fe concentration in sediment leachates

Fe determination in sediment leachates followed the same ICP-MS procedure as described in Section 2.5, except that an 800 to 4000-fold dilution of leachates by 2% Q-HNO_3/0.5% Q-HCl solution was used to bring Fe within the calibration range. Matrix-matched solutions used for instrument tuning and calibration. Samples were procedurally blank corrected and reagent blanks consistently contained <1% of the Fe measured in the leachates.

2.9 TOTAL SEDIMENT DIGESTION USING HF AND PERCHLORIC ACIDS

The determination of total Fe, Mn, and Ti in sediments was achieved by a serial acid attack with heated aqua regia (HCl/HNO_3) and combined hydrofluoric acid and perchloric acid (HF-$HClO_4$) as described in Marsh et al. (2007). A series of United States Geological Survey certified sediment standards were processed in

addition to replicate blanks to assess the accuracy of the method. These are summarised in Table 2-5.

Table 2-5. Comparison of blank corrected determinations of sediment standard compositions compared with consensus values.

Standard	Fe (wt%)	Ti (ppm)	Mn (ppm)	Ba (ppm)	U (ppm)
Consensus values for sediment standards					
MAG-1	4.75 ± 0.21	4500 ± 400	760 ± 70	479 ± 41	2.7 ± 0.3
SGR-1	2.12 ± 0.10	1520 ± 150	267 ± 34	290 ± 40	5.4 ± 0.4
SCO-1	3.59 ± 0.13	3760 ± 390	408 ± 30	570 ± 30	3.0 ± 0.2
Mean measured sediment standard values*					
MAG-1, *n*=3	4.63 ± 0.14	4340 ± 160	776 ± 42	502 ± 50	2.5 ± 0.2
SGR-1, *n*=2	2.04 ± 0.13	1500 ± 70	262 ± 24	299 ± 36	4.8 ± 0.0
SCO-1, n=2	3.50 ± 0.06	3550 ± 80	415 ± 20	620 ± 57	2.9 ± 0.5

*Mean of replicate (*n*) sample digestions

2.9.1 HF-Perchloric sediment digestion procedure

Sediments sample preparation followed that described for sequential sediment leaching (Section 2.8). About 100 mg of each ground sediment sample and sediment standard was accurately weighed into 15 ml Savllex Teflon digestion bombs. These bombs had been pre-cleaned in 10% Decon (24 hrs, 25 ºC), 50% HCl (24 hrs, 60 ºC), and 50% HNO_3 (24 hrs, 60 ºC) respectively. Concentrated analytical grade reagents were used throughout. $HClO_4$ is a powerful oxidiser and dehydrating agent, therefore the aqua regia step was used to remove organic matter and prevent the potential accumulation of explosive $HClO_4$ compounds prior to sample digestion by HF-$HClO_4$.

Aqua regia was prepared by the mixing of HCl and HNO_3 in respective proportion 1:3. Aqua regia (5 ml) was slowly added to each sediment sample using a disposable LDPE 3 ml pipette. The lids were tightly secured and the samples were placed on a hotplate at ~60 ˚C for 24 hours. Samples were then left to cool prior to removing the lids and placing them face up on the hotplate along with the samples. Samples were then re-heated at ~80 ˚C to dryness. HF (3 ml) followed by

2.25 ml of $HClO_4$ was added to each sample using disposable 3 ml LDPE pipettes. Sample lids were securely fastened and the sample bombs were placed on a hot-plate at ~150 ˚C and left to re-flux for 18-24 hours before being left to cool. Lids were carefully removed and placed face up on the hot plate along with the sample bombs, then reduced to incipient dryness by heating at ~180 ˚C. During evaporation of HF-$HClO_4$, sample bombs were continually agitated and tapped on the hotplate to prevent the accumulation of condensates around the rim, and to accelerate the drying process by disturbing the continually forming $HClO_4$ precipitates. Finally, to ensure the effective removal of HF from the sample residue, an additional 2 ml of $HClO_4$ was added to each sample and again the solution was reduced to incipient dryness as described above. Once the samples had cooled, they were re-dissolved in 10 ml of 8M HNO_3; lids were securely fitted to the sample bombs and samples were gently heated at ~50 ˚C to ensure thorough re-dissolution of the digested residue. The final solutions were transferred to 10% HCl cleaned 30 ml LDPE sample bottles, prior to analysis by the ICP-MS procedure described below.

2.9.2 Analysis of sediment digests by ICP-MS

Determination of sediment digest composition followed the same ICP-MS procedure as described in Section 2.5. An exception to this procedure was the preparation of a multi-elemental standard from 1000 μg/ml stock solutions of Fe, Mn, and Ti, and the 1000-4000-fold dilution of digests by 2% Q-HNO_3/0.5% Q-HCl solution prior to analysis to bring individual element concentrations to within the operational calibration range. Samples were blank corrected and procedural blanks were typically <0.1-2% of the measured elemental concentration in the sample.

2.10 OXYGEN DETERMINATIONS

Dissolved oxygen concentrations were determined in two types of sample, spatial variation in pore-fluid concentrations and temporal variation in overlying core-water concentrations. Pore-fluid determinations used a high-resolution micro-electrode (Section 2.10.1) to measure oxygen concentrations at sub-millimeter resolution below the sediment surface. Two different techniques (one for each

different research cruise) were used to determine the concentration of oxygen at 1-6 hourly intervals in incubated overlying core-water as presented in Chapter 4, oxygen determination by Winkler titration (Section 2.10.2) and by Optode Fluorescence (Section 2.10.3).

2.10.1 Oxygen determination by micro-electrode

Shipboard oxygen concentration profiles were measured in surface sediments using Unisense micro-electrode equipment; including micro-sensors with 50 μm tip diameter, M33-2 micromanipulator, LS18 lab stand, MC-232 motor drive, PA2000 Pico-ammeter, and Profix software (Figure 2-7). All analyses were conducted at sea in a controlled temperature laboratory held between 4 °C and 6 °C.

Micro-sensors were calibrated using a Unisense Cal300 calibration chamber. A two point linear dissolved oxygen calibration was obtained from 100% (oxic) and 0% (anoxic) saturated solutions. Firstly the 100% oxygen saturation value was measured by placing the micro-sensor in the calibration chamber with an aerated seawater sample of comparable temperature and salinity to the sediment pore-fluids. The oxic reading was recorded in Volts following a period of stabilisation from the sensor output (typically ~1.0 V). The anoxic oxygen saturation value was then determined by passing nitrogen gas through the chamber for 5 to 10 minutes until the sensor output had decreased and stabilised to within 0.01 V. Unisense recommends a calibration is only used when the anoxic voltage reading is less than 10% of the oxic voltage reading to ensure sufficient accuracy of analyses. In this study the anoxic readings were typically 0.02 V, less than 3% of the oxic value.

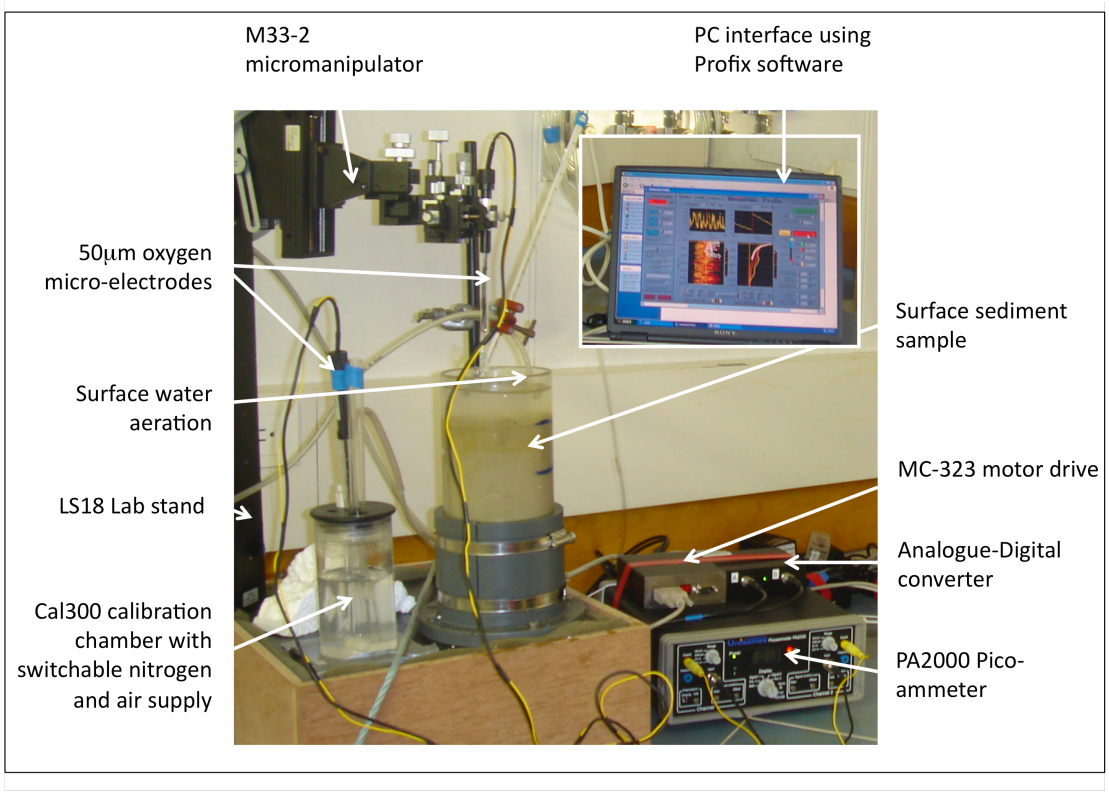

Figure 2-7. Unisense micro-electrode set-up for measuring high-resolution oxygen profiles in surface sediments.

Surface sediment samples were allowed to settle and re-equilibrate for 30 minutes after sub-sampling with a gentle surface water aeration that did not produce any visible disturbance of the surface layer. A minimum of 2 oxygen profiles were recorded from ~1 mm above the sediment surface to a maximum depth of 57 mm and a maximum sampling resolution of 100 μm steps. Recorded oxygen saturation values were converted to molar concentrations using Unisense conversion tables of empirically derived oxygen saturation values for the appropriate temperature and salinity of the sample.

2.10.2 Oxygen measurements by Winkler titration

The chemical determination of oxygen concentrations in seawater is based on the method first proposed by Winkler (1888) and modified by Strickland and Parsons (1968). This method was used for oxygen determination in overlying core-water during sediment-seawater core incubation experiments (Chapter 4), and was considered the best available alternative approach to the Optode fluorescence method used in earlier experiments from a different cruise (Section 2.10.3).

Oxygen in the water sample oxidises iodide ion (I^-) to iodine (I_2) quantitatively. The amount of iodine generated is then determined by titration with a standard thiosulfate ($S_2O_3^{-2}$) solution. From which the amount of oxygen can be computed from the titre using the stoichiometric relationships for these reactions.

Shipboard automated photometric determinations of dissolved oxygen were carried out using a Sensoren Instrument System (SIS) Oxygen Plus Winkler Titrator based on the method of Williams and Jenkins (1982). The apparatus comprised a Metrohm Dosimat 665 auto-titrator, LED light source, photodiode, and stirrer assembly. For a detailed description of the Winkler titration method see Smythe-Wright et al. (1993). A description of the sample handling protocol is outlined below.

Oxygen sampling and sample fixing was carried out in a controlled temperature laboratory at 4-6 ˚C. Samples were collected in glass oxygen bottles with gravimetrically determined internal volumes (~38 ml), a narrow neck and PVC stoppers. Samples were transferred to the oxygen bottles using a Tygon tube from the sample source inserted into the bottom of the oxygen bottle. The oxygen bottle was tapped repeatedly to dislodge any trapped air and the sample was allowed to overflow until the bottle had been flushed with 2-3 times more than the internal volume of the flask. Fixing reagents - 3M Manganese (II) Chloride followed by 8M Sodium Hydroxide/4M Sodium Iodide - were dispensed immediately using Anachem bottle dispensers, which where calibrated to deliver 1 ml of reagent to a manufacturer claimed reproducibility of 0.1%. Stoppers were tightly replaced and the bottles were shaken vigorously ~20 times. The fixed oxygen samples were then left for 30-45 minutes in the controlled temperature laboratory. Prior to analysis the lids were removed and the bottle lip was wiped dry. A 1 ml aliquot of 5 M H_2SO_4 was added to each bottle along with a magnetic stir bar. The oxygen bottle was then placed on the dispensing platform and the automated titration was initiated. The thiosulphate standard was calibrated in triplicate prior to analysis (titre volume: 0.3813 ml) and the reagent blank (expressed as titre units) was evaluated (0.00653 ml).

2.10.3 Oxygen measurements by fibre-optic optode fluorescence

The shipboard determination of dissolved oxygen concentration in incubated overlying core water from the Eel River shelf (Chapter 4), was conducted by and presented here courtesy of Tim Riedel of the University of Southern California. For a full description of the method of analysis, please refer to Klimant et al. (1995). A description of the sampling protocol for oxygen can also be found in Chapter 4.

The instrument used was a ProSens non-invasive Flow-Through Cell (FTC) micro-sensor. The FTC oxygen minisensor is a miniaturised fibre optic chemical sensor integrated in a flow-through cell and connected to a transmitter by an optical fibre. A glass tube with an inner diameter of 2 mm is coated with oxygen sensor at its inner wall and encloses a volume for liquid inside the FTC of about 100 (±10) μL. The FTC was connected via Luer-Lock adapters to silicone tubing to which the glass vessels containing core-water sample could be attached and passed through the cell using a syringe. The accuracy of analyses is reported to be ± 0.4% at 20.9% oxygen saturation, and ± 0.05% at 0.2% oxygen saturation, with a detection limit of 0.03%. The technique is non-pH dependant and the instrument is calibrated using a 2-point calibration between air saturated (100% O_2) and nitrogen-flushed (0% O_2) seawater samples.

2.11 DETERMINATIONS OF SEDIMENT CARBON CONTENT

Two methods were used for the determination of carbon in sediments and in both cases inorganic and organic carbon is totally converted to carbon dioxide. Coulometric carbon dioxide determination was undertaken at NOCS, and infrared detection was undertaken at the University of California, Riverside.

Carbon coulometry uses a partially aqueous medium containing ethanolamine and a colorimetric indicator to quantitatively absorb CO_2 gas. A UIC model 5011 CO_2 Coulometer was used for the analysis of total carbon (TC) and total inorganic carbon (TIC). Total organic carbon (TOC) was calculated by subtracting the measured TIC value from the TC value. CO_2 was introduced to the coulometer cell by an acidification module for conversion of TIC to CO_2 and a combustion furnace for the conversion of TC to CO_2. A description of the sediment sample

preparation can be found in Section 2.8.2. The analytical procedure followed the manufacturers recommended protocol, utilising ~30 mg of sample. Blanks and standards were assessed after every 8 samples. A repeated $CaCO_3$ standard was used for instrument calibration and the reproducibility of measurements was ± 0.2 wt% (2-SD).

TC and TIC were measured by infrared detection on an Eltra CS 500 Carbon / Sulphur Determinator at the University of California, Riverside. The CS-500 has a microcontroller, a high temperature resistance furnace going up to 1550 ˚C and solid-state infrared detectors with auto zero and auto range control. TOC content was calculated from the difference between the measured TIC and TC. For TIC analysis ~100 mg of dried pulverised sediment sample was gravimetrically determined to within 0.0001 g and treated with HCl in an Erlenmeyer flask inside the TIC-module. Oxygen flow purged the evolved CO_2 out of the flask, through to the infrared detector. TC was determined on an additional ~100 mg sample that underwent combustion, and the evolved CO_2 was passed through to the same infrared detection cell as used for TIC determination. Measured sediment standards AR4017 and AR1034 were assessed and were within 1% of the certified values. The analytical precision of this procedure was ± 0.04 wt%.

Determination of low-level organic carbon concentrations may be subject analytical inconsistency between different methodologies. Relatively minor inaccuracies in TC and TIC determinations could lead to larger inaccuracies in the concentration of organic carbon when it represents only a minor fraction of TC. The range of organic carbon measurements presented here for the Crozet islands and measured by the Eltra CS 500, are consistent with the range of measurements made by Hernandez Sanchez (2009) from separate sediment cores collected from the same sites, using the same UIC Model 5011 CO_2 instrument described above for analysis of Montserrat and Eel River shelf sediments. This instrument was also used by Pollard et al., (2009) to determine organic carbon content of sinking particulate matter in the Crozet region, in which the accuracy of the instrument was demonstrated by inter-comparison with other laboratory methods. Therefore the methods described here are inferred to be sufficient for comparison of organic carbon contents down-core and between study sites.

2.11.1 Calculations of sediment organic carbon accumulation rate

Crozet Holocene mean annual organic carbon accumulation rates were calculated from radio-carbon sediment accumulation rates (Hernandez Sanchez, 2009) and the dry bulk density estimated from the empirical relationship between dry bulk density and carbonate content for Southern Ocean sediments (Froelich, 1991). Eel River shelf carbon accumulation rates were estimated from measured TOC and published bulk sediment accumulation rates (Sommerfield and Nittrouer, 1999).

2.12 NUTRIENT ANALYSES

Pore-fluid nitrate + nitrite (hereinafter nitrate) and silicate analyses were undertaken on centrifuged pore-fluid samples (Section 2.3.1) for Crozet and Montserrat sediments, and nitrate on Rhizon sampled pore-fluids (Section 2.3.3) for the Eel River Shelf sediments. Nutrient analyses for Crozet samples were undertaken at sea by Paul Morris (NOCS), on a Skalar Sanplus Auto-analyser following the method of Sanders et al. (2007). Mean procedural blanks were assessed at 0.28 μM nitrate and 0.8 μM silicate. Eel River shelf pore-fluids were refrigerated at ~2 $^{\circ}$C prior to being analysed for nutrients by James McManus at Oregon Sate University, using a Lachat QuikChem 4200 flow injection auto-analyser. Mean procedural blanks for this method were assessed at 0.24 μM nitrate. Montserrat nutrient samples were frozen at sea, and analysed by Debbie Hembury (NOCS) at Plymouth Marine Labs (PML) using a 5 channel Bran and Luebbe AAIII segmented flow autoanalyser, employing quality control tested analytical methodologies for the nitrate and nitrite developed at PML.

Chapter 3 Pore-fluid Fe and Mn geochemistry during volcanogenic sediment diagenesis: Implications for benthic exchange of Fe and Mn

ABSTRACT

The distribution of sediments that sustain dissolved Fe inputs to seawater is largely unknown and despite the prevalence of volcanogenic sediments in ocean basins, they have not yet been considered a potentially significant source of Fe to seawater. Presented here are pore-fluid Fe, and redox-related Mn, concentration data for two dissolved size fractions (<0.02 μm and <0.2 μm) from two contrasting deep-sea volcaniclastic sediment sites: [1] Tephra rich debris flow deposits from Montserrat, Caribbean Sea (1110 m), and [2] bio-siliceous volcaniclastic sediments from the Crozet Islands, Southern Ocean (3000-4200 m). Dissolved (<0.2 μm) pore-fluid Fe content is high in the surface 0-5 cm below the seafloor (cmbsf) at both sites (17-20 μM), with 70-290 μM maxima 10-30 cmbsf at Crozet. Dissolved pore-fluid Mn content is 0.1-4 μM in Crozet and substantially higher (up to 200 μM below 0-12 cmbsf) in Montserrat, with significant diffusive Mn inputs to Montserrat bottom water.

Unique to Crozet sites, pore-fluids are dominantly composed of nano-scale colloidal Fe and Mn between 0.2 and 0.02 μm. The exact origin of these colloids remains unknown, but they are suggested to comprise authigenic-weathering products such as nano-particulate goethite and colloidal smectites from volcanic glass alteration. The apparent stability of colloidal Fe and Mn in oxygenated pore-fluids suggests they are open to exchange with the overlying bottom water, and therefore present a potentially important source of nano-scale colloidal Fe to seawater, the impact of which for biogeochemical cycles is likely to be determined by recycling processes within the benthic boundary layer.

3.1 INTRODUCTION

The behaviour of Fe and Mn in marine biogeochemical cycles is similar due to the different solubility of their oxidised and reduced species in seawater, leading to the enrichment of dissolved Fe and Mn in reducing sediment pore-fluids and relative depletion in oxygenated seawater. Many of the processes governing the diagenetic cycling of Fe between sediments and pore-fluids will also impact Mn, which is a bio-essential micronutrient closely linked to several trace element cycles (Burdige, 1993). For these reasons, whilst the focus of this thesis is on the cycling of Fe between sediments and seawater, the opportunity was taken to assess the pore-fluid geochemistry of both Fe and Mn in this chapter.

Volcanogenic sediments are quantitatively important components of marine sediment, particularly in the proximity of Island arcs where tephra-dominated deposits may be several thousand meters thick. In ocean basins distal from volcanic centers, volcanogenic sediments are important sources of lithogenic material to otherwise biogenic-dominated sediments. Volcanogenic tephra deposits comprise 23% by volume of Pacific Ocean sediments (Straub and Schmincke, 1998), and within them abundant Fe-Mn rich mineral phases undergo substantial alteration during early diagenesis. Therefore the proportion of tephra in ocean sediments, its composition, and its localised accumulation causes significant spatial and temporal variation in oceanic sediments that could have a significant impact on the fluxes of Fe and Mn to the ocean.

The distribution of Fe and Mn in sediment pore-fluids is largely controlled by dissimilatory solubilisation of oxide phases by bacteria in suboxic sediments and diffusion driven transport and precipitation in oxic conditions near the sediment surface (Burdige, 1993). Dissolved Fe fluxes to the overlying seawater are observed in coastal and estuarine sediments, and are increasingly understood to be widespread in low-oxygen, high organic-carbon shelf to shelf-slope environments, where Fe and Mn concentration gradients are sufficient to sustain a diffusive flux to the water column, which is enhanced by bioirrigation by benthic fauna (Sundby and Silverberg, 1985; Johnson et al., 1992; Watson et al., 1993; Tappin et al., 1995; McManus et al., 1997; Warnken et al., 2001; Berelson et al., 2003; Elrod et al., 2004; Lohan and Bruland, 2008). The input of dissolved

and particulate Fe from sediments has also been suggested to impact biogeochemical cycles in open-ocean settings (De Baar and De Jong, 2001; Lam et al., 2006; Nishioka et al., 2007). However the benthic Fe flux from deep-sea sediments to the oceans is yet to be assessed. Benthic Mn inputs to deep-seawater have been identified in the east Atlantic (Statham et al., 1998) but investigations of Mn cycling are yet to constrain the spatial occurrence of benthic input to the deep-sea.

The oxygenated surface-layer of deep-sea sediments is typically of sufficient thickness to prevent diffusion of aqueous Fe^{2+} and Mn^{2+} into the overlying water-column and these species are re-oxidised and trapped as insoluble (oxy)hydroxide precipitates in the sediment (Shaw et al., 1990). However shallow oxygen penetration depths (<1 to 3 cmbsf) have been observed in regions of elevated organic carbon accumulation or volcaniclastic sediment supply, in both shallow (<500 m) and deep-sea (>1000 m) sediments (Cai and Reimers, 1995; Haeckel et al., 2001b). Some deep-sea volcaniclastic regions are therefore likely to exhibit steep Fe and Mn concentration gradients and efflux of dissolved metals from the sediments. Many deep-water sediments are typified by non steady-state behaviour (e.g. episodic supply of organic carbon; seasonal bioturbation by mega-fauna; sediment remobilization by turbidites; and active volcanoclastic deposition) and consequently are likely to experience temporal shifts in the redoxclines of Fe and Mn that may further impact Fe and Mn cycling near the sediment-seawater interface. Deep-sea volcanogenic sediments are therefore an important but previously overlooked sedimentary facies where significant Fe and Mn flux may occur.

In this chapter pore-fluid and solid-phase Fe and Mn content is presented for cores collected from two different volcanogenic settings, a highly active margin sediment facies offshore of the Soufriere Hills volcano, Montserrat in the Caribbean Sea, and a mixed biogenic-volcanogenic sediment facies near the Crozet Island region in the the Southern Ocean. Ancillary dissolved O_2 and NO_3^- data and sediment organic carbon content, allows qualitative evaluation of redox conditions between study sites.

The goals of this study are (1) to use pore-fluid and solid phase sediment data to describe the diagenetic behaviour of Fe and Mn at the two study regions, (2) to

determine environmental factors responsible for differences in Fe and Mn geochemistry between these regions and (3) to consider the potential for volcaniclastic sediment diagenesis in these regions to promote the exchange of dissolved Fe and Mn with the overlying bottom waters.

3.2 THE STUDY AREA

Two regions were used for the study of Fe and Mn geochemistry during volcanogenic sediment diagenesis: (1) tephra-rich sediments (1100 m water depth) close to the volcanic island of Montserrat in the Carribbean Sea; and (2) deep-sea (3200-4200 m water depth) mixed volcaniclastic-biosiliceous sediments from the Indian Ocean sector of the Southern Ocean. Both regions contain significant volcanogenic basaltic components and underlie well-oxygenated bottom waters, but the sediment accumulation and organic carbon supply rates of the two regions differ profoundly. A description of the sampling sites is given below.

3.2.1 Montserrat region sediment description and sampling locations

Montserrat sediments are typical of sediment from the Lesser Antillies region and are dominated by large-scale submarine avalanche deposition from active arc volcanism (Deplus et al., 2001). Tephra-rich debris flows have dominated the sedimentary input in a region ~200 km^2 to the South East of the Soufriere Hills Volcano since 1995 (Trofimovs et al., 2006), and data presented here are from within this region. Pelagic carbonate-rich sedimentation otherwise dominates the background sediment composition in the region, but forms only a minor component of the bulk sediment geochemistry in the cores studied here.

The data presented here are from two cores, JC18_8 and JC18_33 (Figure 3-1). Sites JC18_8 (16°38.70'N 62°02.00'W, 1110 m) and JC18_33 (16°38.40'N 62°02.00'W, 1114 m) are repeat occupations of the same site, which is ~15 km ESE of Soufriere Hills Volcano and is at the depocentre of the 1998, 2003 and 2006 eruption event debris flow deposits. The sites described in this chapter comprise almost entirely tephra sedimentation from this period (90-99.5% tephra)

with little significant contributions of background pelagic sedimentation between tephra deposition events (0.5-10% $CaCO_3$; Appendix III).

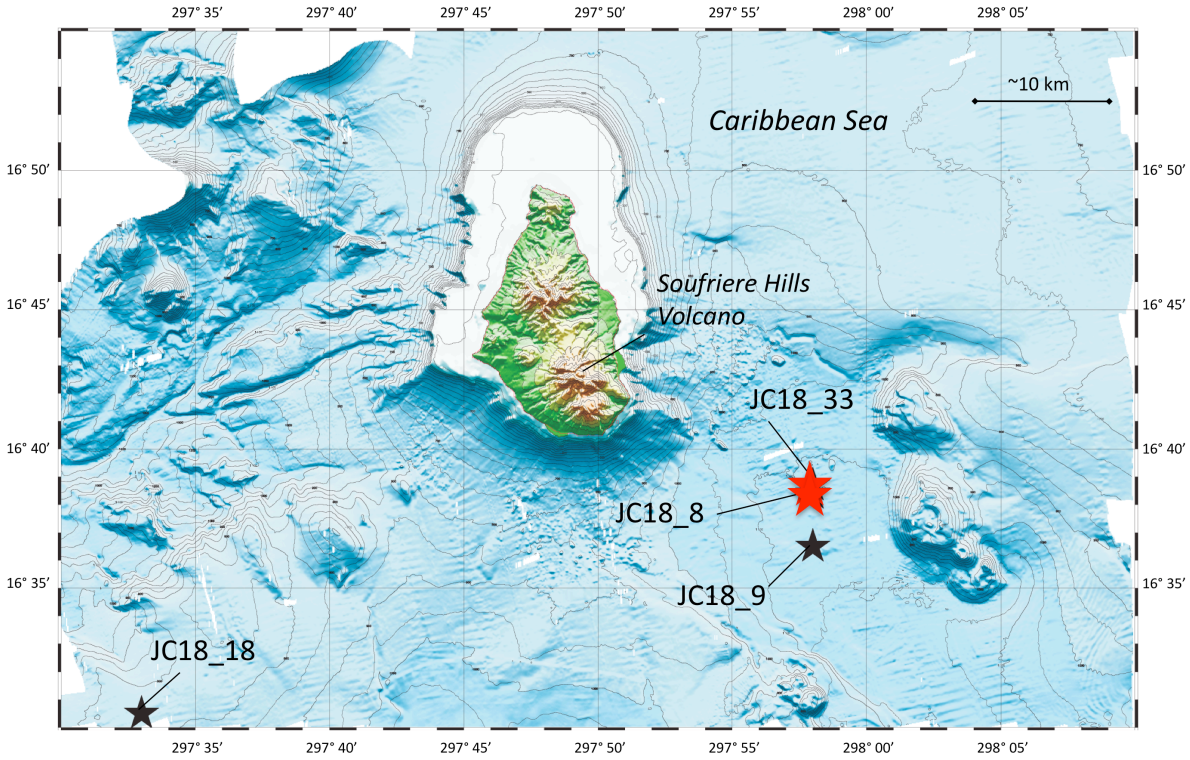

Figure 3-1. Map of Montserrat region showing sediment sampling locations. Sites studied in this chapter (JC18_8, and JC18_33) are highlighted in red, and are within the depocentre of the 1998, 2003 and 2006 Soufriere Hills Volcano dome collapse events. Sites JC18_9 and JC18_18 are discussed in Chapter 4.

3.2.2 Crozet region sediment description and sampling locations

Calcareous and siliceous primary production in the surface waters, and turbidite inputs from the volcanic Crozet islands account for sediment supply to Crozet sites where mixed biogenic-volcanogenic sediments accumulate in deep-water around the Crozet Plateau (Marsh et al., 2007). A 2-fold north-south gradient in annual integrated primary production and carbon export to the sediment is stimulated by Fe inputs from the Crozet Islands to the High-Nutrient Low-Chlorophyll (HNLC) surface waters north of the plateau (Planquette et al., 2007; Pollard et al., 2007).

Sediments and pore-fluids were collected from the Crozet island region 44-49°S,

50-54°E within the Polar Frontal Zone (PFZ) of the Indian sector of the Southern Ocean (Figure 3-2). Holocene mean annual organic carbon accumulation rates are 0.113 gC m^{-2} yr^{-1} north of the Plateau (M10), 0.011 gC m^{-2} yr^{-1} south of the Plateau (M6) and 0.008 gC m^{-2} yr^{-1} east of the Plateau (M5). Sediment focusing at M10 and sediment winnowing at M6 enhances the impact of elevated primary productivity on the gradient in organic carbon accumulation rate between these sites. Bulk sediment geochemistry is described by Marsh et al. (2007), and bulk compositions from this study and Marsh et al. (2007) are summarised in Table 3-1. $CaCO_3$ was determined from inorganic carbon content and lithogenic abundance was calculated from Ti content of sediments in this study (Appendix III), following the method of Marsh et al. (2007). Biogenic opal is calculated as the remaining difference between total and $CaCO_3$ and lithogenics. Lithogenic mineralogy includes volcanic glass, clay, pyroxene, hornblende, olivine, illmanite and amorphous Fe oxides as identified by smear slide petrography (Homoky et al., 2009). Bioturbation and bioirrigation is apparent on macro- and micro-scale (cm to sub-mm) in the sediment structure and sites are characterised by turbiditic emplacements, which are dominated by lithogenic phases at M6 (>7 cmbsf). All near-surface (<15 cmbsf) sediments are Holocene in age (Marsh et al., 2007).

Table 3-1. Bulk sediment composition of Crozet study sites.

Site	Bio-$CaCO_3$ %	Bio-opal %	Litho-basalt %
This study (0-21 cmbsf)			
M10	18	68	14
M5	16	47	37
M6	6	54	40*
Marsh et al. (2007) (0-15 cmbsf)			
M10	10-15	65-85	10-20
M5	9-12	50-60	30-40
M6	1.5-4	60-80	15-20
* of which 0-7cm = 27%, 7-21cm = 47%			

The Crozet region provides an excellent contrast to the Montserrat study area, due to the much slower rates of sediment accumulation, a natural gradient in organic carbon export to the deep-sea in this region (Pollard, 2009) and the different method of delivery of volcanogenic material to these sites (via MORB turbidities in contrast to pyroclastic debris flows). Volcanogenic surface sediments in the Crozet region experience much longer periods of sub-oxic diagenesis than sediments around Montserrat, they contain higher organic

carbon contents and are mixed with significant quantities of biosiliceous material. Furthermore, primary production in this region is in part sustained by sedimentary Fe inputs from the island plateau (Planquette et al., 2007), and therefore offers a novel opportunity to assess the potential for the deep-sea sediments of the Crozet region to supply Fe to the overlying HNLC water-column.

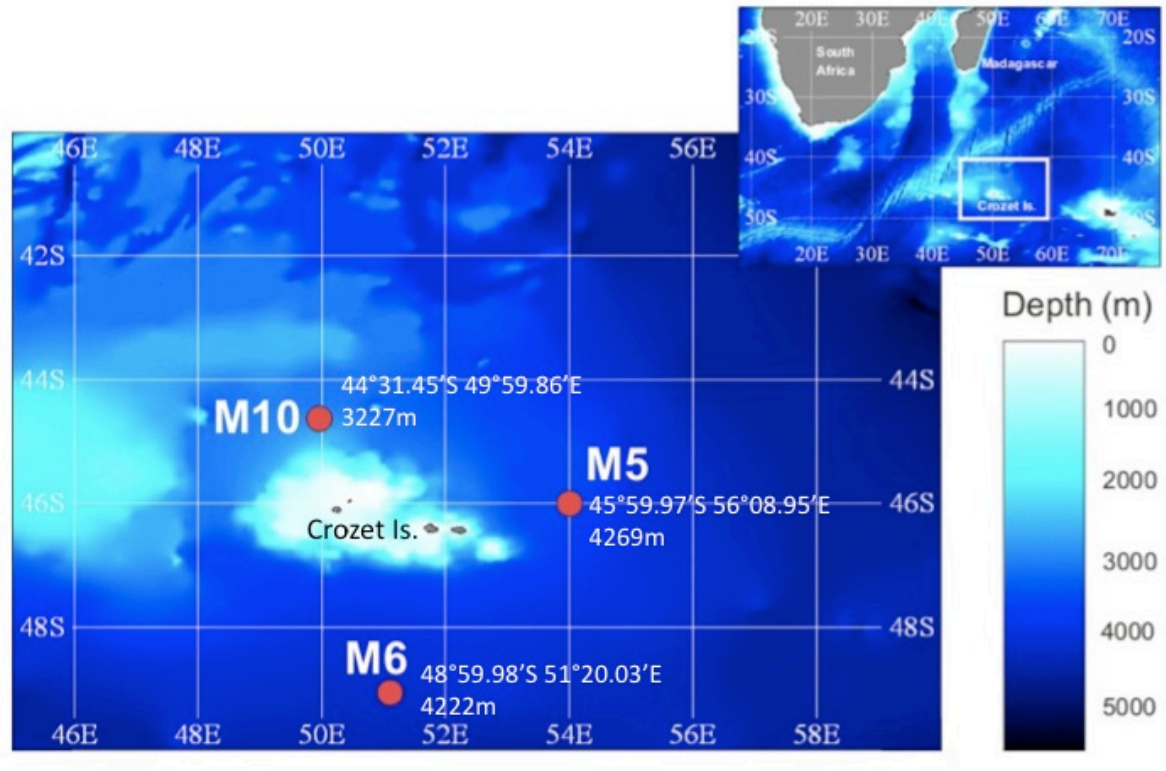

Figure 3-2. Bathymetric map of sampling sites in the Crozet region from CROZEX cruises D268 and D300. Samples used in this study are derived from three sites around the Crozet Islands, M10, M5 and M6.

3.3 METHODS AND ANALYTICAL PROCEDURES

A full description of all sampling methods and analytical procedures used for this chapter are described in Chapter 2. Briefly, pore-fluid Fe and Mn concentrations were measured in 2 operationally defined size fractions (<0.2 μm and <0.02 μm) and provided a means for assessing the partitioning of Fe and Mn between truly dissolved and small colloidal size ranges. Oxygen profiles, pore-fluid nitrate and silicate data, sediment organic carbon content, and solid-phase reactive Fe

phases, and total Fe, Mn and Ti content provide important ancillary data for the interpretation of diagenetic processes in these regions.

3.4 RESULTS AND DISCUSSION

3.4.1 Redox characteristics of Montserrat and Crozet surface sediments

The diagenetic behaviour of Fe and Mn is strongly affected by the reduction and oxidation reactions occurring in surface sediments. In order to facilitate the discussion of Fe and Mn cycling at each site, a brief description of observed redox conditions is presented. Pore-fluid oxygen and nitrate data, along with the organic carbon content of the sediments, are used as qualitative tools to evaluate the status and control of redox conditions at the study sites.

3.4.1.1 Pore-fluid oxygen and nitrate profiles

Dissolved pore-fluid oxygen and nitrate concentrations (Appendix II) are shown in Figure 3-3. Oxygen in Montserrat surface sediments reflects bottom water concentrations in the region (~250 μM), and is depleted below detection limit at 0.5 centimetres below the seafloor (cmbsf). The concentration of nitrate is very low in the surface 0-1 cmbsf (0.3 μM) and below detection limit at 1-2 cmbsf, reflecting rapid utilisation of nitrate between the surface sediment and over-lying bottom water (~28 μM NO_3^- in bottom waters). Bottom water nitrate was determined by Debbie Hembury at site JC18_9 and used for the extrapolation to site JC18_8. These distributions were typical of those observed at other debris-flow sites during the JC18 cruise.

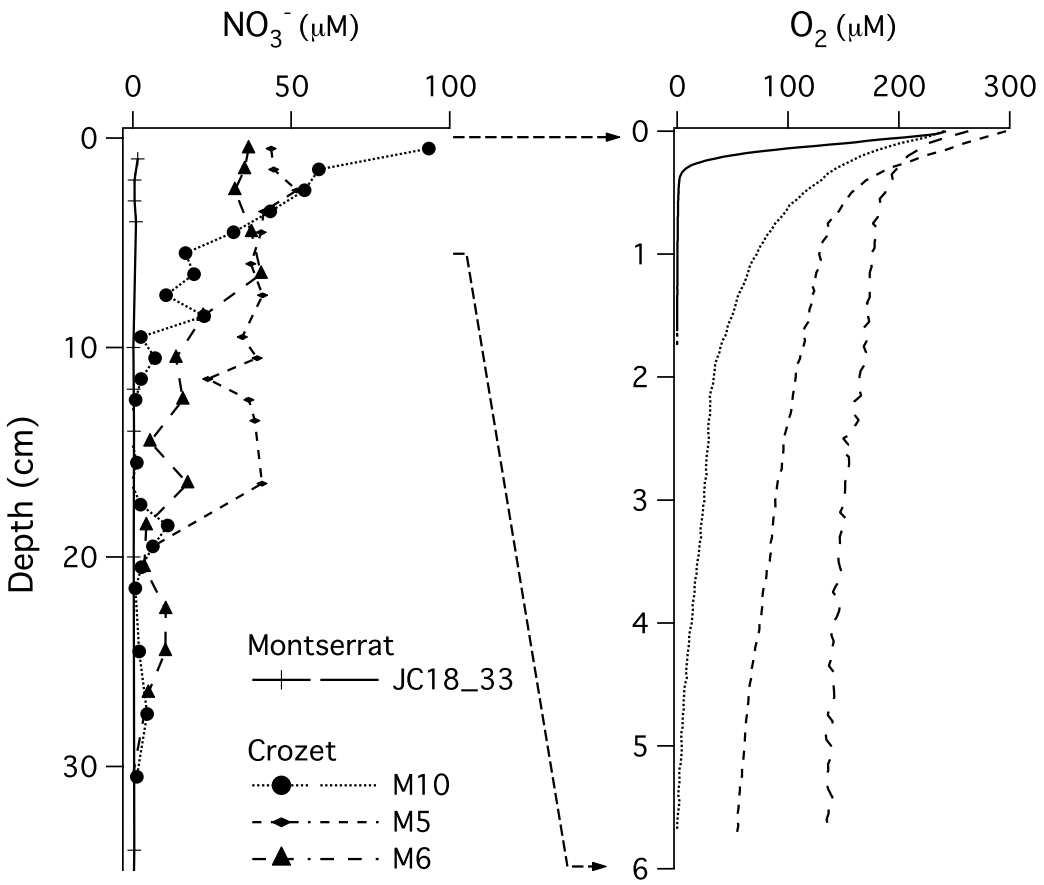

Figure 3-3. Dissolved pore-fluid oxygen and nitrate concentrations in Montserrat and Crozet surface sediments. Crozet oxygen data are derived from cores collected during D300: a return cruise a year after D286, from which all other pore-fluid and solid-phase constituent data originate. Montserrat nitrate data and oxygen data were collected from site JC18_8 and are used here to infer the redox conditions coupled to the Fe and Mn geochemistry at JC18_33 (Figure 3-1).

A gradient in pore-fluid oxygen concentration in the upper 0-6 cmbsf is identified between Crozet sites in the order M10>M5>M6 (Figure 3-3). M10 surface nitrate concentrations are elevated 2-fold above bottom water concentrations (~40 μM; Sanders et al., 2007), while M5 and M6 reflect more closely the overlying seawater values. Pore-fluid oxygen profiles at M10 show complete oxygen consumption by ~5 cmbsf and nitrate consumption by ~10 cmbsf. Measurable nitrate at M10 at 18 and 29 cmbsf is indicative of bioirrigation across the oxic-suboxic interface in these sediments.

Combination of the oxygen microelectrode and pore-fluid nitrate data suggest that oxygen penetration at the M6 is likely to be ~15 cmbsf, and is consistent

with the consumption of oxygen within a turbidite unit identified by Marsh et al. (2007). Nitrate is present throughout this turbidite unit to 20 cmbsf. Persistent bottom water nitrate concentrations at M5 suggest oxygen is present through the upper 20 cm of sediment sampled. The 19.5cm data point for nitrate at M5 may be an artefact of sampling close to the bottom of the core sample.

3.4.1.2 Sediment organic carbon contents

Total carbon content of the Montserrat sediments at JC18_33 is low (up to 1.3 dry weight percent [dwt%]) and almost entirely dominated by inorganic carbon (up to 1.2 dwt%) in the form of $CaCO_3$ (Figure 3-4; Appendix III). Two maxima at 4-6 and 14-16 cmbsf coincide with finer fractions of the sediment lithology and the dissolved Fe maxima within the pore-fluids (Section 3.4.2). Organic carbon content ranges from below detection limit at ~12 cmbsf in the coarse-sand-dominated 2006 debris flow to a maximum of just 0.08 dwt% in the surface 0-1 cmbsf, with a second maximum of 0.07 dwt% at 16 cmbsf. Organic carbon content is therefore very low, and maxima are associated with hemi-pelagic sedimentation between debris flow deposits.

Total carbon content of Crozet sediment is dominated by inorganic carbon in the form of $CaCO_3$. Crozet sediment ranges in organic carbon content from 0.27-0.58 dwt% at 0-1 cmbsf to 0.25-0.3 dwt% at 16-20 cmbsf. These values are nearly an order of magnitude higher than the Montserrat site. M10 has a down core (0-20 cmbsf) depletion of total carbon from ~3.2 to 2.0 dwt% consistent with dilution by lithogenic phases. Organic carbon is also depleted down core from 0.58 to 0.25 dwt%. Total carbon and organic carbon at M5 are distributed similarly to M10, with 2.2 and 0.4 dwt% at 1-2 cmbsf decreasing to 1.9 and 0.25 dwt% at 20 cmbsf respectively. M6 exhibits the reverse trend with total carbon elevated from 0.9-1.1 dwt% in the surface to ~1.3 dwt% at 16 cmbsf, probably due to turbidite inputs to this site.

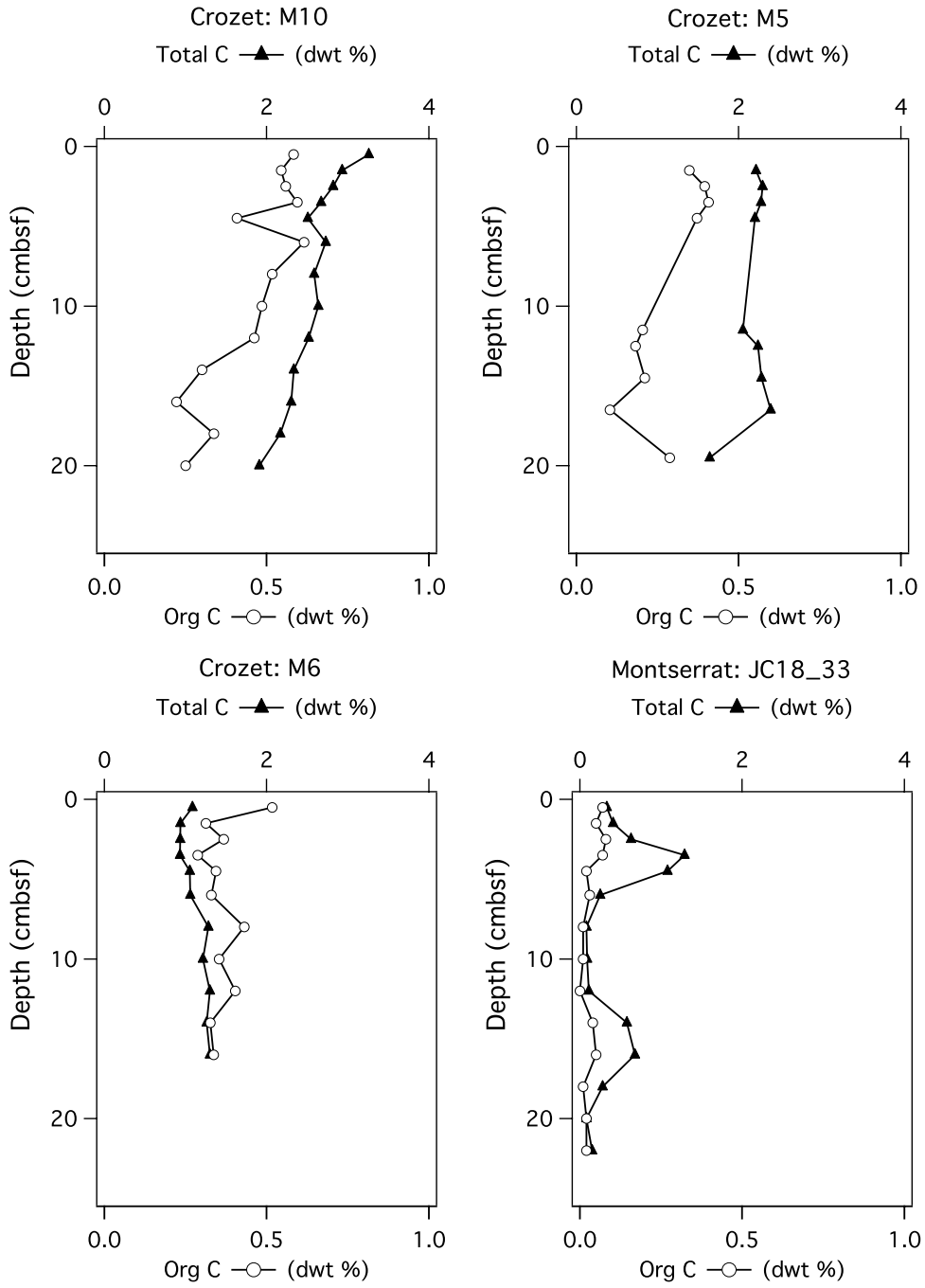

Figure 3-4. Down core variation in total carbon and organic carbon content of Montserrat and Crozet surface sediments.

3.4.1.3 Controls on sediment redox conditions in Montserrat and Crozet

Different processes appear to dominate the redox conditions of Montserrat and Crozet surface sediments; fresh tephra inputs to the Montserrat site are likely to sustain the very shallow oxygen and nitrate penetration depths observed, despite

very low organic carbon contents, while the gradient of mean (0-5 cmbsf) organic carbon content between Crozet sites (M10>M5≅M6) broadly corresponds to the depth of the redoxcline at each site (M10<M5<M6).

Oxygen and nitrate is rapidly consumed in Montserrat sediments in the upper 0-1 cmbsf, and oxygen and nitrate penetration this shallow more closely resembles estuarine and shelf sediment pore-fluids, where sediment organic carbon content is sufficiently high to sustain rapid oxidant utilisation (Aller et al., 1986). However the organic carbon content of Montserrat sediments is at or near detection limit at site JC18_33 (0.01-0.07 dwt %), and appears insufficient to drive the complete reduction of oxygen and nitrate in the upper 0-1 cmbsf. The occlusion of pore-space by weathering products can lead to a reduction in the rate of oxygen diffusion in some sediments, however the observation of highly unconsolidated and mobile sediment layers during recovery of Montserrat sediment cores suggests additional reductants are more likely to control of redox conditions for Fe and Mn in the pore-fluid, than restricted pore-fluid diffusion.

The deposition of tephra in seawater by sub-aerial volcanism results in the deposition of thick lithogenic sequences in the Montserrat region before they have been exposed to extensive chemical weathering. Consequently, the composition of tephra is highly susceptible to chemical alteration by contact with seawater, and experiments have demonstrated that Fe and Mn - among other elements - are readily enriched in seawater by desorption and dissolution from tephra (Frogner et al., 2001; Jones and Gislason, 2008).

Deplus et al. (2001) observed significant quantities of Fe(II) minerals in tephra debris flows east of Montserrat, suggesting a significant pool of Fe minerals exist with the potential for oxidation on contact with seawater. Ash-covered deep-sea sediments of the South China Sea have also been investigated (Haeckel et al., 2001b), and tephra layers are shown to be capable of preventing O_2 from penetrating into the underlying sediments, where O_2 is totally exhausted within ash layers thicker than just 3 cm. The oxygen diffusion length-scale can be also drastically reduced by the reaction with dissolved Mn to form disseminated MnO_2 coatings on grains in situ as well as crusts, thus the redox conditions of Montserrat sediment pore-fluids are likely to be dominated by the inorganic volcaniclastic chemical alteration rather than by organic carbon decomposition.

Seasonally elevated surface water productivity and export across the Crozet sites (Pollard, 2009) coincides with a shallowing of the sediment redoxcline at M10 relative to M5 and M6. The oxygen penetration at all 3 of the Crozet sites is perhaps shallower than would have been anticipated for deep-sea sites in the Southern Ocean, but is comparable with deep-sea (3000-4000 m) measurements from the Western Atlantic off the Amazon shelf where organic carbon content is similar (0.3-0.8 dwt%; Wenzhöfer et al., 2001). Oxygen profiles are not typical of steady-state diffusive fluxes, but show enhanced consumption in the surface 0-1 cmbsf, probably attributed to the episodic nature of carbon supply in this region (Pollard et al., 2007). Consistent with this suggestion, a phytodetrital 'fluff' layer (2-4 mm thick), presumed to be the organic carbon source to these sediments, was observed on the surface of the M5 core used for oxygen determination, and coincided with the end of the surface water primary productivity bloom in Jan 2005. Bottom water NO_3^- in the Crozet region was ~34 μM, and pore-fluid compositions reflect marginal surface enrichments at M5 (0-3 cmbsf) and significantly elevated NO_3^- concentrations at M10 (0-3 cmbsf), consistent with the oxidation of organic matter by oxygen and subsequent generation of nitrate in the pore-fluid, prior to later depletion through organic carbon decomposition deeper in the sediment (Froelich et al., 1979).

The range of organic carbon content reported in the Crozet sediments is similar to other deep-sea abyssal sites of the World's Oceans, at ~0.1-0.3 dwt % (Hedges et al., 1999; Seiter et al., 2004), where organic carbon is the primary reductant controlling pore-fluid Fe and Mn distribution. The gradient in mean organic carbon content (0-20 cmbsf) between M10 (0.45 dwt %) and M6 (0.36 wt %) is broadly consistent with the shallowing of the redoxcline from South to North of the Crozet Islands. The organic carbon content of Crozet sites typically decreases down core as would be expected when organic carbon remineralisation drives the microbial utilisation of oxygen and nitrate during early diagenesis. Thus the episodic supply of organic carbon is inferred to play the dominant role in controlling the redox conditions of surface sediment pore-fluids at Crozet sites.

The diagenetic behaviour of Fe and Mn will now be evaluated in the contrasting depositional conditions represented by the chosen study sites.

3.4.2 Pore-fluid Fe and Mn distributions

Pore-fluid Fe and Mn data can be found in Appendix II. The lowest concentration of dissolved Fe observed in the <0.2 μm fraction of Montserrat pore-fluids is in the surface 0-1 cmbsf, consistent with the oxidative removal of dissolved Fe close to the sediment surface (Figure 3-5). Subsurface maxima of dissolved Fe (18-20 μM) occur at 2-6 and 14-16 cmbsf, coincident with the depth of maximum organic carbon content (Figure 3-4). Dissolved Mn (<0.2 μm) concentrations are also lowest towards the surface oxidised layer, with Mn maxima (~200 μM) persistent below 12 cmbsf, possibly reflecting the saturation concentration of the pore-fluid, leading to rhodochrosite precipitation ($MnCO_3$) or a mixed phase (Ca, Mg, Mn) carbonate (Burdige and Gieskes, 1983) (Figure 3-6). Both Fe and Mn measured in the Montserrat pore-fluids exhibit no analytically significant partitioning between the <0.02 μm and 0.02-0.2 μm dissolved size fractions, suggesting dissolved Fe and Mn are both in a truly dissolved aqueous phase.

Fe and Mn concentrations in Crozet pore-fluids are relatively high (1–20 μM Fe; 0.1–0.3 μM Mn) in the oxic to sub-oxic 0-10 cmbsf as compared with previous measurements from deep-sea Southern Ocean sites (<0.1 µM Fe; King et al., 2000); the equatorial Pacific (<5 µM Fe; Haeckel et al., 2001a); and tropical northeast Atlantic (1-13 µM Fe; Froelich et al., 1979), where Mn and Fe follow classical biogeochemical zonation with depth. The concentration of Fe in the <0.2 μm size fraction in Crozet sites is typically 1 – 50 μM, with maxima of up to 100–300 μM. The Mn content is generally low (0.2-2 μM) and maxima (4-20 μM) are associated with the same depth in the sediment as the highest Fe concentrations. The down core distributions of Fe and Mn in the pore-fluid is highly variable and do not mimic the dissolved Fe and Mn profiles of diffusion-dominated surface sediments, where the oxidative removal of Fe(II) and Mn(II) in the near-surface pore-fluid maintains very low concentrations in the upper sediment column.

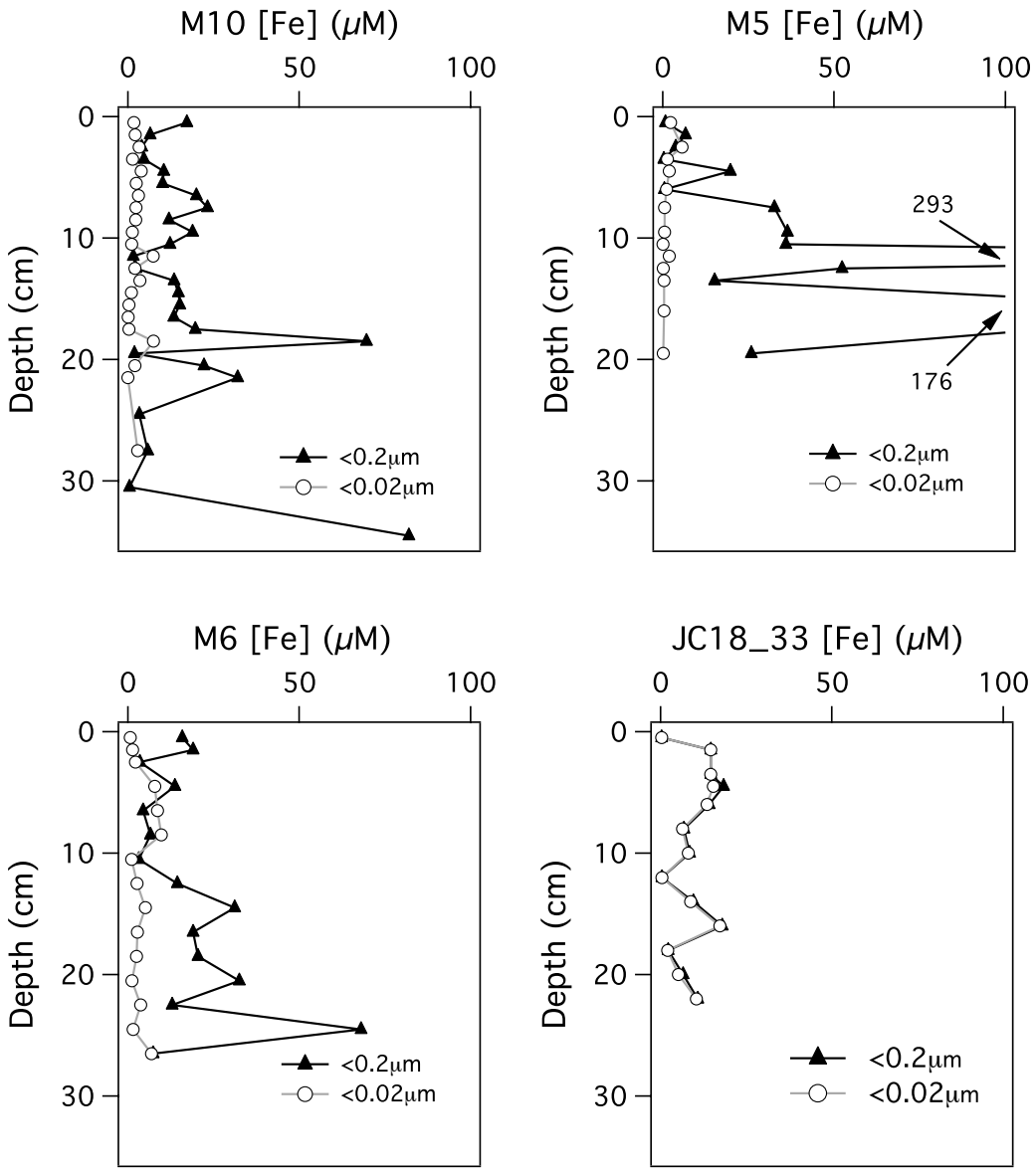

Figure 3-5. Concentration of Fe in surface sediment pore-fluids from Crozet and Montserrat sediments, determined by centrifugation and filtration through 0.2 and 0.02 μm filters.

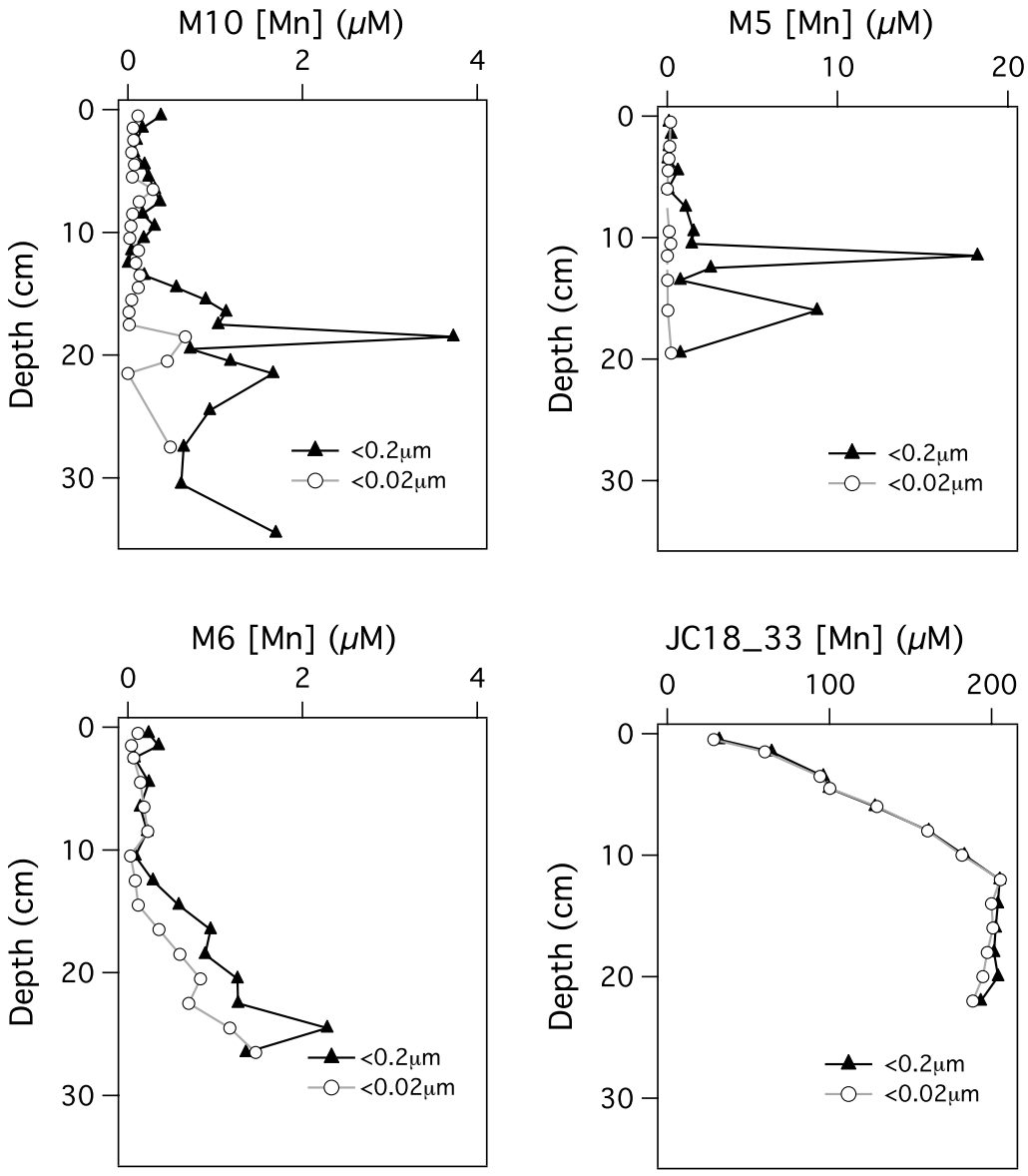

Figure 3-6. Concentration of Mn in surface sediment pore-fluids from Crozet and Montserrat sediments, determined by centrifugation and filtration of pore-fluids through 0.2 and 0.02 μm filters.

Additional processes may add complexity to the distribution of Fe and Mn in the pore-fluids. For example: bioturbation and bioirrigation may serve to inject oxygen into reducing zones in the sediment, producing a 3-dimensional oxic-suboxic interface (Aller, 1990); slumping/re-working of sediments can recycle oxidised metals by mixing sediments and pore-fluids across oxidising and reducing zones (Canfield et al., 1993); and the diffusion rates of aqueous species may be altered by episodic supply of organic matter (Watson et al., 1993; Gehlen et al., 1997).

The concentration of dissolved Fe and Mn is strongly partitioned between <0.02 and 0.02-0.2 μm at Crozet sites, and the proportion of Fe and Mn in the 0.02-0.2 μm dissolved size fraction ranges from 30-99% of the total pore-fluid Fe and Mn pool. The partitioning of Fe and Mn between these size fractions suggests significant proportions of dissolved Fe and Mn are present as small colloids, the origin and composition of which is discussed in Section 3.4.4.

In order to provide an analytical check for the pore-fluid concentrations of Fe in the Crozet region, and to elucidate small-scale heterogeneity in the pore-fluid Fe distributions, additional shipboard DET (Diffusive Equilibrium in Thin-film) Gel probes were utilised for pore-fluid Fe determinations. DET probes were deployed in contemporaneous sediment cores collected from the same Mega-core deployment as used for pore-fluid sampling by centrifugation in Crozet, and from the proximal site JC18_8 in Montserrat. DET gel probes have been demonstrated to provide a robust alternative method for high-resolution sampling of pore-fluid Fe in surface sediments (Fones et al., 2001; Morford et al., 2003). These data are shown in Figure 3-7 and illustrate significant millimetre-scale heterogeneity and a similar range of Fe concentrations (3 to 263 μM) in the upper 0-15 cmbsf at Crozet sites compared with those derived by centrifugation and filtration. Montserrat DET Fe data are of similar concentration to the centrifugation and filtration technique, with the exception of a millimetre-scale maxima of ~125 μM.

The use of DET gel probes in this context highlights important differences between methods of pore-fluid Fe determination. Although the gel probes are likely to equilibrate with a small colloidal fraction of Fe <0.2 μm in diameter, they may also permit the equilibration of larger colloidal material, and discrepancies in the size and rate of diffusion of dissolved and colloidal size fractions may lead to apparent differences in Fe concentration between DET gel probe and centrifugation and filtration methods. The time taken for a Fe colloid to equilibrate with the DET gel is unknown and likely to vary according to the size of the colloid. Furthermore it is possible that some colloids may interact differently with the gel matrix and impose an additional bias when sampling pore-fluid Fe of mixed colloidal origins. Small discrepancies in Fe distribution between methods are therefore likely to have resulted from the uncertainties discussed here.

However the comparison of DET gel probe data demonstrates the concentrations of Fe presented for Montserrat and Crozet pore-fluids are unlikely to have resulted from contamination or from sampling artefacts. They also testify to the significance of millimetre-scale heterogeneity to the pre-fluid Fe composition and the apparent abundance of small-colloidal Fe and Mn in the pore-fluids.

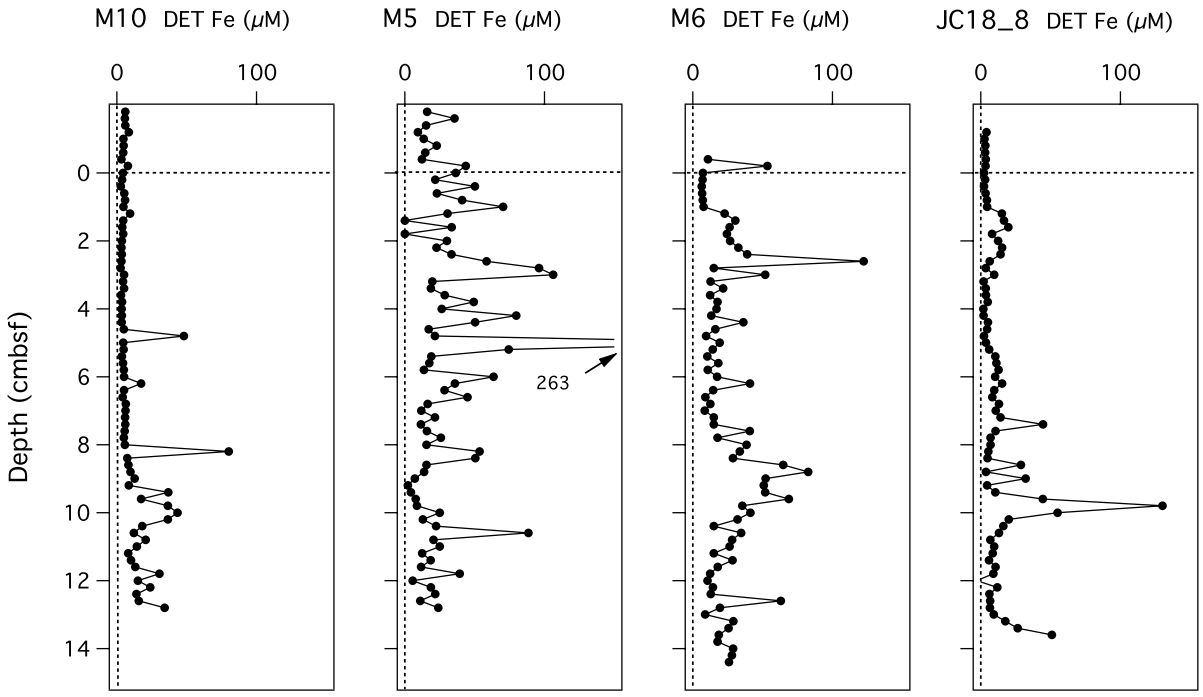

Figure 3-7. Concentration of Fe in surface sediment pore-fluids from Crozet and Montserrat sediments, determined by Diffusive Equilibrium in Thin-film (DET) gel probes from adjacent cores of the same deployment as those used for pore-fluid sampling by centrifugation and filtration in Crozet, and from the proximal site JC18_8 in Montserrat.

3.4.2.1 Evidence for pore-fluid Fe and Mn cycling

A scatter plot of dissolved (<0.2 μm) pore-fluid Fe verses Mn concentration reveals a strong positive correlation in the surface sediments of Crozet sites, which closely resembles the Fe/Mn ratio of Crozet island basalt (Fe/Mn ~69:1; Gunn et al., 1970; Figure 3-8). Deeper pore-fluid concentrations do not sustain this relationship and the data shift toward relatively higher Mn concentrations, indicative of enrichment of dissolved Mn relative to substrate composition.

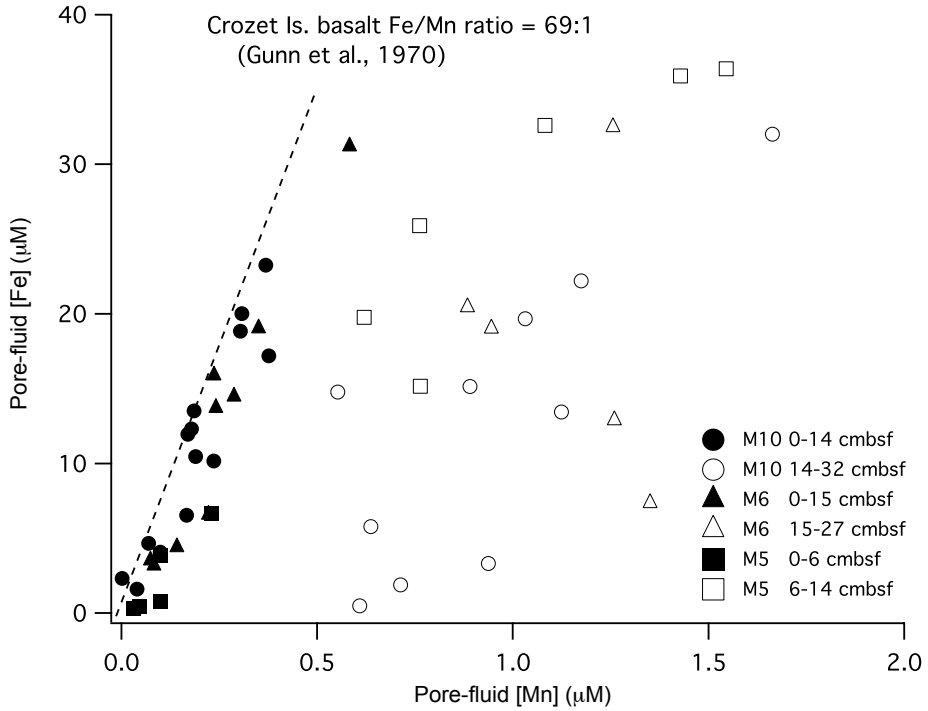

Figure 3-8. Dissolved (<0.2 μm) pore-fluid Fe verses Mn concentration in Crozet surface sediments.

No correlation is observed in the Fe/Mn ratio of Montserrat pore-fluids (Figure 3-9), and all data lie well below the mean Fe/Mn ratio reported for Soufriere Hills volcano basalts (Zellmer et al., 2003). Similar to Crozet however, the Fe/Mn ratio in the Montserrat pore-fluids broadly decreases down-core.

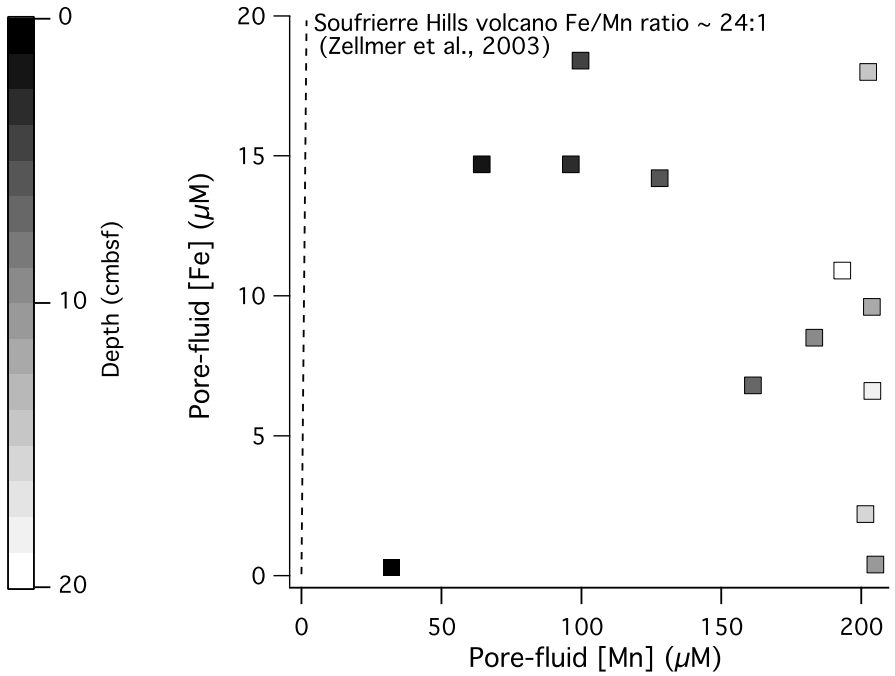

Figure 3-9. Dissolved (<0.2μm) pore-fluid Fe verses Mn concentration in Montserrat surface sediments.

3.4.3 Solid-phase Fe and Mn distribution in Montserrat and Crozet sediment

The titanium (Ti) content of sediments is used here as a tracer of volcanogenic inputs to Crozet and Montserrat surface sediments. Changes in the relative abundance of Fe and Mn with respect to Ti can be used to interpret zones of Fe and Mn removal and/or enrichment in sediment due to early diagenetic cycling of these metals between the sediments and the pore-fluids. These data can be found in Appendix III.

Broadly elevated Fe/Ti ratios are observed at the Crozet site M10, 2-5 cmbsf with additional maxima at 9 and 21 cmbsf (Figure 3-10). The Mn/Ti maxima are closely associated with the Fe:Ti maxima. The zone of elevated Fe and Mn relative to Ti corresponds to the suboxic-oxic transition identified from oxygen and nitrate profiles, and is therefore consistent with the oxidation of upward diffusing Fe and Mn in the surface sediments.

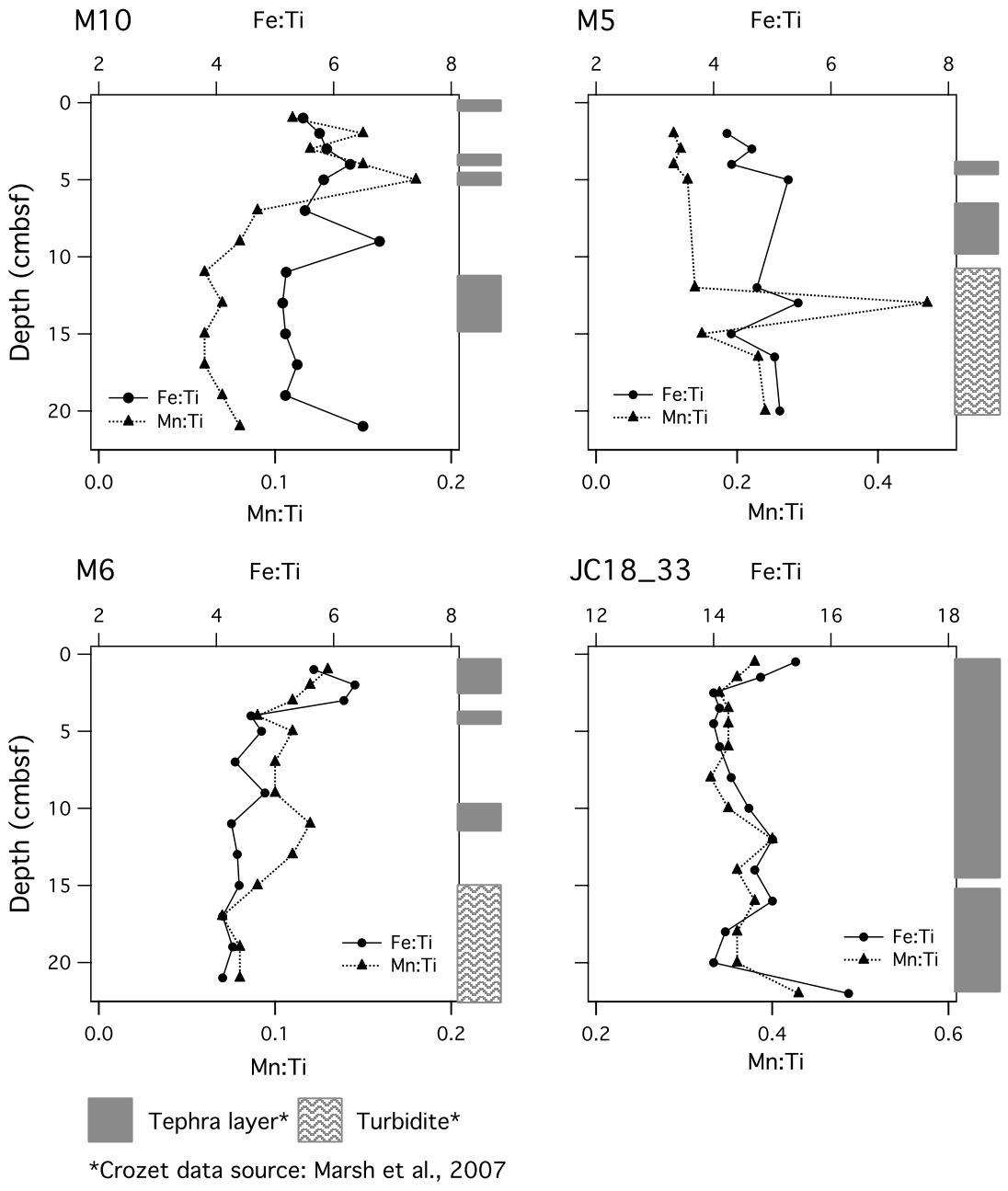

Figure 3-10. Down core variation in solid-phase Fe/Ti and Mn/Ti ratios of Crozet (M10, M5, M6) and Montserrat (JC18_33) surface sediments. Approximate depth of tephra and turbidite layers are shown for comparison.

A zone of turbidite emplacement identified by Marsh et al. (2007) at M5 corresponds to elevated Fe/Ti and Mn/Ti maxima, where as at M6 the lowest Fe/Ti and Mn/Ti ratios are associated with a turbidite layer and elevated Fe/Ti and Mn/Ti more closely correspond to the depth of tephra layers.

In the tephra-dominated Montserrat site, JC18_33, Fe:Ti and Mn:Ti maxima appear in the surface 0-2 cmbsf and are associated with finer sediment fractions at the surface of individual debris flows. This could result from a higher Fe/Ti and Mn/Ti signature to pelagic sedimentation between debris flow events, except this is expected to be a very minor fraction of the bulk sediment composition due to the short intervals between debris flow events (2-3 years). A more plausible explanation is the enhanced precipitation of Fe and Mn oxides between sediment deposition episodes at the sediment surface that have subsequently been buried too rapidly to permit the upward migration of Fe and Mn oxides with the redox front.

The solid-phase Fe, Mn and Ti data indicate Fe and Mn are actively involved in diagenetic cycling in Crozet and Montserrat. The timing and magnitude of tephra and turbidite inputs to each region is likely to impact the distribution of Fe and Mn in the sediments and pore-fluids. To gain further insight into the behaviour of Fe at the study sites, the partitioning of Fe between reactive Fe phases has also been determined (Appendix III).

The diagenetic behaviour of Fe is assessed by comparison of the relative abundances of operationally defined reducible Fe phases in order of their reactivity towards a series of leaching reagents described in Section 2.8; Highly-labile, adsorped and carbonate-associated Fe ($Fe_{h\text{-}lab}$) is the most readily available of these to reduction, followed by hydrous Fe oxides (Fe_{ox1}) and then crystalline Fe oxides (Fe_{ox2}). Collectively these Fe phases comprise the reactive Fe pool (Fe_{reac}), the abundance of which can also be compared to the total Fe pool (Fe_{total}) as a measure of the extent of authigenic Fe oxide enrichment in the sediment. Down core variation in the ratio $Fe_{h\text{-}lab}/[Fe_{h\text{-}lab}+Fe_{ox1}]$ may indicate reaction of $Fe_{h\text{-}lab}$ towards Fe_{ox1}, and similarly a change in the ratio of $Fe_{ox1}/[Fe_{ox1}+Fe_{ox2}]$ may indicate a reaction of Fe_{ox1} towards Fe_{ox2}. A relatively high $Fe_{h\text{-}lab}/[Fe_{h\text{-}lab}+Fe_{ox1}]$ may be indicative of a high degree of redox re-cycling of Fe in surface sediments.

The Fe_{total} content of Crozet sediments ranges from ~0.9 to 3.9 dwt % (Figure 3-11). Bulk (0-21 cmbsf) Fe_{total} content is highest at M6 and lowest M10, and is consistent with the degree of lithogenic dilution by biosiliceous sedimentary components (Marsh et al., 2007). The concentration of Fe_{reac} is also highest at M6 relative to M5 and lowest at M10. However, the proportion of Fe_{reac} relative to Fe_{total}

in the surface 0-5 cmbsf is greatest at M10, followed by M6 and apparently lowest at M5 (Figure 3-12). An increase in the proportion of Fe_{ox1} relative to $[Fe_{ox1}+Fe_{ox2}]$ can indicate a zone of crystalline Fe oxide reaction towards hydrous Fe oxide during early diagenesis; the $Fe_{ox1}/[Fe_{ox1}+Fe_{ox2}]$ ratio is greatest in surface layers at M10 and decreases down core, and is lowest in surface layers at M6 increasing down core. This is consistent with the enrichment of Fe_{ox1} in the surface sediment due to precipitation of hydrous Fe oxides by the oxidation of dissolved Fe in pore-fluids at M10. The relative enrichment of Fe_{ox1} below 15 cmbsf at M6 is coincident with the turbidite emplacement of upper-slope sediments identified by Marsh et al. (2007). This relationship is also reflected in the ratio $Fe_{h\text{-}lab}/[Fe_{h\text{-}lab}+Fe_{ox1}]$, where the greatest proportion of $Fe_{h\text{-}lab}$ is identified in the oxic surface layer at M10 (0-5 cmbsf), and in the turbidite layer at M6. These solid-phase relationships in Fe partitioning indicate that Fe recycling is more intense in the northern M10 site of highest organic carbon supply, and are in agreement with the enhanced rates of oxygen and nitrate utilisation at M10 already discussed. Some of these data and aspects of their interpretation have previously been published in the journal Geology (Homoky et al., 2009; Appendix I).

Montserrat debris flow deposits were identified by lithological changes in the box-core sediment section; sediments coarsen down core from silts to coarse sands between the sediment surface and 15 cmbsf where the coarse sands lie un-conformably on fine-sands also coarsening with depth to ~22 cmbsf. This was interpreted to be the successive 2003 and 2006 debris flow deposits by shipboard sedimentologists on JC_18 (J. Trofimvoss and P. Talling, pers comm).

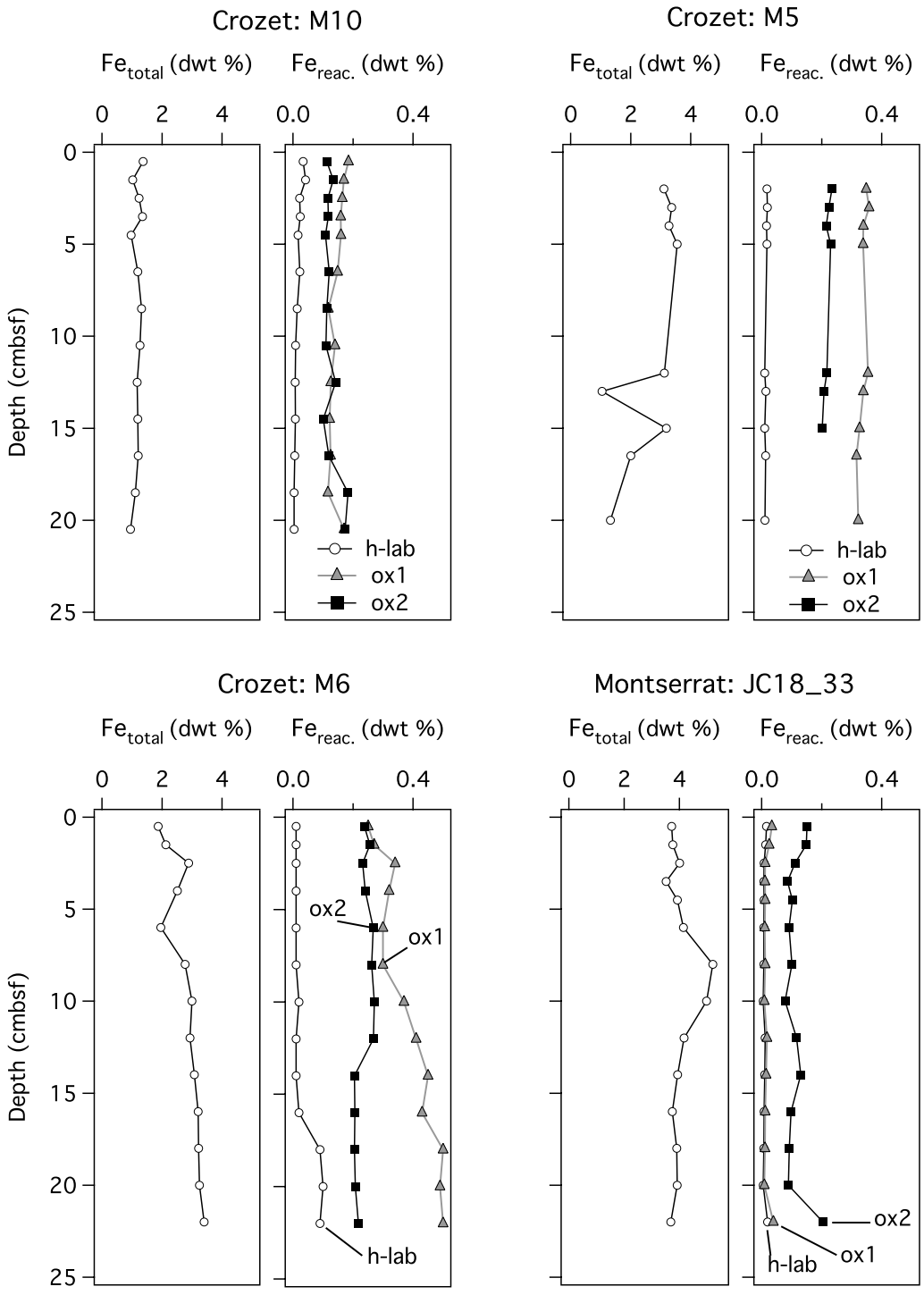

Figure 3-11. Total Fe and reactive Fe contents of Crozet and Montserrat sediments. Reactive Fe (Fe_{reac}) is defined as the sum of highly labile Fe ($Fe_{h\text{-}lab}$) including carbonate associated and adsorped Fe, easily reducible hydrous Fe oxides (Fe_{ox1}) and reducible crystalline Fe oxides (Fe_{ox2}). Reactive Fe determination follows the sequential extraction procedures of Poulton and Canfield (2005).

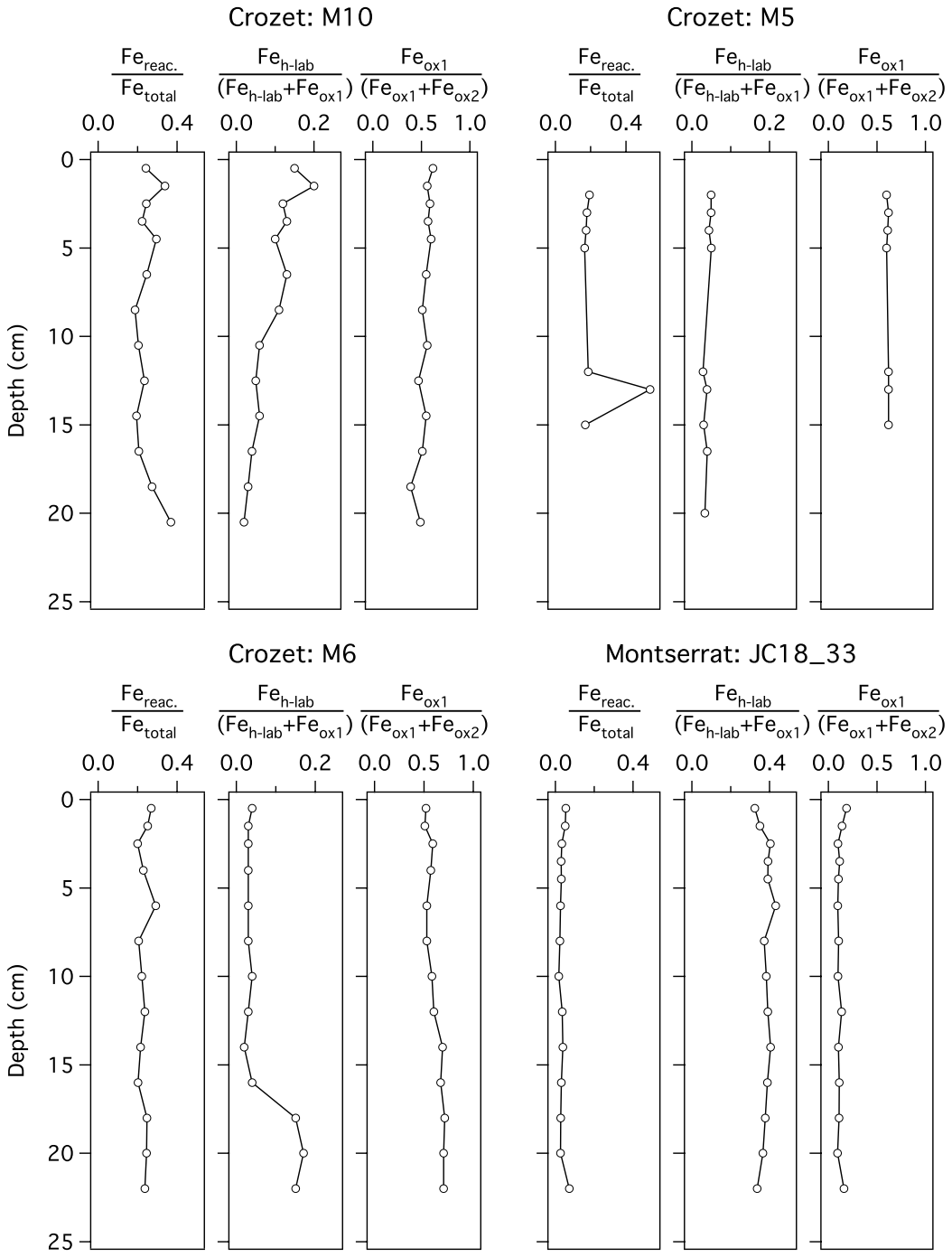

Figure 3-12. Relative proportions of reactive Fe phases in Crozet and Montserrat sediments. Reactive Fe (Fe_{reac}) is defined as the sum of highly labile Fe ($Fe_{h\text{-}lab}$) including carbonate associated and adsorped Fe, hydrous Fe oxides (Fe_{ox1}), and crystalline Fe oxides (Fe_{ox2}), following determination by the sequential extraction procedures of Poulton and Canfield (2005).

Total Fe (Fe_{total}) content of Montserrat sediment ranges from ~3.2 to 5.6 dwt % (0-20 cmbsf) (Figure 3-11). The greatest concentration of Fe_{total} is between 8 and 10

cmbsf, in the centre of the 2006 debris flow deposit. The concentration of reactive Fe phases is typically lower than those found in the Crozet sites, and dominated by Fe_{ox2}. The ratio of reactive Fe relative to the total Fe pool (Fe_{reac} /Fe_{total}) ranges from 0.02 to 0.07, an order of magnitude lower than that observed at Crozet sites Figure 3-12). Fe_{reac} enrichments are identified (0.05-0.07) near the sediment surface and the hemi-pelagic transitions between the 2006 and 2003 (~15 cmbsf) and 2003 and 1998 (~22 cmbsf) debris flow deposits. The Fe_{ox1} /[Fe_{ox1}+Fe_{ox2}] ratio is consistent down core (~0.1) with enrichments (0.15-0.2), at the same depth as the elevated Fe_{reac}/Fe_{total}. The occurrence of crystalline Fe oxides is therefore most strongly associated with lithogenic inputs and hydrous Fe oxides with pelagic sedimentation. The ratio $Fe_{h\text{-}lab}$ /[$Fe_{h\text{-}lab}$+Fe_{ox1}] is substantially higher (0.3-0.4) in Montserrat than any of the Crozet sites, with the strongest enrichment in highly-labile Fe coincident with dissolved Fe maxima in the pore-fluids between 2 and 6 cmbsf.

Montserrat sediments contain relatively little reactive Fe compared with the older mixed volcaniclastic and bio-siliceous sediments in Crozet. Reactive Fe phases in Montserrat sediments are dominated by crystalline Fe oxides, which are inferred to be largely goethite minerals (van der Zee et al., 2003), with the remaining component comprising near-equal quantities of highly-labile Fe and easily reducible Fe oxides, which is inferred to largely comprise ferrihydrite (Poulton and Canfield, 2005). Crozet sediments contain significantly more reactive Fe within the total Fe pool than Montserrat, and are dominated by easily reducible oxides, followed by crystalline Fe oxides. The total and reactive Fe partitioning in Montserrat and Crozet sediments suggests that Crozet sediments have undergone more extensive redox recycling of Fe than Montserrat, despite apparently greater rates of oxidant utilisation in Montserrat surface sediment pore-fluids. The greater extent of redox recycling of Fe probably reflects the longer period of early-diagenesis that exists for surface sediments in Crozet compared with Montserrat. The observation of polychaete worms and burrowing mega-fauna is isolated to mega-cores recovered from Crozet, and is therefore further evidence that bioirrigation and bioturbation may also be enhancing the extent of Fe recycling in Crozet surface sediments.

With improved understanding of the different rates and controls of Fe and Mn cycling between the study sites, we should now consider the possible origins and impacts of the colloidal Fe and Mn identified in Crozet pore-fluids.

3.4.4 Possible origins of colloidal Fe and Mn in Crozet pore-fluids

The distributions of Fe and Mn between Crozet and Montserrat pore-fluids are distinct. Fe and Mn in Crozet pore-fluids are significantly partitioned between the traditionally termed "dissolved" size fractions, while Montserrat pore-fluids show no consistent partitioning of either element (Figure 3-5 and Figure 3-6). Crozet pore-fluid Fe and Mn concentrations are typically higher, and their biogeochemical zonations are less distinct than previous measurements from deep-sea surface sediments (Froelich et al., 1979; Klinkhammer, 1980; King et al., 2000; Haeckel et al., 2001a), and the concentration of Fe and Mn remains elevated in the pore-fluid despite the presence of oxygen. It is inferred therefore that Crozet pore-fluids comprise relatively small quantities of aqueous Fe^{2+} and $Mn^{2=}$, and relatively abundant colloidal phases comprising organically complexed and/or colloidal and/or nano-particulate phases greater than 20 nm in diameter. The possible origin and composition of which will be discussed.

Pore-fluid size fractionation studies are uncommon, and to date only one study in beach sand pore-fluids has examined the partitioning of Fe and Mn (Huerta-Diaz et al., 2007). These authors found Mn to be mainly present in the pore-fluid as truly dissolved species (90%) in contrast to Fe, which was mostly (93 ± 10%) associated with small size colloids (~0.001 µm to 0.45 µm). These findings are consistent with size fractionated Fe concentrations reported for northeast Pacific Ocean seawater, where ~50% of Fe present was a small colloid (<0.2 µm) and water column profiles suggest the colloids may have a sedimentary origin (Nishioka et al., 2001), and for North Atlantic waters where colloial Fe is reported to dominate the variability in the distribution of dissolved Fe (Bergquist et al., 2007).

Variations in the abundance of colloidal phases in the pore-fluids may result from a number of factors affecting the solubilisation, precipitation, and stabilisation of Fe and Mn. These include the episodic supply of organic carbon that is capable of inducing drastic temporal changes to steady-state pore-fluid compositions in the

deep-sea (Gehlen et al., 1997); the vertical mixing of sediments and pore-fluids through slumping and turbidite emplacement in this region (Marsh et al., 2007); the influence of bioirrigation and bioturbation by benthic fauna (Aller, 1990); and the uncertain role of stabilising organic complexes in the pore-fluid environment (Luther III et al., 1992).

A recent study has demonstrated the dominant reactive Fe (oxy)hydroxide in marine sediments is nano-scale goethite crystals rather than what was previously assumed to be 2-line ferrihydrite (van der Zee et al., 2003). This is significant because the relative stability of goethite, its capacity for Mn substitution and cation sorption (Scheinost et al., 2001), and its apparently nano-scale crystal size near oxic-anoxic boundaries in marine sediments make it a potential component of the Fe and Mn colloids measured in Crozet pore-fluids. However, why would nano-goethite appear ubiquitous in Crozet pore-fluids but not in Montserrat pore-fluids? Goethite rather than ferrihydrite precipitation is favoured when an increase in pH and the supply of oxygen for oxidation of Fe^{2+} occurs slowly (van der Zee et al., 2003). The diagenetic rates of Fe and Mn cycling in Crozet sediments are controlled by the supply of reactive organic carbon, where the mean estimated flux is low (~0.05 gC m^{-2} yr^{-1}; Section 0) and early diagenetic reactions in the surface 0-21 cmbsf are likely to occur over a period of thousands of years. By contrast rapid episodes of sedimentation in the Montserrat region produce steep oxygen and pH gradients and are more likely to favour the oxidation of hydrous Fe oxides like ferrihydrite. Consistent with this suggestion, a 2-fold increase in the relative abundance of hydrous Fe oxides (Fe_{ox1}) relative to crystalline Fe oxides (Fe_{ox2}) is observed in the surface 0-2 cmbsf in Montserrat (Figure 3-12). However, bulk Fe_{ox2} content (Fe fraction containing goethite) is also elevated in the surface 0-2cmbsf, meaning this nano-goethite explanation remains uncertain. Presuming less favourable nano-goethite forming conditions may account for the absence of colloidal components in Montserrat pore-fluids, they cannot explain why evidence of nano-goethite formation in other deep-sea pore-fluids has not been observed in previous studies, where pH and oxygen gradients maybe similar in nature to Crozet.

Florindo et al. (2003) observed that low magnetisation occurs in sediments with elevated pore-fluid silicon concentrations that arise from the diagenesis of biogenic silica and/or silicic volcanic ash. . The authors concluded that dissolved

silicon (DSi) concentrations >500 μM can significantly decrease the size of the Eh/pH stability field of magnetite in favour of forming Fe-bearing smectite, a commonly colloidal clay, during oxic-suboxic diagenesis. However, the dissolution of Magnetite in anoxic sediments favours pyrite formation (Canfield and Berner, 1987). Nontronite, an Fe(III) rich member of the smectite group of clay minerals that forms from basaltic weathering, typically consists of more than 30% Fe_2O_3 and commonly substitutes Fe for Mn (Kohler et al., 1994). Crozet surface sediments contain favourable [DSi] (400-800 μM) within the oxic-suboxic zone (~0-20 cmbsf) for authigenic smectite formation, whereas Montserrat sediments contain very low [DSi] (60-100 μM) in predominantly anoxic surface sediments (0-20 cmbsf), and so are unlikely to sustain magnetite-smectite alteration (Figure 3-13; Appendix II). It is therefore hypothesised that volcanogenic mineral alteration is an important source of colloidal and/or nano-particulate Fe to the pore-fluids in Crozet, and that Mn substitution of Fe, or sorption to mineral surfaces, accounts for the correlative Fe and Mn distribution in the colloidal fraction of Crozet pore-fluids.

The true nature of these colloids remains unclear. They are inferred to comprise oxidised and/or adsorbed Fe^{2+}/Fe^{3+} and $Mn^{2+}/Mn^{3+}/Mn^{4+}$ that is mobilised by bacterial reduction in addition to any nano-particulate authigenic weathering products and organic Fe-complexes that are present in the colloidal size range. These data highlight the need to measure different size-fractions in pore-fluids from additional basin-wide sedimentary environments, as a colloidal fraction may represent an important component of metal cycling between sediments and pore-fluids in other marine sedimentary environments. The apparent stability of Fe and Mn colloids in oxygenated pore-fluids at Crozet also highlights the potential for exchange with the overlying bottom waters, and will be discussed further the next section.

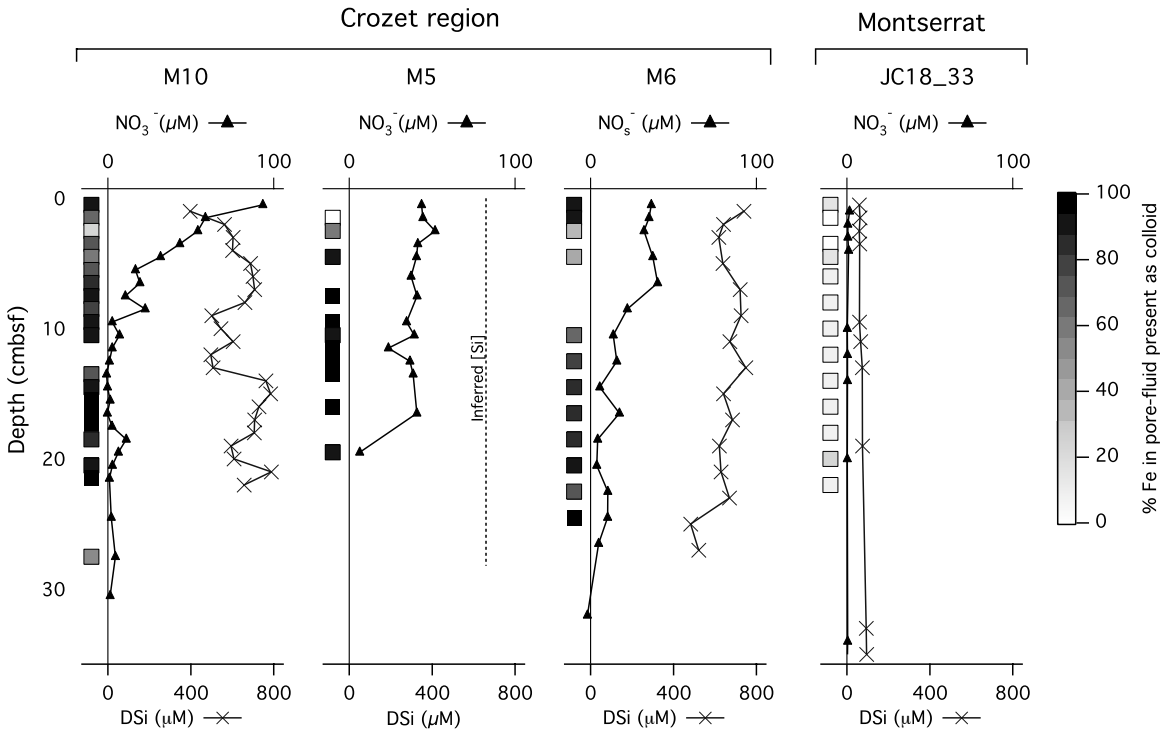

Figure 3-13. The proportion of pore-fluid Fe measured in a colloidal size range (0.02-0.2 μm) compared with dissolved pore-fluid nitrate and silicon concentrations, for Crozet and Montserrat surface sediments. The colloidal abundance of Fe is expressed using a grey-scale. Dissolved Si was not determined for M5; the dashed line is extrapolated from M6 and M10 [DSi]. Dissolved Si was not determined for Montserrat site JC18_33, and has been extrapolated from an earlier occupation of this site: JC18_8.

3.4.5 Implications of pore-fluid Fe and Mn for benthic exchange

Since the earliest Fe measurements in the oceans it has been suggested that colloids may dominate Fe distribution in seawater (Gordon et al., 1982). Small Fe and Mn colloids in the traditionally termed "dissolved" size fraction are reported for the North Atlantic and Southern Oceans and northeast Atlantic shelf (Wells and Goldberg, 1994; Wells, 1998; Wells et al., 2000), where 96% of Fe and 4% of Mn is reported to be in small colloidal forms. However, little is understood about the nature or origin of colloidal Fe. The ubiquity of colloids in ocean environments, concentration gradients towards sedimentary regions and the - albeit limited - measurements of colloids in sediment pore-fluids, suggest that sediments may be a source of colloidal Fe and possibly Mn to seawater. Recent studies have also demonstrated that the deep-sea contains a substantial

proportion of colloidal Fe in a traditionally termed "dissolved" size fraction (Bergquist et al., 2007). However, no studies thus far have measured a colloidal fraction of Fe and Mn in pore-fluids of the deep-sea. It is therefore important to consider the potential for dissolved and colloidal Fe and Mn (DFe, DMn and CFe, CMn) to diffuse from the volcanogenic pore-fluids presented in this study into the overlying bottom waters.

3.4.5.1 Diffusive flux estimation of benthic pore-fluid Fe and Mn exchange with the overlying bottom waters

Diffusive flux calculations of pore-fluid constituents have previously been successful in helping to assess the significance of diagenetic cycling between sediments and seawater (Li and Gregory, 1974; Klinkhammer, 1980; Klinkhammer et al., 1982; Warnken et al., 2001; Elrod et al., 2004). Accurately determining the flux of Fe and Mn from pore-fluids to overlying bottom waters however is not trivial, and beyond the scope of the data available to this study. Pore-fluid profiles presented in this chapter typically do not show characteristic diffusive gradients towards the overlying bottom water. However the measurement of dissolved (<0.2 μm) Fe concentrations in the surface 0-1 cmbsf of deep-ocean sediments ~1000 times greater than the concentration of Fe measured in the deep-ocean suggests a strong concentration gradient exists and in the case of Crozet, without an oxidative barrier to limit the exchange of Fe and Mn with the overlying bottom waters. Possible mineral scale origins of colloidal Fe and Mn in Crozet sediments may also account for the apparently non-diffusive pore-fluid profiles, and be further complicated by seasonal fluctuations to bioturbating macro-fauna. Therefore a linear gradient of dissolved and colloidal Fe and Mn (DFe/Mn and CFe/Mn) at the sediment–seawater interface is estimated and used - as the best available approach - to evaluate the flux potential of Fe and Mn to the overlying bottom water, based on Ficks first law of diffusion (Equation 3-1).

$$F_j = -D_j^{sed}(dC_j/dx) \qquad (3\text{-}1)$$

Where F_j is the flux of metal *j*, which is calculated from the product of the effective diffusion coefficient of metal *j* in the sediment (D_j^{sed}) and the concentration gradient (dC_j/dx). The depth interval (dx) is estimated as the mean

depth of the shallowest pore-fluid sample from the overlying bottom water (e.g. x = 0.5, where *j* is measured at 0-1 cmbsf). The concentration change (dC_j) is estimated from the difference in concentration of *j* in the pore-fluid and the estimated bottom water concentration. Effective diffusion coefficients for Fe^{2+} and Mn^{2+} are based on those calculated by Klinkhammer (1980). These values are estimated from the diffusion coefficients of divalent cations in distilled water between 0 and 25 ºC, and corrected for temperature (2 ºC: Crozet; 6 ºC: Montserrat), porosity (75%: Crozet; 50%: Montserrat) and a tortuosity factor (0.5) based on the extrapolated data of Li and Gregory (1974) from deep-sea sediments in the eastern equatorial Atlantic. The effective diffusion coefficients (D_j^{sed}), calculation parameters and flux estimates are summarised in Table 3-2 and Table 3-3.

Table 3-2. Parameters used for the calculation of diffusive fluxes of colloidal Fe (CFe) and dissolved Fe (DFe) in Crozet and Montserrat.

Site	Temp. (ºC)	D_{Fe}^{sed} (cm^{-2} s^{-1})	d*x* (cm)	dC_{Fe} (nmol cm^{-3})	C_{Fe}^{bw} (nmol cm^{-3})
CFe (0.02-0.2 μm)					
M10	2	1.4×10^{-6}	0.6	17.20	7.5×10^{-4}
M5	2	1.4×10^{-6}	0.6	0.79	7.5×10^{-4}
M6	2	1.4×10^{-6}	0.6	15.89	7.5×10^{-4}
JC18_33	6	1.1×10^{-6}	0.6	0.30	6×10^{-4}
DFe (< 0.02 μm)					
M10	2	1.4×10^{-6}	0.6	1.75	7.5×10^{-4}
M5	2	1.4×10^{-6}	0.6	-	7.5×10^{-4}
M6	2	1.4×10^{-6}	0.6	0.75	7.5×10^{-4}
JC18_33	6	1.1×10^{-6}	0.6	0.26	6×10^{-4}

Diffusive flux calculations are based on Klinkhammer (1980), where F_j is equal to $-D_j^{sed}(dC_j/dx)$. Diffusion coefficients are estimated for aqueous species Fe^{2+}, following the authors' extrapolation of Li and Gregory's (1974) data where tortusoity is 0.5, and adjusted for sediment porosities of 75% and 50% for Crozet and Montserrat, respectively. Changes in Fe concentration (dC_{Fe}) are based on the depth averaged surface 0-1 cmbsf (mean = 0.5 cmbsf) pore-fluid concentrations, minus the bottom water concentrations of Fe (C_{Fe}^{bw}) extrapolated from Klunder et al. (In Press) that are assumed to be present above a diffusive boundary layer thickness of 1 mm (Jorgensen and Revsbech, 1985).

Table 3-3. Parameters used for the calculation of diffusive fluxes of colloidal Mn (CMn) and dissolved Mn (DMn) in Crozet and Montserrat.

Site	Temp. (ºC)	D_{Mn}^{sed} (cm^{-2} s^{-1})	d*x* (cm)	dC_{Mn} (nmol cm^{-3})	C_{Mn}^{bw} (nmol cm^{-3})
CMn (0.02-0.2 μm)					
M10	2	1.3×10^{-6}	0.6	0.38	5×10^{-4}
M5	2	1.3×10^{-6}	0.6	0.10	5×10^{-4}
M6	2	1.3×10^{-6}	0.6	0.24	5×10^{-4}
JC18_33	6	1.0×10^{-6}	0.6	31.5	1×10^{-3}
DMn (< 0.02 μm)					
M10	2	1.3×10^{-6}	0.6	0.11	5×10^{-4}
M5	2	1.3×10^{-6}	0.6	0.18	5×10^{-4}
M6	2	1.3×10^{-6}	0.6	0.12	5×10^{-4}
JC18_33	6	1.0×10^{-6}	0.6	28.2	1×10^{-3}

Diffusive flux calculations are based on Klinkhammer (1980), where F_j is equal to $-D_j^{sed}(dCj/dx)$. Diffusion coefficients are estimated for aqueous species and Mn^{2+}, following the authors' extrapolation of Li and Gregory's (1974) data where tortusoity is 0.5, and adjusted for sediment porosities of 75% and 50% for Crozet and Montserrat, respectively. Changes in Mn concentration (dC_{Mn}) are based on the depth averaged surface 0-1 cmbsf (mean = 0.5 cmbsf) pore-fluid concentrations, minus the bottom water concentrations of Mn (C_{Mn}^{bw}) extrapolated from Statham et al. (1998) that are assumed to be present above a diffusive boundary layer thickness of 1mm (Jorgensen and Revsbech, 1985).

The diffusion coefficients of organically complexed and/or nanoparticulate Fe and Mn phases in pore-fluids have not been quantified, but are likely to differ from those estimated for free cations. The diffusion coefficients of Cu-complexes in distilled water (Phillips and Ellis, 1970) and Pb-complexes in hydro-gels (Scally et al., 2006), are both demonstrated to be ~25% slower than the respective free cation. By extrapolation however, the differences in D_j^{sed} between CFe/Mn and DFe/Mn are likely to be within the uncertainty of the approach presented here, and is consistent with the approach of Huerta-Diaz et al. (2007).

The concentration gradient for Fe and Mn assumes a diffusive boundary layer (DBL) thickness of 1 mm (Jorgensen and Revsbech, 1985) and that the concentration in the bottom waters adjacent to the DBL is equal to the concentration determined for bottom waters within ~100 m of the sediment surface, those closet available data to date. In reality this concentration may be elevated due to imperfect mixing of re-suspended particles in the water column producing a gradient in Fe and Mn concentration in the bottom water nepheloid or benthic boundary layer (BBL) (Statham et al., 1998). Seawater sampling close to the sea floor is impractical by CTD, and overlying core water from mega-core deployments is subject to artificially elevated trace metal concentrations due to disturbance of the surface sediments during core recovery and possible contamination of the overlying seawater, meaning DET gel probes are also unlikely to accurately sample overlying water Fe and Mn concentrations. Thus while CTD measurements of Fe and Mn in the bottom waters provide the best available means for estimating dC_j, the gradient derived for (dC_j/dx) is likely to represent its upper value.

The mechanism of pore-fluid Fe and Mn transport is an additional uncertainty in the absolute flux across the sediment-seawater interface. These diffusive flux estimates fail to account for variations in advective fluxes of Fe and Mn. Montserrat sediments did not appear to compact easily, but their sandy composition may be subject to significant pore-fluid pumping, and bioirrigation and seabed topography has been shown to enhance the advective flux of solutes from sediment pore-fluids to the overlying water column (Huettel et al., 1998; Huettel et al., 2003; Volkenborn et al., 2007). Enhanced advective transport of Fe and Mn is neglected in these calculations, which therefore may underestimate the total Fe and Mn flux in this regard. Thus interpretation of the flux estimates provided here requires careful consideration of the assumptions used in their derivation. Nonetheless they provide an important provisional and best-available estimate of the impact of diagenetic processes on Fe and Mn cycling in the benthic boundary layer of these regions.

3.4.5.2 Implications of Flux estimates for Fe and Mn cycling.

The estimated DFe fluxes from Crozet and Montserrat sediments are 0.06-0.13 and 0.02 μmol cm^{-2} yr^{-1}, respectively (Table 3-4). The highest flux estimates for Fe

are in the colloidal fraction from Crozet (up to 1.13 μmol cm^{-2} yr^{-1}), and values are close to those calculated for the global average of reducing shelf sediments (1.5-19 μmol cm^{-2} yr^{-1}) (Raiswell and Anderson, 2005). Depending on the distribution of Crozet-type pore-fluid compositions, they could have a significant impact on Fe cycling in the deep-sea and for global seawater Fe budgets.

Table 3-4. Summary of estimated colloidal (0.02-0.2 μm) and dissolved (<0.02 μm) Fe and Mn fluxes from Crozet and Montserrat pore-fluids to the overlying bottom water.

Site	Diffusive flux estimates			
	CFe (μmol cm^{-2} yr^{-1})	DFe (μmol cm^{-2} yr^{-1})	CMn (μmol cm^{-2} yr^{-1})	DMn (μmol cm^{-2} yr^{-1})
Crozet				
M10	1.13	0.13	0.03	<0.01
M5	0.06	-	<0.01	0.01
M6	1.11	0.06	0.02	<0.01
Montserrat				
JC18_33	<0.01	0.02	0.17	1.48

The estimated DMn flux is substantially higher in Montserrat (1.48 μmol cm^{-2} yr^{-1}) compared with Crozet (up to 0.01 μmol cm^{-2} yr^{-1}), and is of greater magnitude that the flux observed by Berelson et al. (2003) on the continental margins (~0.4 μmol cm^{-2} yr^{-1}). The DMn flux in Montserrat is therefore likely to reflect an important pathway for diagenetic Mn cycling in this region. Consistent with this interpretation, M. Palmer (pers. comm., 2009) identified Mn oxide crusts in this region in 2004, distal to hydrothermal inputs. This observation supports the prediction of a benthic flux of aqueous Mn to the bottom waters, but also attests to the existence of an effective reservoir for the accumulation of oxidised Mn at the sediment surface. However, discrete Mn crusts were not identified in any cores collected during the Montserrat cruise, and so we infer Mn entrained in the bottom waters to be sufficiently stable for localised benthic transport. These ideas are discussed in further detail in Chapter 4 (Section 4.3.5).

The distribution of volcanic tephra deposits in the Worlds' oceans is large (~23% by volume in the Pacific Ocean; Straub and Schmincke, 1998), however source-proximal deposition such as that which typifies Montserrat site JC18_33

represents only a minor fraction of the volcaniclastic sediment distribution as a whole. The tephra deposition from the 1991 Mt Pinatubo eruption for example, the largest eruption documented in modern history, covers an area of just 0.1% of the oceans' area, of which >95% of the tephra-covered area is less than 5 mm thick, compared with the 10-20 cm thick region of tephra deposit sampled in the Montserrat site. Thus Montserrat sediments represent an important yet relatively small depositional area of the ocean floor. We suggest a pore-fluid Mn flux to bottom waters is likely to be an important component of Mn cycling in this region, but the significance of young tephra-rich deposits for global seawater Mn budgets remains uncertain.

Mixed bio-siliceous, volcaniclastic sediments such as those which exist around Crozet are likely to cover a much greater area of the ocean floor than Montserrat sediments, on the order of an estimated 23% (Straub and Schmincke, 1998) of deep-ocean siliceous sediments, or 1.6% of the oceans area (~5.8 $x10^6$ km^2). We can predict the concentration of Fe and Mn in the oceans that would result from the benthic fluxes estimated from Crozet-type sediments using Equation 3-2:

$$C_{Fe}=(F_{Fe}At_r)/V \qquad (3\text{-}2)$$

Where C_{Fe} is the concentration of Fe, and $(F_{Fe}At_r)/V$ is equal to the product of the benthic Fe flux (F_{Fe}), the area of ocean floor hosting the flux (A), and the mean residence time of Fe in the oceans (t_r), divided by the volume of the oceans (V). If we assume the Crozet region sediments are typical of siliceous deep-sea sediments with a significant volcaniclastic component, then A is likely to be in the region of 1.6 % of the oceans area (5.76 $x10^{12}$ m^2). Assuming the oceanic residence time based on observed Fe and Mn export is ~30 years for Fe (De Baar and De Jong, 2001) and ~60 years for Mn (Martin and Knauer, 1980), the concentration of Fe and Mn in seawater from Crozet-type benthic inputs would be ~1.0 nmol Fe L^{-1} and 0.05 nmol Mn L^{-1}. These predictions are in excess of the mean Fe concentration and approximately half of the mean Mn concentration we observe in the deep-oceans (~0.8 nM Fe, ~0.15 nM Mn: Statham et al., 1998; Ussher et al., 2004; Klunder et al., In Press), and so disagree with the balance of inputs from other well-established sources, including atmospheric, riverine, continental shelf and hydrothermal inputs (Chester, 1990; Duce et al., 1991; Johnson et al., 1992; De Baar and De Jong, 2001; Elrod et al., 2004). The flux

estimates therefore highlight the potential importance of bio-siliceous-volcanogenic sediments for Fe and Mn cycling in the deep-oceans, as well as indicate that additional processes must exist to balance the estimated flux with other sources of Fe and Mn to the oceans. Enhanced rates of aqueous-particulate recycling between pore-fluid, seawater and surface sediments in a benthic boundary layer will probably shorten the true residence time of Fe and Mn close to the seafloor compared with the oceans as a whole. Furthermore, aggregation and settling may restrict the mobility of the colloidal Fe and Mn fraction in pore-fluids and overlying bottom waters. So quantifying the residence time close to the seafloor will be important for evaluating the true impact of these pore-fluid flux predictions. Enhanced sampling resolution near the sediment-seawater interface will greatly improve our understanding of benthic Fe and Mn cycling, and strengthen efforts to quantify the sedimentary impact on seawater Fe and Mn budgets.

The Fe flux calculation derived from Crozet pore-fluid concentrations corresponds to an estimated global input of dissolved Fe, dominated by nano-scale colloids, from deep-sea biosiliceous-volcaniclastic sediments to the oceans of 48 $x10^{9}$ mol yr^{-1}. This is higher than, though of similar magnitude to, the benthic balancing term suggested to account for the global deep-water burial flux of Fe (De Baar and De Jong, 2001) (Figure 3-14). Recycling processes within the benthic boundary layer will likely determine the true impact of deep-sea benthic Fe exchange on global biogeochemical cycles.

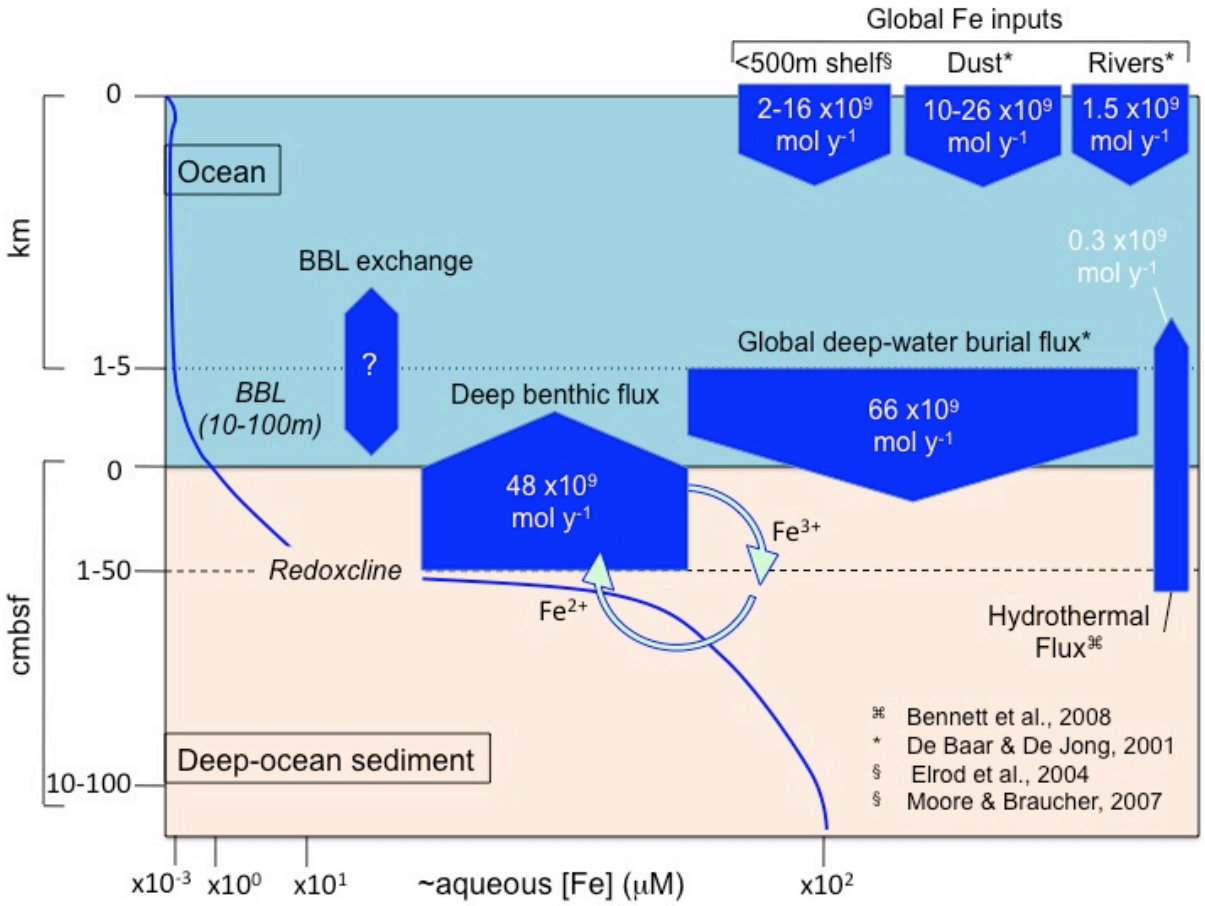

Figure 3-14. Illustration summarising dissolved Fe distribution in the oceans and Crozet-type (biosiliceous, volcaniclastic) deep-ocean sediments (solid blue line). Published fluxes of Fe to and from the oceans are shown in comparison to the deep-sea benthic exchange term estimated in this study.

3.5 CONCLUSIONS

Crozet and Montserrat sediments represent regions of contrasting oxygen utilisation pathways, the Crozet region is primarily driven by organic-carbon oxidation, whereas Montserrat is suggested to be dominated by the oxidation of lithogenic Fe(II) minerals and other mineral phases with metals in their lower oxidation states, as is typical of young tephra-rich deposits in the oceans. Elevated organic carbon supply in the otherwise HNLC-Crozet region and abundant tephra deposition in Montserrat accounts for steep Fe and Mn concentration gradients at the pore-fluid-seawater interface. However, the composition of Fe and Mn in the pore-fluids of these regions is distinct.

Montserrat pore-fluids appear to comprise Fe and Mn in a truly aqueous phase, whereas a colloidal fraction dominates dissolved (<0.2 μm) Fe and Mn distribution in Crozet pore-fluids. The true composition and origin of these colloids remains uncertain; weathering of basalt minerals in the presence of high dissolved silicon concentrations is hypothesised to contribute to the generation of colloidal smectites in Crozet sediment, however the significance of additional authigenic weathering products and organic matter interactions cannot be overlooked. The colloids are inferred to comprise adsorbed Fe^{2+}/Fe^{3+} and $Mn^{2+}/Mn^{3+}/Mn^{4+}$ that may be mobilised by bacterial reduction along with any nanoparticulate authigenic minerals, such as nano-goethite and/or Fe/Mn-bearing smectites, that might be formed by biosiliceous-volcaniclastic weathering.

Diffusive flux calculations for the sediment-seawater exchange of Fe and Mn support the view that deep-water volcanogenic sediments are potentially a significant source Fe and Mn to the deep-ocean. Montserrat sediments are inferred to sustain an important source of dissolved Mn to the bottom waters, of equal or greater magnitude than that determined for continental shelf sediments. Crozet sediments have the potential for an important diffusive flux of dissolved Fe in a colloidal form to the overlying waters. There is significant uncertainty associated with the magnitude of flux estimates presented in this study; a critical question remains, concerning the fate of Fe and Mn in the overlying bottom waters. Differences in the composition of Fe and Mn in the pore-fluids will have important impacts on the residence time, susceptibility to adsorption, scavenging, diffusion and transport of Fe and Mn in deep-water. Knowledge of the origin, composition and ubiquity of these colloidal forms is therefore critical to interpret the impact of Fe and Mn inputs from sediments to the oceans. Future investigations would benefit from direct benthic flux determinations in basin-wide sedimentary environments, with improved sampling resolution across the benthic boundary layer, and the development of novel tracer techniques for benthic exchanges with seawater.

Chapter 4 Microcosm studies of Fe and Mn at the sediment-seawater interface.

ABSTRACT

This chapter investigates the fluxes of dissolved Fe and Mn from surface sediments to overlying bottom waters in shipboard incubation experiments from river-dominated coastal (Eel River shelf), and volcanogenic deep-water (Montserrat), sediment settings. A low-cost portable apparatus was designed to sample ex-situ benthic dissolved metal and oxygen fluxes (Eel River shelf: Fe and O_2; Montserrat: Fe, Mn and O_2). A substantial flux of Fe was measured on the Eel River shelf (6.3 ± 5.9 μmol m^{-2} d^{-1}), which correlates with the rate of sedimentary organic carbon oxidation, demonstrating the link between benthic Fe flux and sediment respiration in shelf sediments. Bioirrigation is suggested to maintain up to a 10-fold increase in the Fe flux of Eel River shelf sediments, and account for high temporal and spatial heterogeneity of Fe flux observations. Changes in bioirrigation, oxidation kinetics and the cycling of Fe between dissolved and particulate phases are likely to account for discrepancies between ex-situ, in-situ and pore-fluid methods of flux derivation. The Eel River shelf has a relatively slow estimated oxidation half-life of Fe(II) ($t_{1/2}$ 3.6-5.9 hrs), compared with Montserrat ($t_{1/2}$ 0.3-0.5 hrs), where an Fe flux could not be identified within the accuracy of the analyses. Montserrat tephra-rich sediments are estimated to sustain a diffusive flux of dissolved Mn, in the region of 27 μmol m^{-2} d^{-1}, and demonstrate susceptibility to compaction-induced episodes of Fe and Mn advection to bottom waters. This study demonstrates that low-cost ex-situ incubation experiments can replicate benthic Fe flux measurements made by in-situ benthic chambers. The findings support the view that continental shelf sediments are important vectors of Fe to seawater and highlight the Fe flux-enhancing role of biota. Volcanogenic sediments dominated by inorganic sediment diagenesis are also shown to be a significant source of dissolved Mn to bottom waters. Recommendations for future studies are made.

4.1 INTRODUCTION

Seawater chemistry is influenced by trace metal fluxes to and from marine sediments. However, the direct measurement of biogeochemical processes at the sediment–seawater interface is typically very difficult to achieve because biogeochemical cycling of trace metals is complicated by the interaction of multiple variables present in natural sediment systems. Controlled microcosm investigations of Fe cycling in the benthic boundary layer are therefore an important complement to any study of sedimentary Fe biogeochemistry, and they will provide a useful comparison to the diffusive flux estimates based on pore-fluid concentration gradients derived in Chapter 3.

Studies have demonstrated that continental shelves are likely to sustain the highest sediment-derived diagenetic flux of Fe to the oceans (Croot and Hunter, 1998; Johnson et al., 1999; Elrod et al., 2004; Raiswell and Anderson, 2005; Lohan and Bruland, 2008). High organic carbon oxidation rates lead to intensified dissimilatory Fe reduction during microbial sediment respiration, and promote the supply of dissolved Fe to near surface pore-fluids. Dissolved Fe diffuses upward in the sediment column following the concentration gradient of dissolved Fe. This gradient is often highest on the continental shelves, resulting in the diffusion of Fe into the overlying bottom water. Similar processes sustain the flux of Mn from continental shelf sediments (Sundby and Silverberg, 1985; Johnson et al., 1992), and are thought to exist in some deep-water sediments (Statham et al., 1998).

The fate of Fe diffusing from the pore-fluids to the overlying bottom water remains unclear. Elevated concentrations of Fe^{2+} and ligand stabilised Fe^{3+} have been identified in shelf waters of the northeast Pacific (Lohan and Bruland, 2008). However, when Fe^{2+} reaches the bottom waters it is subject to intensified rates of oxidation, scavenging and precipitation. A colloidal faction of dissolved Fe entrained in bottom waters, either by oxidative precipitation and agglomeration, and/or through sediment re-suspension may also be involved in the cycling of Fe in the shelf zone (Nédélec et al., 2007). Previous studies indicate these Fe-bearing particles may be a primary source of Fe for phytoplankton (Wells and Mayer, 1991; Croot and Hunter, 1998; Johnson et al., 1999; Nodwell and Price, 2001;

Chase et al., 2005) and that particulate and colloidal Fe may impact open ocean Fe budgets (Wu and Luther III, 1996; Johnson et al., 1997; Lam et al., 2006; Nishioka et al., 2007).

In-situ benthic chamber investigations have been beneficial for advancing our understanding of trace element cycling at the sediment-seawater interface, and for determining the magnitude of sedimentary Fe fluxes (Watson et al., 1993; McManus et al., 1997; Berelson et al., 2003; Elrod et al., 2004). However, some key aspects of sediment-seawater Fe cycling remain to be assessed. For example: the impact of sediment re-suspension on the exchange of dissolved Fe between sediments and seawater; the impact of bioirrigation on Fe fluxes in ex-situ incubation experiments; and a wider range of sedimentary environments, such as low-carbon and volcanic-rich sediments, which represent important large-scale depositional facies, need to be evaluated. An improved understanding of the controls, distribution, magnitude and fate of sedimentary Fe inputs to seawater will inform our understanding of global biogeochemical Fe cycling.

The main objectives of these microcosm studies were 4-fold: (1) to design and build a small-portable unit capable of incubating intact ex-situ sediments and overlying core-water from the northern California shelf and Montserrat in order to measure the concentration of Fe in the over-lying core water over time; (2) to compare and contrast the magnitude of measured fluxes with the predicted fluxes derived from pore-fluid concentration gradients and in-situ studies where available; (3) to assess the impact of biocide additions on the efflux of Fe; and (4) to assess the impact of sediment re-suspension on efflux of Fe. To further address objectives (2) and (4), the opportunity has been taken to assess the magnitude of Mn fluxes in Montserrat sediments due to the high pore-fluid flux predictions calculated in Chapter 3 (Section 3.4.5.1).

4.1.1 Sampling locations and site descriptions

Sediments from 2 regions were sampled for use in the shipboard microcosm studies, the Eel River-dominated California margin of the northeast Pacific Ocean and volcaniclastic sediments from the Montserrat region of the Caribbean Sea.

4.1.1.1 Eel River shelf sites

Eel River shelf (ERS) sediments were collected during RV Wecoma cruise (WE0704E) in September 2007, which was funded through a National Science Foundation research grant aimed at investigating the benthic Fe flux of the California margin. Consequently, this cruise provided an opportunity to sample sediments hypothesised to be a significant source of Fe to the overlying seawater. In-situ benthic lander deployments conducted by Professor William Berelson's research group from the University of Southern California also provide an opportunity to compare these shipboard incubation experiments with in-situ flux determinations. ERS sediments sampling sites are summarised in Table 4-1 and Figure 4-1. This chapter presents incubation experiment data collected from sites ERS-2 and ERS-3. Site ERS-1 was used for the collection of sediments and pore-fluids, these data and an accompanying discussion are presented in Chapter 5. Methods of sediment sampling are described in Chapter 2 (Section 2.1).

Table 4-1. Sampling locations on Eel River Shelf (ERS)

Site (sampling)	Depth (m)	Latitude	Longitude	Date
ERS-1 (pore-fluid)	120	40º 43.7 N	-124º 28.6 W	Apr-07
ERS-2 (Inc. Exp. 1)	125	41º 00.0 N	-124º 20.3 W	Sep-07
ERS-3 (Inc. Exp. 2)	90	40º 57.0 N	-124º 18.2 W	Sep-07

The Eel River is the primary source of Holocene sedimentary material to the shelf region and is typically deposited in the winter to spring months by flood events (Ogston et al., 2004). A mixture of very fine sands, silts and clays occupy the mid-shelf region of 60-120 m water depth, where the mean organic carbon accumulation rate is estimated to be ~26.7 g m^{-2} yr^{-1} (Sommerfield and Nittrouer, 1999). Sediment re-suspension and lateral transport is wave-dominated, and bioturbation and bioirrigation is prevalent across the shelf and shelf slope break.

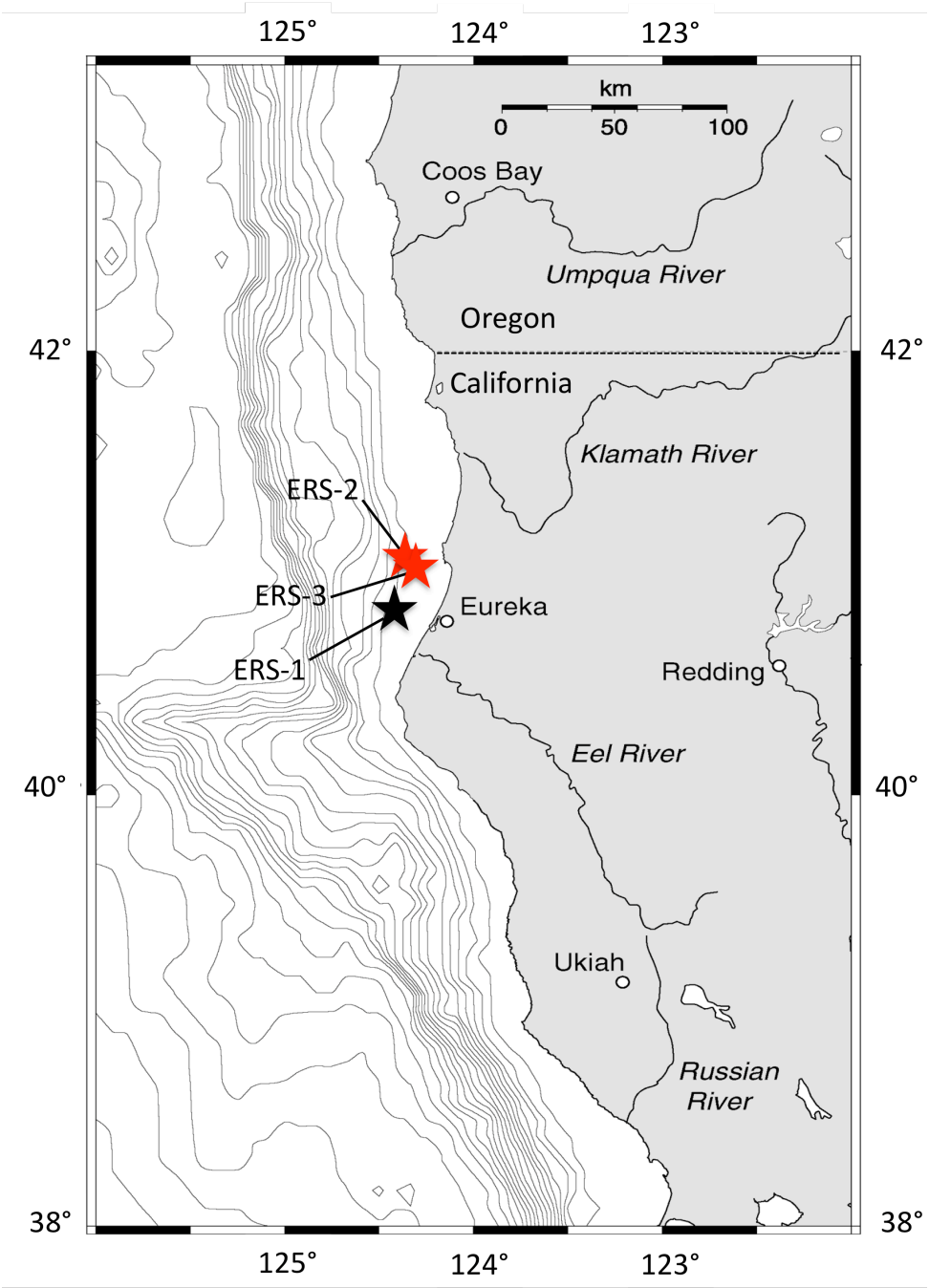

Figure 4-1. Bathymetric map (100 m contours), showing Eel River shelf sampling sites on the northeast Pacific Ocean margin. Sites used for sampling in this chapter are highlighted red.

4.1.1.2 Montserrat sites

Montserrat region sediments were first introduced in Chapter 3, and are described in detail in Section 3.2.1. Briefly, Montserrat region sediments are typical of many sediments in the Lesser Atillies, which are often dominated by

large-scale submarine pyroclastic flow deposition from active arc volcanism (Deplus et al., 2001). Montserrat region sediments are comprised of tephra-rich debris flows that have dominated the sedimentary input in a region ~200 km^2 to the southeast of the Soufriere Hills Volcano since 1995 (Trofimovs et al., 2006), pelagic carbonate-dominated sedimentation otherwise dominates the sediment composition in this region.

The Montserrat sampling sites used in this thesis are summarised in Table 4-2 and Figure 4-2. Sampling sites used for the microcosm experiments presented in this Chapter represent the 2 end-member sediment types in this region: (1) Site JC18_9 lies ~15 km ESE of Soufriere Hills Volcano in the depocentre of the 1998 and 2006 eruption event debris flow deposits, and comprises almost entirely tephra deposits between 2 and 10 years since deposition; (2) Site JC18_18 lies ~30 km SW of the Soufriere Hills volcano, and comprises almost entirely pelagic carbonate sedimentation, in addition to a small fraction of volcanogenic ash inputs.

Table 4-2. Sampling locations in Montserrat

Site	Depth (m)	Latitude	Longitude	Date
JC18_8	1110	16º 38.70 N	-62º 02.00 W	Dec-07
JC18_9	1113	16º 36.50 N	-62º 02.00 W	Dec-07
JC18_18	787	16º 30.50 N	-62º 27.00 W	Dec-07
JC18_33	1114	16º 38.40 N	-62º 02.00 W	Dec-07

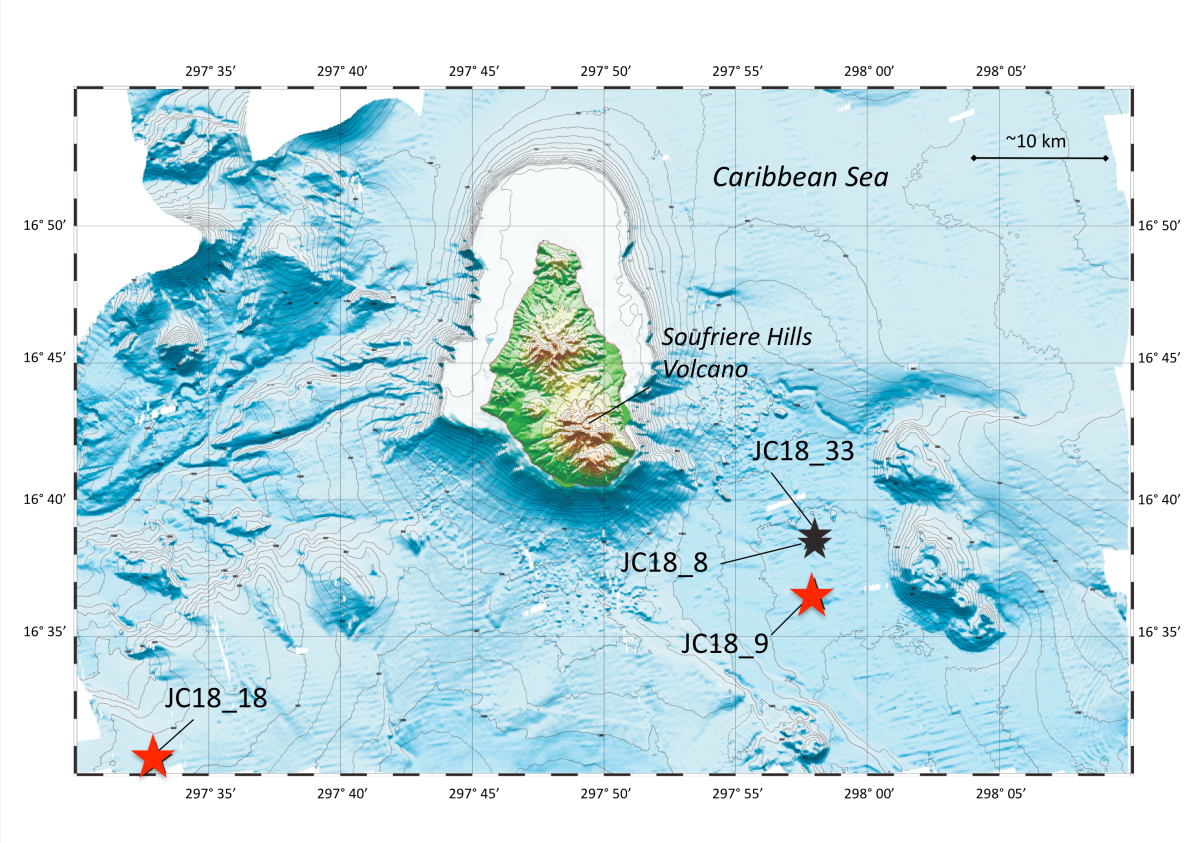

Figure 4-2. Map of sediment sampling locations in the Montserrat Region. Sites used in this chapter are highlighted red.

4.2 EXPERIMENTAL METHODS AND ANALYSES

4.2.1 Incubation apparatus design

A portable and robust chamber was designed and built for shipboard sediment-seawater incubation. In designing these incubation experiments the apparatus that housed the sediment and seawater needed to meet a number of important requirements. These included:

1. Preservation of the sampled sediment-seawater interface;
2. Prevention of oxygen and trace-metal contamination of the sample;
3. Controlled agitation of overlying seawater; and
4. Removal of seawater from the experiment without altering the internal trace-metal and/or oxygen concentrations.

The incubation unit is based on design principles used by the University of Southern California, where the unit is deployed within a polycarbonate sediment

core tube as is illustrated in Figure 4-3. The movement of the piston towards the sediment sample reduces the volume of incubated seawater. Movement of the piston allows for the sampling of seawater via a tap and luer-lock fitting, and the application of positive pressure to the piston prevents atmospheric contamination of the seawater during sampling.

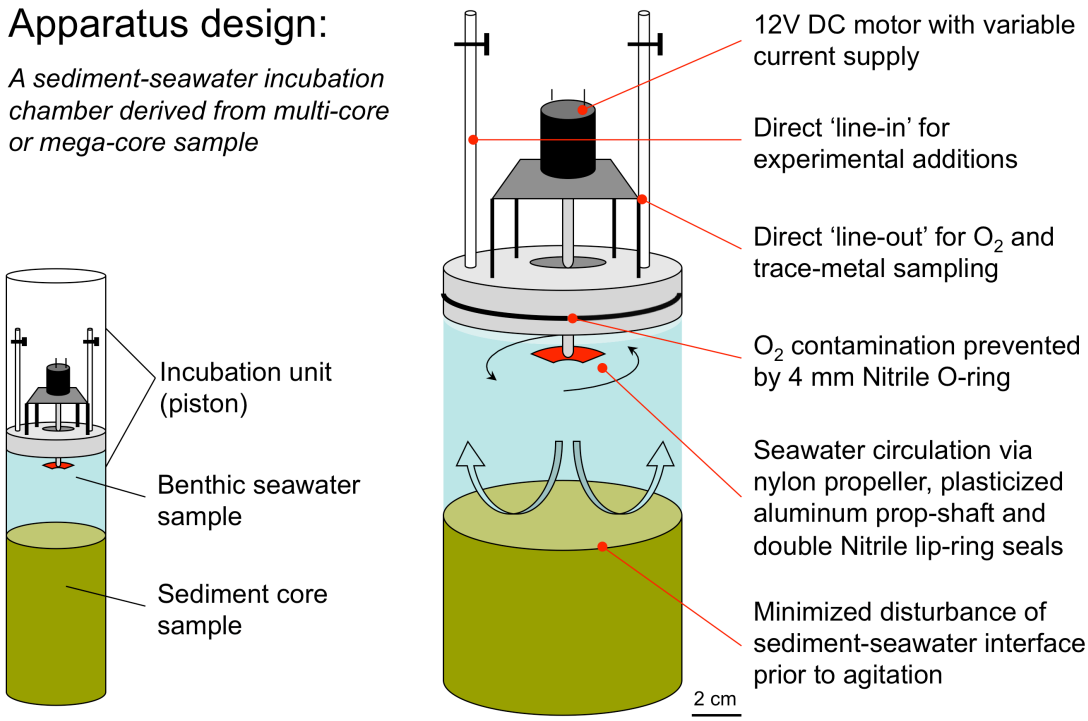

Figure 4-3. Apparatus design for microcosm incubation experiments. An incubated sediment-seawater sample is isolated by insertion of a piston-like incubation unit into a multi-core or mega-core derived sediment core.

Efforts were made to ensure all components of the incubation unit that were potentially in contact with the seawater samples would eliminate or minimise Fe and Mn (and other) trace-metal contamination artefacts. The assembled components are illustrated in Figure 4-4. Polycarbonate, teflon and nylon all have sufficiently low leachable trace metal properties for use in this instance (Howard and Statham, 1997). The materials used that were most susceptible to contaminating the sample were nitrile (o-rings and lip-ring seals), and aluminium (propeller shaft). Nitrile rubber however, is most prone to leaching metals when in contact with reducing solutions. Therefore components were thoroughly rinsed 3 times with Milli-Q prior to use. Aluminium was used for the propeller shaft due to its capacity for heat dissipation and its ability to form an effective seal with the

lip-ring seals. The aluminium shaft could pose a significant artefact in experiments intent on measuring aluminium in samples. While the risk of Fe and Mn contamination was considerably less, as a precaution a PVC plasticised coating was applied to all of the propeller shaft except that which came into contact with the lip-ring seal.

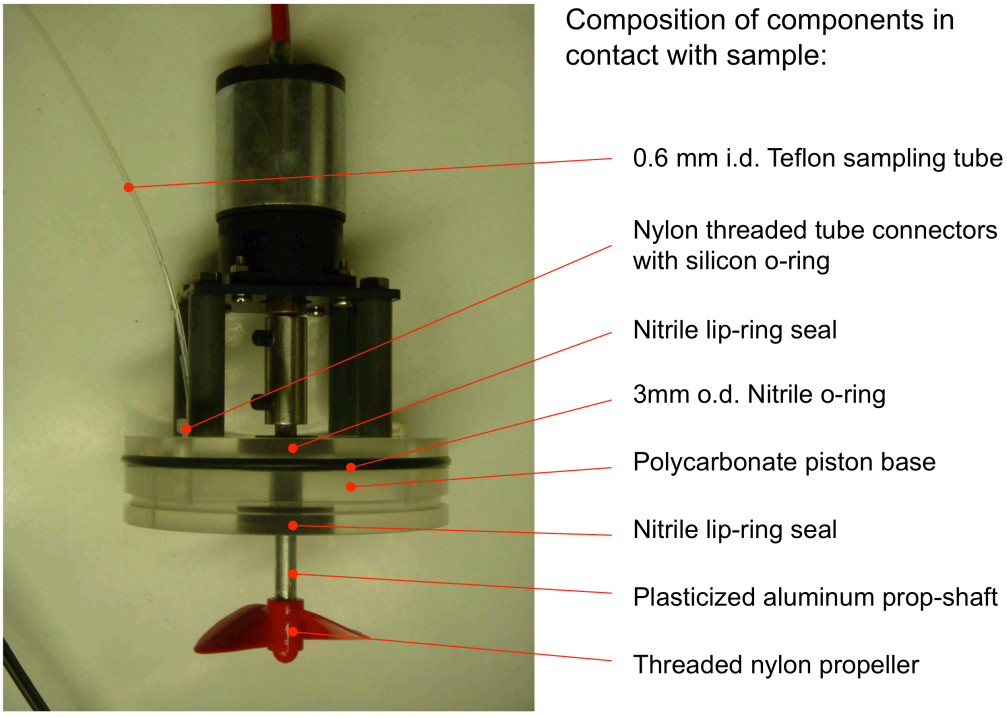

Figure 4-4. Photograph of assembled incubation unit with annotated composition of key sample-sensitive components kept 'trace-metal clean'.

A control experiment that incubated Southampton estuary seawater showed no significant increase in Fe(II) concentration over a period of 72 hours. Seawater was collected in 10% HCl-cleaned and Milli-Q rinsed polycarbonate core tube with LDPE core-cap sealing one end. The incubation unit was Milli-Q-rinsed and left for 72 hours at room temperature, with daily sampling intervals. Fe(II) concentration was measured by the Ferrozine method described in Section 2.6. Measured concentrations were consistently below the method detection limit (MDL: 150 nM Fe), therefore the apparatus was considered sufficiently clean with respect to Fe for incubation of natural sediment-seawater samples, and sufficiently resistant to leaching of Fe by seawater for the duration of experiments presented in this chapter.

Ex-situ incubation experiments may never truly replicate the natural environment. We can, however, assess the impact of individual processes such as sediment re-suspension, and compare different sites by controlling factors at the sediment-seawater interface that affect Fe cycling. Bottom water salinity, pH, and light intensity were maintained by isolating incubated samples in the dark in a controlled temperature laboratory during the shipboard experiments.

4.2.2 Experimental set-up and sampling protocol

The incubation apparatus set-up is shown in Figure 4-5. On both cruises, core liners were secured upright in a controlled temperature laboratory, set at the same temperature as bottom waters, as determined by CTD casts. Core liners and incubation units were acid cleaned (24 hrs 10% HCl) and thoroughly rinsed with Milli-Q prior to utilisation. Cores were recovered either by Multi-core (RV Wecoma) or by push core sub-sampling of box cores (RRS *James Cook*), following Section 2.2. All cores were a minimum 15 cm long (~10 times the oxygen penetration depth). Once cores were transferred to the controlled temperature laboratory, incubation units were immediately inserted into core tubes. A nitrogen gas line was attached to the sample inlet on the piston and allowed to purge air from between the piston and overlying core water to ensure any trapped air was oxygen-depleted. The headspace and excess overlying bottom water was then drained to waste through the sample lines by inserting the piston to a height of ~20 cm above sediment surface (leaving ~1.5 L of incubated seawater, where 1 cm depth = 78 ml seawater). The sample lines were then closed and the core wrapped in aluminium foil. The propeller was set to ~30 rpm (gentle water circulation rate) and left to stand for ~2 hours prior to sampling time “0 hrs” at the start of the experiment.

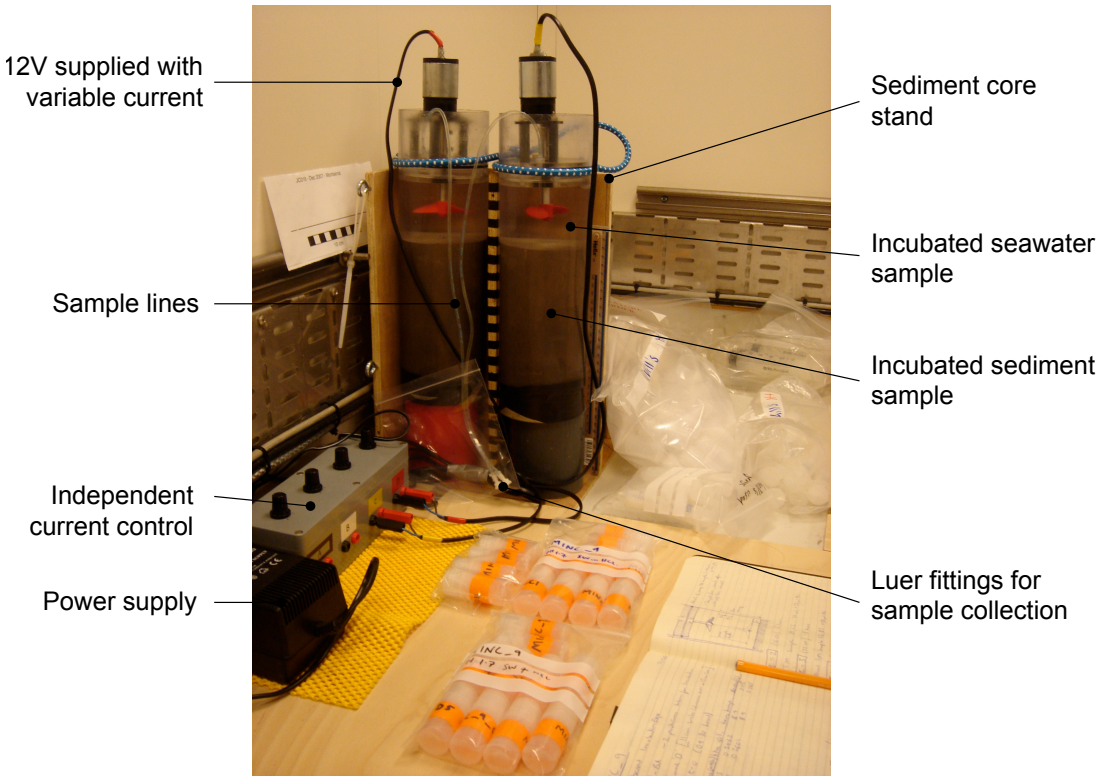

Figure 4-5. Shipboard incubation apparatus set-up in controlled temperature laboratory on the RRS *James Cook*.

During the incubation period samples were collected using the following sampling protocol:

Step 1) Connect acid-clean (72 hrs 20% HCl/72 hrs 20% HNO_3/Milli-Q rinsed) nitrile-free 20 ml syringe to luer-lock of each sample line. Record time. Using a PVC rod specifically designed to distribute pressure on the incubation unit, apply pressure to piston while extracting the 'dead volume' from the sample line into the syringe and eject to waste.

Step 2) For oxygen analysis by Optode fluroescence (RV *Wecoma*): Re-connect a nitrogen-flushed 10 ml open-ended glass vessel with 30 ml syringe joined by silicon tube sleeves and an in-line tap. With tap open, apply pressure to piston and draw a sample 2-3-times the glass volume, tapping continuously to ensure no bubbles are present in the sample vessel. Close tap, and remove glass vessel for immediate oxygen analysis as described in Section 2.10.3.

Step 3) For oxygen analysis by Winkler titration (RRS *James Cook*): Re-connect a nitrogen flushed 60 ml syringe with 5 cm length of tygon tube. Apply pressure to piston and draw a full syringe of sample. Immediately transfer sample to ~30 ml narrow-neck, calibrated glass oxygen bottle. Insert tube to base and fill steadily ensuring no bubbles are entrained in the sample and all air is flushed from sample bottle. Flood the bottle with the entire sample, and immediately fix for analysis as described in Section 2.10.2.

Step 4) Connect a second acid-clean 20 ml Nitrile-free syringe, apply pressure to piston and draw 12 ml sample for trace metal analysis.

Step 5) Disconnect syringe and plug sample line with teflon stopper.

Step 6) Connect nitrate cellulose luer-lock syringe filter (0.2 μm) to syringe and pass 1 ml to waste followed by 10 ml into a 30 ml LDPE sample bottle for acidification to pH 1.7. Store refrigerated prior to analysis (described below).

4.2.3 Incubated seawater sample analysis

Incubated seawater samples from the Eel River shelf were analysed for oxygen and Fe; samples from Montserrat were analysed for oxygen, Fe and Mn. During the California margin cruise all oxygen concentrations were determined by Optode fluorescence (Section 2.10.3). Eel River shelf samples used the ratio of spiked isotope ^{57}Fe to ^{56}Fe determined by ICP-MS to determine the concentration of Fe (Section 2.5.2). Montserrat region samples were analysed for oxygen by Winkler titration (Section 2.10.2), and a low-dilution ICP-MS method was used for the determination of Fe and Mn concentrations (Section 2.5.1).

4.3 RESULTS AND DISCUSSION

Experiment results data tables can be found in Appendix IV.

4.3.1 Eel River shelf incubation experiments

Three incubation experiments were conducted on Eel River shelf sediments (ERS2, ERS3) and seawater. A total of 4 cores (A-D) were used in each of 3 experiments. These experiments measured the dissolved Fe and oxygen

concentration in incubated seawater overlying sediments in an undisturbed state (Exp. 1), following the addition of a biocide to the core-water (Exp. 2), and during and after the agitation of the sediment-seawater interface (Exp. 3).

4.3.1.1 Experiment 1: 'Undisturbed' ERS sediment-seawater incubations

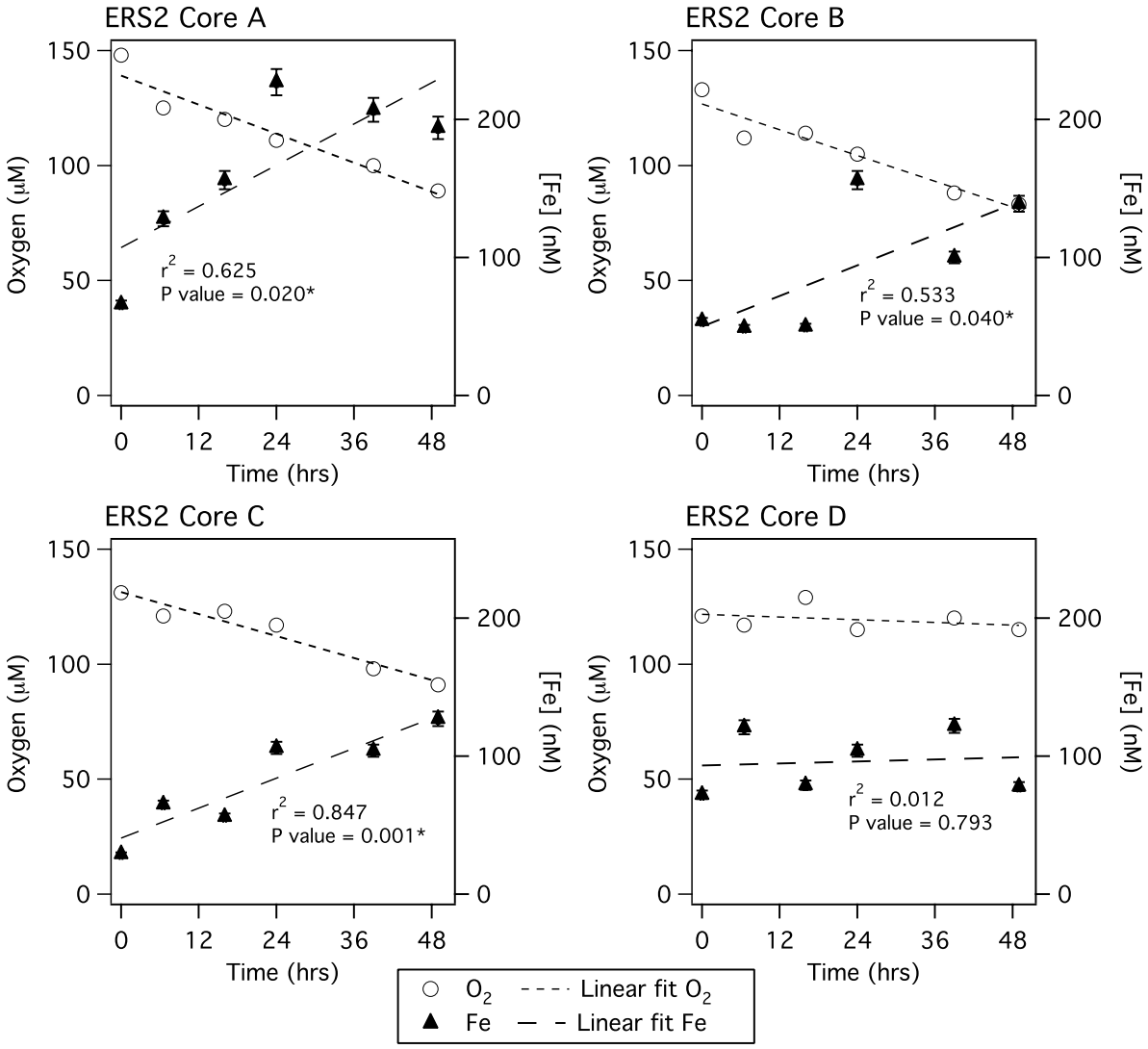

Figure 4-6. Eel River shelf incubation Experiment 1. Dissolved oxygen and Fe (<0.45 μm) concentrations were determined over a period of 49 hours, during which overlying core-water was subject to gentle recirculation. Dashed lines represent the linear best fit to the data, and are used for the derivation of mean fluxes. Error bars are 2-SD. Values of r^2 and P refer to the linear fit of Fe concentration data, where a P

value less than 0.05(Schmidt et al.) indicates a 95% probability the correlation is not due to chance.

Dissolved oxygen concentration decreased linearly during the 49-hour incubation experiment in cores A, B and C (Figure 4-6). Core D exhibited a negligible decrease in oxygen during this time. Cores A, B and C also showed a statistically meaningful net increase in dissolved Fe concentration (P value <0.05) at the end of the incubation experiment, while core D exhibited no significant change in dissolved Fe concentration.

4.3.1.2 Experiment 2: Biocide addition to ERS sediment-seawater incubations

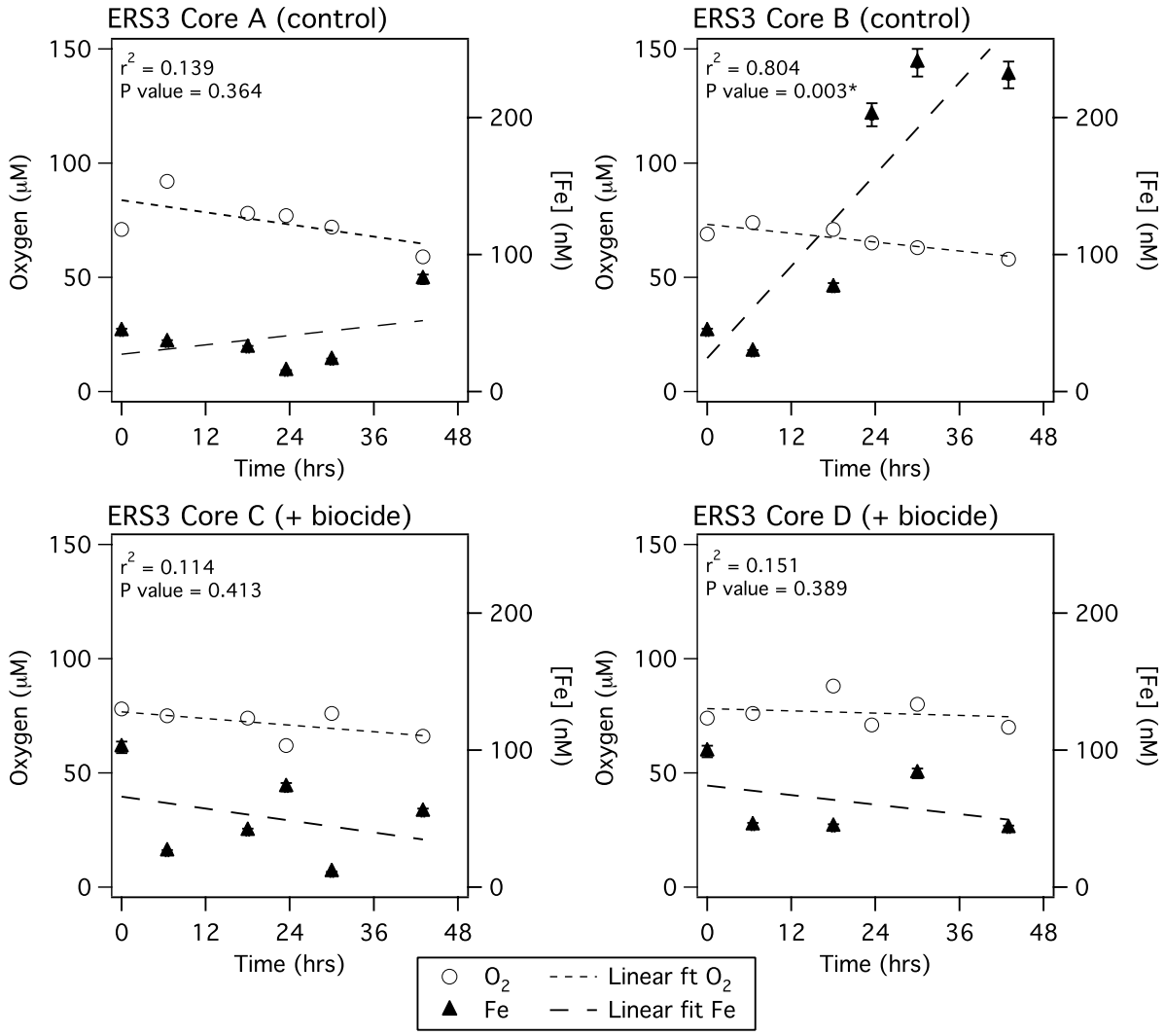

Figure 4-7. Eel River shelf incubation Experiment 2. Dissolved oxygen and Fe (<0.45 µm) concentrations, over a period of 42 hours, during which overlying core-water was subject to gentle recirculation and the addition of a biocide to cores C and D (2 ml of 100% formalin solution [$H_2C(OH)_2$] added to ~1.125 L of incubated core-water = 0.18% formalin). Dashed lines represent the linear best fit to the data, and are used for the derivation of mean fluxes. Error bars are 2-SD. Values of r^2 and P refer to the linear fit of Fe concentration data, where a P value less than 0.05(Schmidt et al.) indicates a 95% probability the correlation is not due to chance.

The addition of a fast acting biocide in low concentration (2 ml of 100% formalin solution [$H_2C(OH)_2$] added to ~1.125 L of incubated core-water = 0.18% formalin) to 2 of 4 incubated cores, was assumed to stop the activity of respiring macro-fauna responsible for bio-irrigation of surface sediments (Giere, 2009), the biocide is inferred to not significantly impact the bacterial diagenetic processes in the sediment during the 48 hr incubation period.

Dissolved oxygen concentrations decrease from ~70-80 μM at the start of the incubations to 60-70 μM after 45 hours (Figure 4-7). The most significant decrease in oxygen is measured in cores A, B and C, with negligible change to oxygen concentration in core D. Dissolved Fe concentrations show a net increase in control cores A and B. The increase in Fe concentration in core B is the highest measured in any of the Eel River shelf incubations (P value <0.005). A net decrease in Fe concentration occurred in cores C and D, which contained ~0.18% formaldehyde in the overlying core water, though the hypothesis that the linear fit through these data is meaningful is rejected at the 95% confidence interval (P value >0.05). Therefore, following the addition of a biocide to the incubated overlying core water, the occurrence of a significant increase in Fe concentration over time decreased from 1 in 2 cores, to 0 in 2 cores.

4.3.1.3 Experiment 3: Incubated re-suspension event of Exp. 2

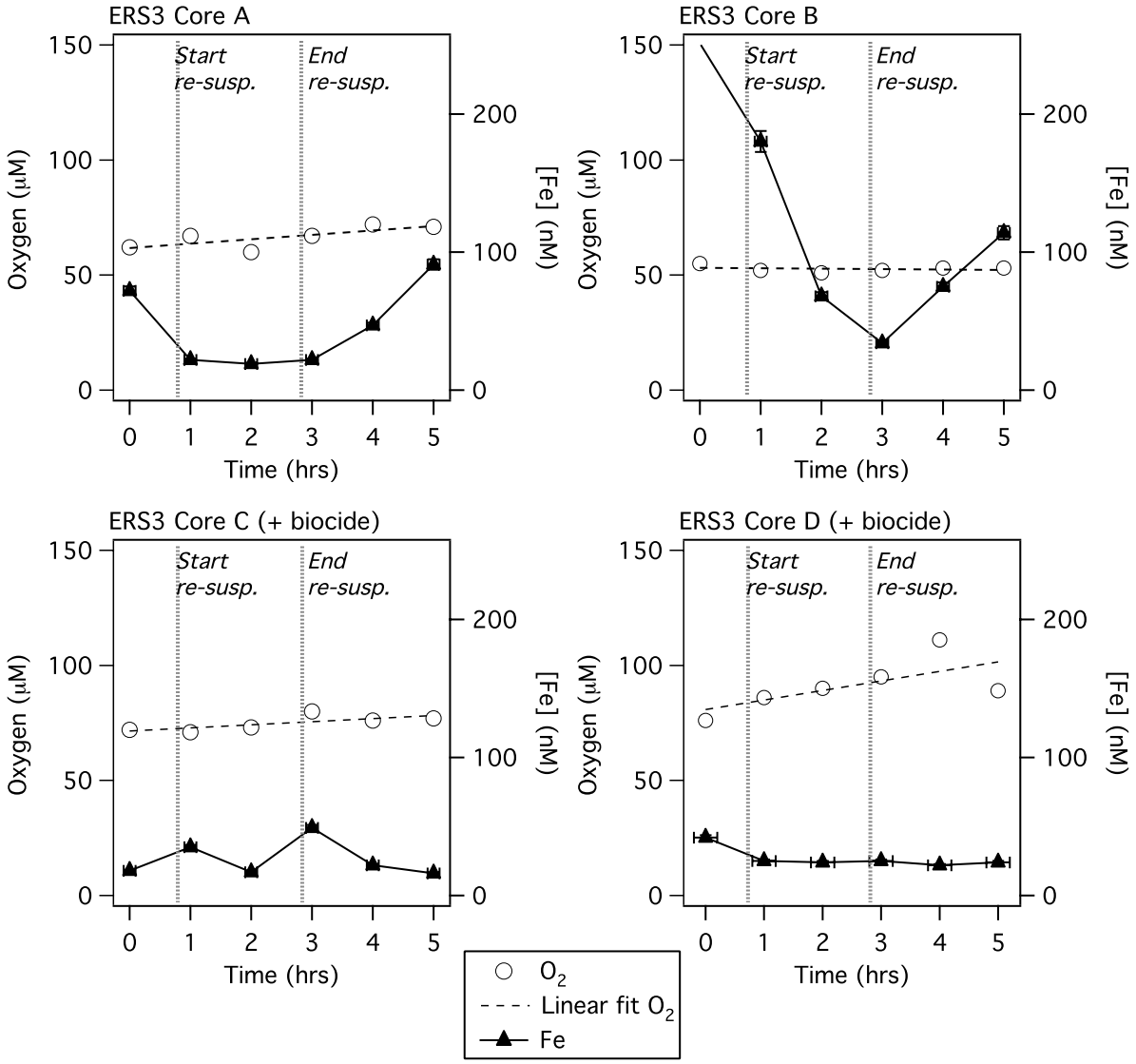

Figure 4-8. Eel River shelf incubation Experiment 3: Dissolved oxygen and Fe (<0.45 µm) concentrations, over a period of 5 hours, during which overlying core-water was subject to a 2-hour period of agitated overlying core-water and sediment re-suspension. This experiment used cores A-D, from experiment 2, which included the biocide addition to Cores C and D. Therefore time = 0 hrs above, is equivalent to time ~45 hours in Exp. 2. Error bars are 2-SD.

A 2-hour period of surface water agitation, which visibly enhanced over-lying core water turbidity, resulted in a decrease in dissolved Fe concentration in Cores A and B, from 45 to 25 nM in Core A and 251 to 23 nM in Core B (Figure 4-8).

Following the re-suspension event, Fe concentrations in A and B increased again to ~100 nM. Biocide cores C and D showed no significant change to Fe concentrations during the experiment, which remained low between 15 and 25 nM. The re-suspension of sediments in this experiment is believed to be insufficient to entrain reducing sediment pore-fluids, as the total thickness of sediment re-mobilised was estimated by sight to be less than 1 mm. No cores recorded a decrease in oxygen concentration during the 5 hour incubation, and in A, C and D, oxygen concentration increased, suggesting the isolation of atmospheric oxygen from the sample may have been compromised during periods of enhanced core-water agitation. Significant contamination can be ruled out as oxygen concentrations remain just 30-40% of saturation, and within the range of values reported for bottom waters on the Eel River shelf (Severmann et al., In prep.).

4.3.2 Evaluation of Eel River shelf incubation results

The concentration of Fe in overlying core water measured at the start of the Eel River shelf incubation experiments (between 20 and 60 nM) is consistent with the total dissolved Fe concentrations previously reported for bottom waters from the Oregon and Washington shelves (Lohan and Bruland, 2008). Initial dissolved oxygen concentrations measured in Experiment 1 (120-150 μM O_2; ERS2) and Experiment 2 (70-75 μM O_2; ERS3) correspond to bottom water oxygen values determined by water column profiles (Severmann, 2008; Severmann et al., In prep.). Dissolved Fe and oxygen concentration data from Experiment 1 and control cores C and D from Experiment 2, are used to estimate the benthic Flux of Fe and oxygen consumption rates. Where the change in Fe concentration over time is derived from the slope of a linear best fit to the dissolved Fe and oxygen concentration data, and the cross-sectional area of the multi-cores used in incubations is 0.0079 m^2. Organic carbon oxidation (C_{ox}) rates are then estimated using the O_2:CO_2 stoichiometry of remineralisation of −1.45 (Hammond et al., 1996). A summary of Fe flux, O_2 consumption and C_{ox} rates is presented in Table 4-3.

Table 4-3. Eel River shelf Fe fluxes derived from incubation studies. Positive values indicate enrichment in the overlying core-water. Negative values indicate depletion.

Site	Core	Fe flux (μmol m^{-2} day^{-1})	O_2 flux (mmol m^{-2} day^{-1})	C_{ox} flux (mmol m^{-2} day^{-1})
ERS2	A	7.5	-3.2	2.2
ERS2	B	5.6	-2.8	2.0
ERS2	C	5.5	-2.4	1.7
ERS2	D	0.4	-0.3	0.2
ERS3	A	1.7	-1.5	1.1
ERS3	B	17	-1.1	0.7
ERS2 mean		*4.8*	*-2.1*	*1.5*
ERS3 mean		*9.4*	*-1.3*	*0.9*
Mean ERS		*6.3*	*-1.9*	*1.3*

The mean flux of Fe from sediments to the overlying bottom waters determined for the Eel River shelf sediments by these incubation studies is within the range of values described by McManus et al. (1997) and Elrod et al. (2004) for the California continental shelf (0.2-11.0 μmol m^{-2} d^{-1}). The derived Fe flux correlates with the organic carbon oxidation rate as anticipated for a benthic Fe flux sustained by microbial sediment diagenesis. The ratio of Fe flux:C_{ox} is also similar to the range of values reported from previous studies on California margin sediments (Figure 4-9).

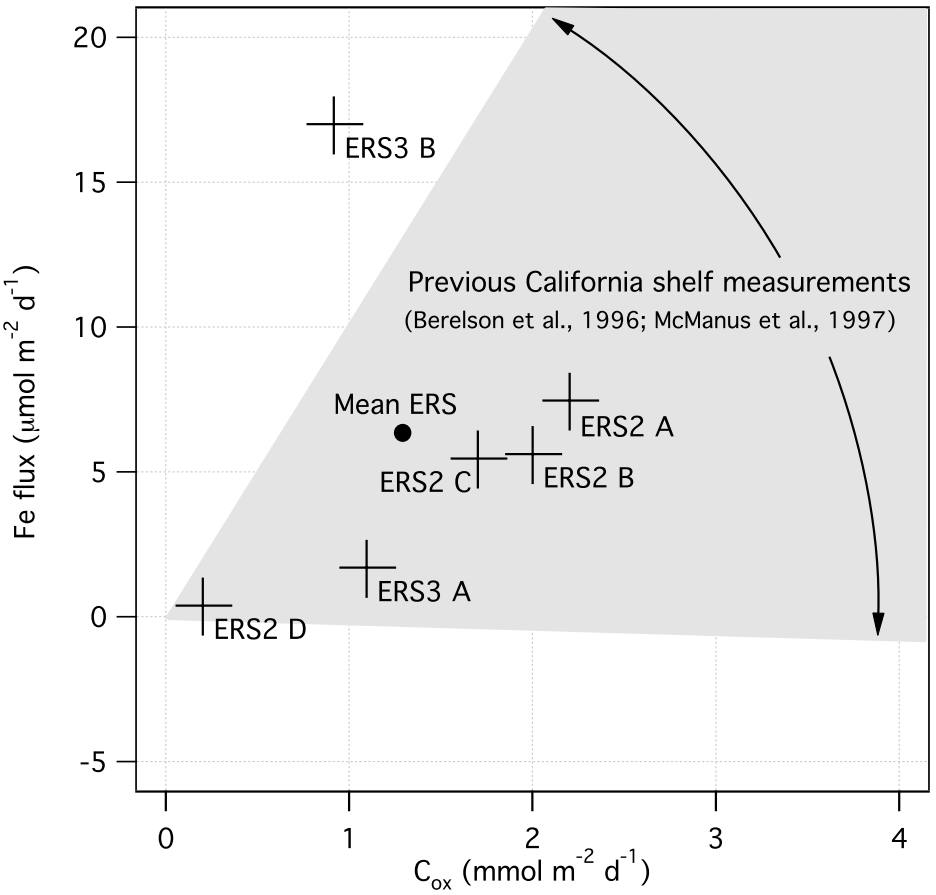

Figure 4-9. Fe flux determinations relative to organic carbon oxidation (C_{ox}) rate for Eel River shelf. Individual core incubations are shown by crosses, and the mean of results by a filled circle. The shaded area represents the range of values described by previous studies on the California margin.

4.3.2.1 Comparison of Eel River shelf flux determinations and the oxidation kinetics of Fe(II)

The flux of Fe to overlying bottom water determined by the sediment core incubations for the ERS is lower than that determined by in-situ benthic lander deployments during the same cruise (Severmann, 2008; Severmann et al., In prep.). Furthermore, both incubation determinations are lower than predicted by pore-fluid Fe concentration gradients (based on ERS1 pore-fluid data presented in Chapter 5, and the diffusive flux calculation used in Chapter 3, Section 3.4.5.1) (Table 4-4).

Table 4-4. Comparison of benthic Fe flux determinations for Eel River shelf

Site	Method of determination	Fe Flux (μmol m^{-2} day^{-1})
ERS2-3	Ex-situ core incubation	4.8-9.4
ERS2-3	In-situ benthic lander (*Severmann et al., In Prep*)	**17-13**
ERS1	Pore-fluid conc. gradient (*Chapters 3 and 5*)	**213**

Factors suggested to account for the discrepancy between flux determinations by in-situ, ex-situ and pore-fluid techniques include: (1) ineffective sample representation of bio-irrigating macro-fauna; (2) enhanced oxygen depletion in incubation chambers; and (3) a particulate and/or colloidal sink for dissolved Fe between the pore-fluids and overlying bottom water.

In-situ benthic chamber deployments have previously been shown to derive greater trace metal fluxes than measured in shipboard sediment core incubations (Berelson et al., 2003). These authors attribute the difference in flux magnitudes to the extent of bioirrigating macro-fauna sampled by the different techniques. The benthic chambers deployed on the Eel River shelf and used previously by Berelson et al. (2003) sample a sediment area of ~0.75 m^2 compared with just 0.008 m^2 in our incubation studies. Consequently, it has been argued that a significant community of bioirrigating macro fauna is excluded from the smaller core samples (Berelson et al., 2003).

The highest recorded Fe flux in this study was from site ERS3, core B. Fe concentration increased sharply by ~120 nM over a period of just 6 hours, inconsistent with the Fe flux/C_{ox} ratio common to the other ex-situ incubations. It is likely this is the result of a ventilating worm tube or burrow, injecting reduced sediment pore-fluid into the overlying core-water and elevating the Fe concentration of the sample (Emerson et al., 1984; Schlüter et al., 2000). A similar result is recorded in Experiment 1, core A, where the Fe concentration between 0 and 24 hours increases by 140 nM, then decreases by 30 nM Fe between 24 and 49 hours. These results indicate that important spatiotemporal dynamics accompany the flux of solutes from Eel River shelf sediments to the

bottom waters, and the ex-situ incubations in this study are unlikely to have comprehensively sampled this flux variability.

Oxygen depletion during incubation experiments will alter the oxidation kinetics of Fe(II) in the overlying core water. Temperature-dependent oxidation kinetics were used to estimate the half-life of Fe(II) in incubation results from ERS2 and from the in-situ lander data of Severmann et al., (In prep.). The oxidation of Fe(II) is composed of several parallel reactions involving various Fe(II) species (Chapter 1; Equation 1-1) and is best described by the pseudo-first-order rate constant, k_{ox}, as a function of pH, temperature and salinity (Equation 4-1), within the typical ranges of the modern ocean (Millero et al., 1987).

$$-d[\mathrm{Fe(II)}]/dt = k_{ox}[\mathrm{Fe(II)}] \quad (4\text{-}1)$$

The overall rate constant, k, is defined in Equation 4-2, and has been empirically derived from experimental data (Equation 4-3), where T = 273.15 + temperature (°C) and I = Ionic strength by Millero et al (1987). All concentrations are Molar, and the derived oxidation rate has units of Mol Fe(II) L^{-1} $60s^{-1}$.

$$-d[\mathrm{Fe(II)}]/dt = k[\mathrm{Fe(II)}][O_2][OH^-]^2 \quad (4\text{-}2)$$

$$\log k = 21.56 - 1545/T - 3.29I^{1/2} + 1.52I \quad (4\text{-}3)$$

Eel River shelf incubated seawater was estimated to have a pH of 7.5, based on Severmann et al., (In prep.) and previous studies on the northeast Pacific ocean upwelling regions (Lohan and Bruland, 2008). Using a bottom water temperature of 8°C, and salinity of 34‰, k_{ox} was estimated to be $4.3 \times 10^{-5} \pm 0.67 \times 10^{-5}$ s^{-1} (±1-SD). The estimated half-life of Fe(II) was derived using Equation 4-4

$$t_{1/2}\mathrm{Fe(II)} = \ln(2)/k_{ox} \quad (4\text{-}4)$$

The calculated Fe(II) oxidation half life is shown in hours as a function of dissolved oxygen concentrations on the Eel River shelf in Figure 4-10.

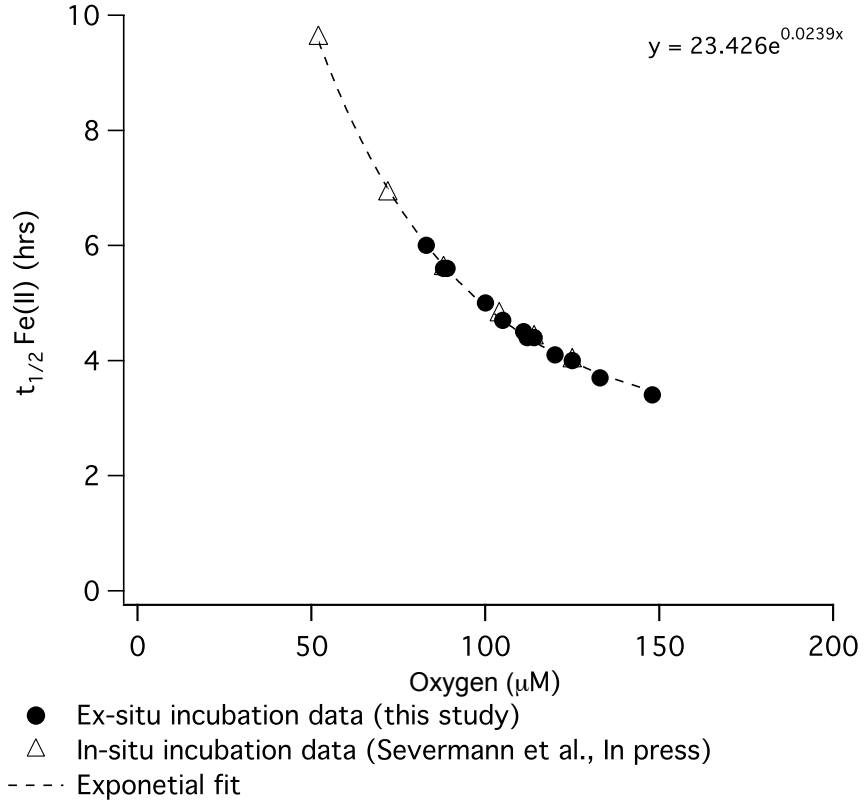

Figure 4-10. Estimated Fe(II) oxidation half-life ($t_{1/2}$) as a function of seawater oxygen concentration, based on ex-situ incubation experiments (this study) and in-situ lander deployments from the same site (Severmann et al., In Prep). The Fe(II) concentration is assumed to equal the total dissolved Fe (<0.45 μm) measured in the incubated seawater.

The range of overlying core-water oxygen concentrations measured in ex-situ incubation experiments (83-148 μM) corresponds to an Fe(II) oxidation half-life between 3.4 and 5.9 hours. When oxygen concentrations are depleted further to 52 μM in the in-situ lander incubation, the Fe(II) oxidation half-life nearly doubles to 9.6 hours. Changes in the oxygen concentration of overlying bottom waters will therefore have a drastic affect on the fate of Fe released from sediments, and these data support similar observations on the Oregon and Washington coasts (Lohan and Bruland, 2008) and in low-oxygen open ocean settings (Moffett et al., 2007). Organic compounds in seawater, such as Fe-binding ligands, are also suggested to slow the kinetics of Fe(II) oxidation (Millero et al., 1987; Statham et al., 2005), and are known to enhance the solubility of Fe(III) in seawater (Millero et al., 1995; Rue and Bruland, 1995; van den Berg, 1995; Wu and Luther III,

1995), perhaps contributing to the elevated Fe concentrations on the Eel River shelf.

The comparison of dissolved Fe and oxygen concentrations over time in bottom waters determined by ex-situ sediment incubations in this study with in-situ lander deployments (Figure 4-11), shows initial changes in Fe concentration are comparable for both methods. When oxygen becomes depleted below 70 μM in the in-situ measurements, the Fe concentrations increase more rapidly. This may result from slower rates of Fe(II) oxidation, or reduced oxygen penetration in surface sediments allowing for a greater Fe(II) flux. In addition, oxygen concentrations may be depleted below a critical threshold, where bioirrigating organisms enhance the ventilation of their burrows to maintain aerobic metabolism (Wohlgemuth et al., 2000), and in doing so increase the rate of Fe exchange with the low oxygen bottom waters.

If flux calculations based on the pore-fluid concentration gradient are greater than the flux determined by in-situ and ex-situ incubation experiments, it is possible that dissolved Fe diffusing up through the sediment column is accumulating in a phase that the <0.45 μm filtration method excludes from the sampling process. Such phases might include Fe adsorped to suspended particles, or Fe associated with aggregating organic colloidal material near the sediment-seawater interface, which is greater than 0.45 μm in size (Figure 4-12). These phases involved in the benthic cycling of Fe may facilitate a return flux of oxidised Fe to the surface sediments. This is consistent with the understanding that ex-situ and in-situ studies will record the net result of Fe inputs and removal from the overlying bottom-water during the incubation period. Additional uncertainty associated with the pore-fluid flux derivations are discussed in Chapter 3 (Section 3.4.5.1).

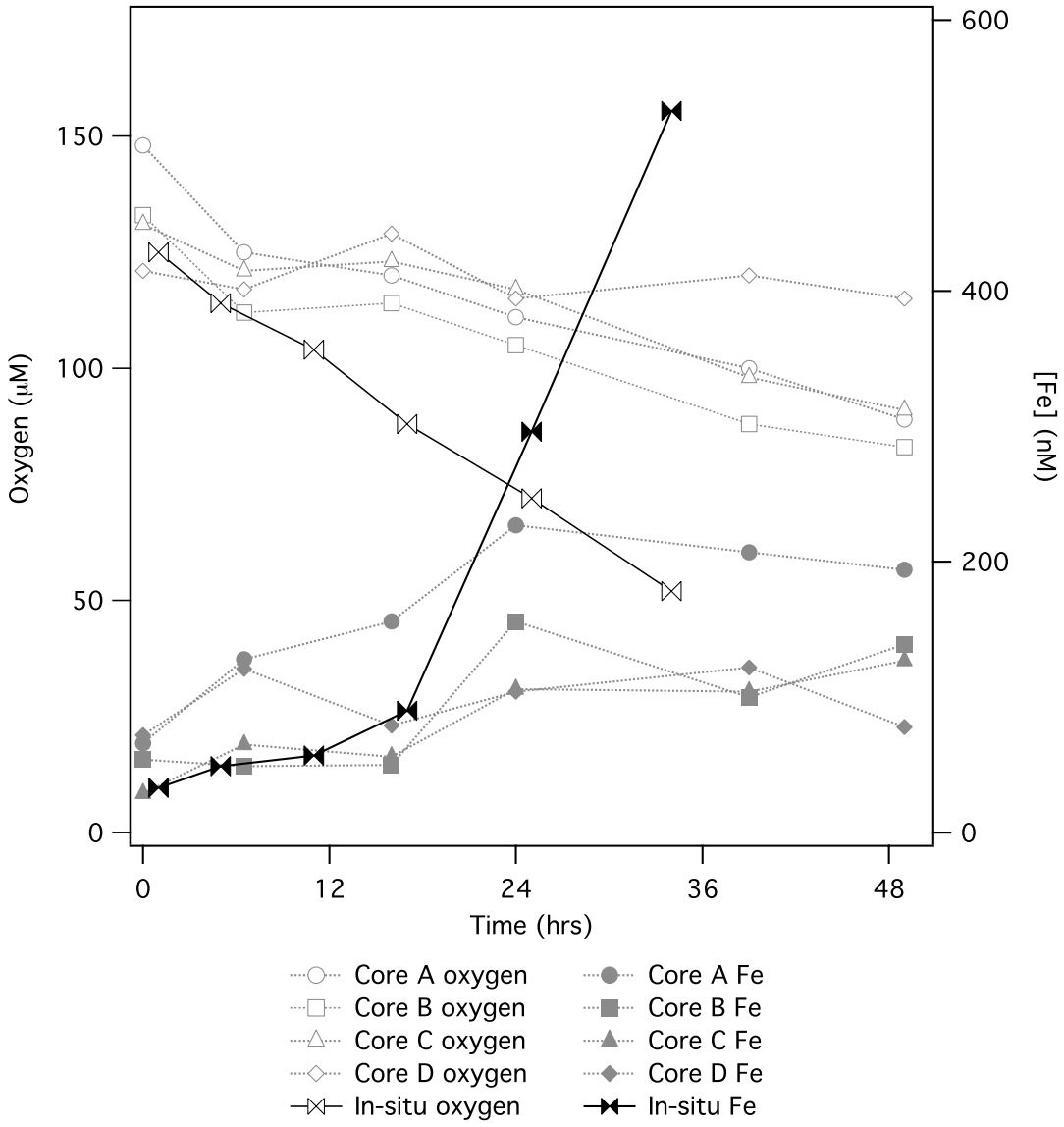

Figure 4-11. Comparison of dissolved Fe and oxygen concentrations over time in Eel River shelf bottom waters, determined by ex-situ sediment incubations (Cores A-D; this study), and in-situ lander deployments (Severmann et al., In Prep.).

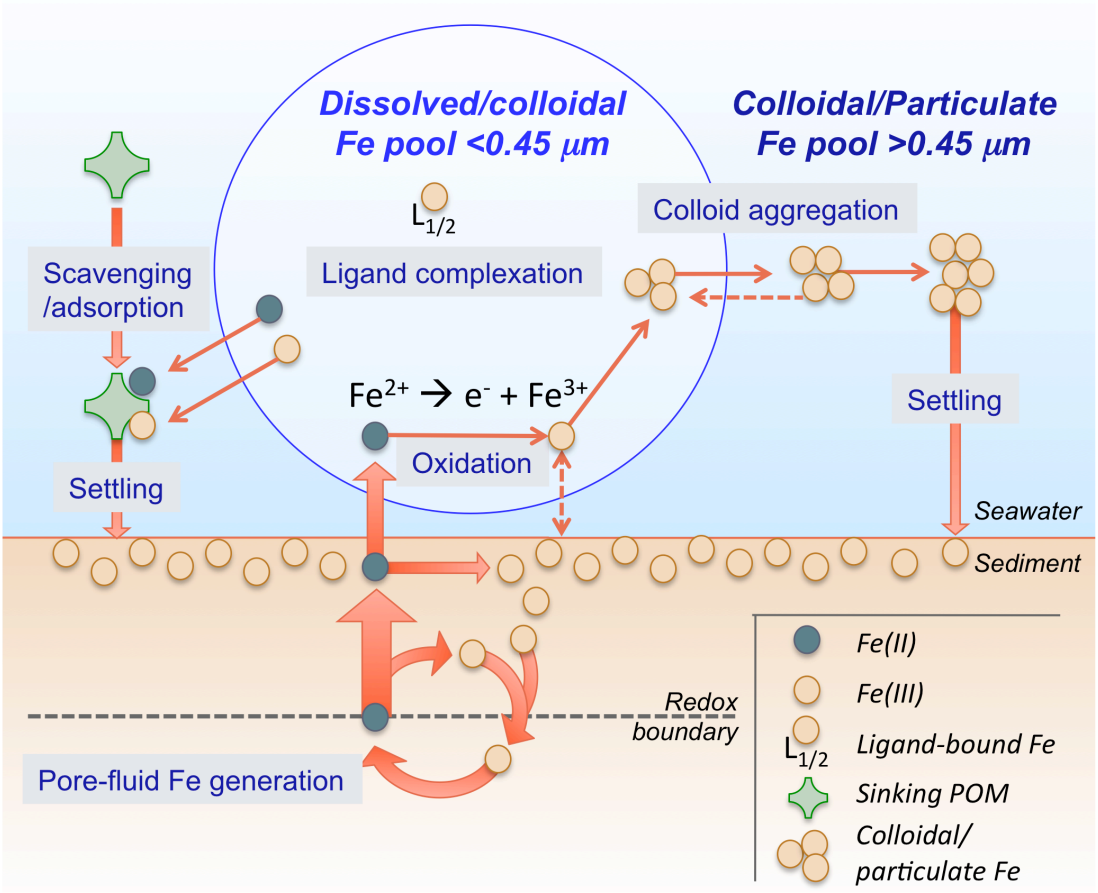

Figure 4-12. The cycling of Fe between dissolved, colloidal and particulate phases in seawater overlying a sedimentary Fe flux. The operationally defined 'dissolved' size fraction (<0.45 μm) is likely to contain a spectrum of truly aqueous Fe, ligand complexes and small colloidal phases, which are subject to exchange with a larger colloidal/particulate Fe pool.

4.3.2.2 Impact of biocide additions on Eel River shelf incubations

There is evidence for a reduction in the Fe flux associated with the addition of a biocide to cores C and D in Experiment 2. The use of formaldehyde is assumed to be sufficient to stop the bio-irrigation of organisms in the surface sediments. Control cores A and B demonstrate the likely significance of macro-fauna in enhancing the Fe flux from Eel River shelf sediments as discussed in the previous section.

4.3.2.3 Impact of sediment re-suspension on Fe flux

The re-suspension of surface sediment during overlying core-water agitation coincides with the reduction of Fe concentration in the overlying core-water in 3 of 4 incubations. It is inferred that organic and/or inorganic particles entrained during re-suspension may adsorb dissolved Fe phases and promote the scavenging of Fe in the core-water. The fate of scavenged Fe is unknown. Fe may be removed from the water column by settling to the sediment, or it may remain in suspension in a colloidal fraction larger than 0.45 μm in diameter. The concentration of Fe does not appear to be scavenged below ~15 nM during re-suspension, suggesting a mechanism of stabilisation exists that prevents scavenging to concentrations below this value. After re-suspension, the dissolved Fe concentration in cores A and B increases towards the end of the experiment. This may either reflect the desorption of Fe from, or disaggregation of, colloidal phases greater than 0.45 μm, or the continued supply of dissolved Fe from the pore-fluids.

4.3.3 Montserrat incubation experiments

Two experiments were conducted on Montserrat sediments from sites JC18_9 and JC18_18 (Section 4.1.1.2). Given the high pore-fluid Mn concentrations indentified in tephra-dominated sediments in this region (Chapter 3), the method used for analysis of incubated seawater samples in Montserrat was modified from that used for the Eel river shelf, to allow for Mn determination. This method is described in Chapter 2, Section 2.4.1. Two cores from each site (tephra-dominated JC18_9, and pelagic-dominated JC18_18) were used for the study of Fe, Mn and oxygen concentration over time in 'undisturbed' sediment-seawater incubations (Experiments 1 and 2), and agitation of the sediment-seawater interface was assessed in 1 core from each site (Experiment 3).

4.3.3.1 Experiment 1: 'Un-disturbed' pelagic-dominated sediment-seawater incubations

Cores B and D record initial Mn concentrations between 1000 and 1300 nM decreasing to ~20 nM after 72 hours (Figure 4-13). The concentration of Fe broadly decreases over time from 85 and 25 nM, in cores B and D respectively, to ~20 nM after 72 hours.

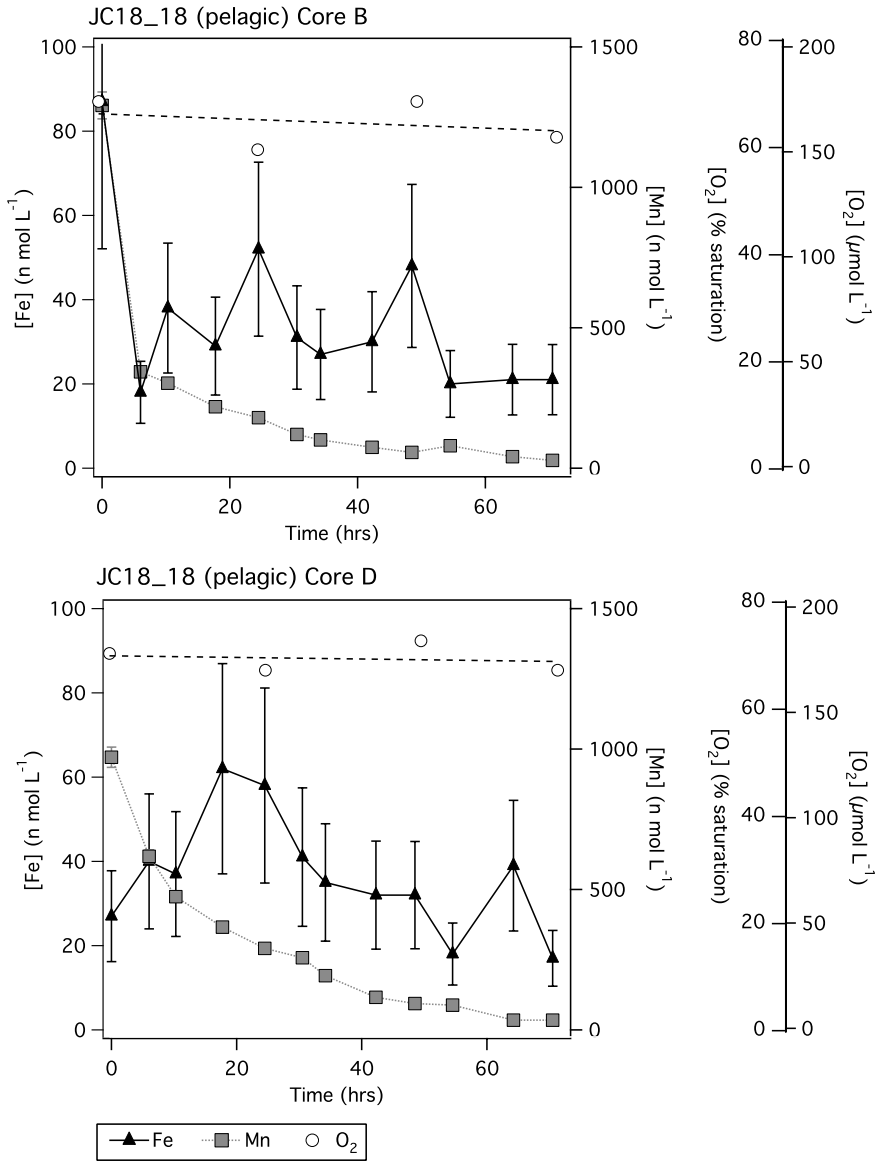

Figure 4-13. Montserrat incubation Experiment 1: Dissolved Fe, Mn (<0.45 μm) and oxygen concentrations in overlying core-water, over a period of 72 hours, during which overlying core-water was subject to gentle recirculation.

4.3.3.2 Experiment 2: 'Un-disturbed' tephra-dominated sediment-seawater incubations

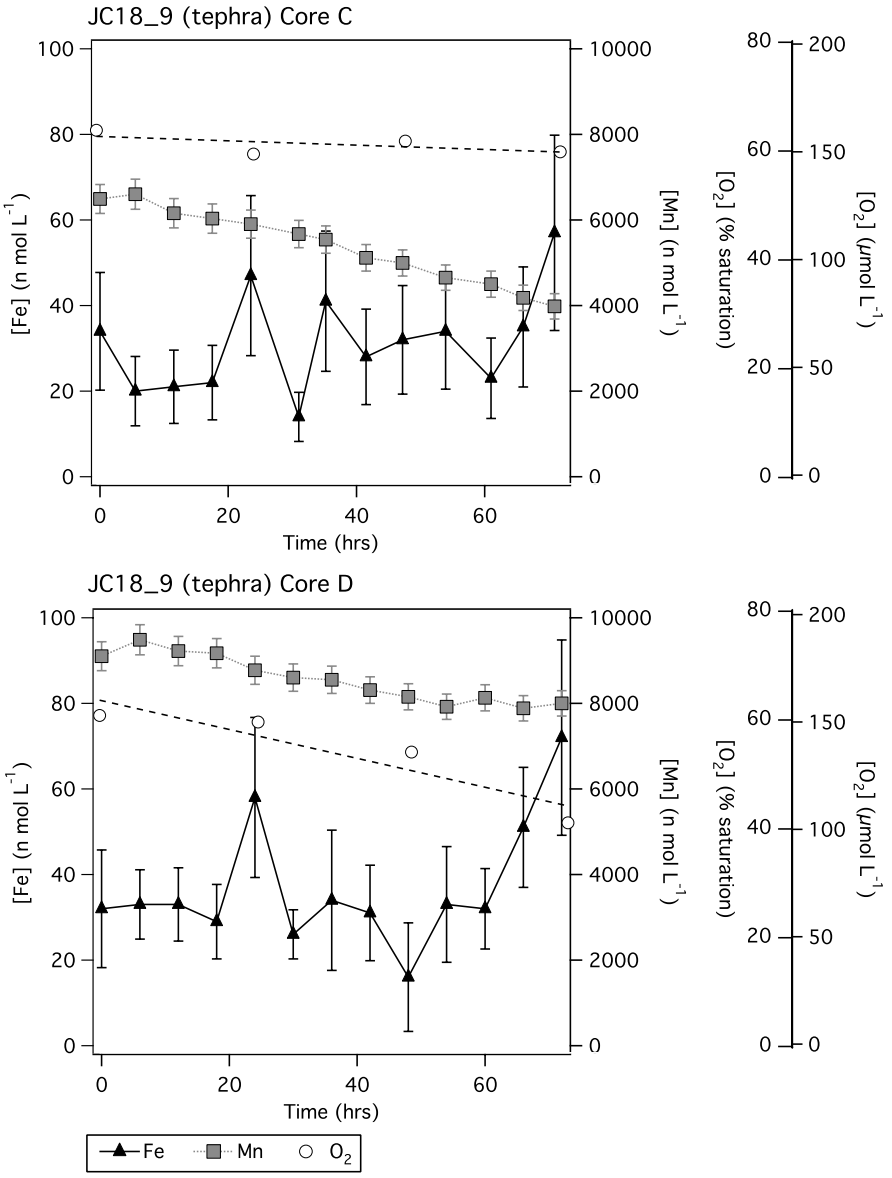

Figure 4-14. Montserrat incubation Experiment 2: Dissolved Fe, Mn (<0.45 μm) and oxygen concentrations in overlying core-water, over a period of 72 hours, during which overlying core-water was subject to gentle recirculation.

Cores C and D are characterised by very high initial Mn concentrations (6500-9000 nM) that decrease during the experiment (4000-8000 nM after 72 hrs) (Figure 4-14). The concentration of Fe increases from ~32 nM to 58 nM (Core C) and 72 nM (Core D) after 72 hours. However, variations in Fe concentration less than 30 nM are difficult to distinguish from analytical uncertainty.

4.3.3.3 Experiment 3: Incubated Montserrat sediment-seawater re-suspension

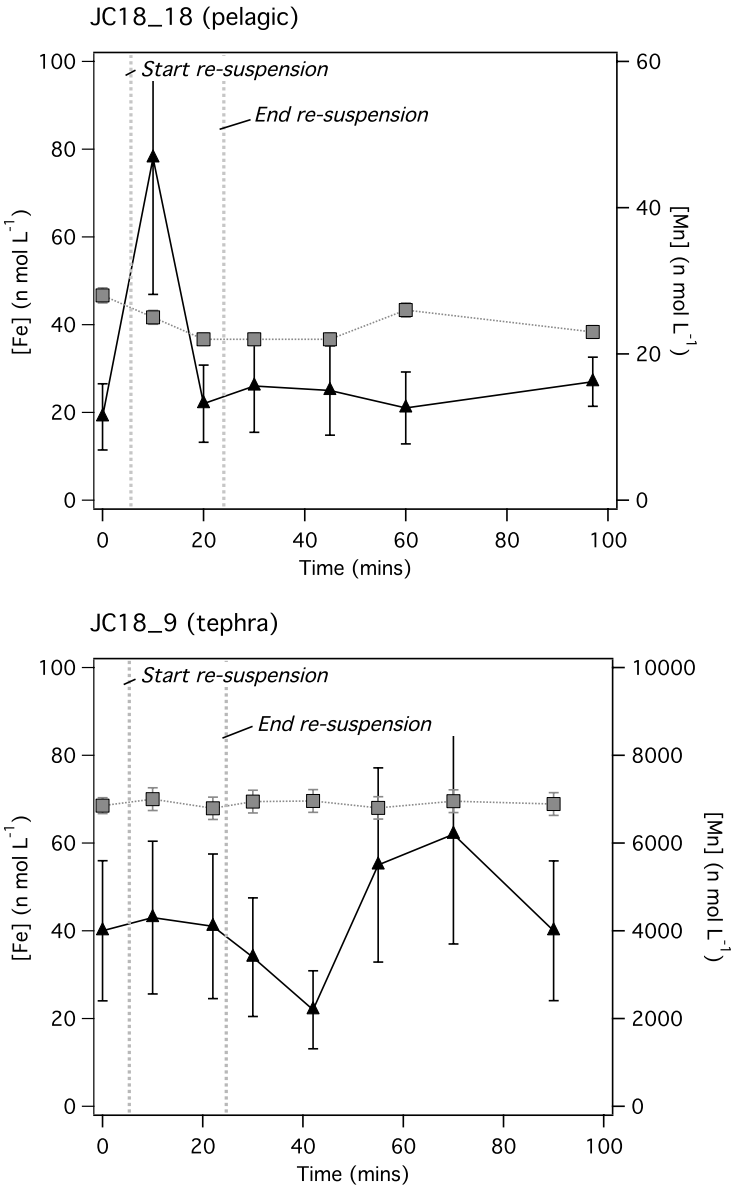

Figure 4-15. Montserrat incubation Experiment 3: Dissolved Fe and Mn (<0.45 µm) in overlying core-water, over a period 90 minutes. Overlying core-water was agitated sufficiently to visibly enhance sediment turbidity for a period of 20 minutes.

A 20-minute period of core-water agitation that produced visibly enhanced sediment turbidity, resulted in a temporarily increased dissolved Fe concentration from 20 to 78 to 22 nM in incubated core-water over pelagic-dominated sediment (Figure 4-15). Over the same period, Mn concentration decreased slightly from 28

to 22 nM. Core-water Fe and Mn concentrations in did not respond to the induced re-suspension of tephra-dominated sediment.

4.3.4 Evaluation of Montserrat incubation experiment results

Typical ocean concentrations for dissolved Fe and Mn are ≤ 1.0 nM (Statham and Burton, 1986; Landing and Bruland, 1987; Sedwick et al., 1997). Elevated nano-molar Fe and Mn concentrations in waters over-lying shelf sedimentary sources are well documented (Sedwick et al., 1997; Johnson et al., 1999; Bucciarelli et al., 2001; Lam et al., 2006), and despite comparatively few sampling efforts, observations of elevated nano-molar Mn concentrations in deep-sea waters have also been made (Statham et al., 1998). However, there has been no previous study of Fe or Mn in seawater close to the sediment surface in the Montserrat region, or any other volcaniclastic sediment site. The concentration of Fe and Mn in overlying core water at the start of these incubation studies was 25-84 nM Fe and 1-1.2 μM Mn at the pelagic site. In the tephra-dominated site starting concentrations were 32-35 nM Fe and 6.5-8.8 μM Mn. Both Fe and Mn concentrations are significantly higher than typical open-ocean values, which suggest (1) the sediment pore-fluids are a source of Fe and Mn to the overlying bottom water and/or (2) the incubated seawater Fe and Mn concentrations are artificially elevated.

Pore-fluid Fe and Mn concentration gradients from site JC18_33 were used to calculate the diffusive flux of Fe and Mn from tephra-dominated sediments in Chapter 3 (Section 3.4.5.1). Based on these fluxes, an increase in the overlying core-water concentration of Fe and Mn is expected to be ~15 nM Fe and ~1500 nM Mn, after 72 hours. The mean standard deviation of repeat Fe analyses is equal to the predicted increase in Fe concentration during the incubation experiment, and it is therefore beyond the resolution of these data to accurately evaluate the predicted Fe flux. The accuracy of Mn analyses is sufficient for evaluation of the flux prediction, however the end of the incubation period is characterised by a deficit in Mn relative to its initial concentration. Removal processes therefore dominate incubation experiments 1 and 2, and in order to evaluate the balance of input and removal processes in the core-water, the oxidation kinetics of Fe and Mn need to be assessed.

It is likely that the overlying core-water was artificially enriched in dissolved Fe and Mn at the start of the incubation experiment. Efforts were made to ensure the incubation units themselves did not contaminate the core-water sample (Section 4.2.1), and Eel River shelf experiments demonstrate the elevated Fe and Mn concentrations are limited to the Montserrat study. Pore-fluid Fe and Mn profiles from neighbouring tephra-dominated site JC18_33 (Chapter 3, Section 3.4.2), testify to the abundance of dissolved Fe (up to 20 μM), and Mn (up to 200 μM), close to the sediment surface. Shipboard observations also record sediments of the debris flow depocentre to be poorly consolidated and permeable with sediment-porosity of ~50% (Hembury et al., 2009). Friction between sediment and the core-tube during sampling can lead to the partial compaction of the sediment core and subsequent loss of pore-fluid from soft sediments to the overlying water column (Zheng et al., 2002). The overlying core-water may therefore be subject to contamination by displaced pore-fluids being driven out of the sediment by compaction either during push-core sub-sampling of open box cores (Section 2.1), or by sediment compaction during box-core recovery.

We can test the push-core induced pore-fluid displacement hypothesis for the tephra-dominated site by calculating the amount of Fe and Mn that would be displaced from the JC18_33 pore-fluid profiles using a standard sediment compaction factor of 0.9 determined by Zheng et al. (2002). A sediment compaction factor of 0.9 means the 30 cm core in JC18-33 would have been approximately 3.3 cm longer when in-situ. With a 10 cm diameter core-tube, this corresponds to a sediment volume deficit of 260 cm^3, and using the porosity estimate of 0.5, a displaced pore-fluid volume of 130 cm^3. Using the depth-averaged concentration for the surface 0-3.5 cmbsf of Fe and Mn from JC18_33, this yields a mean expelled pore-fluid concentration of 10 and 64 μM Fe and Mn respectively, and an elevated overlying core-water concentration of 1.3 μM Fe and 8.3 μM Mn.

Despite not knowing the true amount of sediment compaction associated with the sampling of incubation cores, and relying on near surface pore-fluid Fe and Mn concentrations from an adjacent sampling site, this approach substantiates the pore-fluid displacement hypothesis by describing the initial Mn concentrations observed in the tephra-dominated incubation experiments. The

observed Fe concentrations are significantly lower (maximum 85 nM) than that predicted by the pore-fluid displacement. However, this might be attributed to differences between the pore-fluid Fe and Mn concentrations measured in JC18_33 compared with the true pore-fluid Fe and Mn concentrations at JC18_9, in addition to differences in the oxidation kinetics of Fe and Mn, which will lead to more rapid removal of Fe from the overlying core-water. This idea is explored further in the next section.

4.3.4.1 Oxidation kinetics of Fe in Montserrat incubation experiments

Using the calculation described in Equations 4-1 to 4-4 (Section 4.3.2.1) the Fe(II) oxidation half-life in Montserrat incubation experiments has been determined. The calculation was modified for Montserrat bottom water pH (8.0), temperature (8 ºC) and salinity (35‰). The corresponding oxidation rate constant, k_{ox}, was 6 $x10^{-4} \pm 0.4\ x10^{-4}\ s^{-1}$ (±1-SD). For the range of oxygen concentrations measured in Montserrat incubation experiments (103-174 μM), the Fe(II) oxidation half-life equates to 0.5-0.3 hours. This is significantly shorter than the Fe(II) oxidation half-life calculated for the Eel River shelf (Figure 4-16) and previous low-temperature, low-pH hypoxic shelf environments (Lohan and Bruland, 2008), yet is similar to values reported for the European continental margin in oxygenated waters with an equivalent pH (Ussher et al., 2007).

An Fe(II) oxidation half life of just 0.3 hours could reduce an overlying core-water Fe concentration of 1.3 μM (estimated contamination) to 20 nM after just 2 hours. The time between core recovery and initial core-water sampling was ~2-3 hours, and is therefore consistent with the hypothesis that experiments were subject to pore-fluid displacement during sediment sampling. The corresponding rate of Fe(II) oxidation is greater than the predicted flux from the pore-fluids, so it would appear the sediments are not a significant source of Fe to bottom waters. However, if the concentrations of Fe measured in the incubation experiments were controlled by Fe(II) solubility alone, then they would be much lower than were observed. Therefore the dissolved Fe concentrations probably reflect a portion of stabilised Fe(III) - as outlined earlier in Figure 4-12 - that originated from a diffusive flux.

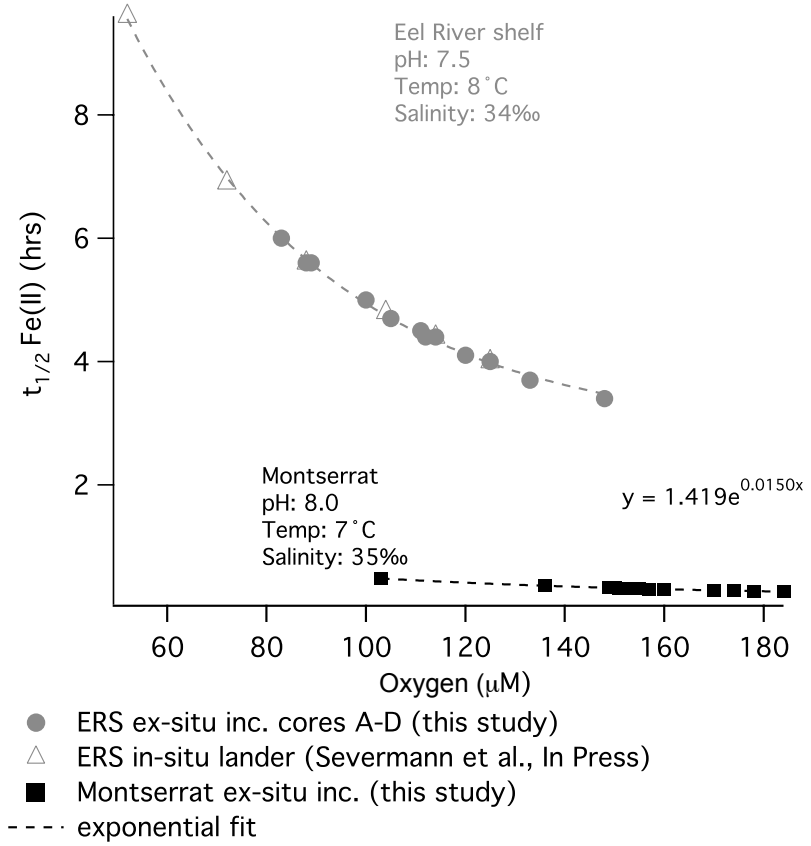

Figure 4-16. Estimated Fe(II) oxidation half-life ($t_{1/2}$) as a function of seawater oxygen concentration for Montserrat ex-situ incubation experiments. The ex-situ and in-situ determinations for the Eel River shelf (Figure 4-10) are included for comparison.

4.3.4.2 Oxidation kinetics of Mn in Montserrat incubation experiments

In order to assess the rate of Mn depletion observed in Montserrat Experiments 1 and 2, a similar equation can be used to derive the Mn(II) oxidation half-life (Equation 4-4), where the oxidation constant, k_{ox}, is described by the homogenous rate Equations 4-5 and 4-6, after von Langen et al. (1997).

$$d[Mn(II)]/dt = k[Mn(II)][O_2][OH^-]^2 \quad (4\text{-}5)$$

$$d[Mn(II)]/dt = k_{ox}[Mn(II)] \quad (4\text{-}6)$$

Where k (1.3×10^{12}) has been derived from empirical data for the appropriate pH, temperature and salinity, k_{ox} becomes $3.3 \times 10^{-6} \pm 0.4 \times 10^{-6}$ s^{-1} (±1-SD), and the corresponding half-life of Mn(II), 9.5 years, similar to that reported for Mn in the

open Pacifc Ocean (Landing and Bruland, 1987) and for some deep-sea waters (Johnson et al., 1996). The rate of Mn removal identified in our incubation experiments suggests the homogenous rate equation over-estimates the true half-life of dissolved Mn measured in the experiments by 2-3 orders of magnitude. Other studies have reported similar discrepancies when Mn(II) concentrations are high (μM) in sediments (Burdige and Gieskes, 1983) and in coastal seawater (Sunda and Huntsman, 1990), and attribute bacterial mediation of Mn(II) oxidation and the auto-catalytic effect of MnO_x formation, which produces rate-enhancing surface sites for the oxidation of Mn(II). Another approach may therefore be needed to assess the observed Mn concentrations in Montserrat incubation experiments.

Based on previous work (Morgan, 1967), Yeats and Strain (1990) derived a rate constant (k = 6.5 x10^{-3} μM^{-2} d^{-1}) for the oxidation of Mn(II) based on coastal and deep-sea field data (Equation 4-7), which assumes a relatively constant seawater pH (8.0) and bottom water temperature (8 ºC).

$$d[Mn(II)]/dt = k[Mn(II)][MnO_x][O_2] \quad (4\text{-}7)$$

MnO_x refers to the concentration of particulate Mn. However, particulate Mn concentration was not determined for these incubation experiments, making an accurate calculation of the Mn(II) oxidation rate using Equation 4-7 unfeasible. Nonetheless, assuming Mn(II) concentration is primarily controlled by its oxidation rate, we can rearrange Equation 4-7 in terms of $[MnO_x]$ (Equation 4-8):

$$[MnO_x] = (d[Mn(II)]/dt)/(k[Mn(II)][O_2]) \quad (4\text{-}8)$$

The concentration of particulate Mn necessary to account for the observed rate of Mn(II) oxidation (d[Mn(II)]/dt) can then be predicted for each incubation experiment (Figure 4-17).

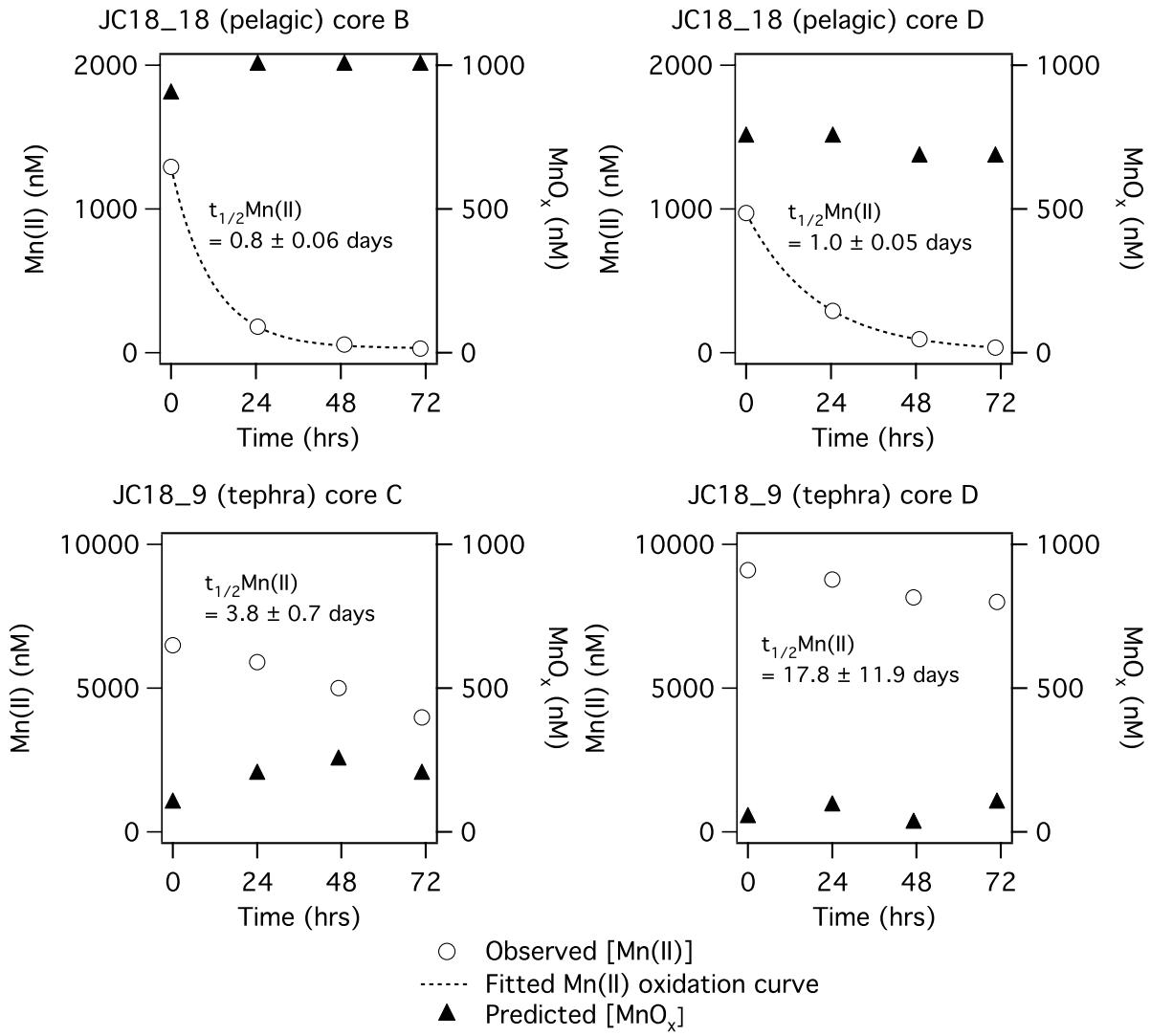

Figure 4-17. Comparison of predicted particulate Mn concentrations ([MnO_x]) during Montserrat incubation experiments. Based on the heterogeneous oxidation of Mn(II) following Yeats and Strain (1990), where the oxidation rate of Mn(II) has been fitted to observed [Mn(II)] over time. The corresponding mean Mn(II) oxidation half-life ($t_{1/2}$Mn(II)) is derived in days (± 1-SD).

This results in a range of particulate Mn concentrations from 30-250 nM for the tephra-dominated incubations to 650-1000 nM for the pelagic dominated incubations. These are comparable to concentrations found in coastal shelf waters (Yeats and Loring, 1991) and the open ocean (Landing and Bruland, 1987), yet indicate very different Mn(II) oxidising conditions between these sites, with corresponding mean oxidation half-lives of 0.8-1.0 days for the pelagic-dominated site (JC18_18) and 3.8-17.8 days for the tephra-dominated site (JC18_9).

Differences in bottom water particulate Mn concentration might result from differences in the surface sediment composition between the slower bottom water Mn(II) oxidation half lives due to low particulate Mn concentrations. Alternatively the concentration of dissolved Mn observed in the tephra-dominated incubation experiments reflects the net contribution of Mn removal by oxidation and Mn addition from a pore-fluid flux to the overlying core-water. The predicted increase in Mn concentration in tephra-dominated incubation Experiments of 1500 nM (after 72 hours), calculated from the JC18_33 pore-fluid gradient (Section 3.4.5.1), is therefore difficult to accurately assess due to the over-printing of Mn addition and removal processes in these experiments.

Assuming dissolved Mn concentration in incubated bottom waters is controlled by the balance of sedimentary flux (pore-fluid derivation = 45 μmol m^{-2} d^{-1}) and oxidative removal (upper estimate of $t_{1/2}$Mn = 0.8 days), an estimate of the net contribution to bottom waters concentration can be made: 27 μmol m^{-2} d^{-1}. Therefore a substantial portion of Mn diffusing from tephra-rich Montserrat sediment pore-fluids is likely to be entrained in the overlying bottom waters, and may be a source of Mn to hydrogenic deposits characteristic of island arc regions (Cronan, 1977).

4.3.4.3 Impact of Montserrat sediment re-suspension on core-water Fe and Mn concentrations

Re-suspension of the pelagic-dominated site resulted in a temporary increase in the concentration of Fe (+60 nM), which decreased to the initial concentration of Fe before the period of re-suspension had ended. It is inferred that the re-suspension of surface sediments is capable of entraining dissolved Fe into the overlying core-water for a matter or minutes, before Fe is effectively oxidised and precipitated and/or scavenged from the dissolved phase within an equally short period of time. The re-suspension of tephra-dominated sediments produced no analytically significant changes in the concentration of Fe or Mn in the overlying core water. It is inferred that the pelagic-dominated surface sediments contain Fe phases more susceptible to Fe dissolution during re-suspension, albeit before subsequent precipitation and/or scavenging.

4.3.5 Implications of experiments for Fe inputs to the oceans.

Microcosm studies on the Eel River shelf have substantiated evidence for the release of Fe from continental shelf sediments to the overlying water-column with a mean Fe flux determination of 6.3 ± 5.9 μmol m^{-2} d^{-1}. Bioirrigation is believed to play an integral role in the release of Fe from Eel River shelf sediments, and is inferred to enhance Fe flux measurements by ~10 times. The comparison of in-situ and ex-situ flux determinations suggests bioirrigation by macro-fauna may be sensitive to enhanced oxygen depletion.

The comparison of the Eel River shelf and Montserrat regions highlights the pH and oxygen dependence of Fe(II) oxidation rates. The relatively low pH and bottom water oxygen concentration of the Eel River shelf extends the oxidation half-life of Fe from minutes to hours compared with the deep-ocean, and may account for the scarce evidence to date of sedimentary Fe inputs from oxygen-rich deep ocean sediments. Despite the very shallow oxygen penetration (<0.5 cmbsf) in the Montserrat region, because bottom waters are nearly saturated with respect to oxygen (~280 μM), Fe will be rapidly re-oxidised close to the sediment surface. Oxygen concentrations in Eel River shelf bottom waters and other continental margin sites of the North East Pacific Ocean are often depleted to between 10 and 100 μM (Cai and Reimers, 1995; Berelson et al., 2003; Lohan and Bruland, 2008; Severmann, 2008). Fe inputs are therefore likely to be maintained for significantly longer periods, allowing for greater vertical mixing in the water column.

The data presented in this study show neither a significant net increase or decrease in dissolved Fe and/or Mn concentrations in overlying sediment core-water during sediment re-suspension episodes. Re-suspended sediments were from the oxic-surface millimetre at the seawater interface and entrained in oxygenated overlying core-water, thus the absence of a significant Fe flux may be expected. Episodic depletion (Eel River shelf) and enrichment (Montserrat-pelagic) in Fe concentration during core-water agitation indicates Fe is being cycled between dissolved, colloidal and particulate forms close to the sediment surface.

4.3.6 Uncertainties affecting incubated flux estimates

Oxygen depletion during 'closed-system' incubation studies can result in enhanced trace metal and nutrient fluxes over time (Berelson et al., 2003). It is argued that this approach is valid for observing a snap-shot of flux magnitudes during short incubation periods (24-48 hours on the Eel River shelf, for example), but for prolonged incubation studies the reduction in oxygen is likely to substantially impact Fe and Mn cycling in the bottom water, and over-estimate the true flux of Fe and Mn. However, oxygen concentration is also a difficult parameter to control; 9 out of 16 incubated cores experienced intermittent oxygen contamination of the overlying core-water between sampling points, suggesting a deficiency in the design of experimental apparatus. Oxygen contamination may have contributed to the loss of Fe from the dissolved Fe pool by enhancing precipitation and/or adsorption to apparatus surfaces during the sampling procedure. Thus the fluxes derived from the incubation studies may underestimate their true magnitude. Without knowledge of the true speciation of Fe and Mn in the overlying core-water, it remains infeasible to accurately describe their oxidation rates.

Changes in pressure and temperature (albeit limited to ~10 ºC) during sediment core recovery may affect microbial and/or bioirrigating macro-faunal physiology in the sediment cores. Speculatively, the dysfunction of bioirrigating organisms would decrease the apparent Fe and Mn flux, as well as reduce the amount of respiration occurring in the bottom waters. The restriction of organic carbon supply to the benthos might further impact biological functioning in the sediment core, and influence the flux observations. As discussed in Section 4.4.1, the area of sediment sampled by multi-core may poorly represent the macro-faunal community intrinsic to sediment processing on the Eel river shelf.

It is likely that a flux of Mn from the tephra-dominated site was contributing to the overlying core-water concentrations during the 3-day incubation period. However, the duration of this flux remains unknown. If the redox boundary depth was altered by compaction during sediment sampling, it will eventually re-equilibrate, and the associated Mn flux may decrease accordingly. These changes are likely to affect calculations of the flux magnitude, rather than dispute the existence of a significant flux.

4.4 CONCLUSIONS

In this chapter, the design, construction and field-testing of a surface-sediment and seawater incubation unit was executed. The reproducibility of incubated core-water [Fe], [Mn] and [O_2] was evaluated, and is consistent with the inherent heterogeneity of natural sediment systems. This study demonstrates low-cost ex-situ incubation experiments can replicate benthic Fe flux measurements made by in-situ benthic chambers. Fe fluxes on the Eel River shelf (6.3 ± 5.9 μmol m^{-2} d^{-1}) correlated with organic carbon oxidation rates, and support the view that benthic Fe flux is controlled by sediment respiration and DIR in shelf sediments, and that shelf sediments are important vectors of Fe to seawater.

The Fe flux-enhancing role of biota has also been highlighted. Biocide addition experiments suggest bioirrigation may increase the Fe flux of Eel River shelf sediments by up to 10 times, and account for high temporal and spatial heterogeneity of Fe flux observations. Changes in bioirrigation, oxidation kinetics and the cycling of Fe between dissolved and particulate phases are likely to account for discrepancies between ex-situ, in-situ and pore-fluid methods of flux derivation (in addition to the uncertainties previously discussed in Chapter 3: Section 3.4.5.1).

The low pH (7.5) and oxygen concentrations (60-120 μM) on the Eel river shelf account for the relatively long oxidation half-life estimated for Fe(II) ($t_{1/2}$ 3.6-5.9 hrs) and are likely to permit greater vertical mixing of sedimentary Fe inputs than Fe diffusing from Montserrat sediments ($t_{1/2}$ 0.3-0.5 hrs) and other oxygenated deep-ocean waters. However, a benthic Fe flux to bottom waters in the Crozet region of the Southern Ocean in unlikely to share the removal rate of Fe in Montserrat bottom waters, due to the dominantly colloidal composition of dissolved Fe in the Crozet pore-fluids (Chapter 3: Section 3.4.5.2).

Contamination of Fe and Mn in Montserrat incubation experiments from pore-fluids displaced during core-sampling has been quantitatively demonstrated, and indicates susceptibility of bottom waters to compaction-induced episodes of Fe and Mn advection. The rate of Mn(II) oxidation in incubation studies remains uncertain, due to unknown particulate Mn (MnO_x) concentrations. The

concentration of MnO_x is inferred to be ~5 times less in tephra-rich incubations compared with pelagic-rich incubations, or else the flux of dissolved Mn contributes to the dissolved Mn concentration at the tephra-rich site, and accounts for the apparently slower oxidative removal of dissolved Mn. A conservative estimate based on the highest Mn(II) oxidation rate for the diffusive flux of dissolved Mn from tephra-rich sediments is ~27 μM m^{-2} d^{-1}. Thus tephra deposits dominated by inorganic sediment diagenesis are shown to be a potentially significant source of dissolved Mn to bottom waters.

Re-suspension of oxic surface sediment (<1 mmbsf) indicates particles entrained in bottom waters may adsorb dissolved Fe phases, and promote the scavenging of Fe in the core-waters from the Eel River shelf. This Fe may be removed from the water column by settling to the sediment, or it may remain in suspension in a size fraction greater than 0.45 μm, where it may be transported to other ocean regions. The concentration of dissolved Fe was not scavenged below ~15 nM during re-suspension, suggesting a mechanism of stabilisation may exist that prevents scavenging to concentrations below this value. Disaggregation of colloids and/or desorption from phases greater than 0.45 μm, may account for increasing Fe concentrations after re-suspension on the Eel River shelf, and during re-suspension in pelagic Montserrat sediment. The dissolved-particulate exchanges of Fe during and after re-suspension of oxic sediments attest to the poorly quantified significance of these processes in bottom waters close to sediments.

4.4.1 Recommendations for future incubation studies

Future designs for shipboard sediment incubation experiments should consider the following recommendations:

1. Consider the importance of time-scales of diagenetic processes and the benefits of 'open' versus 'closed' experimental designs - This study has identified the importance of limiting variation to natural environmental parameters as much as possible. On the Eel River shelf a 'closed' experimental design helped maintain the low oxygen conditions found in bottom waters in this region, but flux derivations were subject to alteration if the incubation period persisted long enough to drastically

reduce oxygen concentrations. In Montserrat, sediment incubation experiments may have benefitted from a longer incubation period to distinguish sampling-induced advective flux artefacts from diffusive fluxes, however a much longer 'closed' experiment duration may have lowered oxygen concentrations unrealistically compared with the natural bottom water conditions.

2. Methods for the determination of Fe and Mn speciation. A knowledge of Fe and Mn speciation would allow for more accurate quantification of the diffusive flux magnitudes and improve understanding of the fate of Fe and Mn entrained in the overlying core-water.

3. Methods for the determination of particulate Fe and Mn concentrations. As above, knowledge of the particulate Fe and Mn concentrations in the overlying core-water would improve calculations of oxidation rates, and interpretation of Fe and Mn cycling between truly dissolved and particulate phases.
4. Real-time sample analyses. Sampling resolution in this study was limited by operational logistics, and sampling itself appeared to induce intermittent oxygen contamination of the incubations, with potential consequences for episodic Fe and Mn oxidation rate changes. Real-time analysis (such as a flow through design) would allow for better identification of data outliers, and improve correlation between oxygen, and particulate and dissolved Fe and Mn cycling.

5. Method for quantification of sediment re-suspension. This study shows sediment re-suspension experiments need to consider variations to the physical properties of different sediments, their susceptibility to re-suspension and the impact of this processes of Fe and Mn fluxes. In order to correlate Fe and Mn fluxes with sediment re-suspension, a means for quantifying the amount of material re-suspended is essential.

6. Number of repeat incubation studies. In order to derive statistically significant results, the number of repeat experiments must be optimised.

Chapter 5 Fe isotopes in pore-fluids from deep-sea and continental margin sediments

This chapter compares the isotopic composition of Fe in surface sediment pore-fluids from the Crozet region to the Eel River shelf. The material presented in this chapter has been published in the journal Geology (Homoky et al., 2009) (Appendix I). With the exception of the pore-fluid Fe isotope compositions (Appendix II), Crozet data is also presented in Chapter 3.

ABSTRACT

Pore-fluid Fe isotopes may be a unique tracer of sediment respiration by dissimilatory Fe reducing bacteria, but to date pore-fluid Fe isotope measurements have been restricted to continental shelf settings. Presented here are the δ^{56}Fe of pore-fluids from 2 distinct sedimentary settings: (1) the river-dominated Eel River shelf on the northern California margin (120 m water depth) and (2) biogenic opal-rich volcaniclastic deep-sea sediments from the Southern Ocean (north and south of the Crozet Plateau; 3000–4000 m water depth). The Fe isotope compositions of Crozet pore-fluids are significantly less fractionated (δ^{56}Fe = +0.12 to –0.01‰) than the Eel River shelf (δ^{56}Fe = –0.65 to –3.40‰) and previous studies of pore-fluid Fe isotopes, relative to average igneous rocks. These data represent the first measurements of Fe isotope compositions in pore-fluids from deep-sea sediments. Comparison of pore-fluid δ^{56}Fe with the relative abundance of highly-labile Fe in the reactive sedimentary Fe pool demonstrates that the composition of Fe isotopes in the pore-fluids reflects the different extent of sedimentary Fe redox re-cycling between these sites. These findings highlight the potential utility of Fe isotopes for tracing inputs from continental shelf sediments, where redox re-cycling of Fe is extensive.

5.1 INTRODUCTION

Iron isotopes have emerged as a new tool to evaluate iron cycling in aquatic environments (Anbar and Rouxel, 2007; Johnson et al., 2008). Incubation experiments have demonstrated that the reduction of Fe(III) in the presence of dissimilatory Fe reducing bacteria produces aqueous Fe^{2+} with $\delta^{56}Fe$ values that are 0.5–2‰ lower than the initial Fe(III) substrate (Beard et al., 1999; Icopini et al., 2004; Crosby et al., 2007). Pore-fluids from sediments where organic matter oxidation proceeds through significant microbial Fe reduction, yield isotope compositions for dissolved Fe^{2+} that are ~1–3‰ lighter than average igneous rocks, suggesting that benthic Fe inputs to the ocean may carry a light isotopic fingerprint (Severmann et al., 2006).

Dissimilatory Iron Reduction (DIR) is a form of chemolithotrophy that is widespread during diagenesis of marine sediments, the rate of which is controlled by organic carbon oxidation and the availability of Fe(III) substrates (Froelich et al., 1979). DIR was one of the earliest metabolic pathways to evolve on earth (Vargas et al., 1998) and it has been suggested that sedimentary Fe isotopes may also be used to reconstruct past Fe cycling in the Archean ocean (Rouxel et al., 2005; Yamaguchi et al., 2005; Severmann et al., 2008).

Pore-fluid Fe isotope measurements have so far been restricted to the continental shelves where DIR is extensive (Bergquist and Boyle, 2006; Severmann et al., 2006). There have been no measurements of Fe isotopes in low organic carbon, sub-oxic sediment pore-fluids, in deep-water settings where sediment accumulation rates are much slower and oxygen penetration deeper than on the continental shelves, or in sediments where potential abiotic processes may significantly imprint the pore-fluid Fe isotope composition. The comparison of Fe isotopes in shallow and deep-water environments has been identified as necessary for advancing our understanding of Fe biogeochemical cycling (Johnson et al., 2008), and characterizing the Fe isotopic fingerprint of DIR in natural, complex aqueous systems is important for the effective interpretation of the sedimentary record, and for developing the potential utility of Fe isotopes as a tracer of benthic Fe fluxes.

This chapter aims to (1) extend measurements of pore-fluid Fe isotope compositions to low-carbon and deep-water environments, (2) assess the diagenetic processes linked to changes in the observed pore-fluid Fe isotope compositions, and (3) elucidate the likely Fe isotopic composition of Fe inputs from sediments to the oceans. In this chapter new δ^{56}Fe data for surface sediment pore-fluids (0–25 cmbsf) from two distinct sedimentary settings is presented: (i) the Eel River-dominated shelf site (ERS-1) on the northern California margin (120m water depth), and (ii) the mixed biogenic opal-rich volcaniclastic sediments from deep-sea Crozet sites M10 (3227 m) and M6 (4222 m), in the Southern Ocean. A full description of the Eel River shelf site (ERS-1) can be found in Chapter 4 (Section 4.2.1.1 and Figure 4-1), and Crozet sites M10 and M6 are described in Chapter 3 (Section 3.2.2 and Figure 3-2). Briefly, the Eel River shelf organic carbon accumulation rate is high (~26.7 gC m^{-2} yr^{-1}; Sommerfield and Nittrouer, 1999) and carbon remineralisation is driven by extensive Fe redox recycling, whereas organic carbon accumulation rates in Crozet are low (M6: ~0.011 gC m^{-2} yr^{-1}; M10: ~0.113 gC m^{-2} yr^{-1}) and diagenetic Fe cycling is limited by the availability of reactive organic carbon. Pore-fluid Fe isotope compositions are compared to the distribution of Fe between reactive sedimentary Fe phases, and used to demonstrate the Fe isotopic expression of benthic Fe redox recycling in the pore-fluids.

5.2 METHODS OF SAMPLING AND ANALYSES

Chapter 2 describes the methods of sediment sampling (Section 2.2) and pore-fluid extraction (Sections 2.3.1-2.3.3). Pore-fluids were analysed for dissolved Fe and Mn concentrations by ICP-MS (Section 2.5). Pore-fluid Fe isotope ratios were measured by a Multi-Collector ICP-MS (Neptune), following the procedure described in Section 2.7. The isotope ratio $^{56}Fe/^{54}Fe$ is reported using standard delta notation, where measured ratios are normalised relative to average igneous rocks, which have an isotope composition of $\delta^{56}Fe = 0 \pm 0.05‰$ (Beard et al., 2003). Pore-fluid nitrate analyses are described in Section 2.12. Sediment determinations of total Fe used a chemical digestion method (Section 2.9) and reactive Fe phases were extracted using the sequential extraction methods of Poulton and Canfield (2005) (Section 2.8). Sediment total carbon and organic carbon content was determined using carbon Coulometry for Crozet sediments

and infrared CO_2 detection for Eel River shelf sediments (Section 2.11). All analyses were carried out as described in Chapter 2, with the exception of pore-fluid Fe and Mn concentration and Fe isotope composition from the Eel RIver shelf, which were analysed by Silke Severmann (formerly at UC Riverside) following the same procedures as described in Sections 2.4 and 2.7.

5.3 RESULTS

Pore-fluid nitrate penetration depth provides a qualitative tool for comparing the sedimentary redox status of the study sites. This depth is greatest at the Crozet site M6 (20–30 cmbsf), intermediate Crozet site M10 (~10 cmbsf) and shallowest at the Eel River shelf site ERS-1 (~5 cmbsf) (Figure 5-1a). The shallowest nitrate penetration depth occurs at the site of highest mean organic carbon content at the Eel River shelf (0.87%, 0–22 cmbsf), which also has the greatest proportion of highly labile Fe phases ($Fe_{h\text{-}lab}$) relative to reactive hydrous Fe oxide (HFO) substrates (63%–69% compared with 2%–20% in Crozet sediments). The relative proportions of $Fe_{h\text{-}lab}$ (Na acetate leachable) and HFO (Hydroxylamine-HCl leachable) were estimated from the sequential sediment extraction procedure of Poulton and Canfield (2005) (Section 2.8). The ratio $Fe_{h\text{-}lab}$ /[$Fe_{h\text{-}lab}$ + HFO] provides an estimate of the extent of diagenetic redox re-cycling of Fe.

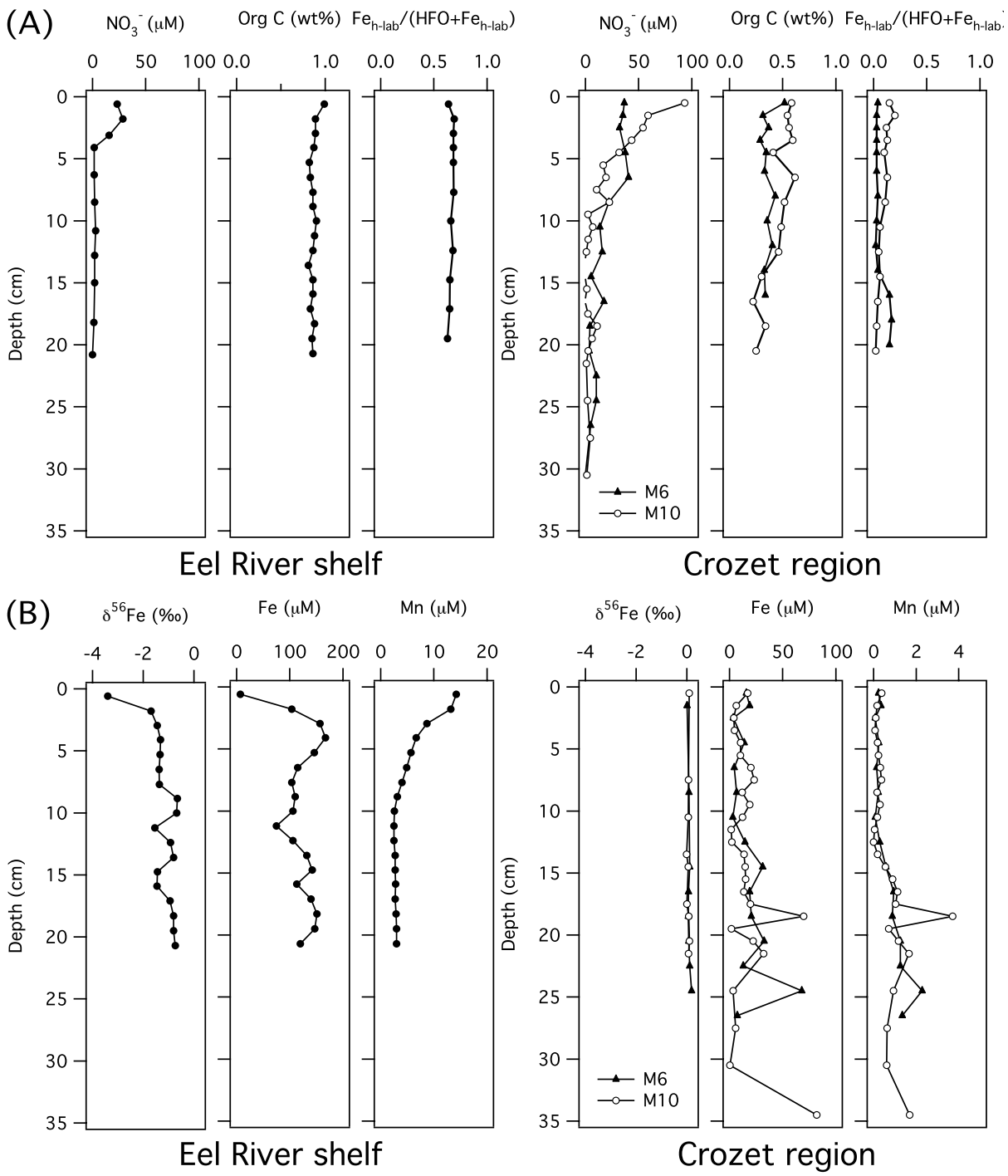

Figure 5-1. (A) Pore-fluid nitrate, solid-phase organic carbon and the proportion of highly-labile Fe ($Fe_{h\text{-}lab}$) relative to Hydrous Fe oxide (HFO) profiles. The $Fe_{h\text{-}lab}$ / (HFO + $Fe_{h\text{-}lab}$) ratio records the relative proportion of highly-labile Fe in a reactive Fe pool utilised during DIR. (B) Concentration of Fe, Mn and $\delta^{56}Fe$ in Crozet region and Eel River shelf pore-fluids.

Crozet region pore-fluid $\delta^{56}Fe$ values range between +0.12 and −0.01‰ relative to average igneous rocks (Figure 5-1b), and closely resemble those of average

continental weathering products (0.2 ± 0.7‰; Beard et al., 2003). In contrast to both these sites, Eel River shelf δ^{56}Fe pore-fluid values lie between -0.65 and -3.40‰, with the greatest isotopic fractionation closest to the sediment-seawater interface (Figure 5-1b). Crozet pore-fluid Fe concentrations are ~1-80 μM at M10 and M6, and are characterised by similar Mn distributions (up to 4 μM), with maxima at ~17 and 25 cmbsf at M10 and M6 respectively. At the Eel River shelf site, pore-fluid Fe concentrations reach a subsurface maximum of 167 μM at 5 cmbsf, and Mn concentrations are highest (14 μM) in the upper 0-5 cmbsf.

5.4 DISCUSSION

5.4.1 Comparison of pore-fluid Fe and Mn distributions, and Fe isotope compositions

The distributions of Fe and Mn in Eel River shelf pore-fluids are broadly consistent with the biogeochemical zonation of respiratory processes (Froelich et al., 1979), indicating the transition from aerobic respiration through to DIR between 0 and 5 cmbsf. However, Fe and Mn in Crozet region pore-fluids are not typical of deep-sea profiles, and are relatively high (1-20 μM Fe; 0.1-0.3 μM Mn) in the upper 10 cm compared with previous measurements from deep-sea Southern Ocean sites (<0.1 μM Fe; King et al., 2000); the equatorial Pacific (<5 μM Fe; Haeckel et al., 2001); tropical northeast Atlantic (1-13 μM Fe; Froelich et al., 1979); and many coastal shelf settings (Canfield et al., 1993; McManus et al., 1997). Additionally, the biogeochemical zonation of NO_3^-, Mn and Fe in the Crozet region pore-fluids is less apparent than at the Eel River shelf site and provides little evidence for DIR-dominated diagenesis (See also Section 3.4.2).

The analysis of 2 different dissolved size fractions (0.2 μm and 0.02 μm) in Crozet region pore-fluids demonstrates that significant colloidal and/or nanoparticulate (herein after 'colloidal') phases are present. It is speculated that these colloids comprise oxidised and/or adsorbed Fe^{2+}/Fe^{3+} that may be utilised during DIR along with any nanoparticulate basaltic weathering products (Section 3.4.4). The distribution of colloidal phases in the pore-fluids is suggested to be influenced by a number of factors affecting the solubilization, precipitation, and stabilization of Fe and Mn. These include the episodic supply of organic carbon

capable of disrupting the steady-state pore-fluid composition (Gehlen et al., 1997); the vertical mixing of volcaniclastic sediments through slumping and turbidite emplacement in this region (Marsh et al., 2007); the influence of bioirrigation and bioturbation (Aller, 1990); and the uncertain role of stabilizing organic complexes in the pore-fluid environment (Luther et al., 1992).

Eel River shelf pore-fluid δ^{56}Fe compositions are consistent with previous studies of Fe-reducing continental margin sediments where DIR catalyses the fractionation of Fe isotopes during redox cycling (Severmann et al., 2006). Crozet region pore-fluid δ^{56}Fe values are significantly less fractionated than previous values reported for sub-oxic pore-fluids (Figure 5-2). Severmann et al. (2006) noted that near-zero δ^{56}Fe values for pore fluids might reflect equilibrium with FeS. Total Sulphur content was analysed in these sediments (CHNS and ICPAES, data not shown) and can be attributed to seawater salts in the Holocene sections for these cores within the accuracy of the analysis. This is consistent with the findings of Marsh et al. (2007), who found no evidence for the onset of sulphide diagenesis in Holocene sediments at the Crozet sites. Therefore the comparison of the Eel River shelf and Crozet region suggests that either a mechanism other than DIR is releasing a substantial amount of Fe (up to 80 μM; δ^{56}Fe ~0.0‰) into the Crozet pore-fluids, or that DIR alone may be insufficient to generate the low-δ^{56}Fe values we observe in continental margin sediments.

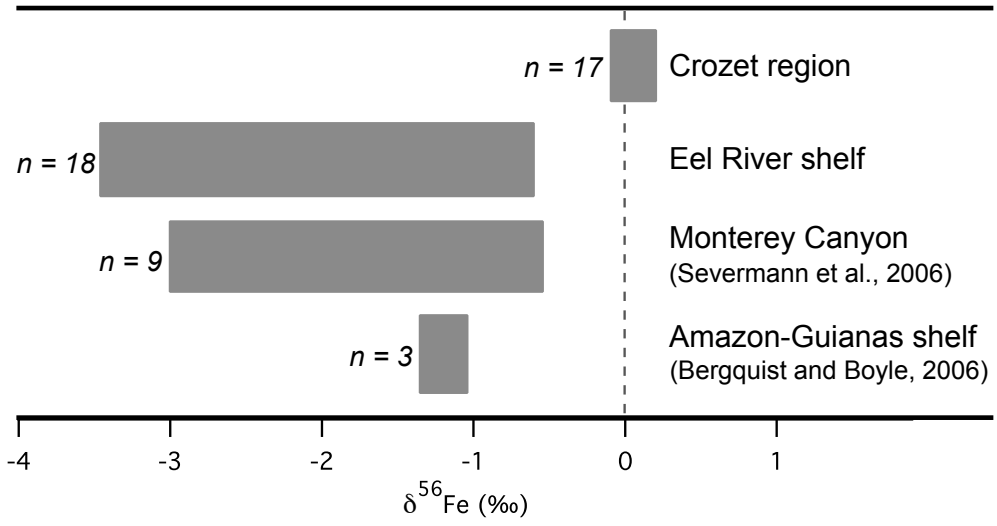

Figure 5-2. Comparison of Crozet and Eel River shelf pore-fluid Fe isotope compositions with published data from DIR-dominated reducing sediments on continental shelves

5.4.2 What accounts for the differences in Fe isotope composition between Crozet and Eel River shelf pore-fluids?

Experiments have shown that Fe isotope fractionations of >1‰ in aqueous systems can also be produced by abiotic processes. For example, ligand-promoted dissolution of mineral substrates, such as goethite, ferrihydrite and hornblende (Brantley et al., 2004), abiotic sorption and surface exchange (Icopini et al., 2004; Crosby et al., 2007), and isotope exchange between free and organically or inorganically complexed Fe (Dideriksen et al., 2008; Hill and Schauble, 2008) could potentially contribute to variations in isotope compositions in nature that are indistinguishable from biological fractionations. Deconvolving these processes in nature presents a major challenge; however it has been argued that abiotic processes alone cannot generate the large inventories of isotopically fractionated Fe that have been identified in continental margin sediments (Johnson et al., 2008). It is hypothesised that the observed variation in Fe isotope composition between the study sites reflects differences in the extent of biogenic benthic recycling of the reactive Fe pool.

The sedimentary reduction and oxidation of Fe during organic carbon oxidation has been estimated to occur 100–300 times prior to ultimate burial below the redoxcline (Canfield et al., 1993), where the extent of bioturbation and bioirrigation may enhance the redox re-cycling of Fe substrates by oxidizing Fe^{2+} and suppressing the onset of sulphide diagenesis (Canfield et al., 1993). The composition of Fe isotopes in sediment pore-fluids is inferred to reflect the extent of redox re-cycling of Fe between DIR-derived Fe^{2+} and the oxidation products (highly-labile Fe phases, such as adsorbed Fe^{3+}) and other reactive Fe(III)(oxy)hydroxides such as ferrihydrite and lepidicrocite (Severmann et al., 2008). Experimental investigations of the mechanism producing Fe isotope fractionation during DIR have shown that the generation of light dissolved Fe^{2+}_{aq} can be attributed to a coupled electron and isotope exchange between sorbed Fe^{2+} (Fe^{2+}_{sorb}) and a reactive Fe(III) ($Fe(III)_{reac}$) component on the surface of the Fe-oxide that is open to exchange (Crosby et al., 2007). These authors argue that changes in the absolute $\delta^{56}Fe$ values of Fe^{2+}_{aq} in their experiments reflect changes in the relative sizes of the reactive Fe pools (Fe^{2+}_{aq}, Fe^{2+}_{sorb} and $Fe(III)_{reac}$), while the isotope fractionation between the dissolved Fe^{2+}_{aq} and the reactive surface layer of

the Fe-oxide layer remains constant. The reactivity of Fe-oxide minerals and the relative proportion of Fe^{2+}_{sorb} may therefore be the primary control on the pore-fluid Fe isotope composition. Consistent with the experimental findings of Crosby et al. (2007), we have measured the lowest pore-fluid δ^{56}Fe values in the Eel River shelf sediments, where a high proportion of reactive Fe occurs as highly-labile Fe phases, as inferred from the much higher $Fe_{h\text{-}lab}$/[HFO+$Fe_{h\text{-}lab}$] ratios compared with Crozet deep-water sediments (Figure 5-3).

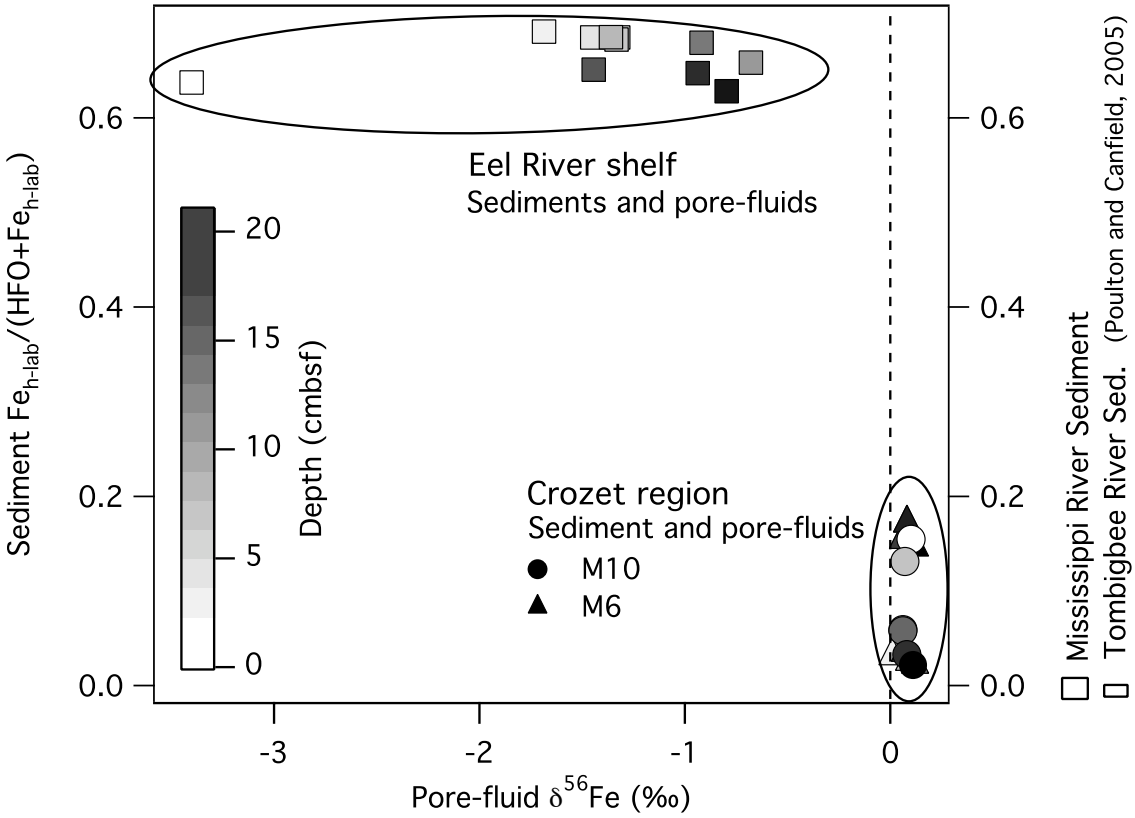

Figure 5-3. Comparison of Eel River shelf and Crozet region (M10 and M6) sediment $Fe_{h\text{-}lab}$/[HFO + $Fe_{h\text{-}lab}$] composition with pore-fluid δ^{56}Fe. The sample depth of data is represented by the grey-scale. The $Fe_{h\text{-}lab}$/[HFO + $Fe_{h\text{-}lab}$] ratio provides an estimate of the relative enrichment of highly-labile Fe phases in the reactive sedimentary pool driven by the extent of redox re-cycling of Fe during sediment diagenesis. The published $Fe_{h\text{-}lab}$/[HFO + $Fe_{h\text{-}lab}$] composition of riverbed sediments provides an end-member composition of the reactive Fe pool prior to the diagenetic redox re-cycling of Fe.

The organic carbon supply to the Eel River shelf appears to be sufficient to sustain DIR, enrich highly-labile Fe phases in the reactive Fe pool and account for

the highest pore-fluid Fe isotope fractionation and elevated $Fe_{h\text{-}lab}$/[HFO+$Fe_{h\text{-}lab}$] ratio. By contrast the low organic carbon input to the deep Crozet region sediments limits DIR. It is speculated that highly seasonal organic carbon inputs to M10 (Pollard et al., 2009) may promote the episodic contribution of DIR to sediment respiration and account for the enrichment of highly-labile Fe at M10 relative to M6. In these circumstances, processes that contribute to the generation of colloids and/or nano-particulates in the pore-fluids (van der Zee et al., 2003) are likely to have near crustal isotope compositions and dilute the isotopic signature of DIR.

5.4.3 Implications for tracing Fe inputs from sediments to the oceans

This chapter substantiates previous observations of light pore-fluid Fe isotope compositions in continental margin sediments: sediments that are known to supply dissolved Fe to the oceans (Chapter 4). Furthermore it has been shown that these light pore-fluid Fe isotope compositions are likely to result from the enhanced rates of diagenetic re-cycling of reactive Fe: a process associated with the shelf sedimentary Fe inputs to the oceans observed to date (McManus et al., 1997; Berelson et al., 2003; Elrod et al., 2004; Severmann et al., 2006; Severmann, 2008; Severmann et al., In prep.). For this reason, Fe isotopes from shelf sediments are likely to carry a unique isotopic signature, significantly lighter than Fe inputs from other sources (Waeles et al., 2007; Bennett et al., 2009; Escoube et al., In Press). Fe inputs from colloidal fractions of deep-sea Crozet pore-fluids, will be isotopically distinct from organic-rich shelf inputs of Fe, but similar to bulk earth compositions, and so are less likely to be traced using Fe isotope compositions in seawater.

5.5 CONCLUSIONS

High dissolved Fe pore-fluid contents arise from the suppression of sulphide diagenesis in Eel River shelf sediments and volcaniclastic weathering in Southern Ocean sediments. It has been demonstrated that the pore-fluid Fe isotope compositions reflect the extent of Fe recycling during early diagenesis, which is driven by supply of reactive organic carbon. Future interpretations of the rock record are invited to consider the importance of Fe isotope processing in carbon-

limited environments. Additionally, the unique isotopic fingerprint of pore-fluid Fe in continental shelf settings is highlighted, drawing further attention to the potential utility of Fe isotopes as a tracer of shelf-derived Fe inputs to seawater.

Chapter 6 Conclusions and future directions

This chapter relates the findings from chapters 3, 4 and 5 to the aims set out in the Chapter 1, namely to evaluate the processes responsible for the generation of sedimentary Fe inputs to seawater, to consider the geographical restrictions/ubiquity of sedimentary Fe inputs to the oceans and their significance for ocean Fe budgets, and the potential directions for future related research.

6.1 CONTROLS ON Fe EXCHANGE BETWEEN SEDIMENTS AND SEAWATER

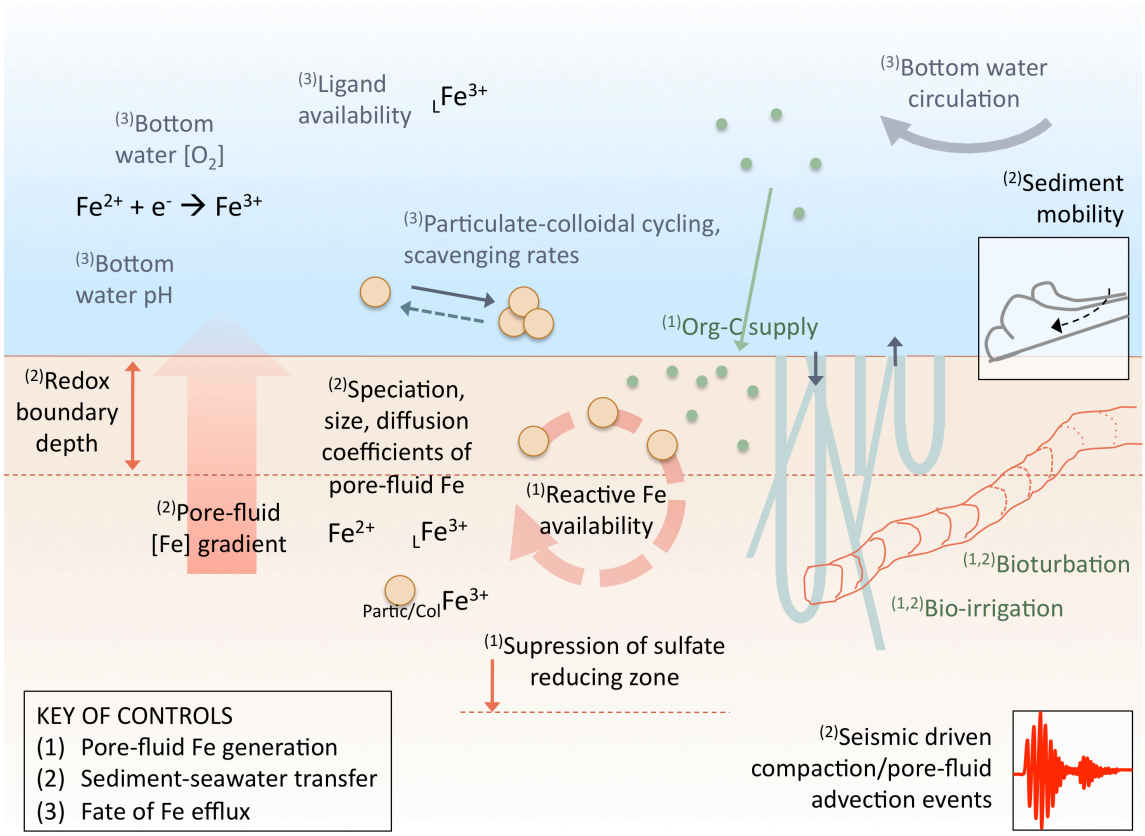

Figure 6-1. Summary of important controls on the generation of dissolved Fe in sediments, the transport to overlying seawater and the fate of sedimentary Fe inputs to seawater.

Factors affecting the exchange of dissolved Fe between sediments and seawater can be grouped into 3 process-related categories: (1) the generation of dissolved Fe in sediment pore-fluids; (2) the transfer of Fe from sediments to seawater; (3) The fate of sediment-derived Fe inputs in seawater. A summary of controls on the generation of dissolved Fe in sediments, the transport of Fe to overlying seawater and the fate of sedimentary Fe inputs in seawater is illustrated in Figure 6-1.

6.1.1 The generation of dissolved Fe in sediment pore-fluids

Pore-fluid Fe generation is necessary to establish and sustain the surface-sediment to bottom-water concentration gradient required to generate a benthic Fe flux. A major driving force for early diagenetic change in surface sediment geochemistry is the supply of organic carbon that comes principally from the surface ocean. Additionally, microbial sediment respiration, and the availability of reactive Fe substrates are important for sustaining the bacterial dissimilatory reduction of Fe. The bioirrigation and bioturbation of sediments suppresses the onset of sulphate reduction in the sediment column and consequently extends the sub-oxic zone favoured by Fe-reducing bacteria, and enhances the concentration of Fe in surface sediment pore-fluids. The oxidation of organic carbon has previously been correlated with benthic Fe fluxes on the continental shelves where organic carbon supply to the sediments is high (Elrod et al., 2004); this thesis has also considered sediments of relatively low organic carbon supply in the Crozet region, and those of inorganically dominated volcaniclastic sediments in the Montserrat region. Colloidal forms of Fe dominate the Crozet pore-fluids and account for Fe concentrations in excess of those predicted for oxic pore-fluids in deep-sea sediments. The origin and composition of these colloids remains unknown, however they appear widespread in mixed biosiliceous-volcaniclastic pore-fluids in this study, and their nano-metre scale suggests they may be subject to similar diffusion processes as truly aqueous Fe. It has been shown that the generation of a high pore-fluid Fe concentration is also achieved in Montserrat sediments, despite very low organic carbon content of surface sediments. Pore-fluid Fe in Montserrat sediments is in a truly dissolved form and is thought to be dominated by dissolution from abundant Fe(II) mineral phases in the young and reactive tephra supplied to this region.

6.1.2 The transfer of Fe from sediments to seawater

Diffusive transport of dissolved Fe between sediments and seawater is primarily controlled by the concentration gradient between source and sink Fe pools. High organic carbon supply typically produces a shallow redoxcline for Fe, thus producing a steep concentration gradient between surface sediments and seawater, and an enhanced Fe flux. However, despite very low organic carbon content in Montserrat sediments, oxygen utilisation by solid-phase Fe(II) and Mn(II) oxidation may lead to depleted pore-fluid oxygen concentrations and a steep Fe concentration gradient in the surface sediment pore-fluids. The rate of pore-fluid diffusion remains subject to sediment porosity and tortuosity parameters, as described in previous studies (Li and Gregory, 1974; Klinkhammer, 1980). This thesis has highlighted the need for accurate determination of the diffusion co-efficient of different dissolved forms of Fe (and Mn) if accurate fluxes are to be determined. The application of a simple ionic diffusion coefficient to colloidal Fe phases is likely to overestimate the true rate of colloidal diffusion, as, for example, the diffusion coefficients of Cu- and Pb-complexes are known to decrease with increasing size of the complexing ligand (Phillips and Ellis, 1970; Scally et al., 2006).

Advective transport of pore-fluid Fe from sediments to seawater is greatly enhanced by bioirrigation of surface sediments, and by bottom water circulation over permeable sediments (Aller, 1990; Huettel et al., 1998; Elrod et al., 2004). The present study has shown that bioirrigation on the Eel River shelf may account for up to a 10-fold increase in Fe Flux from sediments to bottom waters. The study has also drawn attention to the episodic nature of advective transport processes, resulting from seasonal fluctuations in mega-faunal activity in the Crozet and Eel River shelf regions, the response of biota to changing bottom water oxygen conditions, and possibly to sediment compaction episodes in the Montserrat region, which are suggested to be susceptible to seismic-triggers, releasing pore-fluid Fe and Mn to bottom waters. The influence of sediment re-suspension on the sediment-seawater exchange of Fe is yet to be quantitatively assessed. The results of pilot studies on the Eel River shelf and Montserrat sediments suggest re-suspension of sediments below the redoxcline would be necessary to stimulate significant transfer of Fe to bottom waters. However, re-suspension of oxic layers resulted net gains and losses in bottom water Fe

concentration, demonstrating the dynamic nature and probable importance of Fe cycling between particulate and dissolved phases, close to sediments.

6.1.3 The fate of sedimentary inputs of Fe in seawater

Once Fe from sediment pore-fluids has entered the overlying seawater, its fate, and thus its impact on global biogeochemical cycles, depends on a number of important factors. The speciation of Fe is a vital characteristic affecting its solubility. The concentration of oxygen in the bottom waters has a first-order control on the solubility of Fe in seawater, and will oxidise any soluble reduced forms of Fe(II) to Fe(III) in a matter of seconds to hours depending on both the availability of oxygen and the pH (Millero et al., 1987; Johnson et al., 1997; Lohan and Bruland, 2008). Low bottom water oxygen concentrations caused by phytoplankton growth and decay and low seawater pH in appear to slow the oxidation kinetics of Fe inputs from sediments to the water column on the California shelf significantly, compared with Montserrat bottom waters, and is consistent with previous observations on the Washington and Oregon shelves (McManus et al., 1997; Berelson et al., 2008; Lohan and Bruland, 2008; Severmann, 2008). The true nature of Fe and its speciation in these studies, however, remains unclear.

The interaction of Fe with organic ligands and colloids may enhance the stability and subsequent residence time of Fe in bottom waters, facilitating exchange with the open ocean. The speciation, ligand associations, and size of dissolved Fe phases in seawater have been studied in some detail (Wu and Luther III, 1994; Rue and Bruland, 1995; van den Berg, 1995; Kuma et al., 1998; Nishioka et al., 2001; Wu et al., 2001). Fe ligand concentration is known to control the dissolved Fe concentrations in coastal settings (Buck et al., 2007), and is suggested to account for deep-water Fe concentrations (Boye et al., 2001). Size-fractionated Fe colloids have been measured in estuarine sediment pore-fluids (Huerta-Diaz et al., 2007), and the colloid-Fe association attributed to the presence of organic ligand complexes. Coastal sediments have also been suggested to be a source of Cu-complexing ligands to the water column (Skrabal et al., 1997), and therefore invites speculation as to whether or not they may also be a source of Fe ligands.

Very little is known of the role that organic ligand and colloid interactions play in benthic Fe cycling. The present study has shown the production of colloidal Fe (and Mn) phases within a dissolved size fraction that exists in oxic and sub-oxic pore-fluids in the Crozet region (Chapter 3). Yet while up to 50% of dissolved Fe in deep-ocean waters has also been measured in a colloidal fraction (Bergquist et al., 2007), no study has directly linked the colloidal Fe observations in pore-fluids around Crozet with enhanced bottom water Fe concentrations. The closest observations of Fe concentrations in bottom waters close to the deep-sea floor are from the Weddell Basin, Southern Ocean (Klunder et al., In Press), where Fe is elevated ~2-fold within 10-100 m of the seabed relative to overlying deep-ocean concentrations (up to 0.8 nM). These authors did not determine the colloidal fraction of the dissolved Fe phase. It has been shown (Chapter 3) that inorganically dominated volcaniclastic sediments in the Montserrat region exhibit none of the colloidal partitioning found in the biosiliceous-volcaniclastic sediments of Crozet, suggesting biotic processes driving early sediment diagenesis may be important for influencing the generation of Fe colloids/ligands in marine sediments, and subsequent enhanced stability in the pore-fluids and possibly the water column. Transfer of Fe between the benthic boundary layer (BBL) and overlying water column, is therefore likely to involve important internal Fe cycles. These are poorly constrained, yet likely to determine the extent to which benthic Fe fluxes impact biogeochemical cycles in the oceans. An interpretive summary of dissolved and particulate Fe cycling and important vertical fluxes between surface sediments, the BBL and the surface ocean, is illustrated in Figure 6-2.

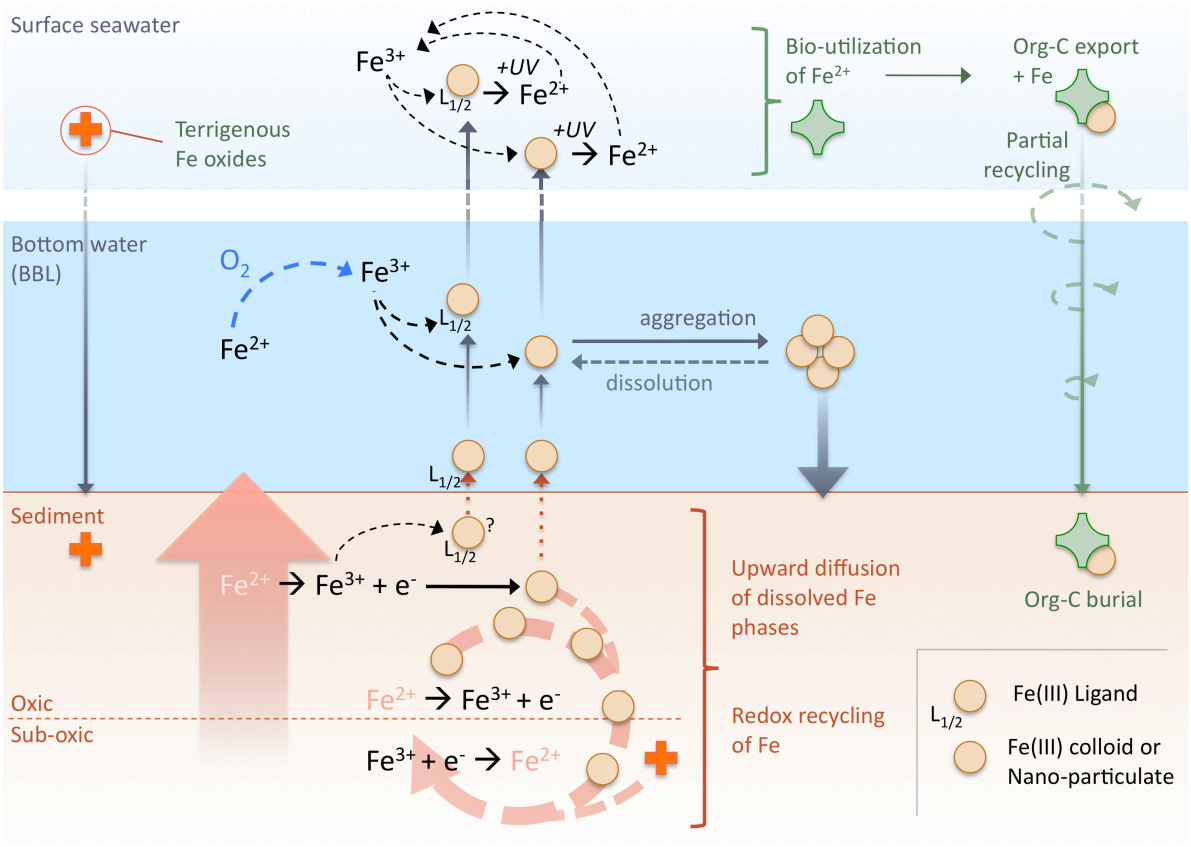

Figure 6-2. Dissolved and particulate Fe cycling and important vertical fluxes between surface sediments, the benthic boundary layer (BBL) and the surface ocean. The benthic boundary layer (BBL) may be characterised by intense dissolved-particulate cycling of Fe.

6.2 THE IMPORTANCE OF SEDIMENTARY Fe SUPPLY TO THE OCEANS

In this thesis the magnitude of Fe fluxes to the overlying bottom waters has been estimated using the pore-fluid concentration gradients across the sediment-seawater interface from 3 contrasting sedimentary settings: Eel River shelf; Montserrat; and Crozet, using the best available estimate of the diffusion coefficient. At 2 of these sites - the Eel River shelf and Montserrat - shipboard incubation experiments were used to evaluate the predicted flux magnitudes (Chapter 4). Both methods of flux derivation have limitations, without knowing the true overlying bottom water concentration of Fe, the pore-fluid concentration

gradient (dC_{Fe}/dx) used in flux calculations (Chapter 3) may overestimate the true Fe flux to the overlying bottom water. The diffusion coefficient for colloidal Fe is not known, but that used is also likely to over-estimate the Fe flux, perhaps by 25%, if other cationic-ligand behaviour may be analogous to Fe (Scally et al., 2006). However, pore-fluid flux calculations did not account for advective properties of the sediments and thus may underestimate the true flux depending on the extent of bioirrigation and sediment compaction. Flux derivations from incubation experiments (Chapter 4) presented additional challenges, as incubated seawater recorded the net result of Fe addition and removal processes. Due to bioirrigation, benthic chamber fluxes have previously been shown to be as much as 75 times higher than those derived by pore-fluid gradients (Elrod et al., 2004). Comparison of Eel River shelf incubations with benthic lander data, however, suggests that artificially low oxygen concentrations my account for the enhanced rates of bioirrigation predicted by Elrod et al. (2004). This study suggests bioirrigation may account for a 10-fold increase in benthic Fe flux on the Eel River shelf.

The characteristics of Fe cycling between sediments and seawater are closely related to the non-steady state behaviour of sediments during early diagenesis. Seasonal fluctuations in sediment accumulation rates, bioirrigation, and reactive Fe utilisation - as well as episodic sediment remobilization and advection - contribute to dynamic pore-fluid and bottom-water environments, and sampling strategies to date have not provided a wholly representative dataset of this variability. A major challenge for future work will be to address the dynamic nature of sediment-seawater exchange of Fe and other pore-fluid constituents to improve the quantification of these processes.

Extrapolation of the benthic Fe inputs to seawater, derived from the incubated Eel River shelf sediments, to the global area of continental margin sediments, yields a mean annual flux of 2-110 $x10^9$ mol yr^{-1} of Fe. This value is based on a global continental shelf area of 27.4 $x10^6$ km^2 (0-200 m) (Raiswell and Anderson, 2005). This lower end of this range of flux magnitude is very close to the minimum global shelf flux predicted by Elrod et al. (2004) of 2.2 $x10^9$ mol yr^{-1}, which is similar to the estimate of Moore and Braucher (2008), 16 $x10^9$ mol yr^{-1}, whilst the upper end of this range is closer to the predicted flux by Raiswell and Anderson (2005) of 400 $x10^9$ mol yr^{-1}. Temporo-spatial variation of reactive Fe supply,

oxygen concentration and bioirrigation on the continental margins is held accountable for the uncertainty reflected in the literature estimates of sedimentary Fe flux to date (Severmann et al., In prep.), some of which is reflected in the range of Fe flux determinations presented in this thesis. This study therefore supports the view that the continental shelves are a significant source of Fe to the oceans, and despite the uncertainties to both source terms, is consistent with claims that shelf sediments provide at least a similar quantity of Fe as aerosols to the oceans dissolved Fe inventory - 2-26 $x10^9$ mol yr^{-1} (De Baar and De Jong, 2001; Jickells and Spokes, 2001).

In addition to fluxes from continental margin sediments, those from deep-sea sediments in the biosiliceous-volcaniclastic Crozet region have been evaluated. Steep pore-fluid Fe concentration gradients have been identified, and the associated fluxes are dominated by colloidal material that appears to be relatively stable in the oxygenated pore-fluids, and so, by inference, open to exchange with the overlying bottom waters. The diffusive flux of this 'dissolved' Fe from Crozet sediments has been extrapolated to deep-sea regions subject to similar biosiliceous-volcaniclastic sedimentation (Crozet sites composition between 10 and 54% volcanogenics). An estimated global deep-sea Fe flux contribution to seawater of 48 $x10^9$ mol yr^{-1}, represents ~73% of the ocean Fe budget (De Baar and De Jong, 2001), sufficient to account for 100% of deep-water Fe concentrations (Bennett et al., 2008), and is therefore a significant over-estimate of the true contribution to the oceans. The quality of these deep-water flux predictions is subject to the validity of a number of assumptions used in their derivation. For example, Fe diffusing into the benthic boundary layer is assumed to share the mean residence time of Fe in the oceans as a whole; in reality, elevated particulate scavenging rates, colloidal aggregation and dissolution are likely to shorten the residence time of Fe in the benthic boundary layer significantly. Seasonal variability in organic carbon inputs, overlying oxygen concentrations and bioirrigation is unaccounted for by the steady-state pore-fluid diffusion equation, and the estimated flux area needs to be verified. The diffusive flux estimates should therefore be considered semi-quantitative at best, and their use limited to assessing the amount of Fe entering bottom waters, and not the oceans as a whole. This study clearly demonstrates the potential importance of Fe inputs from deep-sea sediments to seawater and supports model predictions for a sedimentary sourced Fe input to the deep-sea (Moore and Braucher, 2008).

However, the fraction of Fe escaping the benthic boundary layer is a vital term that needs to be quantified.

This study suggests the predicted diagenetic flux of Fe by De Baar and De Jong (2001) of 33 x10^9 mol yr^{-1}that accounts for the Fe export observed in the oceans, may be in part accounted for by a diagenetic flux from deep-sea sediments as well as the reducing sediments of continental margins.

Organic Fe-complexing ligands have been measured in excess of the dissolved iron concentration at 0.72 ± 0.23 nM (equivalent to an excess of 0.5 nM) in the Southern Ocean (Boye et al., 2001). Recently, the first comprehensive deep-water (4000-5000 m) dissolved Fe profiles in the Southern Ocean were published and show a sharp increase in dissolved Fe concentration from ~0.48 to 0.78 nM within ~100 m of the seafloor in the Weddell Basin (Klunder et al., In Press). These observations are consistent with the saturation of available Fe binding ligands by a benthic Fe source in the Southern Ocean, or benthic inputs of colloidal Fe to an equivalent concentration, and bear witness to the dynamic nature of Fe cycling in the deep-sea that has been previously omitted by limited sampling resolution. The amount of Fe required to escape the BBL that would account for deep-ocean Fe budgets would be just 0.5-1% of the estimated flux from Crozet-type deep-sea sediments. Much remains to be done to quantify Fe cycling between sediments and seawater including the expansion of in-situ observations to basin-wide sedimentary environments and development of high-resolution sampling techniques across the sediment-seawater interface of coastal and, in particular, deep-sea environments.

6.3 TOWARDS ISOTOPE TRACING OF SEDIMENTARY Fe INPUTS TO SEAWATER

Fe isotopes are a promising tool for tracing Fe inputs and internal cycling in the oceans. In Chapter 5 (Homoky et al., 2009) it was demonstrated for the first time that the Fe isotopic signature of pore-fluids from the deep-sea exhibit no isotopic fractionation relative to igneous rocks, in contrast to the Fe isotopic signature of pore-fluids from reducing sediments on continental shelves. Due to the very low concentrations of Fe in the open ocean, the sampling and pre-concentration

methods used to date are insufficient to accurately determine the isotopic composition of Fe in seawater. However, the rapid growth of interest in Fe isotope biogeochemistry and the accuracy of analyses achieved by modern MC-ICP-MS means that it is likely that these measurements will soon be made. This section will consider the potential for tracing sedimentary sources of Fe from the continental shelves to seawater using the isotopic composition of Fe in seawater.

Despite studies of Fe isotope biogeochemistry being in their early stages of development, there has been at least one study of the Fe isotope composition of each of the primary Fe sources to the oceans. Severmann et al. (2006; In prep.), Bergquist and Boyle (2006), and Homoky et al. (2009), provide substantial evidence for the isotopically *light* fingerprint of Fe in reducing sediment pore-fluids from continental shelves and in regions of quantified Fe fluxes to seawater. The greatest pore-fluid Fe isotope fractionations have been observed closest to the sediment surface (Severmann et al., 2006; Homoky et al., 2009), and are consistent with the oxidation of heavier Fe isotopes during diffusion through the upper oxic sediment column. It has therefore been assumed that the mean Fe isotope composition of Fe derived from reducing shelf sediment fluxes is equal to the mean δ^{56}Fe of Fe measured closest to the sediment surface, -3.2 ± 0.2‰. This study (Chapter 5) has also characterised the pore-fluid Fe isotope composition of low-carbon-deep-sea sediment pore-fluids, which are here suggested to contribute to deep-water Fe budgets in the Crozet region. Waeles et al. (2007) and Escoube et al. (In Press) have demonstrated that no significant isotopic fractionation occurs during aerosol dissolution and estuarine mixing of Fe, and that the δ^{56}Fe of aerosol and riverine inputs reflects the isotopic composition of the lithogenic source substrate. Hydrothermal inputs to the deep-ocean have also been shown to contribute to the deep-ocean Fe budget (Bennett et al., 2008) and it is argued that dissolved Fe escaping from hydrothermal plumes has a *heavy* isotopic composition.

The available flux estimates of Fe to the oceans can be used to predict the Fe isotope composition of seawater via the relatively simple isotopic mass-balance calculation shown in Equation 6-1. While Fe inputs to the ocean from riverine, dust and cryogenic sources may in fact vary significantly over glacial to interglacial time scales, the very low solubility of Fe in the oxygenated oceans means that changes in the mean dissolved Fe concentration of seawater since the

LGM are likely to be minor and fall within the uncertainty flux estimates and Fe isotopic compositions already presented here. Moreover, major changes to the magnitude and distribution of Fe inputs due to changes in ice, riverine, and dust reservoirs are not likely to be reflected within the relatively short residence time of Fe in seawater (~30-200 yrs: DeBaar and De Jong, 2001; Johnson et al., 1997). Therefore the mass-balance equation assumes the concentration of Fe in the oceans is in a pseudo-steady-state.

$$\delta^{56}Fe_{sw} = \sum \delta^{56}Fe_i [Fe_i] \quad (6\text{-}1)$$
where $[Fe_{sw}] = \sum [Fe_i]$

The subscript *sw* refers to mean seawater, and the subscript *i* refers to the different inputs of Fe to seawater. We can derive $\delta^{56}Fe_{sw}$ using the isotopic composition of, and annual flux attributed to, riverine (*riv*), continental shelf sediment (*shelf*), deep-sea sediment (*deep*), aerosol (*aer*) and hydrothermal (*ht*) inputs, as derived from this and previous studies (Table 6.1). This calculation is outlined in below.

$$\delta^{56}Fe_{sw} =$$
$$(\delta^{56}Fe_{riv}[Fe_{riv}]) + (\delta^{56}Fe_{shelf}[Fe_{shelf}]) + (\delta^{56}Fe_{deep}[Fe_{deep}]) + (\delta^{56}Fe_{aer}[Fe_{aer}]) + (\delta^{56}Fe_{ht}[Fe_{ht}])$$

Dissolved Fe in the oceans, including Fe entrained from sediment diagenesis, is ultimately exported to, and buried within, marine sediments. There is no to evidence to date for Fe isotopic fractionation in seawater during sedimentation, perhaps due to the relatively low concentrations of Fe in the ocean and high-rates of biological utilization and oxidation. The mass-balance calculation presented above is consistent with the assumption that there is no isotopic fraction of Fe during removal from seawater, though this remains to be unequivocally demonstrated.

Using Equation 6-1, the mean $\delta^{56}Fe$ of total Fe inputs to seawater is predicted to be between -0.1‰ and -3.2‰, depending on the balance of uncertainty between flux estimates to the oceans (Figure 6-3).

Table 6-1. Summary of recent dissolved Fe flux estimates to seawater and the best available constraints on the Fe isotope composition of each flux.

Fe Source	[1]δ^{56}Fe (‰)	[2]Flux (mol yr^{-1})	Data Source
Rivers	0.1	29 x10^9	[1]Escoube et al. (In Press)
- post est.-mixing	0.1	1.5 x10^9	[2]De Baar and De Jong (2001)
Aerosols	0.13	2-26 x10^9	[1]Waeles et al. (2007) [2]De Baar and De Jong (2001) [2]Jickells and Spokes (2001)
Shelf sediments	-3.2	2-400 x10^9	[1]Homoky et al. (2009) [1]Severmann et al. (2006) [2]Elrod et al. (2004) [2]Moore and Braucher (2008) [2](Raiswell and Anderson, 2005)
Deep-ocean sediments	0.1	1.2 x10^9	[1]Homoky et al. (2009) [2]Chapter 3
Hydrothermal inputs	0.75	0.3 x10^9	[1]Bennett et al. (2009) [2]Bennett et al. (2008)

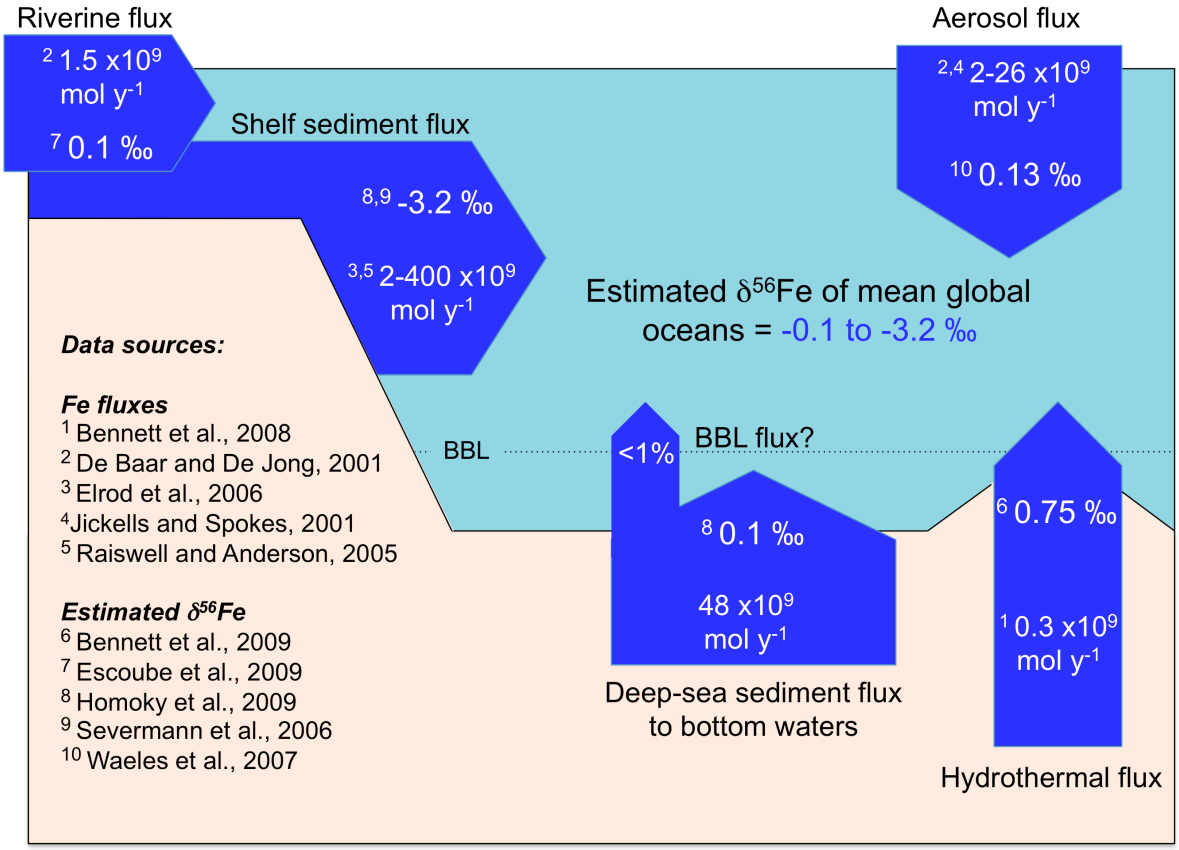

Figure 6-3. Illustration of parameters used to estimate the mean global seawater δ^{56}Fe by isotopic mass-balance. The estimated mean seawater δ^{56}Fe is light relative to average igneous rocks, and reflects the unique, light Fe isotope fingerprint of Fe inputs from continental shelf sediment pore-fluids to seawater. The true mean global seawater δ^{56}Fe value is subject to the further clarification of the isotopic composition of the source Fe fluxes, and improved understanding of Fe isotope fractionation processes in seawater. The BBL exchange term has not been determined, although it is assumed here to be <1% of the deep-sea sediment flux, in order to balance the inputs of Fe to the deep-ocean.

Chu et al. (2006) observed consistently light δ^{56}Fe values (-0.8‰) in Fe-Mn crusts distal to hydrothermal sources in the central Pacific. These authors interpreted the light isotopic signature to represent input from high-temperature hydrothermal vent fluid to the deep-ocean that had been preserved in the Fe-Mn crusts. However, a recent study by Bennett et al. (2008) demonstrates that the isotopic composition of dissolved Fe maintained in deep-ocean waters from high-temperature hydrothermal fluids is isotopically heavy (0.75‰) and disputes the assumptions used in the interpretation by Chu et al. (2006). The range of values derived here for a theoretical mean ocean Fe isotope composition show that the

isotopic composition of Fe-Mn crusts in the central Pacific might instead reflect the mass balance of Fe inputs to the oceans in hydrogenic deposits.

The δ^{56}Fe of seawater will reflect the balance of Fe inputs in different regions, due to the residence time of Fe in seawater (~30-200 yrs: DeBaar and De Jong, 2001; Johnson et al., 1997) being much shorter than the mean ocean mixing time (~1000 yrs). It is therefore likely that the δ^{56}Fe of seawater measured in any single sample will differ to the estimated composition of mean ocean water. Ascertaining the utility of Fe isotopes for tracing continental shelf Fe inputs will be aided by field tests in areas with a quantified understanding of the dissolved Fe budget. For example, we can attempt to use this approach to estimate the isotopic composition of Fe in Crozet surface waters, where Planquette et al. (2007) have estimated an Fe budget for the region (44.5-48ºS, 47-56ºE). These authors attribute 71% of Fe inputs to surface water to have been derived from Fe-rich seawater advecting laterally from the Crozet Islands plateau, 18% from aerosol deposition/dissolution and 11% from a vertical upwelling flux. Assuming the Fe sourced from the the Crozet shelf carries the same Fe isotopic fingerprint as Fe sourced from other continental margin sediments, then the resultant δ^{56}Fe of surface water in this region would be between -2.2 and -2.4‰ (Figure 6-4).

There are some important uncertainties associated with this estimate of Crozet region surface water Fe isotope composition: Firstly, laterally advected waters from the Crozet Island plateau will also be subject to Fe inputs from terrestrial run-off in this area. The magnitude of this Fe input is unknown, though it is assumed to be small relative to the shelf-derived inputs, due to the much larger area of the Crozet Island Plateau compared with the islands themselves. The isotopic composition of Fe derived from run-off has not been determined, but it is likely to reflect the δ^{56}Fe of the weathered substrate (Crozet Island basalt ~0.12 ± 0.1‰) (Bergquist and Boyle, 2006; Escoube et al., In Press). Secondly, the isotopic composition of Fe in deep-water that represents the vertical flux has been assumed to comprise up to 22% Fe from a hydrothermal flux (Bennett et al., 2008), and the remaining 78% from a deep-sea sedimentary flux in this region. The proportion of these vertically upwelling waters (>1000 m deep) sourced from hydrothermal and sedimentary sources relative to waters entrained from outside this region is not known, and the isotopic composition of the vertical flux corresponds to a 2 end-member scenario; either 100% of Fe reflects the mean

ocean values estimated in Figure 6-3, or 100% reflects the deep-sea sediment and hydrothermal inputs in the proportions outlined above.

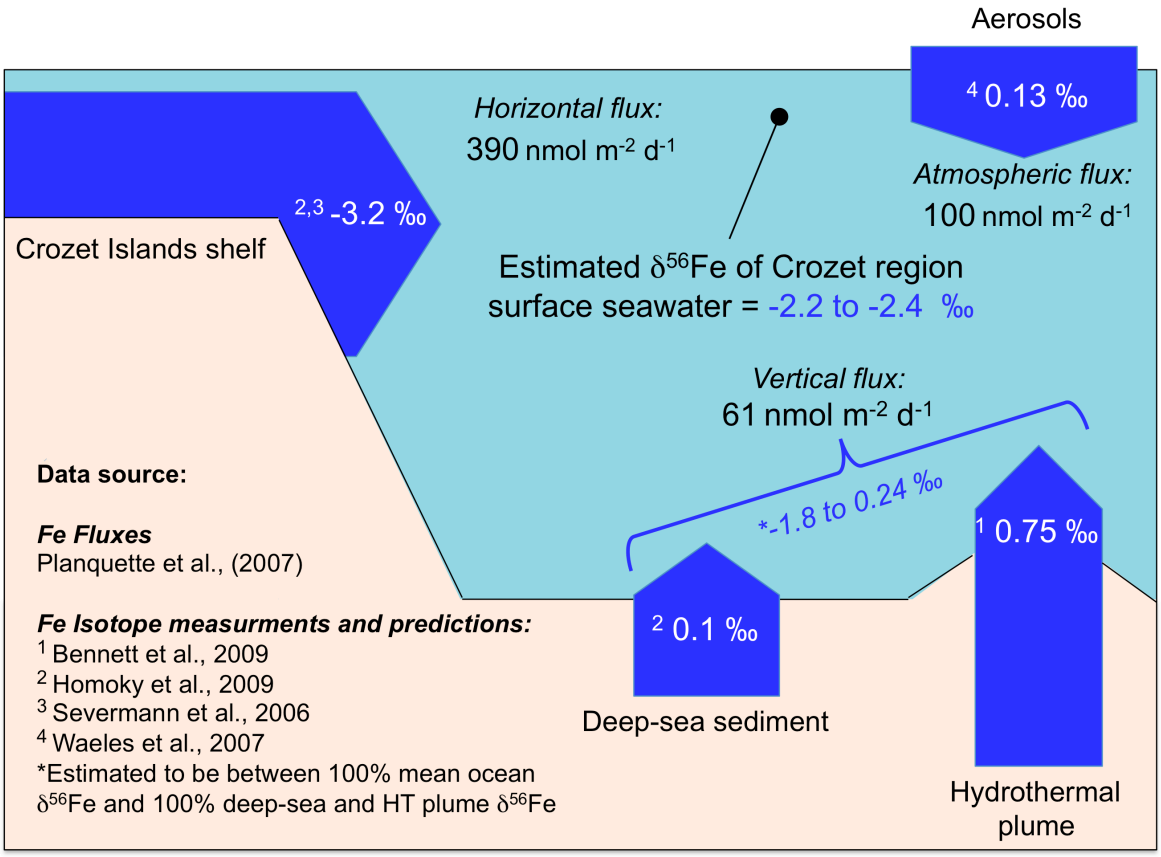

Figure 6-4. Illustration of the parameters used to estimate the δ^{56}Fe of surface waters in the Crozet Region. Fe inputs to Crozet region surface waters are largely sourced from waters that advect laterally across the Crozet Islands plateau. Assuming this Fe flux carries the light Fe isotope fingerprint of continental shelf sediment pore-fluids, the mass balance derivation shows that the Fe isotope composition of Southern Ocean surface water in the vicinity of the Crozet islands could strongly reflect the sedimentary shelf origin of Fe.

Lastly, the internal cycling of Fe in seawater may involve additional Fe isotope fractionating processes that are yet to be identified. For example, adsorption to sinking particles, affinity to organic ligands and colloidal aggregation may all favour isotope fractionation in the water column that could impede attempts to trace the isotopic signature of Fe from the continental shelf sediments.

In spite of the uncertainties outlined above, the Fe budget for Crozet surface waters shows that the isotopic signature of advected Fe inputs will be most

strongly reflected in the surface waters due to its mass balance. Substantial changes in the estimated composition of the vertical flux ($\Delta\ \delta^{56}Fe$ = 2.04‰) impart little change in the resulting surface water Fe isotope composition (± 0.1‰). Therefore these calculations indicate the contributions of sedimentary Fe inputs to some ocean regions may be assessed by Fe isotopes studies. Transport signatures may be most successfully traced in regions where benthic Fe inputs offer a substantial contribution to the dissolved Fe budget, such as the northeast Pacific margin (Lohan and Bruland, 2008; Severmann et al., In prep.) and the sub-arctic pacific (Lam et al., 2006; Nishioka et al., 2007). Attempts to derive the sedimentary Fe flux from Fe isotope compositions in remote ocean regions will need to address the uncertainties of other flux magnitudes and their isotopic compositions.

6.4 IMPLICATIONS OF STUDY FOR FUTURE RESEARCH

This study has illustrated the potential for sedimentary Fe inputs to seawater to be more widespread than previously understood. Future benthic Fe flux investigations should consider examining bio-siliceous-volcaniclastic sediments as highlighted in this thesis as a potential source of nano-scale colloidal Fe to bottom waters. In addition, the following regions may also merit consideration for sedimentary Fe inputs to seawater: 1) oxygen minimum zones, where the reduced Fe(II) oxidation rates may permit the diffusion and accumulation of Fe into overlying bottom waters; 2) sediments subject to episodic carbon supply, such as those underlying surface water productivity blooms, and seasonal sea-ice cover; and 3) mobilised-sedimentary environments, where physical disturbance across the sediment redoxcline may promote the recycling of oxidised and reduced Fe phases, for example storm or wave disturbed sediments, continental shelf slope sediments (Nédélec et al., 2007), sediments subject to scouring by icebergs (Woodworth-Lynas et al., 1991), and sediments subject to anthropogenic disturbance such as deep-sea trawling.

Future efforts to investigate sedimentary Fe flux processes should include consideration of the following:

Dissolved pore-fluid Fe determination. This study has shown that filter sizes traditionally used to separate dissolved from particulate constituents in pore-fluids may also contain colloidal Fe phases.

Fe speciation. This study has shown that it is inadequate to assume pore-fluid Fe is entirely comprised of Fe(II). Knowledge of the true speciation of Fe would enable better quantification of oxidation rates, and improve interpretations of Fe cycling between dissolved and particulate phases.

Colloidal and/or nanoparticulate Fe composition. It has been suggested that authigenic basaltic weathering products may comprise some of the colloidal Fe in Crozet sediment pore-fluids. Knowledge of the composition of Fe phases open to exchange with the dissolved Fe pool would help interpret of the origin and fate of Fe in sediment pore-fluids.

Temporal variation to generation of Fe in pore-fluids. Regions studied in this thesis all exhibit dynamic characteristics to pore-fluid Fe generating processes, due either to episodic sediment supply, to biological ventilation of reducing sediments or to seasonal organic carbon delivery. It is important that temporal variation of these characteristics is represented in future studies.

Fe isotope composition. The coupling of benthic Fe recycling and pore-fluid Fe isotope compositions proposed in this thesis would benefit from additional Fe isotope measurements in other low and high carbon accumulating sedimentary environments. The Fe isotope composition of seawater, proximal and distal to benthic sources, will help constrain the utility of Fe isotopes discussed in this chapter. Of particular importance of for tracing benthic Fe inputs in the oceans, the fractionation of Fe isotopes during BBL exchange processes and during surface ocean bio-utilization needs to be evaluated.

Development of techniques for high-resolution in-situ sampling. There is need and opportunity for the development of high-resolution bottom-water sampling techniques for both coastal shelf and deep-sea sedimentary environments. The concentration gradients of Fe across the sediment-seawater interface may be the largest in the oceans, yet the sampling techniques used to date are incapable of linking pore-fluid and BBL concentration gradients effectively.

Novel experimental designs. Experiments aimed at constraining Fe exchange processes between sediments and seawater will improve our understanding of Fe exchange processes between aqueous Fe^{2+}, ligand-stabilised Fe^{2+}, particulate Fe oxides and colloidal Fe complexes, that are likely to determine the fate of sedimentary Fe inputs to the oceans.

Appendix I. Publication of thesis research

Material presented in this thesis has been published in the Journal Geology:

Homoky, W.B., Severmann, S., Mills, R.A., Statham, P.J., and Fones, G.R., 2009, Pore-fluid Fe isotopes reflect the extent of benthic Fe redox recycling: Evidence from continental shelf and deep-sea sediments: Geology, v. 37, p. 751-754.

A copy of this material is included in this appendix. In addition, the Uniform Reference Locator of an article in Science Magazine that highlights this research is included below:

http://www.sciencemag.org/content/vol325/issue5944/twil.dtl

Editor Nicholas S. Wigginton's article entitled "Heavy Down Below" draws attention to the findings presented in Homoky et al. (2009) and is featured in Science Magazine's "Editor's Choice", Volume 325, Number 5944, Issue of 28 August 2009.

Pore-fluid Fe isotopes reflect the extent of benthic Fe redox recycling: Evidence from continental shelf and deep-sea sediments

W.B. Homoky[1,*], S. Severmann[2], R.A. Mills[1], P.J. Statham[1], and G.R. Fones[3]
[1]National Oceanography Centre, University of Southampton, Southampton SO14 3ZH, UK
[2]Department of Earth and Planetary Sciences, and Institute of Marine and Coastal Sciences, Rutgers University, New Brunswick, New Jersey 08901, USA
[3]School of Earth and Environmental Sciences, University of Portsmouth, Portsmouth PO1 3QL, UK

ABSTRACT

Pore-fluid Fe isotopes may be a unique tracer of sediment respiration by dissimilatory Fe-reducing bacteria, but to date, pore-fluid Fe isotope measurements have been restricted to continental shelf settings. Here, we present δ^{56}Fe values of pore fluids from two distinct sedimentary settings: (1) a riverine-dominated site on the northern California margin (Eel River shelf; 120 m water depth) and (2) biogenic opal-rich volcaniclastic deep-sea sediments from the Southern Ocean (north and south of the Crozet Plateau; 3000–4000 m water depth). The Fe isotope compositions of Crozet region pore fluids are significantly less fractionated (δ^{56}Fe = +0.12‰ to –0.01‰) than the Eel River shelf (δ^{56}Fe = –0.65‰ to –3.40‰) and previous studies of pore-fluid Fe isotopes, relative to average igneous rocks. Our data represent the first measurements of Fe isotope compositions in pore fluids from deep-sea sediments. A comparison of pore-fluid δ^{56}Fe with the relative abundance of highly labile Fe in the reactive sedimentary Fe pool demonstrates that the composition of Fe isotopes in the pore fluids reflects the different extent of sedimentary Fe redox recycling between these sites.

INTRODUCTION

Iron is an essential micronutrient for intracellular processes, and in many macronutrient-replete oceanic regions (high nutrient, low chlorophyll [HNLC]), primary production is limited by the availability of Fe (Martin, 1990). Consequently, the supply of Fe to HNLC regions has been proposed as a major contributing factor to the regulation of carbon drawdown on glacial to interglacial time scales (Martin et al., 1990). Much of the Fe input in HNLC regions has commonly been attributed to aerosol deposition and dissolution, but, increasingly, studies highlight the potential importance of sedimentary Fe sources for the coastal, and even open, ocean (Lam et al., 2006; Nishioka et al., 2007). In continental margin sedimentary settings, the benthic transport of dissolved Fe has been found to be significant (McManus et al., 1997; Berelson et al., 2003; Elrod et al., 2004), and enrichment of Fe in the pore fluids and bottom waters is driven by the reductive dissolution of Fe during organic carbon decomposition.

Iron isotopes have emerged as a new tool to evaluate iron cycling in aquatic environments (Anbar and Rouxel, 2007; Johnson et al., 2008). Incubation experiments have demonstrated that the reduction of Fe(III) in the presence of dissimilatory Fe-reducing bacteria produces aqueous Fe^{2+} with δ^{56}Fe values that are 0.5‰–2‰ lower than the initial Fe(III) substrate (Beard et al., 1999; Icopini et al., 2004; Crosby et al., 2007). Pore fluids from sediments where organic matter oxidation proceeds through significant microbial Fe reduction yield isotope compositions for dissolved Fe^{2+} that are ~1‰–3‰ lighter than average igneous rocks, suggesting that benthic Fe inputs to the ocean may carry a unique isotopic fingerprint (Severmann et al., 2006).

Dissimilatory iron reduction (DIR) is a form of chemolithotrophy that is widespread during diagenesis of marine sediments, and the rate of this process is controlled by organic carbon oxidation and the availability of Fe(III) substrates (Froelich et al., 1979). DIR was one of the earliest metabolic pathways to evolve on Earth (Vargas et al., 1998), and it has been suggested that sedimentary Fe isotopes may be used to reconstruct past Fe cycling in the Archean ocean (Rouxel et al., 2005; Yamaguchi et al., 2005; Severmann et al., 2008).

Pore-fluid Fe isotope measurements have so far been restricted to the continental shelves where DIR is extensive (Bergquist and Boyle, 2006; Severmann et al., 2006). There have been no measurements of Fe isotopes in low–organic-carbon, suboxic sediment pore fluids, in deep-water settings where sediment accumulation rates are much slower and oxygen penetration is deeper than on the continental shelves, or in sediments where abiotic processes such as adsorption or ligand complexation may significantly imprint the pore-fluid Fe isotope composition. The need for comparison of Fe isotopes in shallow- and deep-water environments has been identified (Johnson et al., 2008), and characterization of the Fe isotopic fingerprint of DIR in natural, complex aqueous systems is important for the effective interpretation of the sedimentary record, and for developing the potential utility of Fe isotopes as a tracer of benthic Fe fluxes.

We present here new δ^{56}Fe data for surface sediment pore fluids (0–25 cmbsf [centimeters below seafloor]) from two distinct sedimentary settings: (1) a riverine-dominated site on the northern California margin (Eel River shelf; 120 m water depth), where the organic carbon accumulation rate is high (~26.7 g C m^{-2} a^{-1}; Sommerfield and Nittrouer, 1999) and carbon remineralization is driven by extensive Fe redox cycling, and (2) mixed biogenic opal-rich volcaniclastic sediments from two deep-sea sites in the Southern Ocean (M6: 4222 m; and M10: 3227 m), where organic carbon accumulation rates are low (M6: ~0.011 g C m^{-2} a^{-1}; M10: ~0.113 g C m^{-2} a^{-1}) and diagenetic Fe cycling is limited by the availability of reactive organic carbon (see the GSA Data Repository[1] for additional sample site information).

RESULTS

Pore-fluid nitrate penetration depth provides a qualitative tool for comparing the sedimentary redox status of our study sites. This depth is greatest at the Southern Ocean site (M6; 20–30 cmbsf), intermediate at the Southern Ocean northern site (M10; ~10 cmbsf), and shallowest at the Eel River shelf site (~5 cmbsf) (Fig. 1A). The shallowest nitrate penetration depth occurs at the site of highest mean organic carbon content at the Eel River shelf (0.87%, 0–22 cmbsf), which also has the greatest proportion of highly labile Fe phases ($Fe_{h\text{-}lab}$) relative to reactive hydrous Fe oxide (HFO) substrates ($Fe_{h\text{-}lab}$/[$Fe_{h\text{-}lab}$ + HFO] = 0.63–0.69 for Eel River compared to 0.02–0.20 in Crozet sediments; see Table DR1 in the Data Repository). The relative proportions of $Fe_{h\text{-}lab}$ (Na acetate leachable) and HFO (hydroxylamine-HCl leachable) were estimated using the sequential sediment extrac-

*E-mail: wbh@noc.soton.ac.uk.

[1]GSA Data Repository item 2009180, full description of materials and methods (including sample site descriptions, sampling and analytical procedures, justification of Rhizone sampling for pore-fluid nutrients, and critical evaluation of Crozet region pore-fluid Fe concentrations), is available online at www.geosociety.org/pubs/ft2009.htm, or on request from editing@geosociety.org or Documents Secretary, GSA, P.O. Box 9140, Boulder, CO 80301, USA.

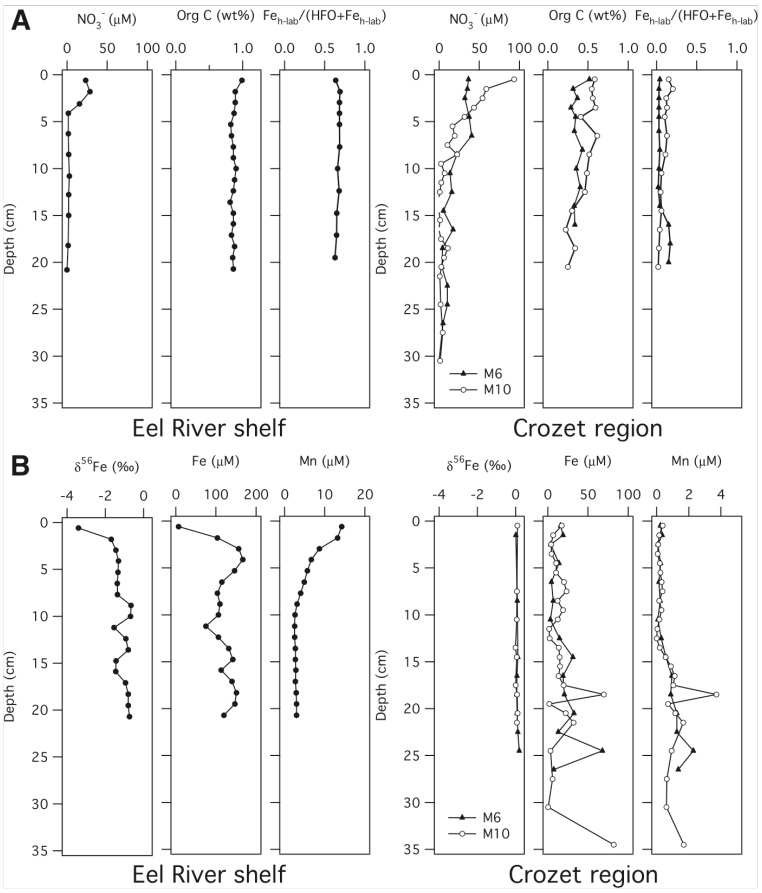

Figure 1. A: Pore-fluid nitrate, solid-phase organic carbon, and the proportion of highly labile Fe ($Fe_{h\text{-}lab}$) relative to hydrous Fe oxide (HFO) profiles. Nitrate penetration depth provides a qualitative tool to assess the redox conditions of the study sites. The $Fe_{h\text{-}lab}/(HFO + Fe_{h\text{-}lab})$ ratio records the relative proportion of highly labile Fe in a reactive Fe pool utilized during dissimilatory iron reduction (DIR). B: Concentration of Fe, Mn, and $\delta^{56}Fe$ in Crozet region and Eel River shelf pore fluids.

tion procedure given in Poulton and Canfield (2005) (see the Data Repository for details of all methods and analyses). The ratio $Fe_{h\text{-}lab}/(Fe_{h\text{-}lab} + HFO)$ provides an estimate of the extent of diagenetic redox recycling of Fe.

Crozet region pore-fluid $\delta^{56}Fe$ values range between +0.12‰ and –0.01‰ relative to average igneous rocks (Fig. 1B) and closely resemble those of average continental weathering products (0.2‰ ± 0.7‰; Beard et al., 2003). In contrast to both these sites, Eel River shelf $\delta^{56}Fe$ pore-fluid values lie between –0.65‰ and –3.40‰, and the greatest isotopic fractionation is closest to the sediment-seawater interface (Fig. 1B). Crozet pore-fluid Fe concentrations are ~1–80 μM at M10 and M6, and they are characterized by similar Mn distributions (up to 4 μM), with maxima at ~17 and 25 cmbsf at M10 and M6, respectively. At the Eel River shelf site, pore-fluid Fe concentrations reach a subsurface maximum of 167 μM at 5 cmbsf, and Mn concentrations are highest (14 μM) in the upper 0–5 cmbsf (see Data Repository Table DR2).

DISCUSSION

The distributions of Fe and Mn in Eel River shelf pore fluids are broadly consistent with the biogeochemical zonation of respiratory processes (Froelich et al., 1979), indicating the transition from aerobic respiration through to DIR between 0 and 5 cmbsf. However, Fe and Mn values in Crozet region pore fluids are not typical of deep-sea profiles, and values are relatively high (1–20 μM Fe; 0.1–0.3 μM Mn) in the upper 10 cm compared with previous measurements from deep-sea Southern Ocean sites (<0.1 μM Fe; King et al., 2000); the equatorial Pacific (<5 μM Fe; Haeckel et al., 2001); tropical northeast Atlantic (1–13 μM Fe; Froelich et al., 1979); and many coastal shelf settings (Canfield et al., 1993; McManus et al., 1997). Additionally, the biogeochemical zonation of NO_3^-, Mn, and Fe in the Crozet region pore fluids is less apparent than at the Eel River shelf site and provides little evidence for DIR-dominated diagenesis.

An analysis of two different dissolved size fractions (0.2 μm and 0.02 μm; see the Data Repository) in Crozet region pore fluids demonstrates that significant colloidal and/or nanoparticulate (herein after "colloidal") phases are present (Fig. 2). We speculate that these colloids are composed of adsorbed and/or organic ligand–bound Fe^{2+}/Fe^{3+} that may be utilized during DIR along with nanoparticulate basaltic weathering products. We suggest that the distribution of colloidal phases in the pore fluids is influenced by the episodic supply of organic carbon, which disrupts the steady-state pore-fluid composition (Gehlen et al., 1997); the vertical mixing of volcaniclastic sediments through slumping and turbidite emplacement in this region (Marsh et al., 2007); the influence of bioirrigation and bioturbation (Aller, 1990); and the uncertain role of stabilizing organic complexes in the pore-fluid environment (Luther et al., 1992).

Eel River shelf pore-fluid $\delta^{56}Fe$ compositions are consistent with previous studies of Fe-reducing continental margin sediments where DIR catalyzes the fractionation of Fe isotopes

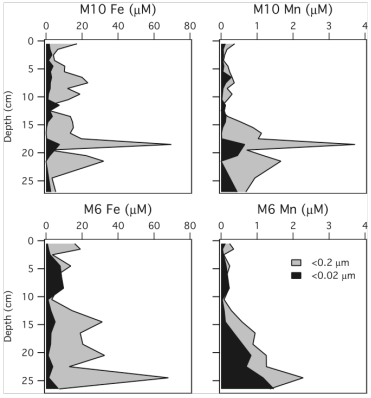

Figure 2. Pore-fluid Fe and Mn concentration at M10 and M6 sampled sequentially by two different filter sizes. Pore-fluid Fe and Mn are partitioned between <0.2 to >0.02 μm, and <0.02 μm size fractions at these sites, and they are inferred to make up a significant colloidal and/or nanoparticulate component of the pore fluids.

during redox cycling (Severmann et al., 2006) (Fig. 3). Crozet region pore-fluid δ^{56}Fe values are significantly less fractionated than previous values reported for suboxic pore fluids (Fig. 3). Severmann et al. (2006) noted that near-zero δ^{56}Fe values for pore fluids might reflect equilibrium with FeS. There is no evidence for sulfide diagenesis in Crozet region Holocene sediments (Marsh et al., 2007). Therefore, the comparison of the Eel River shelf and Crozet region suggests that either a mechanism other than DIR is releasing a substantial amount of Fe (up to 80 μM; δ^{56}Fe ~0.0‰) into the Crozet pore fluids, or that DIR alone may be insufficient to generate the low δ^{56}Fe values we observe in continental margin sediments.

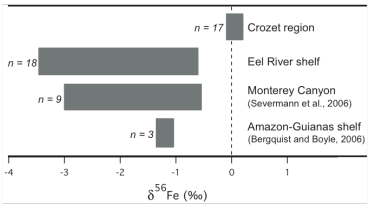

Figure 3. Comparison of Crozet region and Eel River shelf pore-fluid Fe isotope compositions with published data from dissimilatory iron reduction (DIR)–dominated reducing sediments on continental shelves.

Experiments have shown that Fe isotope fractionations of >1‰ in aqueous systems can also be produced by abiotic processes. For example, ligand-promoted dissolution of mineral substrates, such as goethite, ferrihydrite, and hornblende (Brantley et al., 2004), abiotic sorption and surface exchange (Icopini et al., 2004; Crosby et al., 2007), and isotope exchange between free and organically or inorganically complexed Fe (Dideriksen et al., 2008) could potentially contribute to variations in isotope compositions in nature that are indistinguishable from biological fractionations. Deconvolution of these processes in nature presents a major challenge; however, it has been argued that abiotic processes alone cannot generate the large inventories of isotopically fractionated Fe that have been identified in continental margin sediments (Johnson et al., 2008). We hypothesize that the observed variation in Fe isotope composition between our study sites reflects differences in the extent of biogenic benthic recycling of the reactive Fe pool.

The sedimentary reduction and oxidation of Fe during early diagenetic redox recycling has been estimated to occur 100–300 times prior to ultimate burial below the redoxcline (Canfield et al., 1993), where the extent of bioturbation and bioirrigation may enhance the redox recycling of Fe substrates by oxidizing Fe^{2+} and suppressing the onset of sulfide diagenesis (Canfield et al., 1993). The composition of Fe isotopes in sediment pore fluids is inferred to reflect the extent of redox recycling of Fe between DIR-derived Fe^{2+}_{aq} and highly labile oxidation products, such as amorphous Fe-(oxyhdr)oxide (Severmann et al., 2008). Experimental investigations of the mechanism producing Fe isotope fractionation during DIR have shown that the generation of light dissolved Fe^{2+}_{aq} can be attributed to a coupled electron and isotope exchange between sorbed Fe^{2+} and a reactive ferric Fe component on the surface of the Fe-oxide that is open to isotope exchange (Crosby et al., 2007). These authors argue that changes in the absolute δ^{56}Fe values of Fe^{2+}_{aq} in their experiments reflect changes in the relative sizes of the reactive Fe pools. The reactivity of Fe-oxide minerals may therefore be the primary control on the pore-fluid Fe isotope composition. Although we did not quantify the reactive Fe(III) component in the ferric oxide surfaces directly, the coincidence of low pore-fluid δ^{56}Fe values with high $Fe_{h\text{-}lab}$/($Fe_{h\text{-}lab}$ + HFO) in sediments from the Eel River shelf is consistent with the continuous reoxidation of Fe^{2+}_{aq} to amorphous Fe-(oxyhydr)oxides, providing an abundance of surface sites for isotope exchange, which are lacking in the Crozet sediments (Fig. 4).

We interpret the organic carbon supply to the Eel River shelf to be sufficient to sustain DIR and the redox recycling of Fe, thereby enriching highly labile Fe phases in the reactive Fe pool and accounting for the highest pore-fluid Fe isotope fractionation. In contrast, the low organic carbon input to the deep Crozet region sediments limits DIR and redox recycling of Fe. We speculate that highly seasonal organic carbon inputs to M10 (Pollard et al., 2009) may promote the episodic contribution of DIR to sediment respiration and account for the relative enrichment of highly labile Fe in M10 surface sediments and in M6 turbidite layers. In these circumstances, processes that contribute to the generation of colloids and/or nanoparticulates in the pore fluids (van der Zee et al., 2003) are likely to have near crustal isotope compositions and dilute the isotopic signature of DIR.

CONCLUSIONS

High dissolved Fe pore-fluid contents indicate suppression of sulfide diagenesis in Eel River shelf sediments and volcaniclastic weathering in Southern Ocean sediments. We demonstrate that the pore-fluid Fe isotope compositions reflect the extent of Fe recycling during early diagenesis, which is driven by supply of reactive organic carbon and Fe. We invite future interpretations of the rock record to consider the importance of Fe isotope processing in carbon-limited environments. Additionally, the unique isotopic fingerprint of pore-fluid Fe in continental shelf settings is confirmed, drawing further attention to the potential utility of Fe isotopes as a tracer of shelf-derived Fe inputs to seawater.

ACKNOWLEDGMENTS

This work was supported by the UK Natural Environment Research Council grant NE/B502844/1. California margin sampling and isotopic analyses were supported by the U.S. National Science Foundation grant OCE-0624777 (James McManus) and OCE-0624704 (Severmann), and our thanks go to the crew of RV *Wecoma* cruise WE0704E. We thank the crews of RRS *Discovery* cruises D286 and D300, as well as D. Green, P. Morris, S. Taylor, and L. Hep-

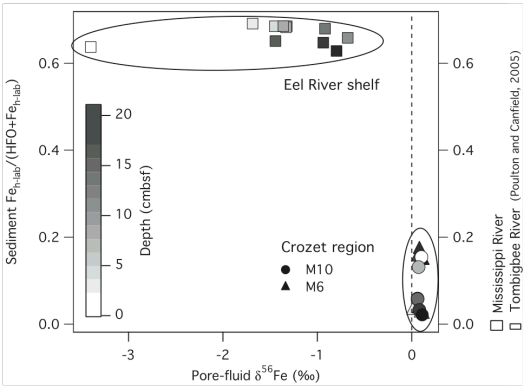

Figure 4. Comparison of Eel River shelf (ER) and Crozet region (M10 and M6) sediment $Fe_{h\text{-}lab}$/(HFO + $Fe_{h\text{-}lab}$) composition with pore-fluid δ^{56}Fe. The sample depth of data is represented by the grayscale. The $Fe_{h\text{-}lab}$/(HFO + $Fe_{h\text{-}lab}$) ratio provides an estimate of the relative enrichment of highly labile Fe phases in the reactive sedimentary pool driven by the extent of redox recycling of Fe during early diagenesis. The published $Fe_{h\text{-}lab}$/(HFO + $Fe_{h\text{-}lab}$) composition of riverbed sediments provides an estimate of the end-member composition of the reactive Fe pool prior to early diagenesis. The contrast between the $Fe_{h\text{-}lab}$/(HFO + $Fe_{h\text{-}lab}$) ratio of the Eel River shelf and Crozet region is attributed to the much greater supply of reactive organic carbon to the Eel River shelf, which enhances the redox recycling of Fe. The slight increase in $Fe_{h\text{-}lab}$/(HFO + $Fe_{h\text{-}lab}$) ratio at M10 (0–8 cmbsf) is attributed to episodic organic carbon inputs to the surface sediments at this site (Pollard et al., 2009), and to a turbidite layer at M6 (15–20 cmbsf; Marsh et al., 2007).

burn for their assistance with geochemical analyses. The authors wish to express their sincere thanks to J. McManus for stimulating discussion. Further, we thank Clark Johnson and Simon Poulton for their insightful reviews.

REFERENCES CITED

Aller, R.C., 1990, Bioturbation and manganese cycling in hemipelagic sediments: Philosophical Transactions of the Royal Society of London, Series A: Mathematical and Physical Sciences, v. 331, p. 51–68, doi: 10.1098/rsta.1990.0056.

Anbar, A.D., and Rouxel, O., 2007, Metal stable isotopes in paleoceanography: Annual Review of Earth and Planetary Sciences, v. 35, p. 717–746, doi: 10.1146/annurev.earth.34.031405.125029.

Beard, B.L., Johnson, C.M., Cox, L., Sun, H., Nealson, K.H., and Aguilar, C., 1999, Iron isotope biosignatures: Science, v. 285, p. 1889–1892, doi: 10.1126/science.285.5435.1889

Beard, B.L., Johnson, C.M., Von Damm, K.L., and Poulson, R.L., 2003, Iron isotope constraints on Fe cycling and mass balance in oxygenated Earth oceans: Geology, v. 31, p. 629–632, doi: 10.1130/0091-7613(2003)031<0629:IICOFC>2.0.CO;2.

Berelson, W., McManus, J., Coale, K., Johnson, K., Burdige, D., Kilgore, T., Colodner, D., Chavez, F., Kudela, R., and Boucher, J., 2003, A time series of benthic flux measurements from Monterey Bay, CA: Continental Shelf Research, v. 23, p. 457, doi: 10.1016/S0278-4343(03)00009-8.

Bergquist, B.A., and Boyle, E.A., 2006, Iron isotopes in the Amazon River system: Weathering and transport signatures: Earth and Planetary Science Letters, v. 248, p. 54–68, doi: 10.1016/j.epsl.2006.05.004.

Brantley, S.L., Liermann, L.J., Guynn, R.L., Anbar, A., Icopini, G.A., and Barling, J., 2004, Fe isotopic fractionation during mineral dissolution with and without bacteria: Geochimica et Cosmochimica Acta, v. 68, p. 3189, doi: 10.1016/j.gca.2004.01.023.

Canfield, D.E., Thamdrup, B., and Hansen, J.W., 1993, The anaerobic degradation of organic matter in Danish coastal sediments: Iron reduction, manganese reduction, and sulfate reduction: Geochimica et Cosmochimica Acta, v. 57, no. 16, p. 3867–3883.

Crosby, H.A., Roden, E.E., Johnson, C.M., and Beard, B.L., 2007, The mechanisms of iron isotope fractionation produced during dissimilatory Fe(III) reduction by *Shewanella putrefaciens* and *Geobacter sulfurreducens*: Geobiology, v. 5, p. 169–189, doi: 10.1111/j.1472-4669.2007.00103.x.

Dideriksen, K., Baker, J.A., and Stipp, S.L.S., 2008, Fe isotope fractionation between inorganic aqueous Fe(III) and a Fe siderophore complex: Mineralogical Magazine, v. 72, p. 313–316, doi: 10.1180/minmag.2008.072.1.313.

Elrod, V.A., Berelson, W.M., Coale, K.H., and Johnson, K.S., 2004, The flux of iron from continental shelf sediments: A missing source for global budgets: Geophysical Research Letters, v. 31, article no. L12307, doi: 10.1029/2004GL020216.

Froelich, P.N., Klinkhammer, G.P., Bender, M.L., Luedtke, N.A., Heath, G.R., Cullen, D., Dauphin, P., Hammond, D., Hartman, B., and Maynard, V., 1979, Early oxidation of organic matter in pelagic sediments of the eastern equatorial Atlantic: Suboxic diagenesis: Geochimica et Cosmochimica Acta, v. 43, p. 1075–1090, doi: 10.1016/0016-7037(79)90095-4.

Gehlen, M., Rabouille, C., Ezat, U., and Guidi-Guilvard, L.D., 1997, Drastic changes in deep-sea sediment porewater composition induced by episodic input of organic matter: Limnology and Oceanography, v. 42, p. 980–986.

Haeckel, M., König, I., Riech, V., Weber, M.E., and Suess, E., 2001, Pore water profiles and numerical modelling of biogeochemical processes in Peru Basin deep-sea sediments: Deep-Sea Research, Part II: Topical Studies in Oceanography, v. 48, p. 3713–3736, doi: 10.1016/S0967-0645(01)00064-9.

Icopini, G.A., Anbar, A.D., Ruebush, S.S., Tien, M., and Brantley, S.L., 2004, Iron isotope fractionation during microbial reduction of iron: The importance of adsorption: Geology, v. 32, p. 205–208, doi: 10.1130/G20184.1.

Johnson, C.M., Beard, B.L., and Roden, E.E., 2008, The iron isotope fingerprints of redox and biogeochemical cycling in modern and ancient Earth: Annual Review of Earth and Planetary Sciences, v. 36, p. 457–493, doi: 10.1146/annurev.earth.36.031207.124139.

King, S.L., Froelich, P.N., and Jahnke, R.A., 2000, Early diagenesis of germanium in sediments of the Antarctic South Atlantic: In search of the missing Ge sink: Geochimica et Cosmochimica Acta, v. 64, p. 1375, doi: 10.1016/S0016-7037(99)00406-8.

Lam, P.J., Bishop, J.K.B., Henning, C.C., Marcus, M.A., Waychunas, G.A., and Fung, I.Y., 2006, Wintertime phytoplankton bloom in the subarctic Pacific supported by continental margin iron: Global Biogeochemical Cycles, v. 20, no. 1, p. GB1006, doi: 10.1029/2005GB002557.

Luther, G.W., III, Kostka, J.E., Church, T.M., Sulzberger, B., and Stumm, W., 1992, Seasonal iron cycling in the salt-marsh sedimentary environment: The importance of ligand complexes with Fe(II) and Fe(III) in the dissolution of Fe(III) minerals and pyrite, respectively: Marine Chemistry, v. 40, p. 81–103, doi: 10.1016/0304-4203(92)90049-G.

Marsh, R., Mills, R.A., Green, D.R.H., Salter, I., and Taylor, S., 2007, Controls on sediment geochemistry in the Crozet region: Deep-Sea Research, Part II: Topical Studies in Oceanography, v. 54, p. 2260, doi: 10.1016/j.dsr2.2007.06.004.

Martin, J.H., 1990, Glacial-interglacial CO_2 change: The iron hypothesis: Paleoceanography, v. 5, p. 1–13, doi: 10.1029/PA005i001p00001.

Martin, J.H., Fitzwater, S.E., and Gordon, R.M., 1990, Iron deficiency limits phytoplankton growth in Antarctic waters: Global Biogeochemical Cycles, v. 4, p. 5–12, doi: 10.1029/GB004i001p00005.

McManus, J., Berelson, W.M., Coale, K.H., Johnson, K.S., and Kilgore, T.E., 1997, Phosphorus regeneration in continental margin sediments: Geochimica et Cosmochimica Acta, v. 61, p. 2891, doi: 10.1016/S0016-7037(97)00138-5.

Nishioka, J., Ono, T., Saito, H., Nakatsuka, T., Takeda, S., Yoshimura, T., Suzuki, K., Kuma, K., Nakabayashi, S., Tsumune, D., Mitsudera, H., Johnson, K.W., and Tsuda, A., 2007, Iron supply to the western subarctic Pacific: Importance of iron export from the Sea of Okhotsk: Journal of Geophysical Research, v. 112, p. C10012, doi: 10.1029/2006JC004055.

Pollard, T.R., and 33 others, 2009, Southern Ocean deep-water carbon export enhanced by natural iron fertilization: Nature, v. 457, p. 577–580.

Poulton, S.W., and Canfield, D.E., 2005, Development of a sequential extraction procedure for iron: Implications for iron partitioning in continentally derived particulates: Chemical Geology, v. 214, p. 209, doi: 10.1016/j.chemgeo.2004.09.003.

Rouxel, O.J., Bekker, A., and Edwards, K.J., 2005, Iron isotope constraints on the Archean and Paleoproterozoic ocean redox state: Science, v. 307, p. 1088–1091, doi: 10.1126/science.1105692.

Severmann, S., Johnson, C.M., Beard, B.L., and McManus, J., 2006, The effect of early diagenesis on the Fe isotope compositions of porewaters and authigenic minerals in continental margin sediments: Geochimica et Cosmochimica Acta, v. 70, p. 2006–2022, doi: 10.1016/j.gca.2006.01.007.

Severmann, S., Lyons, T.W., Anbar, A., McManus, J., and Gordon, G., 2008, Modern iron isotope perspective on the benthic iron shuttle and the redox evolution of ancient oceans: Geology, v. 36, p. 487–490, doi: 10.1130/G24670A.1.

Sommerfield, C.K., and Nittrouer, C.A., 1999, Modern accumulation rates and a sediment budget for the Eel shelf: A flood-dominated depositional environment: Marine Geology, v. 154, p. 227–241, doi: 10.1016/S0025-3227(98)00115-7.

van der Zee, C., Roberts, D.R., Rancourt, D.G., and Slomp, C.P., 2003, Nanogoethite is the dominant reactive oxyhydroxide phase in lake and marine sediments: Geology, v. 31, p. 993–996, doi: 10.1130/G19924.1.

Vargas, M., Kashefi, K., Blunt-Harris, E.L., and Lovley, D.R., 1998, Microbiological evidence for Fe(III) reduction on early Earth: Nature, v. 395, p. 65–67, doi: 10.1038/25720.

Yamaguchi, K.E., Johnson, C.M., Beard, B.L., and Ohmoto, H., 2005, Biogeochemical cycling of iron in the Archean-Paleoproterozoic Earth: Constraints from iron isotope variations in sedimentary rocks from the Kaapvaal and Pilbara cratons: Chemical Geology, v. 218, p. 135–169.

Manuscript received 8 December 2008
Revised manuscript received 31 March 2009
Manuscript accepted 7 April 2009

Printed in USA

Appendix II. Pore-fluid constituent data

Fe, Mn and NO_3^- measurements

Site	Depth	NO_3^- (μM)		Fe (μM)			Mn (μM)		
	(cmbsf)	<0.45 μm	<0.2 μm	<0.45 μm	<0.2 μm	<0.02 μm	<0.45 μm	<0.2 μm	<0.02 μm
Eel River shelf (Lat: 40°43.70'N, Long: 124°28.50'W, Depth: 120 m)									
ERS1	0-1.2	23.1	-	7.1	-	-	14.2	-	-
ERS1	1.2-2.4	28.4	-	104	-	-	13.2	-	-
ERS1	2.4-3.5	15.6	-	157	-	-	8.75	-	-
ERS1	3.5-4.7	1.5	-	167	-	-	6.75	-	-
ERS1	4.7-5.9	-	-	146	-	-	5.71	-	-
ERS1	5.9-7.1	1.5	-	115	-	-	4.93	-	-
ERS1	7.1-8.3	-	-	104	-	-	4.02	-	-
ERS1	8.3-9.4	1.9	-	110	-	-	3.09	-	-
ERS1	9.4-10.6	-	-	106	-	-	2.63	-	-
ERS1	10.6-11.8	2.8	-	75.5	-	-	2.48	-	-
ERS1	11.8-13.0	-	-	106	-	-	2.45	-	-
ERS1	13.0-14.2	1.9	-	132	-	-	2.70	-	-
ERS1	14.2-15.3	-	-	142	-	-	2.67	-	-
ERS1	15.3-16.5	1.9	-	113	-	-	2.75	-	-
ERS1	16.5-17.7	-	-	140	-	-	2.68	-	-
ERS1	17.7-18.9	1.4	-	151	-	-	2.88	-	-
ERS1	18.9-20.1	-	-	147	-	-	3.01	-	-
ERS1	20.1-21.3	0.0	-	120	-	-	3.0	-	-
Crozet (Lat: 45°59.97'S, Long: 56°08.95'E, Depth: 4269 m)									
M5	0-1	-	43.6	-	0.79	2.28	-	0.10	0.18
M5	1-2	-	44.4	-	6.66	5.61	-	0.23	-
M5	2-3	-	51.7	-	3.81	1.36	-	0.10	0.15
M5	3-5	-	41.3	-	0.31	1.90	-	0.03	0.10
M5	4-5	-	40.5	-	19.8	1.13	-	0.62	0.05
M5	5-6	-	37.2	-	0.44	0.53	-	0.05	0.00
M5	6-7	-	40.9	-	32.6	0.55	-	1.08	0.00
M5	7-8	-	34.5	-	36.4	0.09	-	1.54	0.11
M5	8-9	-	39.2	-	35.9	1.90	-	1.43	0.21
M5	9-10	-	23.6	-	294	0.14	-	18.2	0.00
M5	10-11	-	36.6	-	52.4	0.39	-	2.56	0.00
M5	11-12	-	38.5	-	15.2	0.42	-	0.76	0.01
M5	12-13	-	40.7	-	176	0.15	-	8.80	0.04
M5	13-14	-	6.3	-	25.9	2.10	-	0.76	0.24

(Continued…) Fe, Mn and NO_3^- measurements

Site	Depth	NO_3^- (μM)		Fe (μM)			Mn (μM)		
	(cmbsf)	<0.45 μm	<0.2 μm	<0.45 μm	<0.2 μm	<0.02 μm	<0.45 μm	<0.2 μm	<0.02 μm
Crozet (Lat: 44º31.45'S, Long: 49º59.86'E, Depth: 3227 m)									
M10	0-1	-	93.4	-	17.2	1.75	-	0.38	0.11
M10	1-2	-	58.7	-	6.54	2.16	-	0.17	0.06
M10	2-3	-	54.2	-	4.07	3.23	-	0.10	0.06
M10	3-4	-	43.4	-	4.66	1.38	-	0.07	0.04
M10	4-5	-	31.7	-	10.5	3.85	-	0.19	0.07
M10	5-6	-	16.6	-	10.2	2.42	-	0.24	0.05
M10	6-7	-	19.3	-	20.0	3.08	-	0.31	0.29
M10	7-8	-	10.5	-	23.3	2.37	-	0.37	0.13
M10	8-9	-	22.5	-	11.9	2.32	-	0.17	0.05
M10	9-10	-	2.5	-	18.8	1.27	-	0.30	0.03
M10	10-11	-	7.0	-	12.3	1.11	-	0.18	0.02
M10	11-12	-	2.6	-	1.60	-	-	0.04	-
M10	12-13	-	0.9	-	2.31	-	-	BDL†	-
M10	13-14	-	BDL†	-	13.5	3.51	-	0.19	0.14
M10	14-15	-	BDL†	-	14.8	1.01	-	0.55	0.12
M10	15-16	-	1.3	-	15.1	0.29	-	0.89	0.04
M10	16-17	-	BDL†	-	13.4	0.09	-	1.12	0.01
M10	17-18	-	2.4	-	19.7	0.34	-	1.03	0.02
M10	18-19	-	11.0	-	69.7	7.48	-	3.72	0.66
M10	19-20	-	6.3	-	1.88	-	-	0.71	-
M10	20-21	-	2.7	-	22.2	2.06	-	1.17	0.45
M10	21-23	-	0.8	-	32.0	0.01	-	1.66	0.00
M10	23-25	-	2.0	-	3.30	-	-	0.94	-
M10	25-28	-	4.5	-	5.77	2.86	-	0.64	0.49
M10	28-31	-	1.3	-	0.47	-	-	0.61	-
M10	31-35	-	-	-	82.0	-	-	1.69	-

(Continued…) Fe, Mn and NO_3^- measurements

Site	Depth	NO_3^- (μM)		Fe (μM)			Mn (μM)		
	(cmbsf)	<0.45 μm	<0.2 μm	<0.45 μm	<0.2 μm	<0.02 μm	<0.45 μm	<0.2 μm	<0.02 μm
Crozet (Lat: 48º59.98'S, Long: 51º20.03'E, Depth: 4222 m)									
M6	0-1	-	36.6	-	15.9	0.75	-	0.24	0.12
M6	1-2	-	35.3	-	19.0	1.35	-	0.35	0.04
M6	2-3	-	32.2	-	3.52	2.24	-	0.07	0.06
M6	3-5	-	37.5	-	13.7	7.85	-	0.24	0.14
M6	5-7	-	40.5	-	4.40	-	-	0.14	-
M6	7-9	-	22.2	-	6.58	-	-	0.22	-
M6	9-11	-	13.7	-	3.19	1.10	-	0.08	0.03
M6	11-13	-	15.8	-	14.5	2.67	-	0.29	0.08
M6	13-15	-	5.5	-	31.2	5.05	-	0.58	0.12
M6	15-17	-	17.4	-	19.0	2.74	-	0.95	0.35
M6	17-19	-	4.3	-	20.4	2.53	-	0.88	0.59
M6	19-21	-	3.7	-	32.5	1.15	-	1.26	0.83
M6	21-23	-	10.4	-	12.9	3.71	-	1.26	0.70
M6	23-25	-	10.3	-	68.0	1.53	-	2.28	1.17
M6	25-27	-	4.9	-	7.35	-	-	1.35	-
Montserrat (Lat: 16º38.40'N, Long: 62º02.00'W, Depth: 1114 m)									
JC18_33	0-1	-	*1.6	**0.17	0.30	0.26	*16.9	32.0	28.7
JC18_33	1-2	-	*0.6	**5.33	14.7	14.7	*41.3	64.4	60.1
JC18_33	2-3	-	*0.5	-	-	-	-	-	-
JC18_33	3-4	-	*1.0	**7.05	14.7	14.7	*83.2	96.2	94.2
JC18_33	4-5	-	-	**19.6	18.4	15.4	*104	99.7	100
JC18_33	5-7	-	-	**24.1	14.2	13.6	*108	128	129
JC18_33	7-9	-	-	**25.3	6.76	6.38	*142	161	161
JC18_33	9-11	-	*0.2	**9.87	8.45	8.07	*172	183	182
JC18_33	11-13	-	*0.3	**9.78	0.39	0.36	*179	205	205
JC18_33	13-15	-	*0.3	**0.28	9.56	8.83	*201	204	200
JC18_33	15-17	-	-	**24.1	18.0	17.3	*192	202	201
JC18_33	17-19	-	*0.2	**9.15	2.22	2.08	*176	201	197
JC18_33	19-21	-	-	**8.86	6.56	5.16	*194	204	195
JC18_33	21-23	-	-	**15.7	10.9	10.5	*203	193	188

†Below detection limit.

- Not determined.

* Data from JC18_8, an earlier occupation of JC18_33. Analysed by D. Hembury (NOCS).

** Data from 2nd core of single deployment at JC18_33.

Pore-fluid Fe (μM) determination by DET gels

Depth (cmbsf)	Crozet M5	Crozet M6	Crozet M10	Montserrat JC18_8
-2.0	17.2	-	-	-
-1.8	16.0	-	6.1	-
-1.6	35.6	-	5.8	-
-1.4	15.2	-	6.1	-
-1.2	9.4	-	8.6	4.1
-1.0	13.5	-	4.7	2.6
-0.8	22.8	-	4.8	3.2
-0.6	14.6	-	4.5	3.2
-0.4	12.2	10.9	3.2	3.6
-0.2	43.7	53.5	7.9	3.3
0.0	36.5	7.3	4.4	2.3
0.2	21.7	7.0	3.8	3.1
0.4	50.1	6.3	2.8	2.3
0.6	22.9	6.7	5.2	3.4
0.8	41.0	7.1	5.9	4.4
1.0	70.3	7.7	4.6	4.4
1.2	30.5	22.9	9.5	15.1
1.4	0.0	30.5	4.5	16.7
1.6	33.6	26.4	3.8	19.7
1.8	0.0	24.4	4.5	8.1
2.0	30.1	26.7	3.5	12.5
2.2	22.7	32.6	3.2	15.2
2.4	33.5	39.0	3.6	14.2
2.6	58.5	122.3	3.2	6.4
2.8	96.1	15.1	2.7	3.6
3.0	106.3	51.9	5.2	9.6
3.2	19.7	12.7	4.3	2.0
3.4	18.6	21.8	5.1	3.6
3.6	28.5	12.4	3.0	3.7
3.8	49.4	17.7	3.7	5.0
4.0	26.3	17.0	3.4	1.9
4.2	79.7	13.1	3.5	2.0
4.4	50.3	36.2	3.4	5.2
4.6	17.0	16.1	5.0	4.4
4.8	21.5	9.4	48.0	2.3
5.0	0.0	19.3	4.5	3.7
5.2	74.3	14.4	4.9	6.1
5.4	18.9	10.5	3.6	10.4
5.6	17.5	18.3	4.4	11.2
5.8	13.7	10.8	5.0	12.8
6.0	63.5	17.3	5.1	10.3
6.2	35.8	41.1	17.4	15.2

(Continued...) Pore-fluid Fe (μM) determination by DET gels

Depth	Crozet			Montserrat
(cmbsf)	M5	M6	M10	JC18_8
9.6	7.8	68.7	17.4	44.4
9.8	8.6	35.5	36.4	130.1
10.0	25.0	41.2	43.5	55.0
10.2	12.9	32.0	36.5	20.0
10.4	22.3	15.1	18.1	16.1
10.6	88.4	34.7	12.1	13.1
10.8	20.5	28.0	20.6	6.8
11.0	25.0	26.4	14.3	9.7
11.2	12.4	15.1	8.1	8.5
11.4	18.4	28.4	10.2	5.8
11.6	11.7	17.9	13.2	10.5
11.8	39.3	12.4	30.4	9.0
12.0	5.6	10.6	15.0	-3.0
12.2	18.6	14.5	23.8	11.8
12.4	21.7	12.9	14.0	6.2
12.6	11.1	63.0	15.7	6.6
12.8	23.9	19.4	34.2	6.5
13.0	-	8.8	-	9.3
13.2	-	29.0	-	17.5
13.4	-	25.6	-	26.4
13.6	-	18.7	-	50.9
13.8	-	17.7	-	-
14.0	-	28.8	-	-
14.2	-	27.9	-	-
14.4	-	26.0	-	-

Crozet data determined by GFAAS.
Montserrat data determined by ICP-MS at University of Portsmouth, following the same method described in Section 2.5 and analysed by D. Hembury (NOCS).

Fe isotope measurements

Site	Depth (cmbsf)	δ^{56}Fe <0.2μm (‰)	2-SD (±)	δ^{57}Fe <0.2μm (‰)	2-SD (±)	*n*
Eel River shelf (Lat: 40˚43.70'N, Long: 124˚28.50'W, Depth: 120 m)						
ERS1	0-1.2	-3.40	0.07	-5.08	0.39	1
ERS1	1.2-2.4	-1.69	0.06	-2.51	0.29	1
ERS1	2.4-3.5	-1.45	0.13	-1.92	0.33	2
ERS1	3.5-4.7	-1.32	0.13	-1.74	0.33	2
ERS1	4.7-5.9	-1.33	0.02	-1.58	0.22	1
ERS1	5.9-7.1	-1.37	0.15	-1.80	0.36	1
ERS1	7.1-8.3	-1.36	0.13	-2.12	0.33	2
ERS1	8.3-9.4	-0.65	0.21	-0.92	0.46	1
ERS1	9.4-10.6	-0.68	0.13	-1.09	0.33	2
ERS1	10.6-11.8	-1.54	0.05	-2.18	0.16	1
ERS1	11.8-13.0	-0.92	0.13	-1.05	0.33	2
ERS1	13.0-14.2	-0.80	0.08	-1.24	0.39	1
ERS1	14.2-15.3	-1.44	0.25	-2.01	0.09	1
ERS1	15.3-16.5	-1.46	0.09	-2.16	0.63	1
ERS1	16.5-17.7	-0.94	0.22	-1.25	0.39	1
ERS1	17.7-18.9	-0.80	0.13	-1.32	0.33	2
ERS1	18.9-20.1	-0.80	0.37	-1.22	0.19	1
ERS1	20.1-21.3	-0.74	0.13	-0.92	0.33	2
Crozet (Lat: 48º59.98'S, Long: 51º20.03'E, Depth: 4222 m)						
M6	0-1	-	-	-	-	-
M6	1-2	0.01	0.02	-0.06	0.12	2
M6	2-3	-	-	-	-	-
M6	3-5	-	-	-	-	-
M6	5-7	-	-	-	-	-
M6	7-9	0.09	0.02	0.22	0.12	2
M6	9-11	-	-	-	-	-
M6	11-13	-	-	-	-	-
M6	13-15	0.12	0.04	0.15	0.03	1
M6	15-17	0.07	0.03	0.05	0.06	1
M6	17-19	0.06	0.03	0.08	0.09	1
M6	19-21	0.08	0.01	0.12	0.03	1
M6	21-23	0.12	0.02	0.18	0.12	2
M6	23-25	0.19	0.02	0.32	0.22	1
M6	25-27	-	-	-	-	-

(Continued…) Fe isotope measurements

Site	Depth (cmbsf)	δ^{56}Fe <0.2μm (‰)	2-SD (±)	δ^{57}Fe <0.2μm (‰)	2-SD (±)	*n*
Crozet (Lat: 44°31.45'S, Long: 49°59.86'E, Depth: 3227 m)						
M10	0-1	0.10	0.02	0.18	0.12	2
M10	1-2	-	-	-	-	-
M10	2-3	-	-	-	-	-
M10	3-4	-	-	-	-	-
M10	4-5	-	-	-	-	-
M10	5-6	-	-	-	-	-
M10	6-7	0.07	0.02	-0.02	0.12	2
M10	7-8	-	-	-	-	-
M10	8-9	-	-	-	-	-
M10	9-10	-	-	-	-	-
M10	10-11	0.06	0.02	0.02	0.12	2
M10	11-12	-	-	-	-	-
M10	12-13	-	-	-	-	-
M10	13-14	-0.01	0.02	-0.06	0.12	2
M10	14-15	0.06	0.04	0.05	0.13	1
M10	15-16	-	-	-	-	-
M10	16-17	-	-	-	-	-
M10	17-18	0.00	0.02	-0.05	0.12	2
M10	18-19	0.08	0.02	0.13	0.12	2
M10	19-20	-	-	-	-	-
M10	20-21	0.11	0.05	0.18	0.06	1
M10	21-23	0.07	0.07	0.13	0.35	1
M10	23-25	-	-	-	-	-
M10	25-28	-	-	-	-	-
M10	28-31	-	-	-	-	-
M10	31-35	-	-	-	-	-
Mean isotope standards						
IRMM-14		-0.08	0.06	-0.17	0.09	6
IRMM-14 spiked seawater[§]		-0.07	0.12	-0.13	0.05	2
BCR2		-0.18	0.05	-0.29	0.14	6
TAG		-1.01	0.1	-1.54	0.12	3

n = number of istopic analyses

[†]Below detection limit.

[§] Fe stripped seawater samples spiked with 2ug and 5ug IRMM-14 isotope standard.

- Not determined.

Dissolved O_2 measurements (μM)

Crozet				Montserrat		
Depth (cmbsf)	M5	M6	M10	Depth (cmbsf)	JC18_33	JC18_8
-0.10	290	269	271	-0.1	239	239
-0.05	290	269	278	-0.09	239	242
0.00	288	266	241	-0.08	239	245
0.05	285	240	224	-0.07	238	246
0.10	274	220	200	-0.06	238	247
0.15	257	208	181	-0.05	238	247
0.20	241	201	166	-0.04	238	246
0.25	221	199	155	-0.03	238	245
0.30	206	198	144	-0.02	238	244
0.35	196	194	135	-0.01	238	244
0.40	187	194	130	0	236	243
0.45	178	195	121	0.01	230	240
0.50	171	197	114	0.02	217	235
0.55	166	196	109	0.03	199	227
0.60	160	193	102	0.04	178	217
0.65	159	192	98.3	0.05	160	205
0.70	154	193	93.8	0.06	147	192
0.75	151	193	88.3	0.07	139	181
0.80	148	191	85.3	0.08	133	171
0.85	146	192	80.7	0.09	128	161
0.90	142	193	77.8	0.1	125	150
0.95	142	187	73.9	0.11	123	137
1.00	141	186	71.9	0.12	119	124
1.05	138	188	68.2	0.13	114	112
1.10	138	187	65.6	0.14	109	100
1.15	137	183	63.9	0.15	104	89.1
1.20	137	185	62.1	0.16	101	79.2
1.25	135	186	59.8	0.17	97.8	70.2
1.30	135	184	57.0	0.18	95.7	61.9
1.35	136	183	54.3	0.19	94.0	54.2
1.40	137	182	53.2	0.2	92.5	47.2
1.45	137	183	51.5	0.21	91.3	41.1
1.50	136	182	49.7	0.22	90.4	35.5
1.55	136	182	47.2	0.23	89.5	30.3
1.60	135	179	45.1	0.24	89.2	25.7
1.65	132	179	44.2	0.25	89.2	21.6
1.70	133	177	41.3	0.26	89.3	18.1
1.75	132	177	39.2	0.27	89.8	15.0
1.80	130	178	38.2	0.28	89.8	12.5
1.85	130	178	35.9	0.29	90.3	10.4
1.90	129	178	34.3	0.3	90.7	8.6

(Continued...) Dissolved O_2 measurements (μM)

Crozet				Montserrat		
Depth (cmbsf)	M5	M6	M10	Depth (cmbsf)	JC18_33	JC18_8
1.95	128	174	33.7	0.31	91.2	7.2
2.00	127	174	33.0	0.32	91.3	6.0
2.05	126	173	32.5	0.33	91.1	5.0
2.10	127	172	30.8	0.34	90.8	4.2
2.15	125	175	29.4	0.35	91.2	3.5
2.20	124	172	29.9	0.36	91.3	3.0
2.25	124	169	29.6	0.37	91.7	2.6
2.30	123	170	29.9	0.38	91.4	2.4
2.35	122	172	28.7	0.39	91.5	2.2
2.40	123	170	28.1	0.4	90.6	2.0
2.45	120	167	28.2	0.41	89.1	1.9
2.50	119	168	28.6	0.42	86.7	1.7
2.55	118	167	28.2	0.43	84.1	1.6
2.60	117	170	27.4	0.44	81.4	1.6
2.65	117	166	26.5	0.45	78.2	1.5
2.70	116	167	26.3	0.46	76.4	1.4
2.75	114	161	26.0	0.47	74.8	1.3
2.80	114	164	26.5	0.48	73.8	1.3
2.85	113	162	25.1	0.49	71.7	1.2
2.90	109	163	24.8	0.5	69.7	1.2
2.95	105	164	24.2	0.51	67.4	1.2
3.00	107	164	24.8	0.52	65.0	1.1
3.05	106	162	23.5	0.53	61.8	1.0
3.10	106	165	23.1	0.54	58.4	1.0
3.15	104	158	22.5	0.55	54.0	1.0
3.20	102	159	21.8	0.56	50.0	0.9
3.25	101	157	20.9	0.57	46.5	0.9
3.30	99.2	162	21.7	0.58	44.0	0.9
3.35	98.7	158	20.3	0.59	40.7	0.9
3.40	96.3	158	19.9	0.6	37.7	0.8
3.45	96.7	157	19.3	0.61	35.0	0.8
3.50	97.1	157	18.3	0.62	33.6	0.8
3.55	94.8	157	17.5	0.63	32.1	0.7
3.60	92.9	160	17.5	0.64	30.9	0.7
3.65	92.9	157	16.2	0.65	29.0	0.7
3.70	92.5	158	15.7	0.66	27.2	0.7
3.75	90.4	152	15.7	0.67	24.8	0.7
3.80	88.8	154	15.0	0.68	22.6	0.7
3.85	89.0	157	13.9	0.69	20.2	0.7
3.90	89.0	153	14.2	0.7	18.2	0.6
3.95	88.4	153	13.6	0.71	16.1	0.6
4.00	88.2	155	13.2	0.72	14.0	0.6
4.05	85.5	157	11.9	0.73	11.7	0.5

(Continued...) Dissolved O_2 measurements (μM)

Crozet				Montserrat		
Depth (cmbsf)	M5	M6	M10	Depth (cmbsf)	JC18_33	JC18_8
4.10	85.2	155	10.9	0.74	9.6	0.5
4.15	82.7	155	10.9	0.75	7.8	0.5
4.20	81.2	155	10.3	0.76	6.3	0.5
4.25	79.4	152	9.6	0.77	5.1	0.5
4.30	78.3	153	9.1	0.78	4.1	0.5
4.35	78.2	150	8.4	0.79	3.2	0.4
4.40	75.8	148	8.0	0.8	2.5	0.4
4.45	73.9	150	8.7	0.81	1.8	0.4
4.50	75.1	150	7.0	0.82	1.2	0.4
4.55	73.3	148	6.6	0.83	0.9	0.4
4.60	72.1	152	6.2	0.84	0.7	0.4
4.65	70.6	147	5.7	0.85	0.5	0.4
4.70	71.8	149	5.8	0.86	0.5	0.4
4.75	70.3	151	5.2	0.87	0.4	0.4
4.80	70.6	143	5.0	0.88	0.4	0.4
4.85	69.6	147	5.0	0.89	0.4	0.4
4.90	68.5	143	3.7	0.9	0.3	0.4
4.95	69.1	141	3.9	0.91	0.3	0.4
5.00	69.2	145	4.1	0.92	0.3	0.4
5.05	68.4	145	4.1	0.93	0.3	0.4
5.10	68.2	143	3.6	0.94	0.3	0.3
5.15	66.3	144	3.0	0.95	0.3	0.3
5.20	67.4	136	1.8	0.96	0.3	0.3
5.25	67.4	139	2.0	0.97	0.3	0.3
5.30	66.9	143	2.0	0.98	0.3	0.3
5.35	65.0	137	1.2	0.99	0.2	0.3
5.40	66.5	137	0.9	1	0.2	0.3
5.45	67.1	141	2.1	1.01	0.2	0.3
5.50	66.5	140	1.7	1.02	0.2	0.3
5.55	65.3	138	0.7	1.03	0.2	0.3
5.60	64.8	139	0.1	1.04	0.2	0.3
5.65	64.0	140	0.1	1.05	0.2	0.3
5.70	63.4	139	0.0	1.06	0.2	0.2
-	-	-	-	1.07	0.2	0.3
-	-	-	-	1.08	0.2	0.2
-	-	-	-	1.09	0.2	0.2
-	-	-	-	1.1	0.2	0.2

DSi measurements (μM)

Depth (cmbsf)	Crozet*		Montserrat**
	M6	M10	JC18_8
0-1	740	397	59
1-2	641	562	63
2-3	618	604	59
3-4	-	601	61
4-5	638	688	-
5-6	-	700	-
6-7	722	708	-
7-8	-	661	-
8-9	726	500	-
9-10	-	545	60
10-11	6712	604	66
11-12	-	496	-
12-13	748	507	74
13-14	-	762	-
14-15	641	784	-
15-16	-	729	-
16-17	685	708	-
17-18	-	706	-
18-19	620	594	74
19-20	-	608	-
20-21	629	788	-
21-22	-	657	-
22-23	670	-	-
23-24	-	-	-
24-25	482	-	-
25-26	-	628	-
26-27	522	-	-
27-28	-	-	-
28-29	-	618	-
31-32	-	30	-
32-33	-	-	92
33-34	-	-	-
34-35	-	-	94
35-36	-	250	-
36-37	-	-	101

* Analysed by Paul Morris, NOCS.
** Analysed by Debbie Hembury, NOCS
\- Not determined.

Appendix III. Sediment constituent data

TC, TIC, $CaCO_3$ and TOC determinations

Site	Depth (cmbsf)	TC (dwt %)	TIC (dwt %)	*CaCO3 (dwt %)	TOC (dwt %)
Eel River shelf (Lat: 40°43.70'N, Long: 124°28.50'W, Depth: 120 m)					
ERS1	0-1.2	1.03	0.05	0.41	0.99
ERS1	1.2-2.4	0.89	0.05	0.38	0.89
ERS1	2.4-3.5	0.97	0.04	0.38	0.89
ERS1	3.5-4.7	0.92	0.05	0.37	0.87
ERS1	4.7-5.9	0.86	0.06	0.48	0.82
ERS1	5.9-7.1	0.90	0.05	0.44	0.83
ERS1	7.1-8.3	0.90	0.04	0.35	0.86
ERS1	8.3-9.4	0.90	0.04	0.37	0.86
ERS1	9.4-10.6	1.00	0.04	0.32	0.90
ERS1	10.6-11.8	0.87	0.05	0.36	0.88
ERS1	11.8-13.0	0.90	0.04	0.29	0.86
ERS1	13.0-14.2	0.43	0.05	0.43	0.81
ERS1	14.2-15.3	0.94	0.05	0.40	0.86
ERS1	15.3-16.5	0.88	0.05	0.36	0.86
ERS1	16.5-17.7	0.92	0.05	0.39	0.83
ERS1	17.7-18.9	0.84	0.05	0.39	0.88
ERS1	18.9-20.1	0.92	0.04	0.35	0.85
ERS1	20.1-21.3	0.89	0.04	0.32	0.86
Crozet (Lat: 45°59.97'S, Long: 56°08.95'E, Depth: 4269 m)					
M5	1-2	2.21	1.87	15.5	0.35
M5	2-3	2.30	1.90	15.8	0.39
M5	3-4	2.28	1.87	15.6	0.41
M5	4-5	2.20	1.83	15.2	0.37
M5	9-10	2.05	1.85	15.4	0.20
M5	10-11	2.24	2.06	17.1	0.18
M5	12-13	2.28	2.07	17.2	0.21
M5	13-14	2.40	2.29	19.1	0.10
M5	15-16	1.64	1.35	11.3	0.29
Crozet (Lat: 48°59.98'S, Long: 51°20.03'E, Depth: 4222 m)					
M6	0-1	1.09	0.57	4.73	0.52
M6	1-2	0.94	0.62	5.19	0.31
M6	2-3	0.94	0.57	4.73	0.37
M6	3-4	0.93	0.64	5.36	0.29

(Continued…) TC, TIC, $CaCO_3$ and TOC determinations

Site	Depth (cmbsf)	TC (dwt %)	TIC (dwt %)	*CaCO3 (dwt %)	TC (dwt %)
M6	4-5	1.05	0.71	5.92	0.34
M6	5-7	1.06	0.73	6.06	0.33
M6	7-9	1.28	0.85	7.08	0.43
M6	9-11	1.22	0.86	7.18	0.35
M6	11-13	1.30	0.90	7.47	0.40
M6	13-15	1.26	0.94	7.79	0.33
M6	15-17	1.30	0.96	8.03	0.34
Crozet (Lat: 44º31.45'S, Long: 49º59.86'E, Depth: 3227 m)					
M10	0-1	3.26	2.68	22.29	0.58
M10	1-2	2.93	2.39	19.88	0.54
M10	2-3	2.82	2.26	18.83	0.56
M10	3-4	2.67	2.08	17.30	0.59
M10	4-5	2.51	2.10	17.49	0.41
M10	6-7	2.73	2.11	17.60	0.62
M10	8-9	2.59	2.07	17.23	0.52
M10	10-11	2.64	2.15	17.93	0.49
M10	12-13	2.52	2.06	17.13	0.46
M10	14-15	2.34	2.03	16.95	0.30
M10	16-17	2.30	2.08	17.34	0.22
M10	18-19	2.17	1.83	15.24	0.34
M10	20-21	1.91	1.66	13.82	0.25
Montserrat (Lat: 16º38.40'N, Long: 62º02.00'W, Depth: 1114 m)					
JC18_33	0-1	0.33	0.27	2.28	0.07
JC18_33	1-2	0.41	0.37	2.95	0.05
JC18_33	2-3	0.63	0.56	4.58	0.08
JC18_33	3-4	1.29	1.21	10.15	0.07
JC18_33	4-5	1.08	1.06	8.75	0.02
JC18_33	5-7	0.25	0.22	1.76	0.03
JC18_33	7-9	0.08	0.07	0.58	0.01
JC18_33	9-11	0.09	0.08	0.64	0.01
JC18_33	11-13	0.11	0.11	0.95	0.00
JC18_33	13-15	0.58	0.54	4.47	0.04
JC18_33	15-17	0.68	0.63	5.35	0.05
JC18_33	17-19	0.28	0.27	2.24	0.01
JC18_33	19-21	0.08	0.05	0.45	0.02
JC18_33	21-23	0.15	0.13	1.05	0.02

*$CaCO_3$ calculated from inorganic carbon content, where [$CaCO_3$] = 8.33x[TIC]

Total Fe, Mn and Ti determinations

Site	Depth (cmbsf)	Fe (dwt %)	Mn (dwt %)	Ti (dwt %)
Eel River shelf (Lat: 40°43.70'N, Long: 124°28.50'W, Depth: 120 m)				
ERS1	0-1.2	4.73	0.06	0.11
ERS1	1.2-2.4	4.21	0.05	0.45
ERS1	2.4-3.5	4.52	0.06	0.45
ERS1	3.5-4.7	4.25	0.05	0.41
ERS1	4.7-5.9	4.09	0.05	0.44
ERS1	5.9-7.1	4.09	0.05	0.44
ERS1	7.1-8.3	4.06	0.05	0.44
ERS1	8.3-9.4	4.07	0.05	0.45
ERS1	9.4-10.6	4.17	0.05	0.45
ERS1	10.6-11.8	3.96	0.05	0.46
ERS1	11.8-13.0	4.05	0.05	0.44
ERS1	13.0-14.2	4.16	0.06	0.45
ERS1	14.2-15.3	4.32	0.06	0.47
ERS1	15.3-16.5	4.10	0.05	0.44
ERS1	16.5-17.7	4.00	0.05	0.44
ERS1	17.7-18.9	4.12	0.05	0.44
ERS1	18.9-20.1	4.28	0.06	0.45
ERS1	20.1-21.3	4.32	0.06	0.46
Crozet (Lat: 45°59.97'S, Long: 56°08.95'E, Depth: 4269 m)				
M5	1-2	3.11	0.08	0.74
M5	2-3	3.36	0.09	0.72
M5	3-4	3.28	0.08	0.76
M5	4-5	3.55	0.08	0.67
M5	9-10	3.13	0.10	0.66
M5	10-11	1.04	0.09	0.19
M5	12-13	3.19	0.11	0.74
M5	13-14	2.00	0.09	0.40
M5	15-16	1.32	0.06	0.26
Crozet (Lat: 48°59.98'S, Long: 51°20.03'E, Depth: 4222 m)				
M6	0-1	1.87	0.04	0.33
M6	1-2	2.13	0.04	0.34
M6	2-3	2.89	0.05	0.47
M6	3-5	2.51	0.05	0.55
M6	5-7	1.96	0.05	0.41
M6	7-9	2.77	0.06	0.64
M6	9-11	3.00	0.06	0.62

(Continued…) Total Fe, Mn and Ti determinations

Site	Depth (cmbsf)	Fe (dwt %)	Mn (dwt %)	Ti (dwt %)
M6	11-13	2.93	0.09	0.69
M6	13-15	3.08	0.08	0.71
M6	15-17	3.20	0.07	0.73
M6	17-19	3.22	0.06	0.78
M6	19-21	3.25	0.06	0.76
M6	21-23	3.40	0.06	0.83
Crozet (Lat: 44º31.45'S, Long: 49º59.86'E, Depth: 3227 m)				
M10	0-1	1.37	0.03	0.25
M10	1-2	1.02	0.03	0.18
M10	2-3	1.24	0.03	0.21
M10	3-4	1.35	0.03	0.22
M10	4-5	0.97	0.03	0.17
M10	6-7	1.19	0.02	0.22
M10	8-9	1.32	0.02	0.19
M10	10-11	1.27	0.02	0.24
M10	12-13	1.17	0.02	0.23
M10	14-15	1.19	0.01	0.23
M10	16-17	1.21	0.01	0.22
M10	18-19	1.11	0.02	0.21
M10	20-21	0.95	0.01	0.15
Montserrat (Lat: 16º38.40'N, Long: 62º02.00'W, Depth: 1114 m)				
JC18_33	0-1	3.72	0.10	0.27
JC18_33	1-2	3.76	0.10	0.28
JC18_33	2-3	4.01	0.10	0.31
JC18_33	3-4	3.52	0.09	0.27
JC18_33	4-5	3.93	0.10	0.29
JC18_33	5-7	4.15	0.11	0.32
JC18_33	7-9	5.21	0.13	0.39
JC18_33	9-11	4.99	0.13	0.37
JC18_33	11-13	4.17	0.12	0.29
JC18_33	13-15	3.94	0.11	0.29
JC18_33	15-17	3.75	0.10	0.27
JC18_33	17-19	3.91	0.11	0.30
JC18_33	19-21	3.92	0.11	0.30
JC18_33	21-23	3.69	0.11	0.25

Reactive Fe phases

Site	Depth (cmbsf)	$Fe_{h\text{-}lab}$ † (dwt %)	Fe_{ox1} * (dwt %)	Fe_{ox2} ** (dwt %)
Eel River shelf (Lat: 40°43.70'N, Long: 124°28.50'W, Depth: 120 m)				
ERS1	0-1.2	0.296	0.168	0.371
ERS1	1.2-2.4	0.359	0.160	0.233
ERS1	2.4-3.5	0.323	0.149	0.275
ERS1	3.5-4.7	0.317	0.146	0.254
ERS1	4.7-5.9	0.352	0.164	0.268
ERS1	5.9-7.1	-	-	-
ERS1	7.1-8.3	0.414	0.190	0.350
ERS1	8.3-9.4	-	-	-
ERS1	9.4-10.6	0.384	0.199	0.377
ERS1	10.6-11.8	-	-	-
ERS1	11.8-13.0	0.452	0.214	0.374
ERS1	13.0-14.2	-	-	-
ERS1	14.2-15.3	0.494	0.265	0.477
ERS1	15.3-16.5	-	-	-
ERS1	16.5-17.7	0.476	0.260	0.441
ERS1	17.7-18.9	-	-	-
ERS1	18.9-20.1	0.529	0.313	0.508
ERS1	20.1-21.3	-	-	-
Crozet (Lat: 45°59.97'S, Long: 56°08.95'E, Depth: 4269 m)				
M5	1-2	0.018	0.348	0.234
M5	2-3	0.019	0.358	0.224
M5	3-4	0.016	0.339	0.215
M5	4-5	0.018	0.338	0.230
M5	9-10	0.010	0.354	0.217
M5	10-11	0.014	0.339	0.208
M5	12-13	0.010	0.326	0.202
M5	13-14	0.013	0.316	BDL
M5	15-16	0.011	0.322	BDL

(Continued…) Reactive Fe phases

Site	Depth (cmbsf)	$Fe_{h\text{-}lab}$ † (dwt %)	Fe_{ox1} * (dwt %)	Fe_{ox2} ** (dwt %)
Crozet (Lat: 48°59.98'S, Long: 51°20.03'E, Depth: 4222 m)				
M6	0-1	0.010	0.254	0.238
M6	1-2	0.009	0.270	0.256
M6	2-3	0.010	0.336	0.232
M6	3-5	0.009	0.324	0.241
M6	5-7	0.009	0.298	0.267
M6	7-9	0.008	0.298	0.262
M6	9-11	0.017	0.375	0.271
M6	11-13	0.015	0.410	0.268
M6	13-15	0.010	0.445	0.205
M6	15-17	0.016	0.427	0.206
M6	17-19	0.091	0.499	0.205
M6	19-21	0.101	0.487	0.208
M6	21-23	0.086	0.500	0.218
Crozet (Lat: 44°31.45'S, Long: 49°59.86'E, Depth: 3227 m)				
M10	0-1	0.034	0.185	0.113
M10	1-2	0.042	0.169	0.134
M10	2-3	0.022	0.164	0.116
M10	3-4	0.024	0.159	0.118
M10	4-5	0.017	0.160	0.108
M10	6-7	0.023	0.149	0.121
M10	8-9	0.014	0.118	0.113
M10	10-11	0.009	0.140	0.110
M10	12-13	0.007	0.126	0.142
M10	14-15	0.008	0.122	0.101
M10	16-17	0.006	0.125	0.119
M10	18-19	0.004	0.116	0.183
M10	20-21	0.004	0.170	0.174

(Continued…) Reactive Fe phases

Site	Depth (cmbsf)	$Fe_{h\text{-}lab}$ † (dwt %)	Fe_{ox1} * (dwt %)	Fe_{ox2} ** (dwt %)
Montserrat (Lat: 16º38.40'N, Long: 62º02.00'W, Depth: 1114 m)				
JC18_33	0-1	0.016	0.034	0.151
JC18_33	1-2	0.013	0.025	0.149
JC18_33	2-3	0.008	0.012	0.111
JC18_33	3-4	0.007	0.011	0.086
JC18_33	4-5	0.008	0.012	0.102
JC18_33	5-7	0.007	0.010	0.091
JC18_33	7-9	0.007	0.012	0.101
JC18_33	9-11	0.005	0.009	0.078
JC18_33	11-13	0.012	0.018	0.116
JC18_33	13-15	0.010	0.015	0.130
JC18_33	15-17	0.008	0.012	0.098
JC18_33	17-19	0.007	0.011	0.092
JC18_33	19-21	0.005	0.009	0.089
JC18_33	21-23	0.020	0.039	0.204

†Highly-labile Fe, including adsorbed and carbonate associated Fe, extracted by Na acetate.

*Easily reducidble (hydrous) Fe oxides, extracted by hydroxylamine-HCl.

**Reducible Fe oxides (such as goethite), extracted by Na Dithionite.

- Not determined.

Appendix IV. Microcosm experiment data

Eel River shelf microcosm experiment data

Core	Comment	Time (hrs)	O_2 (μM)	Fe (nM)	(± 1-SD)
Experiment 1 (ERS2: 40º 43.7 N -124º 28.6 W, Depth: 125 m)					
A	Circ.	0	148	66	3
A	Circ.	6.5	125	128	5
A	Circ.	16	120	156	7
A	Circ.	24	111	227	10
A	Circ.	39	100	207	9
A	Circ.	49	89	194	8
B	Circ.	0	133	54	2
B	Circ.	6.5	112	49	2
B	Circ.	16	114	50	2
B	Circ.	24	105	156	7
B	Circ.	39	88	100	4
B	Circ.	49	83	139	6
C	Circ.	0	131	29	1
C	Circ.	6.5	121	65	3
C	Circ.	16	123	56	2
C	Circ.	24	117	106	4
C	Circ.	39	98	104	4
C	Circ.	49	91	127	5
D	Circ.	0	121	72	3
D	Circ.	6.5	117	121	5
D	Circ.	16	129	79	3
D	Circ.	24	115	104	4
D	Circ.	39	120	122	5
D	Circ.	49	115	78	3
Experiment 2 (ERS3: 40º 57.0 N -124º 18.2 W, Depth: 90 m)					
A	Circ.	0	71	44	2
A	Circ.	6.5	92	36	2
A	Circ.	18	78	32	1
A	Circ.	23.5	77	15	1
A	Circ.	30	72	23	1
A	Circ.	43	59	82	3
B	Circ.	0	69	44	2
B	Circ.	6.5	74	29	1
B	Circ.	18	71	76	3
B	Circ.	23.5	65	202	8
B	Circ.	30	63	240	10
B	Circ.	43	58	231	10

(Continued…) Eel River shelf microcosm experiment data

Core	Comment	Time (hrs)	O_2 (μM)	Fe (nM)	± 1-SD
C	Circ. + Bio.	0	78	102	4
C	Circ. + Bio.	6.5	75	26	1
C	Circ. + Bio.	18	74	41	2
C	Circ. + Bio.	23.5	62	73	3
C	Circ. + Bio.	30	76	11	0
C	Circ. + Bio.	43	66	55	2
D	Circ. + Bio.	0	74	99	4
D	Circ. + Bio.	6.5	76	45	2
D	Circ. + Bio.	18	88	44	2
D	Circ. + Bio.	23.5	71	-	-
D	Circ. + Bio.	30	80	83	3
D	Circ. + Bio.	43	70	43	2
Experiment 3 (ERS3: 40º 57.0 N -124º 18.2 W, Depth: 90 m)					
Exp.2 A	Circ.	0*	62	72	3
Exp.2 A	Susp.	1	67	22	1
Exp.2 A	Susp.	2	60	19	1
Exp.2 A	Circ.	3	67	22	1
Exp.2 A	Circ.	4	72	47	2
Exp.2 A	Circ.	5	71	91	4
Exp.2 B	Circ.	0*	55	252	11
Exp.2 B	Susp.	1	52	180	8
Exp.2 B	Susp.	2	51	68	3
Exp.2 B	Circ.	3	52	34	1
Exp.2 B	Circ.	4	53	75	3
Exp.2 B	Circ.	5	53	114	5
Exp. 2 C	Circ. + Bio.	0*	72	18	1
Exp. 2 C	Bio. + Susp.	1	71	35	1
Exp. 2 C	Bio. + Susp.	2	73	17	1
Exp. 2 C	Circ. + Bio.	3	80	49	2
Exp. 2 C	Circ. + Bio.	4	76	22	1
Exp. 2 C	Circ. + Bio.	5	77	16	1
Exp. 2 D	Circ. + Bio.	0*	76	42	2
Exp. 2 D	Bio. + Susp.	1	86	25	1
Exp. 2 D	Bio. + Susp.	2	90	24	1
Exp. 2 D	Circ. + Bio.	3	95	25	1
Exp. 2 D	Circ. + Bio.	4	111	22	1
Exp. 2 D	Circ. + Bio.	5	89	24	1

Circ. - Re-circulation of overlying corewater
Bio. - Biocide addition to overlying corewater
Susp. - Re-suspension of surface sediment by enhanced overlying corewater circulation
* Start of Exp.3 (t = 0 hrs) is equivalent to Exp. 2: t = ~45 hrs.

Montserrat microcosm experiment data

Core	Comment	Time (hrs)	O_2 (μM)	Fe (nM)	(± 1-SD)	Mn (nM)	(± 1-SD)
Experiment 1 (JC18_18: 16º 30.50 N -62º 27.00 W, Depth: 787 m)							
B	Circ.	0	174	87	35	1292	48
B	Circ.	6	-	18	7	343	13
B	Circ.	10	-	38	15	303	11
B	Circ.	18	-	29	12	219	8
B	Circ.	25	151	52	21	180	7
B	Circ.	31	-	31	12	120	4
B	Circ.	34	-	27	11	101	4
B	Circ.	42	-	30	12	74	3
B	Circ.	49	174	48	19	56	2
B	Circ.	54	-	20	8	80	3
B	Circ.	66	-	21	8	41	2
B	Circ.	71	157	21	8	28	1
D	Circ.	0	178	27	11	971	36
D	Circ.	6	-	40	16	618	23
D	Circ.	10	-	37	15	474	18
D	Circ.	18	-	62	25	366	14
D	Circ.	25	170	58	23	290	11
D	Circ.	31	-	41	16	257	10
D	Circ.	34	-	35	14	193	7
D	Circ.	42	-	32	13	116	4
D	Circ.	49	184	32	13	94	4
D	Circ.	54	-	18	7	88	3
D	Circ.	66	-	39	16	35	1
D	Circ.	71	170	17	7	35	1
Experiment 2 (JC18_9: 16º 36.50 N -62º 02.00 W, Depth: 1113 m)							
C	Circ.	0	160	34	14	6490	242
C	Circ.	6	-	20	8	6601	246
C	Circ.	12	-	21	9	6157	230
C	Circ.	18	-	22	9	6031	225
C	Circ.	24	149	47	19	5904	220
C	Circ.	32	-	14	6	5671	212
C	Circ.	36	-	41	16	5543	207
C	Circ.	42	-	28	11	5114	191
C	Circ.	48	155	32	13	4997	186
C	Circ.	54	-	34	14	4652	174
C	Circ.	62	-	23	9	4499	168
C	Circ.	67	-	35	14	4182	156
C	Circ.	71	150	57	23	3980	149

(Continued...) Montserrat microcosm experiment data

Core	Comment	Time (hrs)	O_2 (μM)	Fe (nM)	(± 1-SD)	Mn (nM)	(± 1-SD)
D	Circ.	0	153	32	13	9104	340
D	Circ.	6	-	33	13	9488	354
D	Circ.	12	-	33	13	9220	344
D	Circ.	18	-	29	11	9173	342
D	Circ.	24	150	58	23	8774	327
D	Circ.	32	-	26	10	8603	321
D	Circ.	36	-	34	13	8552	319
D	Circ.	42	-	31	12	8308	310
D	Circ.	48	136	16	6	8152	304
D	Circ.	54	-	33	13	7920	296
D	Circ.	62	-	32	13	8128	303
D	Circ.	67	-	51	21	7882	294
D	Circ.	71	103	72	29	7999	298
Experiment 3							
Exp. 1 B	Circ.	0.0*	-	19	8	28	1
Exp. 1 B	Susp.	0.2	-	78	31	25	1
Exp. 1 B	Susp.	0.3	-	22	9	22	1
Exp. 1 B	Circ.	0.5	-	26	11	22	1
Exp. 1 B	Circ.	0.8	-	25	10	22	1
Exp. 1 B	Circ.	1.0	-	21	8	26	1
Exp. 1 B	Circ.	1.6	-	27	11	23	1
Exp. 2 C	Circ.	0.0*	-	40	16	6854	180
Exp. 2 C	Susp.	0.2	-	43	17	6998	261
Exp. 2 C	Susp.	0.4	-	41	16	6790	253
Exp. 2 C	Circ.	0.5	-	34	14	6943	259
Exp. 2 C	Circ.	0.7	-	22	9	6959	260
Exp. 2 C	Circ.	0.9	-	55	22	6801	254
Exp. 2 C	Circ.	1.2	-	62	25	6954	260
Exp. 2 C	Circ.	1.5	-	40	16	6890	257

Circ. - Re-circulation of overlying core water

Bio. - Biocide addition to overlying core water

Susp. - Re-suspension of surface sediment by enhanced overlying core water circulation

* Start of Exp. 3 (t = 0.0) is equivalent to Exp. 1: t = ~96 hrs and Exp. 2: t = ~72 hrs.

- Not determined

References

Aller, R.C., Mackin, J.E., and Cox, J.R.T., 1986, Diagenesis of Fe and S in Amazon inner shelf muds: apparent dominance of Fe reduction and implications for the genesis of ironstones: Continental Shelf Research, v. 6, p. 263-289.

Aller, R.C., 1990, Bioturbation and Manganese Cycling in Hemipelagic Sediments: Philosophical Transactions of the Royal Society of London. Series A, Mathematical and Physical Sciences, v. 331, p. 51-68.

Anbar, A.D., and Rouxel, O., 2007, Metal Stable Isotopes in Paleoceanography: Annual Review of Earth and Planetary Sciences, v. 35, p. 717-746.

Arnold, G.L., Weyer, S., and Anbar, A.D., 2004, Fe Isotope Variations in Natural Materials Measured Using High Mass Resolution Multiple Collector ICPMS: Analytical Chemistry, v. 76, p. 322-327.

Barbeau, K., Rue, E.L., Bruland, K.W., and Butler, A., 2001, Photochemical cycling of iron in the surface ocean mediated by microbial iron(III)-binding ligands: Nature, v. 413, p. 409-413.

Beard, B.L., Johnson, C.M., Cox, L., Sun, H., Nealson, K.H., and Aguilar, C., 1999, Iron Isotope Biosignatures: Science, v. 285, p. 1889-1892.

Beard, B.L., Johnson, C.M., Von Damm, K.L., and Poulson, R.L., 2003, Iron isotope constraints on Fe cycling and mass balance in oxygenated Earth oceans: Geology, v. 31, p. 629-632.

Bennett, S.A., Achterberg, E.P., Connelly, D.P., Statham, P.J., Fones, G.R., and German, C.R., 2008, The distribution and stabilisation of dissolved Fe in deep-sea hydrothermal plumes: Earth and Planetary Science Letters, v. 270, p. 157-167.

Bennett, S.A., Rouxel, O., Schmidt, K., Garbe-Schˆnberg, D., Statham, P.J., and R.German, C., 2009, Iron isotope fractionation in a buoyant hydrothermal plume, 5˚S Mid-Atlantic Ridge: Geochimica et Cosmochimica Acta, v. 73, p. 5619-5634.

Berelson, W., McManus, J., Coale, K., Johnson, K., Burdige, D., Kilgore, T., Colodner, D., Chavez, F., Kudela, R., and Boucher, J., 2003, A time series of benthic flux measurements from Monterey Bay, CA: Continental Shelf Research, v. 23, p. 457.

Berelson, W.M., Riedel, T., McManus, J., and Severmann, S., 2008, The effects of oxygen on benthic flux of nutrients and iron measured with benthic chambers deployed on the Oregon/N.California shelf ASLO Ocean Sciences Meeting: Orlando, Florida.

Bergquist, B.A., and Boyle, E.A., 2006, Iron isotopes in the Amazon River system: Weathering and transport signatures: Earth and Planetary Science Letters, v. 248, p. 54.

Bergquist, B.A., Wu, J., and Boyle, E.A., 2007, Variability in oceanic dissolved iron is dominated by the colloidal fraction: Geochim. Cosmochim. Acta v. 71 p. 2960–2974.

Bollens, G.C.R., and Landry, M.R., 2000, Biological response to iron fertilization in the eastern equatorial Pacific (IronEx II). II. Mesozooplankton abundance, biomass, depth distribution and grazing: Marine Ecology-Progress Series, v. 201, p. 43-56.

Bottrell, S.H., and Morton, M.D.B., 1992, A reinterpretation of the genesis of the Cae Coch pyrite deposit, North Wales: Journal of the Geological Society, v. 149, p. 581-584.

Boyd, P.W., Watson, A.J., Law, C.S., Abraham, E.R., Trull, T., Murdoch, R., Bakker, D.C.E., Bowie, A.R., Buesseler, K.O., Chang, H., Charette, M., Croot, P., Downing, K., Frew, R., Gall, M., Hadfield, M., Hall, J., Harvey, M., Jameson, G., LaRoche, J., Liddicoat, M., Ling, R., Maldonado, M.T., McKay, R.M., Nodder, S., Pickmere, S., Pridmore, R., Rintoul, S., Safi, K., Sutton, P., Strzepek, R., Tanneberger, K., Turner, S., Waite, A., and Zeldis, J., 2000, A mesoscale phytoplankton bloom in the polar Southern Ocean stimulated by iron fertilization: Nature, v. 407, p. 695-702.

Boye, M., and van den Berg, C.M.G., 2000, Iron availability and the release of iron-complexing ligands by Emiliania huxleyi: Marine Chemistry, v. 70, p. 277-287.

Boye, M., van den Berg, C.M.G., de Jong, J.T.M., Leach, H., Croot, P., and de Baar, H.J.W., 2001, Organic complexation of iron in the Southern Ocean: Deep-Sea Research Part I-Oceanographic Research Papers, v. 48, p. 1477-1497.

Boye, M., Aldrich, A.P., Van Den Berg, C.M.G., De Jong, J.T.M., Veldhuis, M.J.W., and De Baar, H.J.W., 2003, Horizontal gradient of the chemical speciation of iron in surface waters of the northeast Atlantic Ocean: Marine Chemistry, v. 80, p. 129-143.

Bucciarelli, E., Blain, S., and Treguer, P., 2001, Iron and manganese in the wake of the Kerguelen Islands (Southern Ocean): Marine Chemistry, v. 73, p. 21-36.

Buck, K.N., Lohan, M.C., Berger, C.J.M., and Bruland, K.W., 2007, Dissolved iron speciation in two distinct river plumes and an estuary: Implications for riverine iron supply Limnology and Oceanography, v. 52, p. 843–855.

Burdige, D.J., and Gieskes, J.M., 1983, A pore water/solid phase diagenetic model for manganese in marine sediments: Am J Sci, v. 283, p. 29-47.

Burdige, D.J., 1993, The biogeochemistry of manganese and iron reduction in marine sediments: Earth-Science Reviews, v. 35, p. 249.

Cai, W.-J., and Reimers, C.E., 1995, Benthic oxygen flux, bottom water oxygen concentration and core top organic carbon content in the deep northeast Pacific Ocean: Deep Sea Research Part I: Oceanographic Research Papers, v. 42, p. 1681-1699.

Canfield, D.E., and Berner, R.A., 1987, Dissolution and pyritization of magnetite in anoxie marine sediments: Geochimica et Cosmochimica Acta, v. 51, p. 645-659.

Canfield, D.E., 1989, Reactive iron in marine sediments: Geochimica Cosmochimica Acta, v. 53, p. 619-632.

Canfield, D.E., Thamdrup, B., and Hansen, J.W., 1993, The anaerobic degradation of organic matter in Danish coastal sediments: Iron reduction, manganese reduction, and sulfate reduction: Geochimica et Cosmochimica Acta ; Vol/Issue: 57:16, p. Pages: 3867-3883.

Chase, Z., Hales, B., Cowles, T., Schwartz, R., and van Geen, A., 2005, Distribution and variability of iron input to Oregon coastal waters during the upwelling season: J. Geophys. Res., v. 110.

Chester, R., 1990, Marine Geochemistry: London, Chapman & Hall, 698 p.

Chu, N.C., Johnson, C.M., Beard, B.L., German, C.R., Nesbitt, R.W., Frank, M., Bohn, M., Kubik, P.W., Usui, A., and Graham, I., 2006, Evidence for hydrothermal venting in Fe isotope compositions of the deep Pacific Ocean through time: Earth and Planetary Science Letters, v. 245, p. 202-217.

Coale, K.H., Johnson, K.S., Fitzwater, S.E., Gordon, R.M., Tanner, S., Chavez, F.P., Ferioli, L., Sakamoto, C., Rogers, P., Millero, F., Steinberg, P., Nightingale, P., Cooper, D., Cochlan, W.P., Landry, M.R., Constantinou, J., Rollwagen, G., Trasvina, A., and Kudela, R., 1996, A massive phytoplankton bloom

induced by an ecosystem-scale iron fertilization experiment in the equatorial Pacific Ocean: Nature, v. 383, p. 495-501.

Coale, K.H., Johnson, K.S., Fitzwater, S.E., Blain, S.P.G., Stanton, T.P., and Coley, T.L., 1998, IronEx-I, an in situ iron-enrichment experiment: Experimental design, implementation and results: Deep-Sea Research Part Ii-Topical Studies in Oceanography, v. 45, p. 919-945.

Coale, K.H., Johnson, K.S., Chavez, F.P., Buesseler, K.O., Barber, R.T., Brzezinski, M.A., Cochlan, W.P., Millero, F.J., Falkowski, P.G., Bauer, J.E., Wanninkhof, R.H., Kudela, R.M., Altabet, M.A., Hales, B.E., Takahashi, T., Landry, M.R., Bidigare, R.R., Wang, X.J., Chase, Z., Strutton, P.G., Friederich, G.E., Gorbunov, M.Y., Lance, V.P., Hilting, A.K., Hiscock, M.R., Demarest, M., Hiscock, W.T., Sullivan, K.F., Tanner, S.J., Gordon, R.M., Hunter, C.N., Elrod, V.A., Fitzwater, S.E., Jones, J.L., Tozzi, S., Koblizek, M., Roberts, A.E., Herndon, J., Brewster, J., Ladizinsky, N., Smith, G., Cooper, D., Timothy, D., Brown, S.L., Selph, K.E., Sheridan, C.C., Twining, B.S., and Johnson, Z.I., 2004, Southern ocean iron enrichment experiment: Carbon cycling in high- and low-Si waters: Science, v. 304, p. 408-414.

Cronan, D.S., 1977, Deep-sea nodules: distribution and geochemistry, *in* Glasby, G.P., ed., Marine Manganese Deposits: Amsterdam, Elsevier, p. 11-44.

Croot, P.L., and Hunter, K.A., 1998, Trace metal distributions across the continental shelf near Otago Peninsula, New Zealand: Marine Chemistry, v. 62, p. 185-201.

Crosby, H.A., Roden, E.E., Johnson, C.M., and Beard, B.L., 2007, The mechanisms of iron isotope fractionation produced during dissimilatory Fe(III) reduction by Shewanella putrefaciens and Geobacter sulfurreducens: Geobiology, v. 5, p. 169-189.

De Baar, H.J.W., and De Jong, J.T.M., 2001, Distributions, Sources and Sinks of Iron in Seawater, *in* Turner, D.R., and Hunter, K.A., eds., The Biogeochemistry of Iron in Seawater, Volume 7: IUPAC series on analytical and physical chemistry of environmental systems: Chichester, John Wiley & Sons, Ltd, p. 123-253.

Deplus, C., Le Friant, A., Boudon, G., Komorowski, J.-C., Villemant, B., Harford, C., SÈgoufin, J., and CheminÈe, J.-L., 2001, Submarine evidence for large-scale debris avalanches in the Lesser Antilles Arc: Earth and Planetary Science Letters, v. 192, p. 145-157.

Duce, R.A., Liss, P.S., Merrill, J.T., Atlas, E.L., Buat-Menard, P., Hicks, B.B., Miller, J.M., Prospero, J.M., Arimoto, R., Church, T.M., Ellis, W., Galloway, J.N., Hansen, L., Jickells, T.D., Knap, A.H., Reinhardt, K.H., Schneider, B., Soudine, A., Tokos, J.J., Tsunogai, S., Wollast, R., and Zhou, M., 1991, The atmospheric input of trace species to the world ocean: Global Biogeochemical Cycles, v. 5, p. 193-259.

Elrod, V.A., Berelson, W.M., Coale, K.H., and Johnson, K.S., 2004, The flux of iron from continental shelf sediments: A missing source for global budgets: Geophysical Research Letters, v. 31, p. art. no.-L12307.

Emerson, S., Jahnke, R., and Heggie, D., 1984, Sediment-water exchange in shallow water estuarine sediments: Journal of Marine Research, v. 42, p. 709-730.

Escoube, R., Rouxel, O.J., Sholkovitz, E., and Donard, O.F.X., In Press, Iron Isotope Systematics in Estuaries: The case of North River, Massachusetts (USA): Geochimica et Cosmochimica Acta, v. In Press.

Feely, R.A., Lewison, M., Massoth, G.J., Robertbaldo, G., Lavelle, J.W., Byrne, R.H., Von Damm, K.L., and Curl, H.C., 1987, Composition and dissolution of

black smoker particulates from active vents on the Juan-De-Fuca Ridge: J. Geophys. Res.- Solid Earth Planets, v. 92, p. 11347-11363.
Florindo, F., A. P. Roberts, and Palmer, M.R., 2003, Magnetite dissolution in siliceous sediments: Geochem. Geophys. Geosyst., v. 4, p. 13.
Fones, G.R., Davison, W., Holby, O., Jorgensen, B.B., and Thamdrup, B., 2001, High-resolution metal gradients measured by in situ DGT/DET deployment in Black Sea sediments using an autonomous benthic lander: Limnology and Oceanography, v. 46, p. 982-988.
Froelich, P.N., Klinkhammer, G.P., Bender, M.L., Luedtke, N.A., Heath, G.R., Cullen, D., Dauphin, P., Hammond, D., Hartman, B., and Maynard, V., 1979, Early oxidation of organic matter in pelagic sediments of the eastern equatorial Atlantic: suboxic diagenesis: Geochimica et Cosmochimica Acta, v. 43, p. 1075-1090.
Froelich, P.N., Malone, P.N., Hodell, D.A., Ciesielski, P.F., Warnke, D.E., Westall, F., Hailwood, E.A., Nobes, D.C., Fenner, J., Mienert, J., Mwenifumbo, C.J., and Müller, D.W., 1991, Biogenic Opal and Carbonate Accumulation Rates in the Subantarctic South Atlantic: The Late Neogene of Meteor Rise Site 704, *in* Ciesielski, P.F., Kristoffersen, Y., et al., ed., Proc. Ocean Drilling Program, Scientific Results, Volume 114, p. 515-550.
Frogner, P., Reynir, G., slason, S., and skarsson, N., 2001, Fertilizing potential of volcanic ash in ocean surface water: Geology, v. 29, p. 487-490.
Gehlen, M., Rabouille, C., Ezat, U., and Guidi-Guilvard, L.D., 1997, Drastic Changes in Deep-Sea Sediment Porewater Composition Induced by Episodic Input of Organic Matter: Limnology and Oceanography, v. 42, p. 980-986.
German, C.R., Campbell, A.C., and Edmond, J.M., 1991, Hydrothermal scavenging at the Mid-Atlantic Ridge: Modification of trace element dissolved fluxes: Earth and Planetary Science Letters, v. 107, p. 101-114.
Giere, O., 2009, Sampling and Processing Meiofauna, Meiobenthology, Springer Berlin Heidelberg, p. 63-86.
Gledhill, M., van den Berg, C.M.G., Nolting, R.F., and Timmermans, K.R., 1998, Variability in the speciation of iron in the northern North Sea: Marine Chemistry, v. 59, p. 283-300.
Gordon, R.M., Martin, J.H., and Knauer, G.A., 1982, Iron in north-east Pacific waters: Nature, v. 299, p. 611-612.
Gunn, B.M., Ramon, C.-Y., Watkins, N.D., Abranson, C.E., and Nougier, J., 1970, Geochemistry of an Oceanite-Ankaramite-Basalt Suite from East Island, Crozet Archipelago: Contributions to Mineralogy and Petrology, v. 28, p. 319-339.
Haeckel, M., König, I., Riech, V., Weber, M.E., and Suess, E., 2001a, Pore water profiles and numerical modelling of biogeochemical processes in Peru Basin deep-sea sediments: Deep Sea Research Part II: Topical Studies in Oceanography, v. 48, p. 3713-3736.
Haeckel, M., van Beusekomb, J., Wiesnerc, M.G., and Koniga, I., 2001b, The impact of the 1991 Mount Pinatubo tephra fallout on the geochemical environment of the deep-sea sediments in the South China Sea: Earth and Planetary Science Letters, v. 193, p. 151-166.
Hammond, D.E., McManus, J., Berelson, W.M., Kilgore, T.E., and Pope, R.H., 1996, Early diagenesis of organic material in equatorial Pacific sediments: stpichiometry and kinetics: Deep Sea Research Part II: Topical Studies in Oceanography, v. 43, p. 1365-1412.
Hedges, J.I., Hu, F.S., Devol, A.H., Hartnett, H.E., Tsamakis, E., and Keil, R.G., 1999, Sedimentary organic matter preservation; a test for selective degradation under oxic conditions: Am J Sci, v. 299, p. 529-555.

Hembury, D., Palmer, M.R., Fones, G.R., and Jones, M.T., 2009, Oxygen uptake during marine diagenesis of fresh volcanic material, Goldschmidt, Volume Conference Abstracts: Davos, Switzerland, p. A521.

Hernandez Sanchez, M.T., 2009, Productivity variations around a naturally Iron-fertilised region of the ocean: The Crozet Plateau, Southern Ocean: Bristol, University of Bristol.

Homoky, W.B., Severmann, S., Mills, R.A., Statham, P.J., and Fones, G.R., 2009, Pore-fluid Fe isotopes reflect the extent of benthic Fe redox recycling: Evidence from continental shelf and deep-sea sediments: Geology, v. 37, p. 751-754.

Howard, A.G., and Statham, P.J., 1997, Trace Inorganic Analysis: Philosophy and Practice: Chichester, John Wiley.

Huerta-Diaz, M.A., Rivera-Duarte, I., Sanudo-Wilhelmy, S.A., and Flegal, A.R., 2007, Comparative distributions of size fractionated metals in pore waters sampled by in situ dialysis and whole-core sediment squeezing: Implications for diffusive flux calculations: Applied Geochemistry, v. 22, p. 2509.

Huettel, M., Ziebis, W., Forster, S., and Luther, G.W., 1998, Advective Transport Affecting Metal and Nutrient Distributions and Interfacial Fluxes in Permeable Sediments: Geochimica et Cosmochimica Acta, v. 62, p. 613-631.

Huettel, M., Røy, H., Precht, E., and Ehrenhauss, S., 2003, Hydrodynamical impact on biogeochemical processes in aquatic sediments: Hydrobiologia, v. 494, p. 231-236.

Icopini, G.A., Anbar, A.D., Ruebush, S.S., Tien, M., and Brantley, S.L., 2004, Iron isotope fractionation during microbial reduction of iron: The importance of adsorption: Geology, v. 32, p. 205-208.

Jickells, T.D., and Spokes, L.J., 2001, Atmospheric Iron Inputs to the Oceans, *in* Turner, D.R., and Hunter, K.A., eds., The Biogeochemistry of Iron in Seawater, Volume 7: IUPAC series on analytical and physical chemistry of environmental systems: Chichester, John Wiley & Sons, Ltd, p. 85-121.

Johnson, C.M., Beard, B.L., and Roden, E.E., 2008, The Iron Isotope Fingerprints of Redox and Biogeochemical Cycling in Modern and Ancient Earth: Annual Review of Earth and Planetary Sciences, v. 36, p. 457-493.

Johnson, K.S., Berelson, W.M., Coale, K.H., Coley, T.L., Elrod, V.A., Fairey, W.R., Iams, H.D., Kilgore, T.E., and Nowicki, J.L., 1992, Manganese Flux from Continental Margin Sediments in a Transect Through the Oxygen Minimum: Science, v. 257, p. 1242-1245.

Johnson, K.S., Coale, K.H., Berelson, W.M., and Michael Gordon, R., 1996, On the formation of the manganese maximum in the oxygen minimum: Geochimica et Cosmochimica Acta, v. 60, p. 1291-1299.

Johnson, K.S., Gordon, R.M., and Coale, K.H., 1997, What controls dissolved iron concentrations in the world ocean?: Marine Chemistry, v. 57, p. 137-161.

Johnson, K.S., Chavez, F.P., and Friederich, G.E., 1999, Continental-shelf sediment as a primary source of iron for coastal phytoplankton: Nature, v. 398, p. 697-700.

Jones, M.T., and Gislason, S.R., 2008, Rapid releases of metal salts and nutrients following the deposition of volcanic ash into aqueous environments: Geochimica et Cosmochimica Acta, v. 72, p. 3661-3680.

Jorgensen, B.B., and Revsbech, N.P., 1985, Diffusive Boundary Layers and the Oxygen Uptake of Sediments and Detritus: Limnology and Oceanography, v. 30, p. 111-122.

King, S.L., Froelich, P.N., and Jahnke, R.A., 2000, Early diagenesis of germanium in sediments of the Antarctic South Atlantic: in search of the missing Ge sink: Geochimica et Cosmochimica Acta, v. 64, p. 1375.

Klimant, I., Meyer, V., and Kuhl, M., 1995, Fibre-optic microsensors, a new tool in aquatic biology: Limnology and Oceanography, v. 40, p. 1159-1165.

Klinkhammer, G., Heggie, D.T., and Graham, D.W., 1982, Metal diagenesis in oxic marine sediments: Earth and Planetary Science Letters, v. 61, p. 211-219.

Klinkhammer, G.P., 1980, Early diagenesis in sediments from the eastern equatorial Pacific, II. Pore water metal results: Earth and Planetary Science Letters, v. 49, p. 81-101.

Klunder, M., Laan, P., Middag, R., and de Baar, H.J.W., In Press, Dissolved Iron in the Southern Ocean: Deep Sea Research Part II Oceanographic Research Papers, v. Polarstern ANT XXIV/3 Special issue.

Kohler, B., Singer, A., and Stoffers, P., 1994, Biogenic nontronite from marine white smoker chimneys: Clays and Clay Minerals, v. 42, p. 689-701.

Kuma, K., Katsumoto, A., Nishioka, J., and Matsunaga, K., 1998, Size-fractionated iron concentrations and Fe(III) hydroxide solubilities in various coastal waters: Estuarine, Coastal and Shelf Science, v. 47, p. 275-283.

Kuma, K., Isoda, Y., and Nakabayashi, S., 2003, Control on dissolved iron concentrations in deep waters in the western North Pacific: Iron(III) hydroxide solubility: Journal of Geophysical Research-Oceans, v. 108, p. art. no.-3289.

Lam, P.J., J.K.B. Bishop, C.C. Henning, M.A. Marcus, G.A. Waychunas, and Fung., I.Y., 2006, Wintertime phytoplankton bloom in the Subarctic Pacific supported by continental margin iron: Global Biogeochemical Cycles, v. 20(1), p. GB1006.

Landing, W.M., and Bruland, K.W., 1987, The contrasting biogeochemistry of iron and manganese in the Pacific Ocean: Geochimica Cosmochimica Acta, v. 51, p. 29-43.

Landing, W.M., and Powell, R.T., 1999, The biogeochemistry of iron in the Atlantic Ocean: Abstracts of Papers of the American Chemical Society, v. 217, p. 090-GEOC.

Li, Y.-H., and Gregory, S., 1974, Diffusion of ions in sea water and in deep-sea sediments: Geochimica et Cosmochimica Acta, v. 38, p. 703.

Lohan, M.C., and Bruland, K.W., 2008, Elevated Fe(II) and Dissolved Fe in Hypoxic Shelf Waters off Oregon and Washington: An Enhanced Source of Iron to Coastal Upwelling Regimes: Environmental Science & Technology, v. 42, p. 6462-6468.

Lovley, D.R., and Phillips, E.J.P., 1986, Organic matter mineralization with reduction of ferric iron in anaerobic sediments: Appl. Environ. Microbiol., v. 51, p. Pages: 683-689.

Lovley, D.R., 1991, Dissimilatory Fe(III) and Mn(IV) reduction: Microbiol. Mol. Biol. Rev., v. 55, p. 259-287.

Luther III, G.W., Kostka, J.E., Church, T.M., Sulzberger, B., and Stumm, W., 1992, Seasonal iron cycling in the salt-marsh sedimentary environment: the importance of ligand complexes with Fe(II) and Fe(III) in the dissolution of Fe(III) minerals and pyrite, respectively: Marine Chemistry, v. 40, p. 81-103.

Marsh, R., Mills, R.A., Green, D.R.H., Salter, I., and Taylor, S., 2007, Controls on sediment geochemistry in the Crozet region: Deep Sea Research Part II: Topical Studies in Oceanography, v. 54, p. 2260.

Martin, J.H., and Knauer, G.A., 1980, Manganese cycling in the northeast Pacific waters: Earth and Planetary Science Letters, v. 51, p. 260-274.

Martin, J.H., 1990, Glacial-interglacial CO_2 change: The iron hypothesis: Paleoceanography, v. 5, p. 1-13.

Martin, J.H., Coale, K.H., Johnson, K.S., Fitzwater, S.E., Gordon, R.M., Tanner, S.J., Hunter, C.N., Elrod, V.A., Nowicki, J.L., Coley, T.L., Barber, R.T., Lindley, S., Watson, A.J., Van Scoy, K., Law, C.S., Liddicoat, M.I., Ling, R., Stanton, T.P., Stockel, J., Collins, C., Anderson, A., Bidigare, R., Ondrusek, M., Latasa, M., Millero, F.J., Lee, K., Yao, W., Zhang, J.Z., Friederich, G.E., Sakamoto, C., Chavez, F.P., Buck, K., Kolber, Z., Greene, R.M., Falkowski, P., Chisholm, S.W., Hoge, F., Swift, R., Yungel, J., Turner, S., Nightingale, P., Hatton, A., Liss, P.S., and Tindale, N.W., 1994, Testing the iron hypothesis in ecosystems of the equatorial Pacific Ocean: Nature, v. 371, p. 123-129.

McManus, J., Berelson, W.M., Coale, K.H., Johnson, K.S., and Kilgore, T.E., 1997, Phosphorus regeneration in continental margin sediments: Geochimica et Cosmochimica Acta, v. 61, p. 2891.

Millero, F.J., Sotolongo, S., and Izaguirre, M., 1987, Oxidation kinetics of Fe(II) in sea water: Geochim. Cosmochim. Acta, v. 51, p. Pages: 793-801.

Millero, F.J., Yao, W., and Aicher, J., 1995, The speciation of Fe(II) and Fe(III) in natural waters: Marine Chemistry, v. 50, p. 21-39.

Millero, F.J., 1998, Solubility of Fe(III) in seawater: Earth and Planetary Science Letters, v. 154, p. 323-329.

Moffett, J.W., Goepfert, T.J., and Naqvi, S.W.A., 2007, Reduced iron associated with secondary nitrite maxima in the Arabian Sea: Deep Sea Research Part I: Oceanographic Research Papers, v. 54, p. 1341-1349.

Moore, J.K., Doney, S.C., Glover, D.M., and Fung, I.Y., 2002, Iron cycling and nutrient-limitation patterns in surface waters of the World Ocean: Deep-Sea Research Part Ii-Topical Studies in Oceanography, v. 49, p. 463-507.

Moore, J.K., and Braucher, O., 2008, Sedimentary and mineral dust sources of dissolved iron to the world ocean: Biogeosciences, v. 5, p. 631-656.

Morford, J., Kalnejais, L., Martin, W., François, R., and Karle, I.-M., 2003, Sampling marine pore waters for Mn, Fe, U, Re and Mo: modifications on diffusional equilibration thin film gel probes: Journal of Experimental Marine Biology and Ecology, v. 285-286, p. 85-103.

Morgan, J.J., 1967, Chemical equilibria and kinetic properties of manganese in natural waters, *in* Faust, S.D., and Hunter, J.V., eds., Principles and Applications of Water Chemistry, Wiley, p. 561-623.

Nédélec, F., Statham, P.J., and Mowlem, M., 2007, Processes influencing dissolved iron distributions below the surface at the Atlantic Ocean-Celtic Sea shelf edge: Marine Chemistry, v. 104, p. 156-170.

Nishioka, J., Takeda, S., Wong, C.S., and Johnson, W.K., 2001, Size-fractionated iron concentrations in the northeast Pacific Ocean: distribution of soluble and small colloidal iron: Marine Chemistry, v. 74, p. 157-179.

Nishioka, J., Ono, T., Saito, H., Nakatsuka, T., Takeda, S., Yoshimura, T., Suzuki, K., Kuma, K., Nakabayashi, S., Tsumune, D., Mitsudera, H., Johnson, K.W., and Tsuda, A., 2007, Iron supply to the western subarctic Pacific: Importance of iron export from the Sea of Okhotsk: Journal Geophysical Research, v. 112, p. C10012.

Nodwell, L.M., and Price, N.M., 2001, Direct use of inorganic colloidal iron by marine mixotrophic phytoplankton: Limnology and Oceanography, v. 46, p. 765-777.

Ogston, A.S., Guerra, J.V., and Sternberg, R.W., 2004, Interannual variability of nearbed sediment flux on the Eel River shelf, northern California: Continental Shelf Research, v. 24, p. 117-136.

Phillips, R.E., and Ellis, J.H., 1970, A rapid method of measurement of diffusion coefficients in aqueous solutions: Soil Science, v. 110, p. 421-425.

Pirrie, D., and Marshal, J.D., 1990, Diagenesis of Inoceramus and Late Cretaceous paleoenvironmental geochemistry; a case study from James Ross Island, Antarctica: PALAIOS, v. 5, p. 336-345.

Pirrie, D., Ditchfield, P.W., and Marshall, J.D., 1994, Burial diagenesis and pore-fluid evolution in a Mesozoic back-arc basin; the Marambio Group, Vega Island, Antarctica: JOURNAL OF SEDIMENTARY RESEARCH, v. 64, p. 541-552.

Planquette, H., Statham, P.J., Fones, G.R., Charette, M.A., Moore, C.M., Salter, I., Nedelec, F.H., Taylor, S.L., French, M., Baker, A.R., Mahowald, N., and Jickells, T.D., 2007, Dissolved iron in the vicinity of the Crozet Islands, Southern Ocean: Deep Sea Research Part II: Topical Studies in Oceanography, v. 54, p. 1999.

Polerecky, L., Volkenborn, N., and Stief, P., 2006, High Temporal Resolution Oxygen Imaging in Bioirrigated Sediments: Environmental Science & Technology, v. 40, p. 5763-5769.

Pollard, R., Sanders, R., Lucas, M., and Statham, P., 2007, The Crozet Natural Iron Bloom and Export Experiment (CROZEX): Deep Sea Research Part II: Topical Studies in Oceanography, v. 54, p. 1905.

Pollard, T.R., et al., 2009, Southern Ocean deep-water carbon export enhanced by natural iron fertilization: Nature, v. 457, p. 577-580.

Poulton, S.W., and Canfield, D.E., 2005, Development of a sequential extraction procedure for iron: implications for iron partitioning in continentally derived particulates: Chemical Geology, v. 214, p. 209.

Raiswell, R., and Anderson, T.F., 2005, Reactive iron enrichment in sediments deposited beneath euxinic bottom waters: constraints on supply by shelf recycling: Geological Society, London, Special Publications, v. 248, p. 179-194.

Raiswell, R., Benning, L.G., Davidson, L., and Tranter, M., 2008, Nanoparticulate bioavailable iron minerals in icebergs and glaciers: Mineral Mag, v. 72, p. 345-348.

Rouxel, O.J., Bekker, A., and Edwards, K.J., 2005, Iron Isotope Constraints on the Archean and Paleoproterozoic Ocean Redox State: Science, v. 307, p. 1088-1091.

Rue, E.L., and Bruland, K.W., 1995, Complexation of iron(III) by natural organic ligands in the Central North Pacific as determined by a new competitive ligand equilibration/adsorptive cathodic stripping voltammetric method: Marine Chemistry, v. 50, p. 117-138.

Sanders, R., Morris, P.J., Stinchcombe, M., Seeyave, S., Venables, H., and Lucas, M., 2007, New production and the f ratio around the Crozet Plateau in austral summer 2004-2005 diagnosed from seasonal changes in inorganic nutrient levels: Deep Sea Research Part II: Topical Studies in Oceanography, v. 54, p. 2191.

Sarthou, G., Baker, A.R., Blain, S., Achterberg, E.P., Boye, M., Bowie, A.R., Croot, P., Laan, P., de Baar, H.J.W., Jickells, T.D., and Worsfold, P.J., 2003, Atmospheric iron deposition and sea-surface dissolved iron concentrations in the eastern Atlantic Ocean: Deep-Sea Research Part I-Oceanographic Research Papers, v. 50, p. 1339-1352.

Scally, S., Davison, W., and Zhang, H., 2006, Diffusion coefficients of metals and metal complexes in hydrogels used in diffusive gradients in thin films: Analytica Chimica Acta, v. 558, p. 222-229.

Scheinost, A.C., Stanjek, H., Schulze, D.G., Gasser, U., and Sparks, D.L., 2001, Structural environment and oxidation state of Mn in goethite-groutite solid-solutions: American Mineralogist, v. 86, p. 139-146.

Schlüter, M., Sauter, E., Hansen, H.-P., and Suess, E., 2000, Seasonal variations of bioirrigation in coastal sediments: modelling of field data: Geochimica et Cosmochimica Acta, v. 64, p. 821-834.

Schmidt, M.A., Zhang, Y., and Hutchins, D.A., Assimilation of Fe and carbon by marine copepods from Fe-limited and Fe-replete diatom prey., Source: Journal of Plankton Research; VOL. 21, NO. 9, pp. 1753-1764; 1999.

Sedwick, P.N., Edwards, P.R., Mackey, D.J., Griffiths, F.B., and Parslow, J.S., 1997, Iron and manganese in surface waters of the Australian subantarctic region: Deep-Sea Research I, v. 44, p. 1239-1253.

Seeberg-Elverfeldt, J., Schlüter, M., Feseker, T., and Kölling, M., 2005, Rhizon sampling of pore waters near the sediment/water interface of aquatic systems Limnology and Oceanography: Methods, v. 3, p. 361-371.

Seiter, K., Hensen, C., Schrˆter, J.r., and Zabel, M., 2004, Organic carbon content in surface sediments--defining regional provinces: Deep Sea Research Part I: Oceanographic Research Papers, v. 51, p. 2001-2026.

Severmann, S., Johnson, C.M., Beard, B.L., and McManus, J., 2006, The effect of early diagenesis on the Fe isotope compositions of porewaters and authigenic minerals in continental margin sediments: Geochimica et Cosmochimica Acta, v. 70, p. 2006-2022.

Severmann, S., Lyons, T.W., Anbar, A., McManus, J., and Gordon, G., 2008, Modern iron isotope perspective on the benthic iron shuttle and the redox evolution of ancient oceans: Geology, v. 36, p. 487-490.

Severmann, S., McManus, J., Berelson, W.M., and Hammond, D.E., In prep., The continental shelf benthic iron flux and its isotope composition.

Severmann, S., McManus, J., Berelson, W.M., Riedel, T.E., Owens, J., Homoky, W.B., 2008, The benthic flux of Iron from river-dominated continental shelves of the North Pacific, ASLO Ocean Sciences Meeting: Orlando, Florida.

Shaw, T.J., Gieskes, J.M., and Jahnke, R.A., 1990, Early diagenesis in differing depositional environments: The response of transition metals in pore water: Geochimica et Cosmochimica Acta, v. 54, p. 1233-1246.

Skrabal, S.A., Donat, J.R., and Burdige, D.J., 1997, Fluxes of strong copper-complexing ligands from estuarine sediments: A source to the water column?: Abstracts of Papers of the American Chemical Society, v. 213, p. 161-GEOC.

Smythe-Wright, D., Paylor, R., and Holley, S.E., 1993, Chemical tracer studies at IOSDL-4: The measurement of oxygen in seawater by photometeric and amperometric techniques, Volume 303, Institute of Oceanographic Sciences Deacon Laboratory, p. 47.

Sommerfield, C.K., and Nittrouer, C.A., 1999, Modern accumulation rates and a sediment budget for the Eel shelf: a flood-dominated depositional environment: Marine Geology, v. 154, p. 227-241.

Statham, P.J., and Burton, J.D., 1986, Dissolved Manganese in the North-Atlantic Ocean, 0-35 Degrees-N: Earth and Planetary Science Letters, v. 79, p. 55-65.

Statham, P.J., Yeats, P.A., and Landing, W.M., 1998, Manganese in the eastern Atlantic Ocean: processes influencing deep and surface water distributions: Marine Chemistry, v. 61, p. 55-68.

Statham, P.J., German, C.R., and Connelly, D.P., 2005, Iron (II) distribution and oxidation kinetics in hydrothermal plumes at the Kairei and Edmond vent

sites, Indian Ocean: Earth and Planetary Science Letters, v. 236, p. 588-596.
Statham, P.J., Skidmore, M., and Tranter, M., 2008, Inputs of glacially derived dissolved and colloidal iron to the coastal ocean and implications for primary productivity: Global Biogeochem. Cycles, v. 22.
Stookey, L.L., 1970, Ferrozine - a new spectrophotometric reagent for iron: Analytical Chemistry, v. 42, p. 779-781.
Straub, S.M., and Schmincke, H.U., 1998, Evaluating the tephra input into Pacific Ocean sediments: distribution in space and time: Geologische Rundschau, v. 87, p. 461-476.
Stricktland, J.D.H., and Parsons, T.R., 1968, Determination of dissolved oxygen: A Practical Handbook of Seawater Analysis, v. 167, p. 71-75.
Sunda, W.G., and Huntsman, S.A., 1990, Diel Cycles in Microbial Manganese Oxidation and Manganese Redox Speciation in Coastal Waters of the Bahama Islands: Limnology and Oceanography, v. 35, p. 325-338.
Sundby, B., and Silverberg, N., 1985, Manganese fluxes in the benthic boundary layer: Limnology and Oceanography, v. 30, p. 372-381.
Tappin, A.D., Millward, G.E., Statham, P.J., Burton, J.D., and Morris, A.W., 1995, Trace metals in the central and southern North Sea Estuarine, Coastal and Shelf Science, v. 41, p. 275-323.
Thamdrup, B., 2000, Bacterial Manganese and Iron Reduction in Aquatic Sediments: New York, Kluwer Academic/Plenum Publishers.
Trofimovs, J., Amy, L., Boudon, G., Deplus, C., Doyle, E., Fournier, N., Hart, M.B., Komorowski, J.C., Le Friant, A., Lock, E.J., Pudsey, C., Ryan, G., Sparks, R.S.J., and Talling, P.J., 2006, Submarine pyroclastic deposits formed at the Soufrière Hills volcano, Montserrat (1995-2003): What happens when pyroclastic flows enter the ocean?: Geology, v. 34, p. 549-552.
Ussher, S.J., Achterberg, E.P., and Worsfold, P.J., 2004, Marine Biogeochemistry of Iron: Environmental Chemistry, v. 1, p. 67-80.
Ussher, S.J., Worsfold, P.J., Achterberg, E.P., Laës, A., Blain, S., Laan, P., and de Baar, H.J.W., 2007, Distribution and redox speciation of dissolved iron on the European continental margin Limnology and Oceanography, v. 52, p. 2530-2539.
van den Berg, C.M.G., 1995, Evidence for organic complexation of iron in seawater: Marine Chemistry, v. 50, p. 139-157.
—, 2006, Chemical speciation of iron in seawater by cathodic stripping voltammetry with dihydroxynaphthalene: Analytical Chemistry, v. 78, p. 156-163.
van der Zee, C., Roberts, D.R., Rancourt, D.G., and Slomp, C.P., 2003, Nanogoethite is the dominant reactive oxyhydroxide phase in lake and marine sediments: Geology, v. 31, p. 993-996.
Vargas, M., Kashefi, K., Blunt-Harris, E.L., and Lovley, D.R., 1998, Microbiological evidence for Fe(III) reduction on early Earth: Nature, v. 395, p. 65-67.
Viollier, E., Inglett, P.W., Hunter, K., Roychoudhury, A.N., and Van Capellen, P., 2000, The ferrozine method revisited: Fe(II)/Fe(III) determination in natural waters: Applied Geochemistry, v. 15, p. 785-790.
Volkenborn, N., Polerecky, L., Hedtkamp, S.I.C., Beusekom, J.E.E.v., and Beer, D.d., 2007, Bioturbation and bioirrigation extend the open exchange regions in permeable sediments: Limnology and Oceanography, v. 52, p. 1898-1909.
von Langen, P.J., Johnson, K.S., Coale, K.H., and Elrod, V.A., 1997, Oxidation kinetics of manganese (II) in seawater at nanomolar concentrations: Geochimica et Cosmochimica Acta, v. 61, p. 4945-4954.

Waeles, M., Baker, A.R., Jickells, T., and Hoogewerff, J., 2007, Global dust teleconnections: aerosol iron solubility and stable isotope composition: Environmental Chemistry, v. 4, p. 233-237.

Warnken, K.W., Gill, G.A., Griffin, L.L., and Santschi, P.H., 2001, Sediment-water exchange of Mn, Fe, Ni and Zn in Galveston Bay, Texas: Marine Chemistry, v. 73, p. 215-231.

Watson, A.J., 2001, Iron Limitation in the Oceans, *in* Turner, D.R., and Hunter, K.A., eds., The Biogeochemistry of Iron in Seawater, Volume 7: IUPAC series on analytical and physical chemistry of environmental systems: Chichester, John Wiley & Sons, Ltd, p. 9-39.

Watson, P., Frickers, P., and Howland, R., 1993, Benthic fluxes of nutrients and some trace metals in the Tamar estuary, SW England: Aquatic Ecology, v. 27, p. 135-146.

Wells, M.L., and Mayer, L.M., 1991, The Photoconversion of Colloidal Iron Oxyhydroxides in Seawater: Deep-Sea Research Part a-Oceanographic Research Papers, v. 38, p. 1379-1395.

Wells, M.L., and Goldberg, E.D., 1994, The distribution of colloids in the North Atlantic and Southern Oceans: Limnology and Oceanography, v. 39, p. 286-302.

Wells, M.L., 1998, Marine colloids: A neglected dimension: Nature, v. 391, p. 530-531.

Wells, M.L., Smith, G.J., and Bruland, K.W., 2000, The distribution of colloidal and particulate bioactive metals in Narragansett Bay, RI: Marine Chemistry, v. 71, p. 143-163.

Wenzhöfer, F., Holby, O., and Kohls, O., 2001, Deep penetrating benthic oxygen profiles measured in situ by oxygen optodes: Deep Sea Research Part I: Oceanographic Research Papers, v. 48, p. 1741-1755.

Williams, P.J.L., Jenkinson, N. W., 1982, A Transportable Microprocessor-Controlled Precise Winkler Titration Suitable for Field Station and Shipboard Use: Limnology and Oceanography, v. 27, p. 567-584.

Winkler, L.W., 1888, Die Bestimmung des in Wasser gelösten Sauerstoffen: Berichte der Deutschen Chemischen Gesellschaft, v. 21, p. 2843-2855.

Wohlgemuth, S.E., Taylor, A.C., and Grieshaber, M.K., 2000, Ventilatory and metabolic responses to hypoxia and sulphide in the lugworm Arenicola Marina(L.): The Journal of Experimental Biology, v. 203, p. 3177-3188.

Woodworth-Lynas, C.M.T., Josenhans, H.W., Barrie, J.V., Lewis, C.F.M., and Parrott, D.R., 1991, The physical processes of seabed disturbance during iceberg grounding and scouring: Continental Shelf Research, v. 11, p. 939-961.

Wu, J., and Luther III, G.W., 1994, Size-fractionated iron concentrations in the water column of the western North Atlantic Ocean: Limnology and Oceanography, v. 39, p. 1119-1129.

—, 1995, Complexation of Fe(III) by natural organic ligands in the Northwest Atlantic Ocean by a competitive ligand equilibration method and a kinetic approach: Marine Chemistry, v. 50, p. 159-177.

—, 1996, Spatial and temporal distribution of iron in the surface water of the northwestern Atlantic Ocean: Geochimica et Cosmochimica Acta, v. 60, p. 2729-2741.

Wu, J.F., Boyle, E., Sunda, W., and Wen, L.S., 2001, Soluble and colloidal iron in the olgotrophic North Atlantic and North Pacific: Science, v. 293, p. 847-849.

Yamaguchi, K.E., Johnson, C.M., Beard, B.L., and Ohmoto, H., 2005, Biogeochemical cycling of iron in the Archean-Paleoproterozoic Earth:

Constraints from iron isotope variations in sedimentary rocks from the Kaapvaal and Pilbara Cratons: Chemical Geology, v. 218, p. 135-169.
Yeats, P.A., and Strain, P.M., 1990, The oxidation of manganese in seawater: Rate constants based on field data: Estuarine, Coastal and Shelf Science, v. 31, p. 11-24.
Yeats, P.A., and Loring, D.H., 1991, Dissolved and particulate metal distributions in the St. Lawrence estuary: Canadian Journal of Earth Sciences, v. 28, p. 729-742.
Zellmer, G.F., Hawkesworth, C.J., Sparks, R.S.J., Thomas, L.E., Harford, C.L., Brewer, T.S., and Loughlin, S.C., 2003, Geochemical Evolution of the Soufriere Hills Volcano, Montserrat, Lesser Antilles Volcanic Arc: J. Petrology, v. 44, p. 1349-1374.
Zheng, G., Takano, B., Matsuo, M., and Tanaka, Y., 2002, Compaction of Modern Soft Sediments during Core Sampling--An In Situ Investigation at an Estuary Site: Environmental Geosciences, v. 9, p. 109-114.